UNIVERSITY OF TRENTO

DEPARTMENT OF CIVIL, ENVIRONMENTAL AND MECHANICAL ENGINEERING

DOCTORAL SCHOOL IN
ENGINEERING OF CIVIL AND MECHANICAL STRUCTURAL SYSTEMS
XXVIII CYCLE

PIETRO POLLACI

THEORETICAL AND NUMERICAL MODELS ON THE DIFFUSIVE AND HEREDITARY PROPERTIES OF BIOLOGICAL STRUCTURES

ADVISOR
PROF. LUCA DESERI

CO-ADVISORS
PROF. KAUSHIK DAYAL
PROF. MASSIMILIANO ZINGALES

TRENTO, THURSDAY 17 DECEMBER, 2015

University of Trento
University of Bergamo
University of Brescia
University of Padova
University of Trieste
University of Udine
University IUAV of Venezia

Head of the Doctoral School:
Prof. Paolo Scardi   Università di Trento (IT)

Final Examination: Thursday 17$^{\text{th}}$ December, 2015

Board of Examiners:
Prof. Nicola Pugno   Università degli Studi di Trento (IT)
Prof. Maria Adelaide Vittoria Parisi   Politecnico di Milano (IT)
Dr. Giuseppe Zurlo   National University of Galway (IE)

To my beloved family,
their precious support and encouragement
gave me the force for being here.

E a mia Nonna,
perchè nessuno muore sulla terra
finchè vive nel cuore di chi resta.

Summary

The human body is composed by more than 1 billion of cells. For this reason, they are considered the basic elements of life. The building block of almost all biological membranes and other living organisms are the so-called *lipid bilayers*, structures with a thickness of the order of some nanometers. Because biological membranes surround each cell, they play a very important role in all cell lifetime processes, such as endo- and exo-cytosis; understanding their behavior due to chemical and/or mechanical input is highly important in many fields, such as in the design of drug delivery or in the monitoring of organs healthy.

For these reasons, in **Chapter 1** a review of the main features of this kind of compound is presented. The mechanical behavior of biological membranes is regulated by the interaction of an extremely rich list of features [59, 195], such as their thinness, their special constitutive nature which enables them to sustain bending moments but not in-plane shear stresses (unless their viscosity is accounted for), their chemical composition and, furthermore, their capability of undergoing ordering-disordering phenomena. The model developed in [55, 210] reveals the possibility of describing the geometrical (shape) and conformational (state of order) behavior of the lipid bilayer on the basis of one single ingredient: the in-plane membrane stretching elasticity, regulating the material response with respect to local area changes on the membrane mid-surface. In essence, the major point in the employed model is that the bilayer stretching elasticity is enough to describe its order-disorder transition. In this Thesis it will be shown how, by making use of the results obtained in [55, 210], it is possible to establish a precise connection among

several features of lipid bilayers: line tension, area compressibility modulus, bending moduli and order-disorder transition zone (see [52, 55]).

The main bulk of this Thesis is focused on the response of cell membranes due to chemical and mechanical stimuli. **Chapter 2, 3 and 4** are devoted to deduce how the key aspect of the cell response activated by chemical signaling can be predicted by a simplified energetics, making use of both theoretical models and numerical simulations. In this regard, the attention is focused on cell membranes embedding G protein-coupled receptors (GPRCs), the most import family of biological receptors. By analyzing the behavior of cell membranes, one can isolate three main contributions in order to model their response: (1) diffusion of receptors and transporters embedded in the lipid membrane; (2) conformational changes of the receptors; (3) membrane elasticity. By assuming a proper kinematics, it is possible to use a dimensional reduction procedure [52, 55] and simplify the problem under investigation. The introduction of a unique conformational field owes coupling between the rearrangement of receptors, membrane stretches and the conformational field itself. First of all, a proper energetics is constructed based on experimental data and pragmatical observations. Therefore a phenomenological local energy dependening on temperature and adhesion is assumed. Finally, the energy of receptor-ligand bonds, the energy due to loss of diffusional entropy of the activated GPRCs, and the newly deduced energy due to conformational changes in the transmembranal (TM) domains in the current configuration meet the elastic energy. This is due to the surrounding lipid membrane. Moreover, the interplay between TM conformational changes and lateral pressure of the lipid membrane against such TMs is introduced. The chemical potential of the receptor-ligand compound, deduced as the variational derivative of such energy, is compared with the one calculated by accounting for the work done by the lateral pressure introduced above. The result yields a relationship between the conformational field, the mechanical field (interpreted as either the thickness change or the areal change) and the distribution of the compounds receptor-ligand. The analysis of such resulting constitutive equation among those three quantities shows that, essentially, the reason why ligand-GPRCs compounds prefer to live on lipid raft is that the interplay between the work performed by the lateral pressure and the need of TMs to change their conformation dur-

ing ligand binding. Henceforth, mechanobiology gives a justification to the experimental findings of Nobel Prizes 2012, Kobilka [117] and Leifkovitz [127].

It is possible to show that lipid membranes are subjected to material instabilities whenever areal stretches characterizing homogeneous configurations lie inside the spinoidal zone of the free energy density, and bifurcations from such configurations can be shown to occur as oscillatory perturbations of the in-plane displacement. Furthermore, experimental observations [66] show a power-law in-plane viscous behavior of lipid structures. This observation allows one for considering an effective viscoelastic behavior of lipid membranes, which falls in the framework of Fractional Hereditariness. The unstable behavior, both in elastic and in viscoelastic case, of such structures is deeply investigated in **Chapter 5**. There, first the elastic and then the viscoelastic response are studied. Whenever the membrane is assumed to be purely elastic, perturbations of the phase ordering of lipids are predicted to form bifurcated shapes, sometimes of large periods relative to the reference thickness of the bilayer. The corresponding membrane stress changes are also oscillatory. In the second part of the Chapter also the viscosity of the compound is taken into account. Time synchronous variations are considered for finding the boundary conditions and the field equations governing the problem. Such equations yield a non-classical fractional eigenvalue problem to be analyzed through the method of separation of variables. Because bifurcations of the areal stretch from the spinoidal zone are analyzed, the spatial modes are still found to be oscillatory. The period of oscillation is shown to decrease with the ratio of (dimensionless) generalized local and nonlocal moduli and, hence, the number of oscillation increases with respect to the elastic case. As the ratio just mentioned above increases, for a given number of oscillations, the interval of stretches for which bifurcation can occur gets larger if compared with the one determined by the purely elastic behavior. These results can be also found in [58].

Side issues emerging from phenomenological investigations during the study of the hereditary behavior of the biological structures gave rise to two papers [54, 57] dealing with time-hereditary of biological tissues (such as bones) and with a related mathematical question, e.g. the determination of

the state of free energy for materials exhibiting power-law decay (aka Fractional Hereditary Materials, FHM). Hierarchical materials exhibit marked hereditary and diffusion features that could be understood by seeking for a unified approach. The theoretical models need to be combined with accurate numerical strategies, such as modified Newton-Raphson methods, multigrid methods or numerical methods based on the Cauchy-Born rule. This should be done in order to validate hypothesis of new, although existing, and novel mechanical/multiphysics models and to predict the behavior of hierarchical materials and structures. All the notions coming from these fields have to converge to the common result of giving both valid models and useful design tools for the Engineers. A very important role is played by micromechanics and hierarchical methods; with regards to this in [148] it is written that "*a lot of scientific efforts are still required in the micromechanics of hierarchical materials, before these approaches can converge and achieve the level, at which the computational design of materials with optimally tailored multiscale microstructures can be realized*". Indeed, a good understanding of the underlying nano-structure of any given material, not just biological structures, is needed in order to study the properties and behavior of larger aggregates and, hence, to obtain their effective properties. The goal of this work is to give a contribution for understanding the behavior of natural materials through the development of models able to predict their response.

Accordingly to the considerations above , **Chapter 6** of this Thesis focuses the attention on the notion of state for Fractional Hereditary Materials. By using the definition recalled in [47] for linear viscoelastic materials, one can state that if two states are different then there must be some process (of arbitrary duration) starting from such state which produces different responses with the two states as initial ones. Materials showing hereditary features and undergoing relaxation test possess a residual stress that could be measurable. Henceforth, at first the concept of state is investigated for Fractional Hereditary Materials (FHMs) by means of advanced Fractional Calculus tools [182] and by employing strain functions that are locally of Special Bounded Variation (SBV) in time. The state of "non-virgin materials" is addressed by assuming the strain as independent variable and recasting the expression in terms of Caputo fractional derivatives. The description

of two rheological models, formed by proper arrangement of springs and dashpots, has enabled to reproduce the hereditary features of such materials. Deeper insights about the micromechanics related to the scheme of the rheological elements introduced in the treatment concludes the section.

Mechanical, biological, electrical properties and other material physical features depend on the observation scale. It is well known that material properties may show different features if they are measured either at nanoscale or at micro/macro scale. This phenomenon is particularly relevant whenever the characteristic length of the material microstructure and the size of the sample are comparable. Experimental observations show that in presence of defects in the inner structure at meso/nano scale the material properties exhibit decay laws with respect to the same properties measured at the macroscale, and this holds true for properties such as elasticity, strength and toughness. Under these considerations, the design of a specific material owning high mechanical, thermal and electrical properties at microstructure could be not led to satisfying features at higher observation scales.

Self-similarity of microstructure at several observation scales is the main feature of certain biological tissues. Henceforth it is possible to call them as *hierarchic structures*, since the macro-scale properties can be obtained by measures done at micro-scale and by using a proper (in most cases not-integer) factor scale. This feature is examined in **Chapter 7**. There, as example the bone tissue is considered, since it shows several levels of hierarchy (at least 7) in which hard platelets are embedded in soft (extra-cellular) matrix. Generally, hard elements are hydroxyapatite and soft matrix is collagen. This arrangement at different observation scales provides to bone amazing properties of strength, elasticity, stiffness, toughness and lightness at macro-scale [113, 122, 209]. In order to posses an effective tool for designing good material it is important to handle a proper hierarchic mechanical model, which is able to describe the power-law hereditariness of these materials by using power-law exponents of fractional order. In the case of bones, here taken as example, this exponent is in the range $0 \leq \beta \leq 1$. This behavior arises during creep/relaxation test, whenever a load (displacement) is applied following a ramp up the prescribed value and

held constant during the test. A predictive model of such behavior is needed to design bio-inspired material with the same features. Two rheological models, formed by springs and dashpots are presented in this Chapter and it is shown that they are strictly related with the fractional operators and able to reproduce the power-law behavior in the ranges $0 \leq \beta \leq 1/2$ and $1/2 \leq \beta \leq 1$. Moreover, the related numerical methods used to model the bone response are discussed. The microstructure of bone tissue can not be explained in the classical framework of Euclidean geometry; moreover, the observation of the cross-section at several observation scales shows an anomalous scaling of both geometrical and mechanical properties. The geometric bone features are studied by employing the Hausdorff dimension with the aid of the fractal geometry: it is shown that the value of the fractal dimension is strictly related with the exponent of the power-law obtained by fitting experimental data collected in literature with the fractional springpot model.

Acknowledgements

First and foremost, I bring my deepest gratitude to my advisor, Professor Luca Deseri, for his remarks, suggestions and encouragements throughout this research work. I appreciate all his contributions of time and ideas, and his always present understanding: all my struggles would have not been possible. His constant optimism and overwhelming passion for Mechanics have contribute to my scientific and personal growth.

I deeply acknowledge Professor Kaushik Dayal for having hosted me at Carnegie Mellon twice during my Ph.D. He was essential for overtaking all the numerical issues. It was an honor to meet him.

My best acknowledgments are for Professor Massimiliamo Zingales, who advised me for the *third* time. He was constantly present in my academic-life during the last 7 years. I am very thankful for having introduced me in the world of Academia.

A special acknowledgement is dedicated to Dr. Laura Lunghi, her contribution was fundamental for handling as best as possible the biological side of this Thesis.

I am deeply grateful to all the members of the "Solid and Structural Mechanics Group" at the University of Trento, Prof. Davide Bigoni, Prof. Nicola Pugno, Prof. Massimiliano Gei, Prof. Andrea Piccolroaz, Dr. Francesco Dal Corso, Dr. Roberta Springhetti, Dr. Fiorella Pantano. I would like to thank all my colleagues for being part of my daily life in the last few years:

<div align="right">
With my deepest consideration,

Pietro
</div>

Published papers

The main results presented in this Thesis have been summarized in the following papers:

⋄ L. Deseri, M. Di Paola, M. Zingales and P. Pollaci, "***Power-law hereditariness of hierarchical fractal bones***", International Journal for Numerical Methods in Biomedical Engineering 29 (12), 1338-1369, doi:10.1002/cnm.2572 (2013)

⋄ L. Deseri, M. Zingales and P. Pollaci, "***The State of Fractional Hereditary Materials (FHM)***", Discrete and Continuous Dynamical Systems Series B, 19 (7), doi:10.3934/dcdsb.2014.19.2065 (2014)

⋄ L. Deseri, P. Pollaci, M. Zingales, K. Dayal, "***Fractional Hereditariness of Lipid Membranes: Instabilities and Linearized Evolution***", Accepted for publicaton on Journal of the Mechanical Behavior of Biomedical Materials (2016)

The Writer hopes that the main results obtained in this Thesis, namely what is showed in Chapters 2-4, can spread into scholarly papers suitable for publication in professional journals.

Contents

Introduction

The human body is composed by a huge number of cells, probably more than 1 billion. The boundary of a cell (also known as *cell membrane*, the barrier separating inside and outside the cell) is identified by its external barrier, almost composed by lipid bilayers, structures typically 5 nanometers thick. For this reason, the lipid bilayers are recognized to be building blocks of almost all biological membranes and other living organisms. The scientific interest on this kind of stuctures is dated back in the early 1970s [24, 96, 189], but the recent spread of experimental techniques and imaging elaborations produced an increasing interest in the topic in the last decade.

The lipid structure is composed by a hydrophilic head and a hydrophobic tail. The chemical stability of the constituents forces the formation of structures in which two layers of lipids face each other in such a way the heads look outward and the tails look each other. Each lipid molecule can show two different shape conditions of the tail, either straightened and taller (also known as *ordered state*, L_o), or curly and shortened (also known as *disordered state*, L_d). Which of these state is assumed depends on several conditions, but mainly on temperature of the surrounding and chemical composition of the lipid mixture. The mechanical and chemical response of these amazing structures depends on a very long list of parameters, such as the shape of the membrane, temperature of the environment, osmotic pressure, chemical composition of lipid mixture [3, 4, 12, 13, 15, 38, 104, 105, 107, 155, 179, 202], among others.

Depending on the presence, or not, of embedded specialized proteins into the lipid membrane, several predicting models and theory have been developed [4, 19, 24, 52, 55, 112, 210]. Most of them are based on the characteri-

zation of the energy, with the aim to predict the so called ordered-disordered phenomena arising in transition regions for contrasting the external stimuli. Indeed, thickness reduction of the bilayer is observed by changing the mechanical and chemical conditions in the environment surrounding the cell. For this reason, several Authors adopted the change in thickness as order parameters for studying such kind of compound [88, 163, 179].

GPCRs receptors

Biological membrane are characterized by the presence of embedded specialized proteins able to triggering chemo-mechanical signal transmission and modulation [2, 167]. Thanks to them, it is possible to convert extracellular stimulus into one or more intracellular signals or responses. This process is also knwon as *transmembrane* (TM) *signal transduction*, and it involves mainly three kind of proteins: ion-channel receptors, enzyme-linked receptors and G protein-coupled receptors (GPCRs), also known as seven transmembrane receptors. The name derives from the fact they pass through the cell membrane seven times [199]: alternated intracellular and extracellular loops link the transmembrane domains.

The GPCRs trigger several signal transducion pathways, mainly (i) the cyclic adenosine monophosphate (cAMP) signal pathway and (ii) the phosphatidylinositol signal pathway [86], both of them deeply involved in the most essential process for the life of the cell. In particular, they regulate the response to hormones, neurotransmitters, metabolites, ions, fatty acids, pathogens, and physical stimuli. Thanks to this feature of responding to several nature of stimuli and because they are deeply involved in many diseases (such as cardiovascular, metabolic, neurodegenerative, psychiatric, cancer and infectious pathologies), this family of receptors is widely used as target in drugs delivery (about 40% of all modern medicinal drugs [72, 162]), especially in disorders of neural, immune, cardiovascular and endocrine systems, and cancer [6, 144, 200].

The family of GCPRs is mainly composed by two subfamilies, named α and β, which differ for both chemical properties (e.g. ligand specificity) and downstream effector mechanisms [28, 93]. Some years ago, it has been demonstrated the presence of β-2 adrenergic receptors (β2AR) in HTR-

2

8/SVneo cell line, a well characterized first-trimester human extravillous trophoblast-derived cell line [17]. This presence is strongly connected with several phenomena during pregnancy [92, 125], e.g. limited trophoblast invasion of maternal vessels has been correlated with fetal growth restriction [131]. In this Thesis, the attention will be focused on β2AR in HTR-8/SVneo cell.

The external surface of the membrane plays a fundamental role in the process of ligand binding, since it hosts receptors. Whenever a receptor binds an external ligand, a downstream involving the G-protein is activated. The membrane exhibits a conformational change, while some chemical processes are triggered. The G-protein, indeed, can inhibit or activate various effector enzymes and/or ion channels. The cAMP production follows either a rotation of TM6 and a tilting of TM6 toward TM5 [85], showing a strong connection with conformational changes.

Nowadays GPCR signaling is recognized to be more complex that was originally understood [117]. In the case here analyzed, the formation of β2AR bounds trigger a second messenger named cyclic adenosine monophosphate (cAMP) production. The produced second messenger can activate many downstream signaling pathway inside the cell [127]. Indeed these receptors can activate more than one G protein isoform, and they can also signal using a G protein-independent path-way involving beta-arrestin [117].

Experimental evidences [17] suggest that cAMP can reach the external environment of the cell. This flow is regulated by the presence of a specific proteins called transporters. Among other, the most important has been recognized to be Multidrug Resistant Proteins (MRPs) [18]. It is still not clear the role of extracellular physiological cAMP, but one suggestion is that they may contribute to regulate of the intracellular nucleotide levels [103].

The structure, activation, and signaling of a GPCR is heavily influenced by the bilayer environment. This influence seems likely to involve either indirect bilayer effects, specific membrane–GPCR interactions, or a combination of both [29, 64, 157, 161, 166]. Some subsets of GPCRs are preferentially segregated to discrete regions of the membrane defined as *lipid rafts*. The very reasons why this turns out to be the case are still unknown. Lipid rafts are planar domains of cell membranes enriched by lipids and proteins. In particular, they can be viewed as dynamic nanoscale

assemblies, where a high glycosphingolipid and cholesterol content in the outer leaflet of the lipid bilayer is present. This composition gives them a gel-like liquid-ordered organisation in comparison with the surrounding phospholipid-rich disordered membrane [29, 129].

The main goal of this Thesis is understanding why GPCRs prefer to live on rafts. In this regard, the surrounding environment of these *islands* must be taken into account, i.e. the lipid bilayer and its proximities. Many features are involved in the physical description of the membrane behavior, such as the possibility to sustain in-plane normal forces, bending moments, while the absence of a proper model including the viscosity does not allow for trasmitting shear stresses. The very large variety of configurations exhibit by biological membranes and the order-disorder phenomena are strongly regulated by chemical composition, temperature or osmotic pressure [15, 38, 107, 179]. In this framework, models involving bending elasticity have been deeply used for studying the equilibrium shapes of red blood cells [112] and GUVs (Giant Unilamellar Vesicle) [24, 96], whereas the effects of embedded proteins or rod-like inclusions in the lipid membrane have been fruitfully exploited [4, 19], together with the analysis of buds formation [130] with the coexistence of domains characterized by different bending rigidities [3, 13]. Particular regards have been devoted to the prediction and understanding of the order-disorder transition [5, 27, 59, 70, 88, 107, 109, 116, 163, 164] and to the effects of special molecules (such as cholesterol) on such transition [120, 165, 176]. There exist several models able to give reasonable prediction of this phenomena by employing proper energy functional of such a structure [4, 30, 52, 59, 138, 174, 175, 191, 202, 210].

In particular, there exist a model [52, 55, 210] in which, thanks to the constraint of "quasi-incompressibility" of the environment, chemical composition and stretching elasticity are enough to describe its order-disorder transition, i.e. for describing the membrane profile and boundary layers, and the connected line tension and rigidities in both phases.

Fractional Order Materials

Collaterally to the main topic of this Thesis, mainly focused on the study of biological membranes, some attention is dedicated to Fractional Order

4

Materials(FHM).

Starting from the first half of the twentieth century, the increasing importance of the science of material, with correlated execution of several mechanical tests, showed that many materials posses an intimate time-dependent behavior, sometimes very-well described by mean of proper power-law models [156, 185]. This behavior, also called *macroscopic hereditariness*, clearly arises in presence of tests regarding stress relaxation and creep compliance.

The use of the term *hereditariness* implies that the current response of the material in terms of stress/displacement for example, is deeply influenced by all its past history. Two mechanical tests are mainly used in order to observe these phenomena. The relaxation test is performed by held a constant value of strain, with subsequent monitoring of the value of the stress, which appears to be a decreasing function of time. On the contrary, in a creep test a fixed value of stress is imposed, while it is monitored the value of the strain, which appears to be an increasing function of time. The analysis of these tests clearly suggest that the past undergone stress or strain history influence the future response of the specimen.

The main charatestic of these time-dependent materials is the presence of a response with a very long tail [111]. Classically, the rheological models employed for catching this behavior consist in approximating the response by means of exponentials. It has been shown [54, 57] that the use of power laws would give a more accurate tools able to handle the mathematical description of both creep and relaxation, by inserting these behaviors in the framework of the Fractional Hereditariness. The recent interest in the development of effective bioinspired materials and biological structure focus again the attention on the subject of proper tools for the responsive prediction of materials (see e.g. [111, 133, 152, 184, 188]).

Indeed, the optimization and effective design of engineered devices passes through the chance to employ proper mathematical models of material behavior. In particular, in the case of biological and bioinspired materials, a key aspect is the chance to introduce a multiscale approach for governing the response and the behavior of the material from the nano- to the macrolevel. This aspect is particularly crucial in biomedical and biological applications, where beside the requirement of exact mechanical properties,

5

the physiological functionality of such devices determines their success. The features of biological tissues are essential for design and optimizing devices able to interact at different scales with the environment in which the device is embedded.

In the field of the biological materials, such kind of time-dependent behavior has been observed in mineralized tissues as ligaments and tendons. Indeed, they appear as a composite materials in which high ductile collagen proteic matrix accommodate higher stiff (but also higher brittle) hydroxyapatite crystals. Such compound possesses high strength [80], and at the same time its hereditary response spans several time scales, from pico to nano seconds [16, 97, 114], especially due to the hereditariness of the collagen proteic matrix.

Mineralized bone tissues represent another example of amazing structure that one can encounter in nature. Beside the classical common features required to biological tissues, such as stiffness, strength, toughness, permeability, porosity, thermal conductivity among others [8, 146, 187], they must be able to carry important loads, since they sustain all the weight of the body. It is interesting to note that they show a very marked time-dependent behavior under applied loads [57]. A closer observation of the intimate structure of this tissue reveals that it exhibits a hierarchic self-organization of collagen matrix and mineral crystals, i.e. it presents the same structural organization regardless of the observation scale [122, 150, 153]. It is recognized that bone possess 7 observation scales at which the same basic elements of the material give rise to different arrangements of the structure [122, 150, 153]. For this reason, it is proper to assert that the bone section exhibits a fractal-like self-organization, which determines the exceptional properties of strength, stiffness and toughness. From the point of view of viscoelasticity, this hierarchical arrangement of the assembly provoke multiple relaxation times, experimentally observed on both trabecular and cortical bones and with peculiar continuous time spectra (see e.g. [14, 90, 108]).

Moreover, this particular structural assembly determines an anomalous scaling of stiffness and viscosity coefficients. This scaling can be explained by introducing a mechanical hierarchy dubbed *fractance*, in close relation with fractal geometry.

6

Structure of the Thesis

Following the introductive discussion, this Thesis is composed by two parts. In the first part, the aim is understanding why GPCRs prefers to live on rafts. The problem is faced in the frame of mechanobiology, where tools typically used in Solid Mechanics and approaches typically employed in chemistry and physics meet for combining their capabilities and giving a synergy for exploring the topic. On the other hand, the second part of this Thesis is focused on the notion of Fractional Hereditary Materials, i.e. materials in which the current response is strongly influenced by the past history. In this regard, bones represent a very interesting case of study. The topics discussed in this Thesis will be presented as follows:

- **PART I: Mechanobiology of Cell Membranes**

  - Review on the behavior of lipid membranes
  - A novel constitutive model
  - Balanced configurations
  - Numerical simulations
  - Unstable behavior of lipid membranes

- **PART II: Hereditary behavior of Fractional Order Materials**

  - Notion of state for Fractional Hereditary Materials
  - Power-law hereditariness of hierarchical fractal bones

References

[2] R. Abrol and W. A. Goddard. "Extracellular and intracellular signaling". Ed. by J. A. Adams and K. K. Parker. Royal Society of Chemistry, 2011. Chap. G-protein-coupled receptors: conformational "gatekeepers" of transmembrane signal transduction and diversification (cit. on p. 2).

[3] A. Agrawal and D. Steigmann. "Coexistent Fluid-Phase Equilibria in Biomembranes with Bending Elasticity". *Journal of Elasticity* 93.1 (2008), pp. 63–80 (cit. on pp. 1, 4, 72).

[4] A. Agrawal and D. Steigmann. "Modeling protein-mediated morphology in biomembranes". *Biomechanics and Modeling in Mechanobiology* 8.5 (2009), pp. 371–379 (cit. on pp. 1, 4, 153).

[5] S. Akimov, P. Kuzmin, and Z. J. "An elastic theory for line tension at a boundary separating two lipid monolayer regions of different thickness". *Journal of Electroanalytical Chemistry* 564 (203), pp. 13–18 (cit. on pp. 4, 23).

[6] J. Allard et al. "Mechanical modulation of receptor-ligand interactions at cell-cell interfaces". *Biophysical Journal* 102 (2012), pp. 1–9 (cit. on p. 2).

[8] P. Ammann and R. Rizzoli. "Bone strength and its determinants". *Osteoporosis International* 14 (2003), S13–S18 (cit. on p. 6).

[12] T. Baumgart, W. Webb, and S. Hess. "Imaging coexisting domains in biomembrane models coupling curvature and line tension". *Nature* 423.821Ð824 (2003) (cit. on pp. 1, 21).

[13] T. Baumgart et al. "Membrane Elasticity in Giant Vesicles with Fluid Phase Coexistence". *Biophysical Journal* 89 (2005), pp. 1067–1080 (cit. on pp. 1, 4, 72).

[14] M. Baumgärtel and H. H. Winter. "Interrelation between continuous and discrete relaxation time spectra". *Journal of Non-Newtonian Fluid Mechanics* 44 (1992), pp. 15–36 (cit. on p. 6).

[15]   H. Bermúdez, D. Hammer, and D. Discher. "Effect of Bilayer Thickness on Membrane Bending Rigidity". *Langmuir* 20 (2004), pp. 540–543 (cit. on pp. 1, 4).

[16]   R. Bhowmik et al. "Probing molecular interactions in bone biomaterials: Through molecular dynamics and Fourier transform infrared spectroscopy". *Materials Science and Engineering C* 27 (2007), pp. 352–371 (cit. on p. 6).

[17]   C. Biondi et al. "Prostaglandin E2 inhibits proliferation and migration of HTR-8/SVneo cells, a human trophoblast-derived cell line". *Reproductive Biology and Endocrinology* 27.6-7 (2006), pp. 592–601 (cit. on p. 3).

[18]   C. Biondi et al. "cAMP efflux from human trophoblast cell lines: a role for multidrug resistance protein (MRP) 1 transporter". *Molecular Human Reproduction* 16.7 (2010), pp. 481–91 (cit. on pp. 3, 63–66, 72, 74, 87).

[19]   P. Biscari and F. Bisi. "Membrane-mediated interactions of rod-like inclusions". *The European Physical Journal E* 7 (2002), pp. 381–386 (cit. on pp. 1, 4).

[24]   P. Canham. "The minimum energy of bending as a possible explanation of the biconcave shape of the human red blood cell". *Journal of Theoretical Biology* 26 (1970), 61Ð80 (cit. on pp. 1, 4, 22).

[27]   L. Chen, M. Johnson, and R. Biltonen. "A Macroscopic Description of Lipid Bilayer Phase Transitions of Mixed-Chain Phosphatidylcholines: Chain-Length and Chain-Asymmetry Dependence". *Biophysical Journal* 80 (2001), pp. 254–270 (cit. on p. 4).

[28]   V. Cherezov et al. "High resolution crystal structure of an engineered human beta2-adrenergic G protein-coupled receptor". *Science* 318.5854 (2007), pp. 1258–65 (cit. on p. 2).

[29]   B. Chini and M. Parenti. "G-protein coupled receptors in lipid rafts and caveolae: how, when and why do they go there?" *Journal of Molecular Endocrinology* 32.2 (2004), pp. 325–38 (cit. on pp. 3, 4).

[30] R. Choksi, M. Morandotti, and M. Veneroni. "Global minimizers for axisymmetric multiphase membranes". *arXiv preprint* (2012), p. 1204.6673 (cit. on p. 4).

[38] S. Das, A. Tian, and T. Baumgart. "Mechanical Stability of Micropipet-Aspirated Giant Vesicles with Fluid Phase Coexistence". *The Journal of Physical Chemistry B* 112.11625Ð11630 (2008) (cit. on pp. 1, 4, 72).

[47] L. Deseri, M. Golden, and M. Fabrizio. "The Concept of a Minimal State in Viscoelasticity: New Free Energies and Applications to PDEs". *Archive for Rational Mechanics and Analysis* 181 (2006), pp. 43–96 (cit. on pp. vi, 165, 168, 194, 195, 198, 201).

[52] L. Deseri, M. Piccioni, and G. Zurlo. "Derivation of a new free energy for biological membranes". *Continuum Mechanics and Thermodynamics* 20.5 (2008), pp. 255–273. DOI: `10.1007/s00161-008-0081-1` (cit. on pp. iv, 1, 4, 23, 25, 26, 40, 153, 154, 168, 193).

[54] L. Deseri, M. Zingales, and P. Pollaci. "The State of Fractional Hereditary Materials (FHM)". *Discrete and Continuous Dynamical Systems B* 19.7 (2014), pp. 2065–2089 (cit. on pp. v, 5, 197, 202, 204, 208, 211, 217).

[55] L. Deseri and G. Zurlo. "The stretching elasticity of biomembranes determines their line tension and bending rigidity". *Biomechanics and Modeling in Mechanobiology* 12 (2013), pp. 1233–1242. DOI: `doi: 10.1007/s10237-013-0478-z` (cit. on pp. iii, iv, 1, 4, 23–26, 30, 40, 72, 153, 154, 168, 193).

[57] L. Deseri et al. "Power-law hereditariness of hierarchical fractal bones". *International Journal for Numerical Methods in Biomedical Engineering* 29.12 (2013), pp. 1338–1360 (cit. on pp. v, 5, 6, 227, 228, 230, 233, 234, 238, 239, 241, 243, 245).

[58] L. Deseri et al. "Fractional Hereditariness of Lipid Membranes: Instabilities and Linearized Evolution". *Journal of The Mechanical Behavior of Biomedical Materials* (2015) (cit. on pp. v, 163, 164, 166, 179–181, 183, 185).

10

[59]   M. Deserno. "Fluid lipid membranes: From differential geometry to curvature stresses". *Chemistry and Physics of Lipids* 185 (2014), pp. 11–45 (cit. on pp. iii, 4, 22, 23, 72).

[64]   M. T. Drake, S. K. Shenoy, and R. J. Lefkowitz. "Trafficking of G protein-coupled receptors". *Circulation Research* 99.6 (2006), pp. 570–582 (cit. on p. 3).

[66]   G. Espinosa et al. "Shear rheology of lipid monolayers and insights on membrane fluidity". *PNAS* 108.15 (2011), pp. 6008–6013. DOI: `www.pnas.org/cgi/doi/10.1073/pnas.1018572108` (cit. on pp. v, 154, 165, 167).

[70]   M. Falkovitz et al. "Theory of periodic structures in lipid bilayer membranes". *PNAS* 79 (1982), pp. 3918–3921 (cit. on pp. 4, 25, 27).

[72]   D. Filmore. "It's a GPCR world". *Modern Drug Discovery (American Chemical Society)* (Nov. 2004), pp. 24–28 (cit. on p. 2).

[80]   H. Gao. "Application of fracture mechanics concepts to hierarchical biomechanics of bone and bone-like materials". *International Journal of Fracture* 138 (2006), pp. 101–137 (cit. on p. 6).

[85]   P. Ghanouni et al. "Functionally different agonists induce distinct conformations in the G protein coupling domain of the beta 2 adrenergic receptor". *The Journal of Biological Chemistry* 276.27 (2001), pp. 24433–6. (Cit. on pp. 3, 37).

[86]   A. Gilman. "G proteins: transducers of receptor-generated signals". *Annual Review of Biochemistry* 56.1 (1987), pp. 615–49 (cit. on p. 2).

[88]   R. Goldstein and S. Leibler. "Structural phase transitions of interacting membranes". *Physical Review Letters A* 40.2 (1989), pp. 1025–1035 (cit. on pp. 2, 4, 25, 27, 28, 72).

[90]   R. Guedes, J. Simoes, and J. Morais. "Viscoelastic behaviour and failure of bovine cancellous bone under constant strain rate." *Journal of Biomechanics* 39.1 (2006), pp. 49–60 (cit. on p. 6).

[92]   J. Hanna et al. "Decidual NK cells regulate key developmental processes at the human fetal-maternal interface". *Nature Medicine* 12.1065-1074 (2006) (cit. on p. 3).

[93] M. A. Hanson et al. "A specific cholesterol binding site is established by the 2.8 A structure of the human beta2-adrenergic receptor". *Structure* 16.6 (2008), pp. 897–905 (cit. on p. 2).

[96] W. Helfrich. "Elastic properties of lipid bilayers: theory and possible experiments". *Zeitschrift für Naturforschung C* 28.11 (1973), pp. 693–703 (cit. on pp. 1, 4, 22, 26).

[97] C. Hellmich, J. F. Barthélémy, and L. Dormieux. "Mineral-collagen interactions in elasticity of bone ultrastructure - a continuum micromechanics approach". *European Journal of Mechanics A/Solids* 23 (2004), pp. 783–810 (cit. on p. 6).

[103] A. M. Hofer and K. Lefkimmiatis. "Extracellular calcium and cAMP: second messengers as "third messenger"?" *Physiology (Bethesda)* 22 (2007), pp. 320–7 (cit. on p. 3).

[104] A. Honerkamp-Smith et al. "Line Tensions, Correlation Lengths, and Critical Exponents in Lipid Membranes Near Critical Points". *Biophysical Journal* 95 (2008), pp. 236–246 (cit. on pp. 1, 23).

[105] M. Hu, J. Briguglio, and M. Deserno. "Determining the Gaussian Curvature Modulus of Lipid Membranes in Simulations". *Biophysical Journal* 102.1403Ð1410 (2012) (cit. on p. 1).

[107] A. Iglic, ed. *Advances in planar lipid bilayers and liposomes.* 1st Edition. Vol. 15. Academic Press, 2012 (cit. on pp. 1, 4).

[108] T. Iyo et al. "Anisotropic viscoelastic properties of cortical bone". *Journal of Biomechanics* 37 (2004), pp. 1433–1437 (cit. on p. 6).

[109] F. Jahnig. "Critical effects from lipid-protein interaction in membranes". *Biophysical Journal* 36 (1981), pp. 329–345 (cit. on pp. 4, 25).

[111] A. Jaishankar and G. H. McKinley. "Power-law rheology in the bulk and at the interface: quasi-properties and fractional constitutive equations". *Proceedings of the Royal Society A* 469 (2013). DOI: doi: 10.1098/rspa.2012.0284 (cit. on pp. 5, 193, 194).

[112] J. Jenkins. "Static equilibrium configurations of a model red blood cell". *Journal of Mathematical Biology* 4.2 (1977), pp. 149–169 (cit. on pp. 1, 4).

12

[113] B. Ji and H. Gao. "Mechanical properties of nanostructure of biological materials". *Journal of Mechanics and Physics of Solids* 52 (2004), pp. 1963–1990 (cit. on p. vii).

[114] D. R. Katti, S. M. Pradhan, and K. S. Katti. "Directional dependence of hydroxyapatite-collagen interactions on mechanics of collagen". *Journal of Biomechanics* 43 (2010), pp. 1723–1730 (cit. on p. 6).

[116] C.-I. Kim and D. J. Steigmann. "Distension-induced gradient capillarity in lipid membranes". *Continuum Mechanics and Thermodynamics* 27 (2015), pp. 609–621 (cit. on p. 4).

[117] B. Kobilka and X. Deupi. "Conformational complexity of G-protein-coupled receptors". *Trends in Pharmacological Sciences* 28.8 (2007), pp. 397–406 (cit. on pp. v, 3, 36, 48, 147, 252).

[120] S. Komura et al. "Lateral phase separation in mixtures of lipids and cholesterol". *Europhysics Letters* 67.2 (2004), p. 321 (cit. on pp. 4, 27, 72).

[122] R. Lakes. "Materials with structural hierarchy". *Nature* 361 (1993), pp. 511–515 (cit. on pp. vii, 6, 226, 244).

[125] P. Le Bouteiller and J. Tabiasco. "Killers become builders during pregnancy". *Nature Medicine* 12 (2006), pp. 991–992 (cit. on p. 3).

[127] R. Lefkowitz. "Seven transmembrane receptors: something old, something new". *Acta Physiol* 190 (2007), pp. 9–19 (cit. on pp. v, 3, 36, 48, 147, 252).

[129] D. Lingwood and K. Simons. "Lipid rafts as a membrane-organizing principle". *Science* 327.5961 (2010), pp. 46–50 (cit. on p. 4).

[130] R. Lipowsky. "Budding of membranes induced by intramembrane domains". *Journal de Physique II France* 2 (1992), pp. 1825–1840 (cit. on pp. 4, 23, 25).

[131] L. Lunghi et al. "Control of human trophoblast function". *Reproductive biology and endocrinology : RB&E* 5 (2007), p. 6. ISSN: 1477-7827. DOI: 10.1186/1477-7827-5-6 (cit. on pp. 3, 74, 75).

[133] R. L. Magin. "Fractional calculus models of complex dynamics in biological tissues". *Computers & Mathematics with Applications* 59.5 (2010), pp. 1586–1593 (cit. on pp. 5, 167).

[138] M. Maleki, B. Seguin, and E. Fried. "Kinematics, material symmetry, and energy densities for lipid bilayers with spontaneous curvature". *Biomechanics and Modeling in Mechanobiology* 12.5 (2013), pp. 997–1017. DOI: `doi:10.1007/s10237-012-0459-7` (cit. on p. 4).

[144] S. Mary et al. "How ligands and signaling proteins affect G-protein-coupled receptors' conformational landscape". *Biochem Soc Trans* 41 (2013), pp. 144–147 (cit. on p. 2).

[146] R. Metzler and J. Klafter. "The random walk's guide to anomalous diffusion: A fractional dynamics approach". *Physics Reports* 399 (2000), pp. 1–77 (cit. on p. 6).

[148] L. Mishnaevsky Jr. "Micromechanics of hierarchical materials: A brief overview". *Review on Advavend Material Science* 30 (2012), pp. 60–72 (cit. on p. vi).

[150] R. Muller. "Hierarchical microimaging of bone structure and function". *Nature Reviews* 5 (2009), pp. 373–381 (cit. on p. 6).

[152] S. Nawaz et al. "Cell viscoelasticity measured with AFM and vertical optical trapping at sub-micrometer deformations". *PLoS ONE* e45297 (2012). DOI: `doi:10.1371/journal.pone.0045297` (cit. on p. 5).

[153] S. Nikolov and D. Raabe. "Hierarchical Modeling of the Elastic Properties of Bone at Submicron Scales: The Role of Extrafibrillar Mineralization." *Biophysical Journal* 94 (2008), pp. 4220–4232 (cit. on p. 6).

[155] D. Norouzi, M. Müller, and D. M. "How to determine local elastic properties of lipid bilayer membranes from atomic-force-microscope measurements: A theoretical analysis". *Physical Review Letters E* 74.061914 (2006) (cit. on p. 1).

[156] P. Nutting. "A new general law of deformation". *Journal of The Franklin Institute* 191 (1921), pp. 679–685 (cit. on pp. 5, 193, 196).

[157] J. Oates and A. Watts. "Uncovering the intimate relationship between lipids, cholesterol and GPCR activation". *Current Opinion in Structural Biology* 21.6 (2011), pp. 802–7 (cit. on p. 3).

[161] R. S. Ostrom and P. A. Insel. "The evolving role of lipid rafts and caveolae in G protein-coupled receptor signaling: implications for molecular pharmacology". *British of Journal Pharmacology* 143 (2004), pp. 235–45 (cit. on p. 3).

[162] J. Overington, B. Al-Lazikani, and A. Hopkins. "How many drug targets are there?" *Nature Reviews. Drug Discovery* 5.12 (2006), pp. 993–6 (cit. on p. 2).

[163] J. Owicki and H. McConnell. "Theory of protein-lipid and protein-protein interactions in bilayer membranes". *PNAS* 76 (1979), pp. 4750–4754 (cit. on pp. 2, 4, 25, 27).

[164] J. Owicki, M. Springgate, and H. McConnell. "Theoretical study of protein-lipid interactions in bilayer membranes". *PNAS* 75 (1978), pp. 1616–1619 (cit. on pp. 4, 25, 27, 72).

[165] J. Pan, S. Tristram-Nagle, and J. Nagle. "Effect of cholesterol on structural and mechanical properties of membranes depends on lipid chain saturation". *Physical Review E* 80.021931 (2009) (cit. on p. 4).

[166] H. H. Patel, F. Murray, and P. A. Insel. "G-protein-coupled receptor-signaling components in membrane raft and caveolae microdomains". *Handbook of Experimental Pharmacology* 186 (2008), pp. 167–84 (cit. on p. 3).

[167] R. Phillips et al. "Emerging roles for lipids in shaping membrane-protein function". *Nature* 459 (2009), pp. 379–85 (cit. on p. 2).

[174] P. Rangamani and D. J. Steigmann. "Variable tilt on lipid membranes". *Proceedings of the Royal Society A* 470 (2015), p. 20140463 (cit. on p. 4).

[175] P. Rangamani et al. "Small scale membrane mechanics". *Biomechanics and Modeling in Mechanobiology* 13 (2014), pp. 697–711 (cit. on p. 4).

[176] W. Rawicz et al. "Effect of Chain Length and Unsaturation on Elasticity of Lipid Bilayers". *Biophysical Journal* 79 (2000), pp. 328–339 (cit. on p. 4).

[179]   E. Sackmann. "Handbook of biological physics". Ed. by R. Lipowsky and E. Sackmann. Elsevier, 1995. Chap. 5. Physical Basis of Self-Organization and Function of Membranes: Physics of Vesicles, pp. 213–303 (cit. on pp. 1, 2, 4, 25, 27).

[182]   S. G. Samko, A. A. Kilbas, and O. I. Marichev. *Fractional Integrals and Derivatives. Theory and Applications*. Londn - New York: Gordon & Breach Science Publishers, 1987 (cit. on pp. vi, 167).

[184]   N. Sarkar and A. Lahiri. "Effect of fractional parameter on plane waves in a rotating elastic medium under fractional order generalized thermoelasticity". *International Journal of Applied Mechanics* 4 (2012). DOI: `doi:10.1142/S1758825112500305` (cit. on p. 5).

[185]   G. Scott Blair. "The role of psychophysics in rheology". *Journal of Colloid Science* 2 (1947), pp. 21–32 (cit. on pp. 5, 193, 230).

[187]   E. Seeman and P. D. Delmas. "Bone Quality — The Material and Structural Basis of Bone Strength and Fragility". *The New England Journal of Medicine* 354 (2006), pp. 2250–2261 (cit. on p. 6).

[188]   V. Sharma et al. "Rheology of globular proteins: apparent yield stress, high shear rate viscosity and interfacial viscoelasticity of bovine serum albumin solutions". *Soft Matter* 7 (2011), pp. 5150–5160. DOI: `doi:10.1039/c0sm01312a` (cit. on p. 5).

[189]   E. J. Shimshack and H. M. McConnell. "Lateral phase separation in phospholipid membranes". *Biochemistry* 12.12 (1973), pp. 2531–2360 (cit. on pp. 1, 22).

[191]   D. Steigmann. "A model for lipid membranes with tilt and distension based on three-dimensional liquid crystal theory". *International Journal of Non-Linear Mechanics* 56 (2013), pp. 61–70 (cit. on p. 4).

[195]   M. Terzi, K. Dayal, and M. Deserno. "Revisiting the Link between Lipid Membrane Elasticity and Microscopic Continuum Models". *Biophysical Journal* 108.2 (2015), 87a–88a (cit. on p. iii).

[199]   B. Trzaskowski et al. "Action of molecular switches in GPCRs–theoretical and experimental studies". *Science* 318.5854 (2012), pp. 1258–65. DOI: `doi:10.1126/science.1150577` (cit. on p. 2).

16

[200] H. Unal and S. Karnik. "Domain coupling in GPCRs: the engine for induced conformational changes". *Trends in Pharmacological Sciences* 33.2 (2012), pp. 79–88 (cit. on p. 2).

[202] N. Walani, J. Torres, and A. Agrawal. "Endocytic proteins drive vesicle growth via instability in high membrane tension environment". *PNAS* (2015), E1423–E1432. DOI: `www.pnas.org/cgi/doi/10.1073/pnas.1418491112` (cit. on pp. 1, 4).

[209] H. Yao and H. Gao. "Multi-scale cohesive laws in hierarchical materials". *Internatiol Journal of Solids and Structures* 44 (2007), pp. 8177–8193 (cit. on p. vii).

[210] G. Zurlo. "Material and geometric phase transitions in biological membranes". PhD thesis. Doctorate of Philosophy in Structural Engineering, University of Pisa, 2006 (cit. on pp. iii, 1, 4, 23, 25, 27, 40, 72).

Part I

Mechanobiology of Cell Membranes

Chapter 1

A review on the behavior of Lipid Membranes

Lipid membranes are soft structures arising by proper arrangement of lipids. There exist several type of lipids, but only three of them are mainly found in biological membranes, i.e. phospholipids, glycolipids, and cholesterol. The main feature of lipids is that they are composed by a hydrophilic head soluble in water (also known as the *polar* part) and a hydrophobic tail (also known as the *nonpolar* part. Mostly because of this chemical composition, lipid membrane are self-organized bilayer compounds, i.e. structures in which the polar part (i.e the heads) is pointing outward and the nonpolar part (i.e. the tail) is pointing inward. The biological purpose of this formation is keeping separated the watery environment *outside* the membrane by the the watery environment *inside*.

These self-assembled structures often reveal amazing shapes, sometime breathless intricate patterns at micro and nano scales [12], such as fluid films spanning macroscopic lateral scales but thick just few nanometers (i.e. structures in which lateral extension exceeds lipid size by several orders of magnitude).

A closer analysis of lipid membranes reveals that slight changes in temperature and/or pressure may provoke shape rearrangements with the occurrence of thin and thick zones, namely phase transitions between zones of *straight* and *curly* configurations of lipids (see Figure 1.1). This phenomenon,

nowadays recognized as *raft formation*, was noticed for the first time in 1997 by Simons and Ikonen [190]: it is shown that there exist a range of given temperature, chemical composition and pressure (among other physical parameters) in which different phases coexist, organizing themselves in proper domains. Although this observation is quite recent, the coexistence of several phases in binary or ternary mixtures of different kind of lipids dates back to the early 1970s [189]. The raft formation is often studied in the framework of the so called *order-disorder theory*, in which "liquid ordered" (L_o) and "liquid disordered" (L_d) phases coexist. It is possible to relate the liquid order phase to the straight configuration of lipids, and the curly configuration to the disordered phase, respectively. Recently, the coexistence of two or more phases have been studied extensively [11, 71, 201].
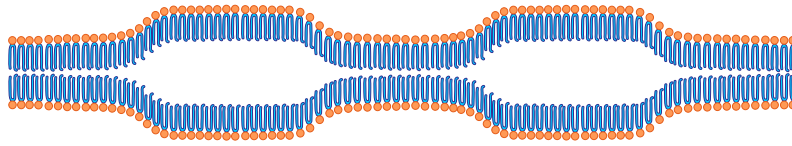
Figure 1.1: Schematic of transition regions between curly and straight lipids, also known as *raft regions*.

Some models for predicting lipid membrane response have been developed under the assumption of (i) "in-plane fluidity" and (ii) elasticity of the membrane, i.e in-plane shear stress cannot arise [24, 96], but it is assumed that changes of the membrane profile are allowed as strategy for responding to the external solicitations. It has been widely shown [59, 106] that the behavior of the membrane is governed by a very small number of material parameters. Among these, the most effective are the *mean* and the *Gaussian curvature* modulus, in the sequel denoted by κ and $\bar{\kappa}$, respectively. It is worth noting that lipid bilayer assemblies are very hard to stretch but easy to bend. The equilibrium of a lipid bilayer can be studied through a functional, introduced for the first time by Helfrich [96], having the following form:

$$\mathcal{E}[\Omega] = \int_{\Omega} \left[\frac{1}{2}\kappa \left(K - K_0 \right)^2 + \bar{\kappa} K_G \right] \mathrm{d}A \qquad (1.1)$$

where Ω is the geometry describing the surface of the membrane and, after defining c_1 and c_2 the two local principal curvatures, $K = c_1 + c_2$ denotes the total curvature and $K_G = c_1 c_2$ is the Gaussian curvature, while K_0 denotes the bilayer curvature, even if this term vanishes often because some material and geometrical symmetries can be taken into account [59, 106].

It has been also shown [52, 55] that, beside bending rigidities, also the line tension plays a very important role in the equilibrium of such a structures, especially in the case of observed non-spherical configurations [5, 104, 130, 197].

1.1 The membrane elasticity theory for the lipid bilayers

In this **Section** the main results obtained in [52, 55, 210] are briefly recalled, and a schematic description of the approach followed in these papers is provided. For a fixed temperature of $30°C$, the Authors assumed that the membrane *natural* configuration $\mathscr{B}_0$ coincides with the flat prismatic shape of constant thickness h_0 (with ordered phase L_o) embedded in a orthonormal reference frame $(\boldsymbol{e}_1, \boldsymbol{e}_2, \boldsymbol{e}_3)$. The membrane geometry is split into two entities, the two-dimensional mid-plane and the thickness, hence, points belonging to $\mathscr{B}_0$ are described by:

$$\boldsymbol{x} = \mathsf{x} + z\boldsymbol{e}_3, \tag{1.2}$$

where $\mathsf{x} = x\,\boldsymbol{e}_1 + y\,\boldsymbol{e}_2$ denotes locations of a flat mid-surface Ω, and z spans the whole thickness. In this Thesis, it is considered a membrane that in the reference configuration $\mathscr{B}_0$ has a thin flat prismatic shape of homogeneous thickness h_0 in direction $\boldsymbol{e}_3$, width B in direction $\boldsymbol{e}_2$ and length L in direction $\boldsymbol{e}_1$. The reference membrane mid-surface θ corresponds to $z = 0$, and its edges are defined by $x = \pm L/2$ and $y = \pm B/2$.

The formulation of the model is based on the following assumptions:

(i) the effects leading to a spontaneous or natural curvature of the bilayer are ignored, i.e. it is assumed that the natural configuration is flat;

(ii) the membrane kinematics is restricted to the class of normal preserving

23

deformations, i.e. the normal vector $\boldsymbol{n}$ remains always normal to the mid-surface (lipid molecules remain orthogonal to the bilayer mid-surface);

(iii) no proteins are taken into account, i.e. only lipid membranes are studied.
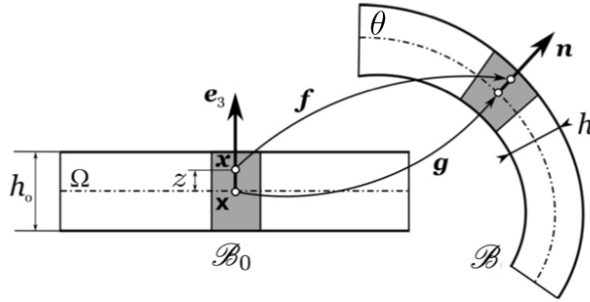
Figure 1.2: Schematic representation of the deformation (1.6) of a prismatic, plate-like reference configuration $\mathscr{B}_0$ into the current configuration $\mathscr{B}$. The gray box depicts the space occupied by two lipid molecules, their volume being conserved during the deformation. Courtesy of [55].

Under these assumptions, a simplified version of the elastic energy related to the change of the membrane geometry is obtained. The deformation mapping is denoted by $\boldsymbol{f}$, while its gradient is $\mathbf{F} = \nabla \boldsymbol{f}$. The stored Helmholtz free-energy can be then expressed as

$$\mathcal{E}(\boldsymbol{f}) = \int_{\mathscr{B}_0} \Psi(\boldsymbol{f}) \, dV = \int_{\Omega} \int_{-h_0/2}^{h_0/2} \Psi(\boldsymbol{f}) \, \mathrm{d}z \, \mathrm{d}\Omega, \qquad (1.3)$$

where Ψ denotes the Hemholtz energy density per unit of referential volume. It easy to recognize that the surface density energy has the form:

$$\psi(\boldsymbol{f}) = \int_{-h_0/2}^{h_0/2} \Psi(\boldsymbol{f}) \, \mathrm{d}z. \qquad (1.4)$$

Experimental evidences suggest that lipid membrane own the so-called *in-plane fluidity*, i.e. the absence of viscosity does not allow for sustaining shear

in planes perpendicular to $\boldsymbol{e}_3$. Based on this constitutive assumption, it is possibile [52, 55] to find a relationship for the energy density Ψ depending on the three invariants of the deformation gradient, namely

$$\mathscr{I}(\boldsymbol{x}) = \{\tilde{J}(\boldsymbol{x}),\, \det \mathbf{F}(\boldsymbol{x}),\, \bar{\phi}(\boldsymbol{x})\}, \tag{1.5}$$

i.e. the areal stretch of planes perpendicular to the direction $\boldsymbol{e}_3$, the volume change and the stretch in direction $\boldsymbol{e}_3$, respectively. The latter term can be also interpreted as the thickness stretch $\bar{\phi}(\boldsymbol{x}) = h(\boldsymbol{x})/h_0$.

Some experiments [130, 179] strongly suggest that the volume of lipid membranes does not change significantly, although geometrical changes occur. Some Authors [88, 164] showed also that the volume of biological membranes can be assumed constant at several values of temperature . In order to find an explicit relationship between Ψ and $\mathscr{I}(\boldsymbol{x})$, the following Ansatz (see Figure 1.2) is assumed:

$$\boldsymbol{f}(\boldsymbol{x}) = \boldsymbol{g}(\mathbf{x}) + z\phi(\mathbf{x})\,\boldsymbol{n}(\mathbf{x}), \tag{1.6}$$

where $\boldsymbol{g}(\mathbf{x}) = \boldsymbol{g}(x, y, 0)$ represents the current mid-surface of the membrane (i.e $\theta = \boldsymbol{g}(\Omega)$), $\boldsymbol{n}$ denotes the outward normal to θ, and $\phi(\mathbf{x}) = h(\mathbf{x})/h_0$ is the thickness stretch, defined as the ratio of the current thickness h_0 over the reference value h_0. The assumption of the Ansatz (1.6) must be coupled with the quasi-incompressibility constraint mentioned above in the following form:

$$\det \mathbf{F}(\mathbf{x}, 0) = \tilde{J}(\mathbf{x}, 0)\phi(\mathbf{x}) = 1. \tag{1.7}$$

It is worth noting that the quasi-incompressibility is a first-oder approximation only of the incompressibility requirement. Indeed, relationship (1.7) holds exactly only in the case of planar deformations, where $\det \mathbf{F}(\boldsymbol{x}) = \det \mathbf{F}(\mathbf{x}, 0) + O(z)$. This will be the special case considered in this Thesis. Relationship (1.7) has been widely adopted as constraint in literature [70, 88, 109, 110, 163, 164, 179], therefore either the areal stretch J or the tick stretch ϕ have been used as coarse-grained order parameter. An explicit expansion of equation (1.4) in powers of the reference thickness h_0 (see [52, 55, 210]) can be done by taking into account the choice of the constraint (1.7). Therefore, a restriction ψ of the energy density Ψ to Ω is considered

by taking into account the requirement (1.7):

$$\psi(J) = \Psi(\tilde{J}, \det \mathbf{F}, \bar{\phi})\Big|_{z=0} = \Psi(J, 1, J^{-1}), \qquad (1.8)$$

where $J(\mathbf{x}) = \tilde{J}(\mathbf{x}, 0)$. At this point, under Ansatz (1.6) and the assumptions of in-plane fluidity and bulk incompressibility, the expansion of equation (1.4) up to third order therm h_0^3 gives

$$\psi = \varphi(J) + \kappa(J)H^2 + \kappa_G(J)K + \alpha(J) \| \left(\text{grad}_\theta \widehat{J}\right)_m \|^2, \qquad (1.9)$$

where H and K are the mean and Gaussian curvatures of the mid-surface θ, respectively, $\kappa(J)$ and $\kappa_G(J)$ are the corresponding bending rigidities, $\varphi(J)$ represent the so-called *local energy* and

$$\alpha(J) = \frac{h_0^2}{24} \frac{\varphi'(J)}{J^5} \qquad (1.10)$$

is a function related to the nonlocal part of the energy density. In equation (1.9), $\hat{J}$ is the spatial description of J, defined by the composition $\hat{J} \circ g = J$, grad_θ is the gradient with respect to points of the current mid-surface θ, and $(\cdot)_m$ gives his material description. On the other hand, it is possible to show [52, 55] that the energy is also described as:

$$\psi = \varphi(J) + h_0^2 \left[k_1 H^2 + k_2 \left(K + \frac{1}{2} \frac{\|\nabla J\|}{J^2} \right) \right] \qquad (1.11)$$

where $\varphi(J)$ is the local term of the energy, the part depending on the gradient of the areal stretch $\|\nabla J\|$ is the non-local part and $h_0^2 \left(k_1 H^2 + k_2 K \right)$ is the bending term. There, the mean and the saddle-splay bending stiffnesses, k_1 and k_2, take the forms:

$$k_1 := \frac{\varphi_{,JJ}(J)}{6}, \qquad (1.12a)$$

$$k_2 := \frac{\varphi_{,J}(J)}{12J}. \qquad (1.12b)$$

The term (1.11) recovers exactly the Helfrich energy [96] if J is constant.

26

The main ingredient of the two-dimensional membrane model derived in (1.9) is the surface Helmholtz energy $\varphi(J)$, which regulates the in-plane stretching behavior of the membrane and describes the phase transition phenomena taking place in lipid bilayers.

The fundamental point is then computing the local energy $\varphi(J)$. In the lack of specific information, $\varphi(J)$ can be constructed, as a polynomials of the power of the order parameters, i.e the change in thickness (see, *e.g.*, [70, 88, 120, 163, 164]), in analogy with the procedure employed in the framework of Landau phase transition.. This approach results to be very useful since it allows for relating the coefficients of the polynomial expansions to quantities (such as the transition temperature, the latent heat and the order parameter jump) that one can measure by setting up proper experiments (see [88] and the treatise [179] for a detailed discussion).

As mentioned above, by assuming that the membrane natural configuration $\mathscr{B}_0$ coincides with the flat, ordered L_o phase (i.e. $J = J_o = 1$) at the considered temperature, the Landau expansion of stretching energy [210] takes the form:

$$\varphi(J) = a_0 + a_1 J + a_2 J^2 + a_3 J^3 + a_4 J^4, \tag{1.13}$$

where the parameters a_i $(i = 0 \div 4)$ depend in general on temperature and chemical composition. Because of the lack of avalaible experimental data, these parameters have been calibrated [210] by considering experimental estimates provided by [88, 119, 120], and for a temperature $T \sim 30°C$ they have been determined as:

$$a_0 = 2.03, \quad a_1 = -7.1, \quad a_2 = 9.23, \quad a_3 = -5.3, \quad a_4 = 1.13, \tag{1.14}$$

dimensionally expressed in $[J][m]^{-2}$. The related local stress, defined as the first derivative of the local energy with respect to the order parameter J, i.e.

$$\tau(J) = \frac{\mathrm{d}\varphi(J)}{\mathrm{d}J}, \tag{1.15}$$

owns the typical S-shaped form, as shown in Figure 1.3, revealing more on the properties of such an energy. Accordingly to the analysis done by Coleman and Newman [31], in the same Figure the remarkable points of
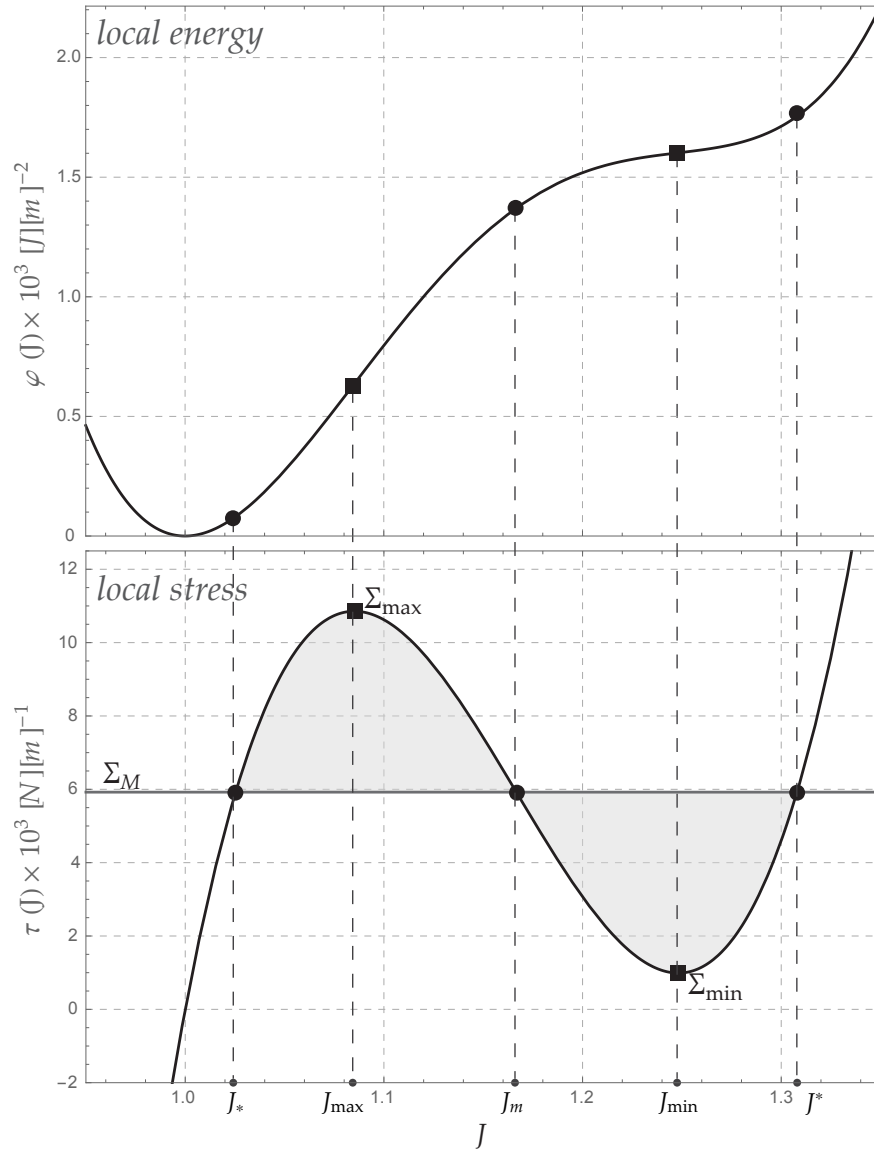
Figure 1.3: The stretching energy $\varphi(J)$ (top) adapted from [88] for a temperature $T \sim 30°$, with related local stress $\varphi'(J) = \tau(J)$ (bottom). The areal stretch $J_o = 1$ corresponds to the unstressed, reference configuration $\mathscr{B}_0$.

interest of the local stress are highlighted. The locations where the maximum $\Sigma_{\max}$ and the minimum $\Sigma_{\min}$ of the local stress occur are denoted by $J_{\max}$ and $J_{\min}$, respectively, and highlighted with squares, while the value of the Maxwell stress (determined by the equal area rule) is drawn as a straight horizontal dark-grey line. Whenever a generic stress Σ is considered, it is also possible to identify three intersections between such a stress and the local stress curve. In the case of the Maxwell stress, these three intersections are denoted with black circles, and the corresponding areal stretch values are called J_*, J_m and J^* from left to right. As an example, Table 1.1 collects the numerical values of these quantities for the local stretching energy obtained by using the coefficients in (1.14).

Table 1.1: Characteristic values of the membrane stretching energy at $T \sim 30°$. Stress expressed as $[\Sigma] = [J/m^2] \times 10^{-3}$

Σ_M	$\Sigma_{\max}$	$\Sigma_{\min}$	J_*	J_m	J^*	$J_{\max}$	$J_{\min}$
5.922	10.855	0.989	1.025	1.167	1.308	1.085	1.248

1.2 Planar case

The study of the equilibrium for a planar lipid membrane described by the energy (1.13) (for instance, by supplying this entity with the constants given by parameters (1.14)) permits to elucidate the emergence of thickness inhomogeneities in the membrane. Moreover, this simple energetics allows one to calculate the corresponding rigidities and the shape of the boundary layer between the ordered and disordered phases. Whenever no curvature changes are experienced by the lipid bilayer, the elastic energy density in (1.9) takes the form:

$$\psi(J) = \varphi(J) + \alpha(J)||\nabla J||^2, \tag{1.16}$$

or equivalently

$$\psi(J) = \varphi(J) - \frac{1}{2}\gamma(J)||\nabla J||^2, \tag{1.17}$$

29

where the function

$$\gamma(J) = -\frac{h_0^2}{12} \frac{\tau'(J)}{J^5} = -2\,\alpha(J) \tag{1.18}$$

can be interpreted as a *transition function*, since it drives the boundary layer wherever transitions between two phases occur. Accordingly with the geometry introduced above, the three-dimensional membrane deformation is further restricted with respect to equation (1.6), according to

$$\boldsymbol{f}(\boldsymbol{x}) = g(x)\boldsymbol{e}_1 + y\boldsymbol{e}_2 + z\phi(x)\boldsymbol{e}_3 \tag{1.19}$$

so that the width B is kept constant and its gradient takes the following form

$$\nabla \boldsymbol{f} = \begin{bmatrix} g_x & 0 & 0 \\ 0 & 1 & 0 \\ z\phi_x & 0 & \phi \end{bmatrix}, \tag{1.20}$$

where the subscript x denotes differentiation with respect to x. The displacement component along $\boldsymbol{e}_1$ is $u(x) = g(x) - x$. After setting

$$\lambda(x) = g_x(x) \tag{1.21}$$

for the stretch in direction $\boldsymbol{e}_1$, the relationships $\det \mathbf{F} = \lambda\phi = 1$ and $J = \lambda$ are found. Hence $\phi = \lambda^{-1}$, so that the membrane deformation is completely determined by $J = \lambda$.

The set of equilibria of a elastic body undergoing the same kinematics (1.19) and governed by the stretching energy density (1.17) are deeply studied in [55] in presence of a stress acting at the edges. For the sake of simplicity, let now consider a one-dimensional case., i.e.

$$\psi(J) = \varphi(J) - \frac{1}{2}\gamma(J)J_x^2. \tag{1.22}$$

The use of the principle of minimum of energy in that specific case [55] allows for obtaining the Euler-Lagrange equation for such kind of structure in the form:

$$\gamma(J)\,J + \frac{1}{2}\gamma(J)\,J_x^2 + \tau(J) = \Sigma, \tag{1.23}$$

where Σ is a force per reference length at the edges $x = \pm L/2$. In such conditions, it is easy to show that homogeneous configurations are in the set of equilibria. Indeed, whenever an homogeneous configuration is considered, the higher-order terms drop to zero and the equilibrium equation reads as:

$$\tau(J) = \Sigma. \tag{1.24}$$

It is also interesting to note that for each choice of stress Σ there exist three admissible homogeneous balanced configurations, because of the characteristic S-shape local stress, shown in Figure 1.3.

References

[5]   S. Akimov, P. Kuzmin, and Z. J. "An elastic theory for line tension at a boundary separating two lipid monolayer regions of different thickness". *Journal of Electroanalytical Chemistry* 564 (203), pp. 13–18 (cit. on pp. 4, 23).

[11] T. Bartels et al. "Raftlike mixtures of sphingomyelin and cholesterol investigated by solid-state 2H NMR spectroscopy." *Journal of the American Chemical Society* 130 (2008), pp. 14521–32 (cit. on p. 22).

[12] T. Baumgart, W. Webb, and S. Hess. "Imaging coexisting domains in biomembrane models coupling curvature and line tension". *Nature* 423.821Ð824 (2003) (cit. on pp. 1, 21).

[24] P. Canham. "The minimum energy of bending as a possible explanation of the biconcave shape of the human red blood cell". *Journal of Theoretical Biology* 26 (1970), 61Ð80 (cit. on pp. 1, 4, 22).

[31] B. Coleman and D. Newman. "On the rheology of cold drawing. I.Elastic Materials". *Journal of Polymer Science: Part B: Polymer Physics* 26 (1988), pp. 1801–1822 (cit. on pp. 27, 96).

[52] L. Deseri, M. Piccioni, and G. Zurlo. "Derivation of a new free energy for biological membranes". *Continuum Mechanics and Thermodynamics* 20.5 (2008), pp. 255–273. DOI: 10.1007/s00161-008-0081-1 (cit. on pp. iv, 1, 4, 23, 25, 26, 40, 153, 154, 168, 193).

[55]   L. Deseri and G. Zurlo. "The stretching elasticity of biomembranes determines their line tension and bending rigidity". *Biomechanics and Modeling in Mechanobiology* 12 (2013), pp. 1233–1242. DOI: `doi:10.1007/s10237-013-0478-z` (cit. on pp. iii, iv, 1, 4, 23–26, 30, 40, 72, 153, 154, 168, 193).

[59]   M. Deserno. "Fluid lipid membranes: From differential geometry to curvature stresses". *Chemistry and Physics of Lipids* 185 (2014), pp. 11–45 (cit. on pp. iii, 4, 22, 23, 72).

[70]   M. Falkovitz et al. "Theory of periodic structures in lipid bilayer membranes". *PNAS* 79 (1982), pp. 3918–3921 (cit. on pp. 4, 25, 27).

[71]   G. W. Feigenson. "Phase boundaries and biological membranes". *Annual Review of Biophysics and Biomolecular Structure* 36 (2007), pp. 63–77 (cit. on p. 22).

[88]   R. Goldstein and S. Leibler. "Structural phase transitions of interacting membranes". *Physical Review Letters A* 40.2 (1989), pp. 1025–1035 (cit. on pp. 2, 4, 25, 27, 28, 72).

[96]   W. Helfrich. "Elastic properties of lipid bilayers: theory and possible experiments". *Zeitschrift für Naturforschung C* 28.11 (1973), pp. 693–703 (cit. on pp. 1, 4, 22, 26).

[104]   A. Honerkamp-Smith et al. "Line Tensions, Correlation Lengths, and Critical Exponents in Lipid Membranes Near Critical Points". *Biophysical Journal* 95 (2008), pp. 236–246 (cit. on pp. 1, 23).

[106]   M. Hu, P. Diggins IV, and M. Deserno. "Determining the bending modulus of a lipid membrane by simulating buckling". *The Journal of Chemical Physics* 214110 (138). DOI: `doi:10.1063/1.4808077` (cit. on pp. 22, 23).

[109]   F. Jahnig. "Critical effects from lipid-protein interaction in membranes". *Biophysical Journal* 36 (1981), pp. 329–345 (cit. on pp. 4, 25).

[110]   F. Jahnig. "What is the Surface Tension of a Lipid Bilayer Membrane?" *Biophysical Journal* 71 (1996), pp. 1348–1349 (cit. on p. 25).

[119]   S. Komura and N. Shimokawa. "Tension-Induced Morphological Transition in Mixed Lipid Bilayers". *Langmuir* 22 (2006), pp. 6771–6774 (cit. on p. 27).

[120]   S. Komura et al. "Lateral phase separation in mixtures of lipids and cholesterol". *Europhysics Letters* 67.2 (2004), p. 321 (cit. on pp. 4, 27, 72).

[130]   R. Lipowsky. "Budding of membranes induced by intramembrane domains". *Journal de Physique II France* 2 (1992), pp. 1825–1840 (cit. on pp. 4, 23, 25).

[163]   J. Owicki and H. McConnell. "Theory of protein-lipid and protein-protein interactions in bilayer membranes". *PNAS* 76 (1979), pp. 4750–4754 (cit. on pp. 2, 4, 25, 27).

[164]   J. Owicki, M. Springgate, and H. McConnell. "Theoretical study of protein-lipid interactions in bilayer membranes". *PNAS* 75 (1978), pp. 1616–1619 (cit. on pp. 4, 25, 27, 72).

[179]   E. Sackmann. "Handbook of biological physics". Ed. by R. Lipowsky and E. Sackmann. Elsevier, 1995. Chap. 5. Physical Basis of Self-Organization and Function of Membranes: Physics of Vesicles, pp. 213–303 (cit. on pp. 1, 2, 4, 25, 27).

[189]   E. J. Shimshack and H. M. McConnell. "Lateral phase separation in phospholipid membranes". *Biochemistry* 12.12 (1973), pp. 2531–2360 (cit. on pp. 1, 22).

[190]   K. Simons and E. Ikonen. "Functional rafts in cell membranes". *Nature* 5.387 (1997), pp. 569–72 (cit. on p. 22).

[197]   M. Trejo and M. Ben Amar. "Effective line tension and contact angles between membrane domains in biphasic vesicles". *The European Physical Journal E* 34.8 (2011), pp. 2–14 (cit. on p. 23).

[201]   S. Veatch and S. Keller. "Seeing Spots: Complex Phase Behavior in Simple Membranes," *Biochim. Biophys. Acta - Molecular Cell Research* 1746 (2005), pp. 172–185 (cit. on p. 22).

[210]   G. Zurlo. "Material and geometric phase transitions in biological membranes". PhD thesis. Doctorate of Philosophy in Structural Engineering, University of Pisa, 2006 (cit. on pp. iii, 1, 4, 23, 25, 27, 40, 72).

Chapter 2

A novel constitutive model

The aim of this Chapter is to highlight the key aspects of the cell response activated by GPCRs through the use of a proper simplified energetics. The energy functional governing the membrane behavior employed here takes contribution from the energy of receptor-ligand bonds, the energy due to loss of diffusional entropy of the activated GPRCs, the deduced energy due to conformational changes in the TM domains in the current configuration and, last but not least, the elastic energy due to the surrounding lipid membrane. The elasticity of the cytoskeleton is not explicitly treated in this approach, but its manifestation is incorporated in the adhesion energy, which augments the membrane elasticity. Furthermore, the interplay between TM conformational changes and lateral pressure of the lipid membrane against such TMs is introduced. The chemical potential of the receptor-ligand compound, deduced as the variational derivative of such energy with respect to the density of active receptors, is compared with the one calculated by accounting for the work done by the lateral pressure. The result yields a relationship between the conformational field, the mechanical field (interpreted as either the thickness change or the areal stretch) and the distribution of the compounds receptor-ligand.

Later in this Chapter, the attention is focused on the analysis of such resulting constitutive equation among those three quantities. The main outcome of this analysis shows that, essentially, the reason why ligand-GPRCs compounds prefer to live on lipid raft. This comes out from the

interplay between the work performed by the lateral pressure and the need of TMs to change their conformation during ligand binding. Henceforth, mechanobiology gives a justification to experimental findings of Chemistry Nobel Prizes 2012, Kobilka [117] and Leifkovitz [127].

2.1 The Helmholtz free energy for the system

The structure formed by the cell membrane does include several components which are involved in very complex processes while stimulated by exogenous and endogenous agents. Nevertheless, a few main effects may be singled out while attempting to model the response of cell aggregates to external ligands. In particular, here the Helmholtz free energy is constructed by taking into account three main contributions, and they are recognized to be the following three items:

- diffusion of receptors and transporters;

- conformational changes of the receptors;

- membrane elasticity.

At this stage, the analysis will be done by focusing the attention on single cells.

2.1.1 Receptor and transporter diffusional entropy

The TM-receptors are interpreted to diffuse to lower the energy of the system in a purely entropic way (see e.g. [81]), i.e.

$$\mathcal{H}_d^{(\xi)} = K_B T \ \xi \left(-e_{RL} + \log \left(\frac{\xi}{\xi_0} \right) \right), \tag{2.1}$$

where K_B is the Boltzmann constant, T is the absolute temperature of the bath in which the cells are living, ξ represents the distribution function of active receptors density, ξ_0 is a referential value of such field and e_{RL} is the specific activation energy for the complex ligand-receptor. In this context, and in the sequel, the quantity ξ_0 denotes the average density computed by

assuming that all the receptors embedded in the cell membrabe are active; for the sake of simplicity, this quantity is named *density of activable receptors*. The result (2.1) is a generalization of the work done by some authors, e.g. as Finkelstein et al. [73] and Murray et al. [151], measuring the entropic changes while accounting for deformation of the membrane.

In analogy with the receptors, the active cAMP transporters, whose density is denoted by ζ, diffuse throughout the cell membrane. Hence, the corresponding contribution to the Helmholtz free energy density reads as follows:

$$\mathcal{H}_d^{(\zeta)} = K_B T \zeta \left(-e_{RT} + \log \left(\frac{\zeta}{\zeta_0} \right) \right), \tag{2.2}$$

where ζ_0 is a referential value of such field defined in analogy with ξ_0 and e_{RT} is the specific activation energy for the complex cAMP-transporter.

As a first approximation, the contribution of the conformational changes observed in transporters are neglected. This assumption implies that *only the entropic term contributes to their total energy*.

2.1.2 Conformational energy

Conformational changes in GPCR receptors are mainly known to be characterized by a rotation ω of TM6 about its axis and by a translation μh of the TM6 domain with respect to TM3 and TM5 (see e.g. Ghanouni et al. 2001 [85]), where h is the value of the membrane thickness in the current configuration and μ is the corresponding shear, as depicted in Figure 2.1. A schematic of the kinematics of the cell membrane in the presence of conformational changes is displayed in Figure 2.2. Here *Structured Deformations* [41, 42, 49–51] are used to describe the geometrical changes of the cell membrane due to both the conformational changes mentioned above together with the deformation of the lipid bilayer.

In particular, on the top-left side of Figure 2.2, a schematic of a piece of the membrane in its "ideally" virgin configuration is sketched; there only the TMs involved in the conformational changes of a single GPCR are drawn. Besides the reference thickness h_0, the quantities highlighted there are the normal $\mathbf{N}$ to the mid-plane, the reference value ϕ_T of the diameter of each TM, and the available diameter ϕ_0 for such movements to arise. After denoting as $\rho_T := \phi_0/\phi_T$ the *room space* available between the TMs for
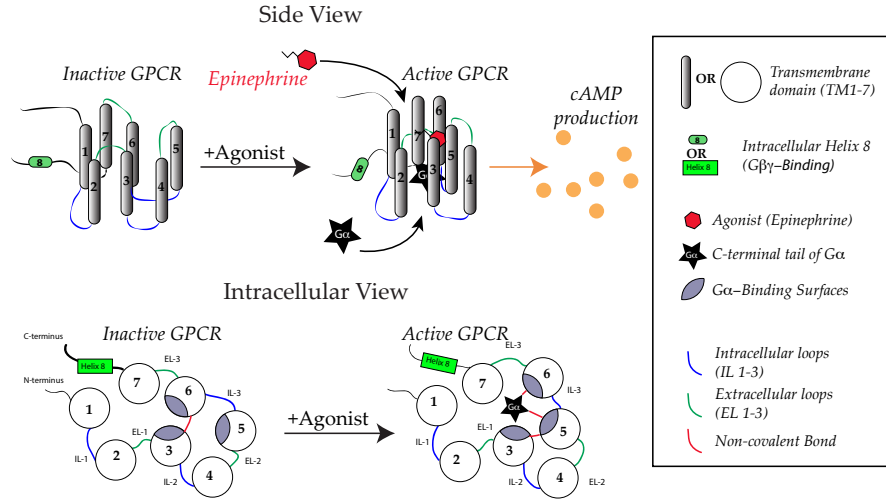
Figure 2.1: Schematic of GPCRs movements caused by the action of epinephrine (inspired by `https://commons.wikimedia.org/wiki/File:GPCR_activation.jpg`)
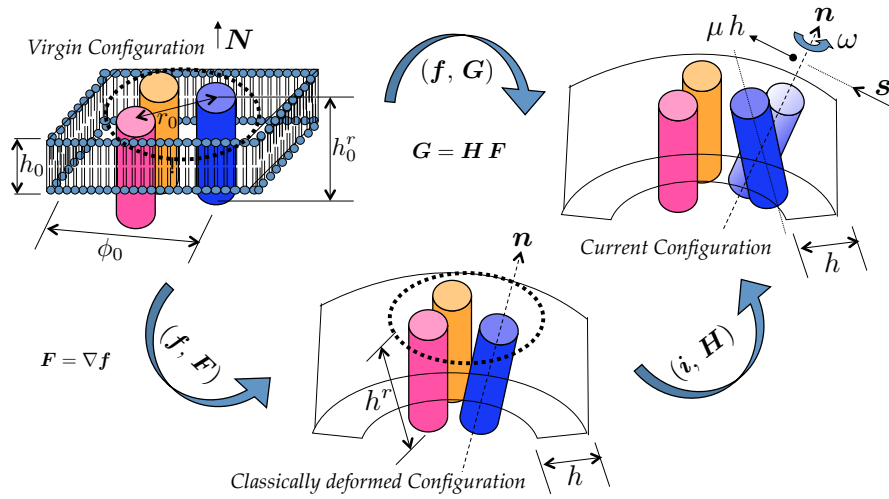
Figure 2.2: Conformational changes and membrane deformation.

Figure 2.3: Schematic of the degree of packing, or *room space*, ρ_T: (a) receptor domain involved, (b-c) minimum $(1 + 2/\sqrt{3}$ and maximum (3) allowed packing configurations, respectively.

conformational changes in the reference configuration, this indicates the *degree of packing* of the TMs. The minimum value of the *room space* ρ_T is estimated to be $1 + 2/\sqrt{3}$ (closest packing of the three domains involved in the movements), hence its value is taken to be betwee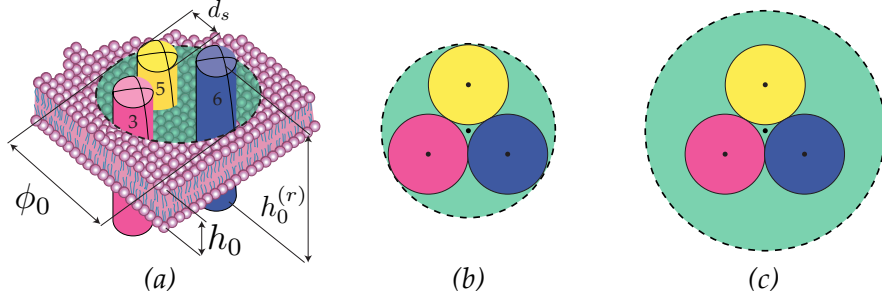n such a value and 3, corresponding to the available room space of a TM in the middle of TM3, 5 and 6, as shown in Figure 2.3.

The current configuration is represented on the top right side of Figure 2.2 and, mathematically, this is described through the pair $(\mathbf{y}, \mathbf{G})$, where $\mathbf{y}$ is the deformation mapping from the virgin configuration, and $\mathbf{G}$ is a tensor field which would be equal to the gradient of $\mathbf{y}$ if no conformational changes would occur. The lower part of the Figure 2.2 offers an explanation of such interpretation through the multiplicative decompostition of the pair $(\mathbf{y}, \mathbf{G})$ introduced above. An intermediate classically deformed configuration is represented in the bottom of this figure where $(\mathbf{y}, \mathbf{F})$, with $\mathbf{F} = \mathrm{Grad}\,\mathbf{y}$, maps points in the virgin configuration in this intermediate one. Furthermore, a pair $(\mathbf{i}, \mathbf{H})$ is visualized in Figure 2.2: here $\mathbf{i}$ is the identity mapping (and, hence, it leaves the first entry untouched), while $\mathbf{H}$ is a tensor field accounting for all the local conformational changes. Although one could use its 9 components to characterize such changes, as a starting point for modeling them, the attention is focused on the main aspects of the observed changes in geometry for the TMs, namely the rotation ω and the shear μ. The change in Helmholtz free energy per unit surface and per unit receptor

due to the changes discussed above can be then interpreted as a result of two contributions, both arising from the classically deformed configuration. For both of such terms, the change in entropy per unit area and per unit receptor is evaluated. The change of entropy due to rotation is accounted for by generalizing the result obtained in [73], namely

$$\varphi_{CR}^{(1)} = A \log \left(\frac{\omega}{2\pi^{2/3}} \right) \tag{2.3}$$

where ω represents the rotation of the TM domains involved in the conformational change about the normal $\mathbf{e}_3$ to the mid-plane of the membrane in the current configuration and $A \cdot K_B T$ represents the conformation energy level per unit receptor per unit area at the reference angle $\omega^* = 2\pi^{2/3}e$ (see footnote[1]).

The change of entropy due to translational changes is also evaluated in the current configuration. The local translation measure is relative to the free volume available for the conformational changes, calculated by multiplying the current value of the thickness h of the cell membrane by the available area $r_0^2 J$, where r_0 represents the referential radius of the involved domains. As h_0 denotes the reference value of the membrane thickness, the field

$$J = \left(\frac{h}{h_0} \right)^{-1} \tag{2.4}$$

represents the inverse of the thickness change measure. It is worth recalling that J depends on the location $\mathbf{x} := (x_1, x_2)$ of the mid plane of the bilayer. It has been shown (see Chapter 1 for details) that J is the order parameter in lipid membranes (see e.g. [52, 55, 210]), allowing for discriminating whether or not lipids exhibit ordered ($J < 1$, more straight configuration of the lipid tails) or disordered phase ($J > 1$, curlier configuration). Henceforth, the resulting change in entropy due to translational changes may be written as

---

[1] The reference angle is estimated as follows:

$$1 = \log \left(\frac{\omega^*}{2\pi^{2/3}} \right) \implies e = \frac{\omega^*}{2\pi^{2/3}} \implies \omega^* = 2\pi^{2/3}e$$

follows:

$$\varphi_{CR}^{(2)} = A \log \left(\frac{\mu \, h}{\left(J \, r_0^2 \, h \right)^{1/3}} \right),$$ (2.5)

where $\mu \, h$ represents a measure of the local translation of the TMs with respect to current location and $\left(J \, r_0^2 \, h \right)^{1/3} = \left(r_0^2 \, h_0 \right)^{1/3}$ is a reference measure of such translation.

The total conformational energy density per unit area and per unit receptor is obtained as the sum of both contributions (2.3) and (2.5) above, i.e.

$$\varphi_{CR} = \varphi_{CR}^{(1)} + \varphi_{CR}^{(2)}.$$

Finally, the relationship for describing the change due to conformational movements reads as:

$$\begin{aligned}
\varphi_{CR} &= A \log \left(\frac{\omega}{2\pi^{2/3}} \frac{\mu h}{(J r_0^2 h)^{1/3}} \right) = A \log \left(\frac{\eta}{J} \frac{h_0^{2/3}}{2\pi^{2/3} r_0^{2/3}} \right) \\
&= A \log \left(\frac{\eta}{J} \frac{1}{2^{1/3}} \left(\frac{2 \, h_0}{\pi d_0} \right)^{2/3} \right) = A \log \left(\frac{\eta}{J} \frac{1}{2^{1/3}} \left(\frac{2 \, h_0}{\pi d_s \rho_T} \right)^{2/3} \right) \\
&= A \log \left(K \frac{\eta}{J} \right)
\end{aligned}$$ (2.6)

where

$$\eta := \omega \, \mu$$ (2.7)

represents the *conformational field* and K is a dimensionless geometric constant defined as follows:

$$K = \frac{1}{2^{1/3}} \left(\frac{2 \, h_0}{\pi \, d_s \, \rho_T} \right)^{\frac{2}{3}}.$$ (2.8)

Equation (2.6) describes conformational changes at the level of GPCRs by combining shear and rotation as a unique parameter that may occur at the level of transmembrane domains. Accordingly to equation (2.8) and the reasonable range of geometric quantities collected from literature in Table 2.1, a range for K can be then determined to be $0.93 \le K \le 2.59$. In the sequel the notation $K_{\min} = 0.93$, $K_{\max} = 2.59$ and $K_m = (K_{\min} + K_{\max})/2 = 1.76$

will be used.

Table 2.1: Reasonable values of geometrical parameters assumed from literature [102, 126], while the room space ρ_T is estimated from Figure 2.3.

thickness h_0 [nm]	diameter d_s [nm]	room space ρ_T -
$3 \div 6$	$0.3 \div 0.5$	$2.15 \div 3$
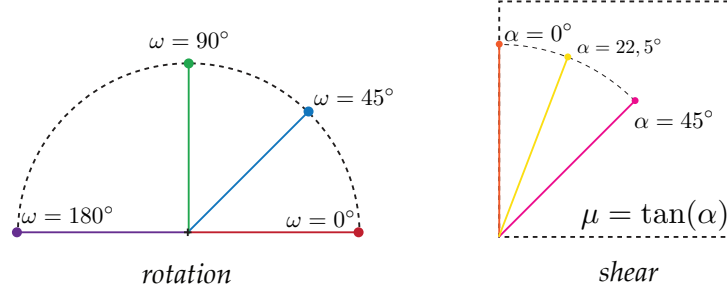
Figure 2.4: Extreme geometric configuration of a single TM.

The range of admissible values of the conformational changes η can be estimated by considering extreme configurations of a single TM, as shown in Figure 2.4. It would be worth bearing in mind that η is composed by two basic movements, a rotation ω in the range $[0, \pi]$, and a shear $\mu = \tan \alpha$ measured through the tangent of an out of plane $(x - z)$ plane, see Figure 2.2) angle α in the range $[0, \pi/4]$, due to the presence of the surrounding TMs. Then, this range for the conformational field is found as $0 \leq \eta \leq \pi$.

2.1.3 Membrane Elasticity and Total Helmholtz free energy

The last contribution to the energy functional lies in the elasticity of the lipid bilayer. Chapter 1 showed a deeper review of a specific stretching energy model recently presented in literature. Henceforth, the local energy

density here employed takes the form:

$$\psi = K_B\,T\,\psi^* = \varphi(J) - \frac{1}{2}\gamma(J)\nabla J^2,$$

where ψ^* denotes the elastic energy density per unit of $K_B\,T$. By summing up all the contributions, the Helmholtz free energy $\mathcal{H}$ of the system is obtained in the following form:

$$\frac{\mathcal{H}}{K_B T} = \int_\Omega \xi\left[-e_{RL} + \log\left(\frac{\xi}{\xi_0}\right) - \varphi_{CR}\right]\,\mathrm{d}A +$$
$$+ \int_\Omega \left(\zeta\left[-e_{RT}\log\left(\frac{\zeta}{\zeta_0}\right)\right] + \psi^*\right)\,\mathrm{d}A. \tag{2.9}$$

2.2 Conformation as the interplay between energetics and lateral pressure

The resulting energetics described before depends on the fields describing distribution function of receptors density ξ and transporters density ζ, conformational change η and areal stretch J. In the sequel it will be shown that both densities of receptors ξ and transporters ζ regulate the production, diffusion and transport of the cAMP, while the last two fields, η and J, are certainly governed by the energetics.

The fact that ξ measures the density of active receptors implies that this quantity is certainly related to the amount of conformational changes η of such GPCRs. Furthermore, because ξ measures this density in the current configuration, the dependence on the local membrane stretch J must be accounted for. Henceforth, an unknown relationship $\xi = \tilde{\xi}(\eta, J)$ is assumed to hold. For a given stretch, a correspondence between density of active receptors and amount of conformational changes also must hold. If such a correspondence is one-to-one, then the latter relationship is invertible in such variables, and

$$\eta = \tilde{\eta}(\xi, J) \tag{2.10}$$

can be taken as its inverse. From the phenomenological point of view, there is the physically reasonable expectation that, for a given J, the higher the

density of active receptor gets, the higher the magnitude of the conformation will be. Finding an explicit expression for the relationship (2.10) is one of the main goal of this Thesis.

The first and second law of thermodynamics can be specified to the system through partition of the power (chemical and mechanical) and thanks to the knowledge of the Helmholtz free energy above. Among other consequences, from this procedure it is standard (see e.g. [48, 91]) to see that the chemical potential of the species is delivered by the variational derivative of such free energy with respect to the specific species itself.

For instance, the variational derivative of the Helmholtz free energy with respect to the chemical species ξ yields the chemical potential μ_{RL} of the compound receptor-ligand,

$$\frac{\mu_{RL}}{K_B T} = \frac{1}{K_B T} \frac{\delta \mathcal{H}}{\delta \xi} = -e_{RL} + 1 + \ln\left(\frac{\xi}{\xi_0}\right) - (\xi\,\varphi_{CR})_{,\xi}\,, \qquad (2.11)$$

where the dependence of η entering φ_{CR} on ξ remains to be determined. Relationship (2.11) witnesses the fact that ξ itself is indeed measuring the *density of active receptors*, namely the ones bound with ligands. On the other hand, the chemical potential of the compound Ligand-Receptor (RL), which represents the free energy per unit receptor and per unit area of such compound, has the meaning of the configurational force driving the conformational changes of the active receptors. This certainly is determined by the (specific) work done by the *lateral pressure* arising against moving TMs for the presence of a quasi-incompressibility watery liquid-like medium, as will be shown in the next section.

2.2.1   Lateral pressure arising in TMs-lipid interactions

Lateral pressure in lipid membranes is known to arise in bilayers even without receptors, due to quasi-incompressibility induced by their acqueous environment. This is known to contribute to the stress across the thickness and it acts as the reaction to incompressibility, thereby *not affecting the elastic (stored) energy*. When it comes to consider the membrane stress, the lateral pressure is indeed the reactive part of such stress. In turn, the lateral pressure changes in the presence of proteins (see e.g. [25, 126, 142,

160]) and it influences their chemical potential. In Figure 2.5 it is shown a schematic of a TM domain involved in the conformational changes and the lateral pressure profile $\pi(\mathbf{x}, z)$ (in green). Indeed, this lateral pressure
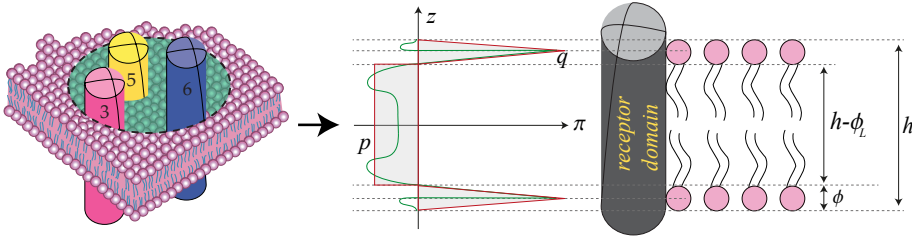
Figure 2.5: Schematic representation of the lateral pressure between a TM domain and the lipid bilayer (see also [142]).

exhibits higher magnitudes in the zones where the lipid heads interact with the top and bottom sites of the TMs. Therefore the lateral pressure induces a local area change $J(\mathbf{x}, z)$ (depending on the location z through thickness as well as on $\mathbf{x}$) against which $\pi(\mathbf{x}, z)$ performs work. The latter is a specific quantity, measured per unit receptor and per unit area (hence is integrated through thickness $h(\mathbf{x}) = h_0/J(\mathbf{x})$), namely:

$$\mathcal{W}(J(\mathbf{x}, t)) = \pi \, d_s \frac{h_0}{J(\mathbf{x}, t)} \int_{-\frac{h_0}{2} J(\mathbf{x}, t)}^{\frac{h_0}{2} J(\mathbf{x}, t)} \pi(\mathbf{x}, z, t) J(\mathbf{x}, z, t) \, \mathrm{d}z \qquad (2.12)$$

where $J(\mathbf{x}, t) := J(\mathbf{x}, 0, t)$ can be evaluated by considering a piecewice linear approximation of the pressure profile, by relating such quantity to the corresponding asymptotic approximation of $J(\mathbf{x}, z, t)$. It is worth noting that in relationship (2.12) the time-dependence is explicitly showed for the sake of completeness, but it will not be taken into account in the sequel. One can account for the surface interactions through the surface energy γ_{RL} between the receptors (R), through the TMs involved in the conformational changes, and the surrounding lipid heads (L), whose diameter is denoted by ϕ_L. It is not difficult to show that this yields a simple expression for the specific work.

Let start by considering a piecewise function able to describe approxi-

mately the lateral pressure profile, i.e.

$$
\pi(\boldsymbol{x}, z) := \begin{cases} -p & 0 < z < \dfrac{h}{2} - \dfrac{\phi_L}{2} \\[2mm] \dfrac{q}{\phi_L/4}\left[z - \left(\dfrac{h}{2} - \dfrac{\phi_L}{2} \right) \right] & \dfrac{h}{2} - \dfrac{\phi_L}{2} < z < \dfrac{h}{2} - \dfrac{\phi_L}{4} \\[2mm] q - \dfrac{q}{\phi_L/4}\left[z - \left(\dfrac{h}{2} - \dfrac{\phi_L}{4} \right) \right] & \dfrac{h}{2} - \dfrac{\phi_L}{4} < z < \dfrac{h}{2} \end{cases}
$$

(2.13)

where q denotes the value of repulsive pressure arising because of the contrast of the headgroup against the receptor domain, and p is the value of the pressure along the hydrocarbon chain region arising fol self-balancing the pressure profile. The introduction of equation (2.13) in (2.12) allows, after some calculations (see Appendix D.1 for more details), for finding an expression for the work done by the lateral pressure as:

$$
\mathcal{W}(\mathbf{x}, t) = \pi \, \phi \, \gamma_{RL} \, (h(\mathbf{x}, t) - h_0) \leq 0
$$

(2.14)

ore equivalently

$$
\mathcal{W}(J(\mathbf{x}, t)) = \pi \, h_0 \gamma_{RL} \, \phi_L \left(\dfrac{1}{J(\mathbf{x}, t)} - 1 \right)
$$

(2.15)

which is consistent with the asymptotic approximation of the quantities above. Whenever the membrane undergoes thinning, the chemical potential would *facilitate* the formation of a new species, then it is decreasing; consequently, the work done by the surrounding pressure (depending on the quantity $h - h_0$) against the lateral expansion (under the assumption of incompressibility, a decreasing thick involves an increasing plane area) is negative, i.e. $\mathcal{W} < 0$. The chemical potential of the compound Receptor-Ligand can be written accounting for of the specific work just obtained. Henceforth such chemical potential can be written as:

$$
\dfrac{\mu_{RL}}{K_B T} = \dfrac{\mu_{RL}^0}{K_B T} + \ln\left(\dfrac{\xi}{\xi_0} \right) + \dfrac{\mathcal{W}(J)}{K_B T}.
$$

(2.16)

Consistency between equations (2.11) and (2.16) implies that the following

relation must hold:

$$(\xi \, \varphi_{CR})_{,\xi} = \frac{\mathcal{W}(J)}{K_B T}. \tag{2.17}$$

Integration of relationship (2.17) delivers the following result:

$$-\xi\varphi_{CR} = \frac{\mathcal{W}(J)}{K_B T}\xi + c(J)$$

where $c(J)$ represents a constant that must be determined, then it is assumed that the conformational field η for the reference density ξ_0 is zero for all J. This normalization allows for determining the constant as:

$$c(J) = -\frac{\mathcal{W}(J)}{K_B T}\xi_0 \tag{2.18}$$

and, consequently, finding a different expression for the energy density related to the conformational field as:

$$-\xi\varphi_{CR} = \frac{\mathcal{W}(J)}{K_B T}\left(\xi - \xi_0\right),$$

namely

$$-\varphi_{CR} = \frac{\mathcal{W}(J)}{K_B T}\left(1 - \frac{\xi_0}{\xi}\right). \tag{2.19}$$

A comparison of relationships (2.5) and (2.19) (see Appendix D.2) yields the following relationship between the density of active receptors ξ, the conformational field η and the membrane strain J:

$$\left(\frac{\xi}{\xi_0}\right)^{-1} = 1 - \frac{C\,J}{1-J}\ln\left(K\frac{\eta}{J}\right), \tag{2.20}$$

where

$$C := \frac{K_B T A}{\pi \phi_T h_0 \gamma_{RL}}. \tag{2.21}$$

Equation (2.20) is the constitutive relationship previously sought (see the introduction part, Section 2.2)

2.3 Constitutive relationships and admissible domains

For the sake of understanding, it is more revealing to express the constitutive relationship (2.20) in terms of the local lipid height ratio, namely:

$$\left(\frac{\xi}{\xi_0}\right)^{-1} = 1 - \frac{C}{\dfrac{h}{h_0} - 1} \ln\left(K\frac{h}{h_0}\eta\right). \tag{2.22}$$

Although equation (2.22) represents a surface in the space defined by ξ, h and η, in Figure 2.10 slices obtained by fixing values of η are shown, namely the quantity $X = \xi/\xi_0$ as a function of the thickness change $H = h/h_0$. In this Thesis, the attention is focused on the occurrence of thinning, i.e $h/h_0 \leq 1$. In particular, taking inspiration from experiments [117, 127], the attention is focused on the occurrence in which the higher the thickness, the higher is the density of active receptors. As matter of fact, the conditions allowing for monotonically increasing relationships between these quantities are of interest.

It will be shown that the density of active receptors and the parameter h/h_0 predict that relative membrane thickening increases the active receptor density, thereby finding that they manifest themselves with higher density on lipid rafts. This result, here obtained directly from the proper energetics employed in the model, is found to be in agreement with the experimental findings of Lefkovitz [127] and Kobilka [117], who showed that in a purification process the addition of cholesterol to the membrane induced rafts formation, i.e. induced the transition to ordered lipids, as displayed in Figure 2.6.

Equation (2.22) delivers a relationship between density of active receptors, thickness change and conformational field. For the sake of illustration, in the sequel the following notation (already used above) will be explicitly employed:

$$X := \frac{\xi}{\xi_0} \tag{2.23a}$$

$$H := \frac{h}{h_0} \tag{2.23b}$$
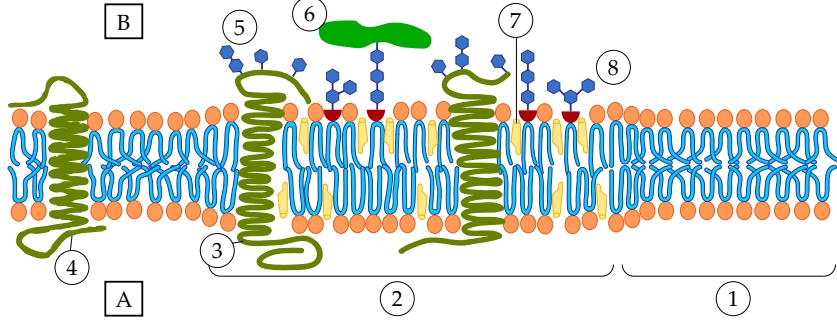
Figure 2.6: Schematic of raft in a membrane: A) cytosol, B) extracellular space, 1) non-raft membrane, 2) lipid raft, 3) lipid raft associated transmembrane protein, 4) non-raft membrane protein, 5) glycosylation modification, 6) GPI-anchored protein, 7) cholesterol, 8) glycolipid. Reproduction from http://cellbiology.med.unsw.edu.au/units/science/lecture0803.html.

One of the most important parameter of the model presented above is the quantity C, but it is tricky to choose a proper value for this parameter. Indeed, although a deeper investigation in literature was done at the best of the Writer's capabilities, neither existing experiments or sources useful for determining the value of the constant C were found. The lack of this piece of information can be filled by considering that, in this framework, it is clear that the conformational field η must increase wherever the thickness change $H = h/h_0$ gets higher values, i.e. $\partial\eta/\partial H > 0$, or explicitly:

$$\frac{\partial\eta}{\partial H} = \frac{1}{C\,H^2\,K\,X}\exp\left(-\frac{(1-H)(1-X)}{C\,X}\right)(H - C\,X - H\,X) > 0$$

Bearing in mind this condition, equation (2.28b) delivers a relationship for C in the following form:

$$C < \frac{H(1-X)}{X} \qquad (2.24)$$

At this stage, the employee of a reverse engineering approach can be useful for determining the order of magnitude of C. In this regard, a closer analysis of (2.21) reveals that the only unknown quantity for computing C is the conformation energy level per unit receptor and per unit area,

49

namely A. Indeed, all the other quantities depend on the geometry of receptor domains. This observation allows for developing the following approach: (i) a parameter a based on known quantities only is introduced; (ii) a relationship for computing A from the constitutive equation (2.20) is computed; (iii) numerical experiment are performed in order to analyze the results and choosing the proper values of A and, consequently, of C. As first step, the following relationship is introduced:

$$C = \frac{A}{a}, \tag{2.25}$$

where

$$a := \frac{\pi \phi_T h_0 \gamma_{RL}}{K_B T}. \tag{2.26}$$

The coefficient a is dimensionless, and it depends on the diameter of the domain, the thickness of the membrane, surface energy and temperature, henceforth it can be easily computed. All the uncertainty lies on the value of A, which represents a ratio between molecules currently in the compound. An inverse relationship for computing A can be found from the constitutive equation (2.20) as

$$A = -\frac{a}{\log\left(K\,\eta\,H\right)} \frac{(H-1)(X-1)}{X}. \tag{2.27}$$

The analysis of equation (2.27) allows for a parametric study of the the constant A as function of the conformational field η whenever the geometry is fixed (i.e. a is known) using as parameter the receptor density $X = \xi/\xi_0$ and the height ratio $H = h/h_0 = J^{-1}$. However, this approach leads to a wide range of possible values for A, and consequently for C. The use of further numerical experiments (see Figure 2.7), allows for limiting C in the range $[0.05 \div 0.75]$, even if the more reliable value is $C = 0.3$ (see Chapter 4 for the numerical simulation on the conformational change). These values will be used in the sequel of this Chapter for the analysis of the constitutive equations.

Manipulation of the constitutive equation (2.20) allows one to get explicit forms of several constitutive relationships very useful for closer mathematical
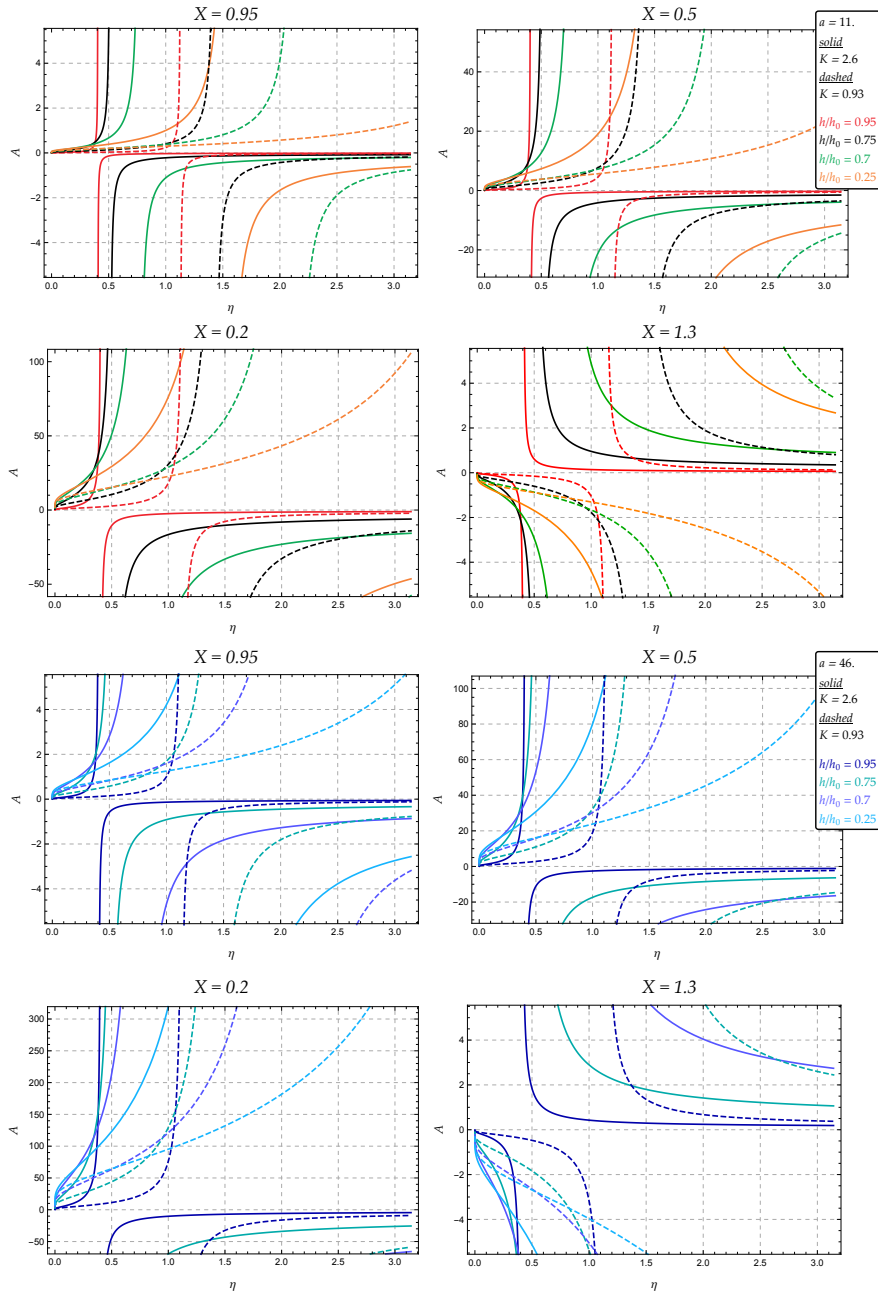
Figure 2.7: Examples of the reserve engineering approach for determining the parameter A: numerical experiments using $a = 11$ and $a = 46$ for given values of K and K.

Table 2.2: Estimated values for C. For each choice of parameters, the first row is referred to $A = 0.5$, the second to $A = 2$. Values of γ_{RL} come from literature [142, 160].

$h_0\,[nm]$	$\phi_T\,[nm]$	$\gamma_{RL}\,[mN/m]$	a	C
3	0.5	10	11.01	0.045 0.182
6	0.3	10	13.21	0.038 0.151
3	0.5	35	38.52	0.013 0.052
6	0.3	35	42.22	0.011 0.043

inspections and revealing more on the model itself:

$$X = \frac{1}{1 - \dfrac{C \log{(K\,\eta\,H)}}{1 - H}}, \qquad (2.28a)$$

$$\eta = \frac{1}{HK} \exp{\left(-\frac{(1 - H)(1 - X)}{C\,X} \right)}. \qquad (2.28b)$$

A closer analysis of (2.28a) provides both an upper and a lower bound for the field of admissible conformational changes. Indeed, receptor density is a positive definite quantity $(X > 0)$ and at the same time the case of interest is regarding when it is an increasing function of the height ratio $(\partial X / \partial H > 0)$. The simultaneous occurrence of both these conditions implies that:

$$\eta < \frac{1}{K\,H} \exp{\left(\frac{1 - H}{C} \right)} = \eta_{UB}, \qquad (2.29a)$$

$$\eta \geq \frac{1}{K\,H} \exp{\left(\frac{H - 1}{H} \right)} = \eta_{LB}. \qquad (2.29b)$$

for given values of H, C and K.

52
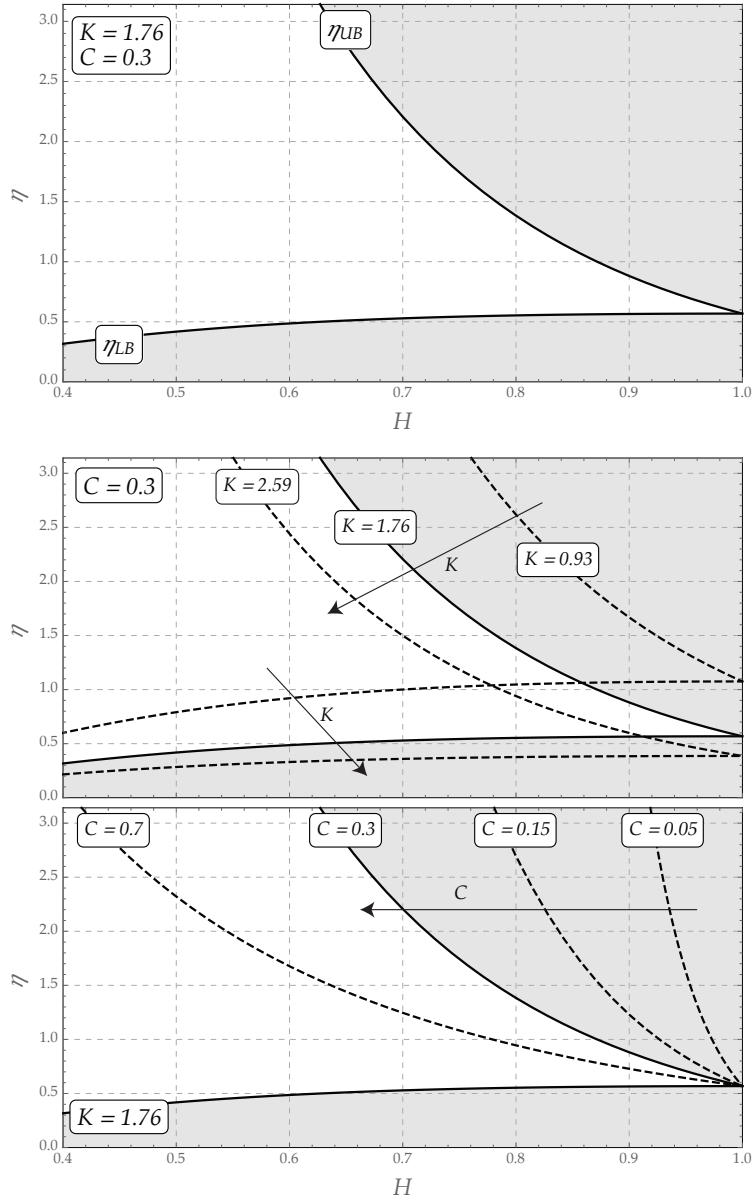
Figure 2.8: Lower and upper bounds on the plane (η, H): (top) given values of K and C; (middle) influence of K on the limit curves; (bottom) influence of C on the limit curves.

Relationships (2.29) allow for determining an admissible region on the plane defined by thickness change H versus receptor density ratio X at the top ofFigure 2.8. Here, the not-admissble movements are denoted as a grey area. This result highlights that for a fixed geometry (i.e. for given values of H, K, C) only some movements of the domains (represented by the conformational field $\eta = \omega \, \mu$) are allowed. The bounds depends on the chosen couple (K, C), as shown at the middle and the bottom of Figure 2.8. It is easy to recognize that an increasing value of K (whenever C is fixed) gives more space for the movements (indeed the the lower bound assumes smaller values with increasing K), whereas increasing values of C (whenever K is fixed) influence the position of the upper bound, that seems to limit the chance to get great movement in correspondence of small thinning. The strong influence of C could be expected since it drives the decay rate of the exponential function in (2.28b).

It would be worth noting that the model is able to predict the absence of conformational changes whenever both the density of receptors is vanishing and the height ratio is very close to zero, i.e $H \to 0$ and $X \to 0$. Indeed, the argument of the exponential function (2.28b) tends to $-\infty$, and thus:

$$\lim_{X \to 0, \ H \to 0} \exp(f(X, H)) \to 0, \tag{2.30}$$

as expected.

Besides equation (2.28a), relationship (2.28b) together with the conditions $X > 0$ and $\partial X / \partial H > 0$ provides an admissible region on the plane defined by (H, X) whenever the conformationl change value is used as parameter. In particular, the following relationship must hold:

$$\frac{\partial X}{\partial H} > 0 \quad \Rightarrow \quad X > \frac{H}{C + H}, \tag{2.31}$$

It is worth bearing in mind that the curves $X(H)$ whenever η is a parameter can be obtained as the projection of the surface $\eta(H, X)$ on the plane $H - X$. A closer inspection of (2.28a) together with the result (2.31) shows that the limit curves become more *flat* as C increases (see Figure 2.9), as equation (2.31) suggests. In this analysis, a special value of conformational change, η^*, is introduced. This value represents the value of η needed for reaching

54

the minimum value of allowed conformational change, namely η_{LB}, whenever the reference configuration $H = 1$ is chosen. This curve is drawn with a red line in Figure 2.10. In the same drawing, the grey area delimited by a dashed line represents locations that are not reachable, since it is out of the admissible region.
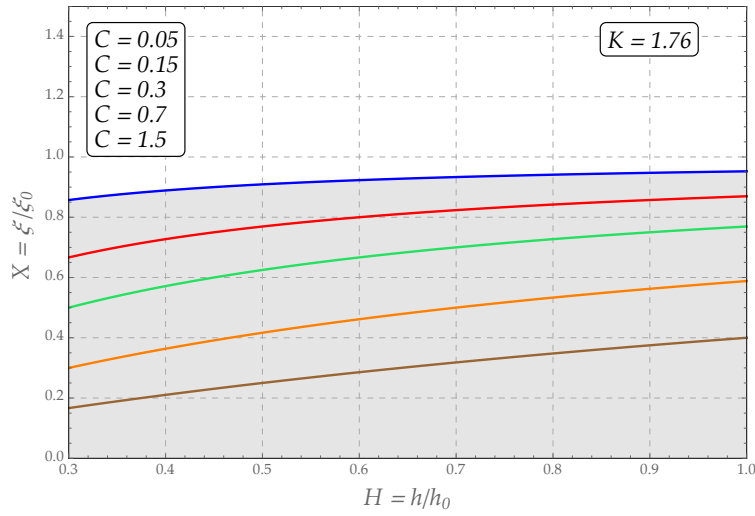
Figure 2.9: Changes in the lower bound for $X = \xi/\xi_0$ depending on C.

In order to complete the series of analysis coming from the constitutive relationships (2.20) and (2.28), the dependence of the behavior of the conformational field η on both height ratio H and receptor density X is studied, and the graphical results are shown in Figure 2.11 and Figure 2.12. As expected, whenever the membrane exhibits thinning (i.e the height ratio H moves from 1 to smaller values) and a fixed value of receptor density is assumed, the conformational changes is increasing, since more movements are needed. On the other hand, as predicted experimentally, whenever the height ratio H is fixed, the value of conformational field η increases as the receptor density increases.
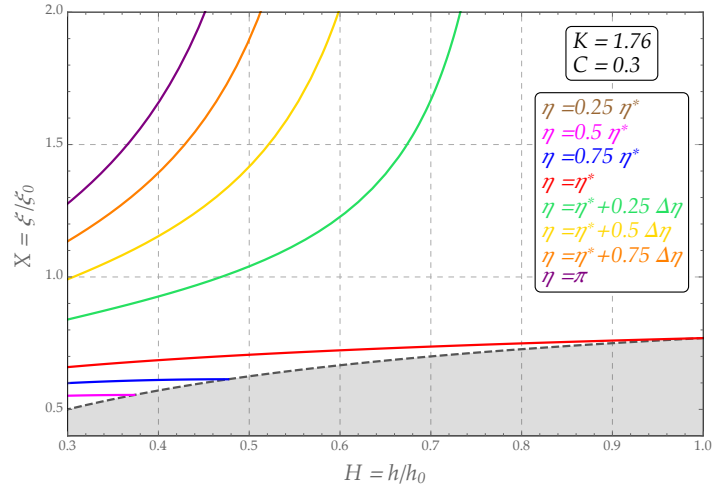
Figure 2.10: Behavior of ξ/ξ_0 vs h/h_0 using η as parameter. Here $\eta^* = 1.07$ and $\Delta\eta = 2.06$.
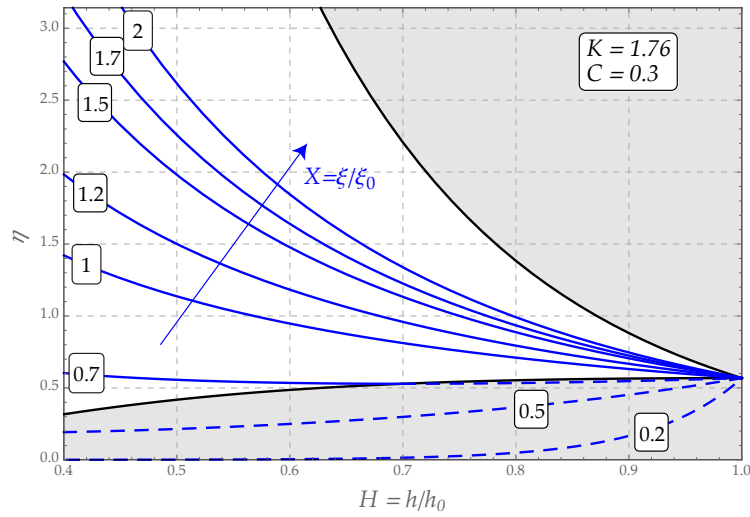
Figure 2.11: Behavior of η vs h/h_0 using the ratio ξ/ξ_0 as parameter. The grey area represents the non-admissible region.
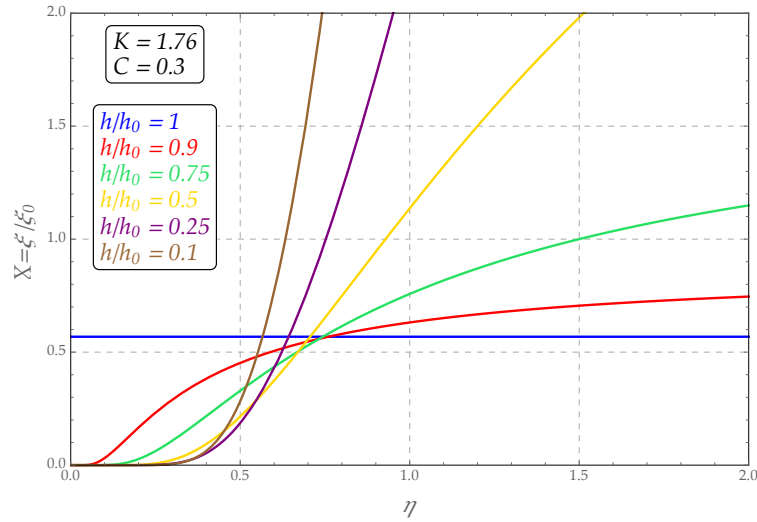
Figure 2.12: Behavior of η vs ξ/ξ_0 using the ratio h/h_0 as parameter. The grey area represents the non-admissible region.

References

[25] R. S. Cantor. "Lipid composition and the lateral pressure profile in bilayers". *Biophysical journal* 76 (1999), pp. 2625–2639. DOI: 10.1016/S0006-3495(99)77415-1 (cit. on p. 44).

[41] G. Del Piero and D. Owen. "Structured Deformations of Continua". *Archive for Rational Mechanics and Analysis* 124 (1993), pp. 99–155 (cit. on p. 37).

[42] G. Del Piero and D. Owen. "Integral-Gradient Formulae for Structured Deformations". *Archive for Rational Mechanics and Analysis* 131 (1995), pp. 121–138 (cit. on p. 37).

[48] L. Deseri, G. Marcari, and G. Zurlo. "UNESCO". 2009. Chap. Thermodynamics (cit. on p. 44).

[49] L. Deseri and D. R. Owen. "Toward a field theory for elastic bodies undergoing disarrangements". *Journal of Elasticity* 70.I (2003), pp. 197–236 (cit. on pp. 37, 226).

[50] L. Deseri and D. R. Owen. "Submacroscopically Stable Equilibria of Elastic Bodies Undergoing Disarrangements and Dissipation". *Mathematics and Mechanics of Solids* 15.6 (2010), pp. 611–638 (cit. on pp. 37, 154, 226).

[51] L. Deseri and D. R. Owen. "Moving interfaces that separate loose and compact phases of elastic aggregates: a mechanism for drastic reduction or increase in macroscopic deformation". *Continuum Mechanics and Thermodynamics* 25 (2012), pp. 311–341. DOI: `10.1007/s00161-012-0260-y` (cit. on pp. 37, 226).

[52] L. Deseri, M. Piccioni, and G. Zurlo. "Derivation of a new free energy for biological membranes". *Continuum Mechanics and Thermodynamics* 20.5 (2008), pp. 255–273. DOI: `10.1007/s00161-008-0081-1` (cit. on pp. iv, 1, 4, 23, 25, 26, 40, 153, 154, 168, 193).

[55] L. Deseri and G. Zurlo. "The stretching elasticity of biomembranes determines their line tension and bending rigidity". *Biomechanics and Modeling in Mechanobiology* 12 (2013), pp. 1233–1242. DOI: `doi: 10.1007/s10237-013-0478-z` (cit. on pp. iii, iv, 1, 4, 23–26, 30, 40, 72, 153, 154, 168, 193).

[73] A. V. Finkelstein and J. Janin. "The price of lost freedom: entropy of bimolecular complex formation". *Protein Engineering* 3.1 (Oct. 1989), pp. 1–3. ISSN: 0269-2139. URL: `http://www.ncbi.nlm.nih.gov/pubmed/2813338` (cit. on pp. 37, 40).

[81] H. Gao, W. Shi, and L. Freund. "Mechanics of receptor-mediated endocytosis". *PNAS* 102.27 (2005), pp. 9469–9474 (cit. on pp. 36, 115).

[85] P. Ghanouni et al. "Functionally different agonists induce distinct conformations in the G protein coupling domain of the beta 2 adrenergic receptor". *The Journal of Biological Chemistry* 276.27 (2001), pp. 24433–6. (Cit. on pp. 3, 37).

[91] M. Gurtin, E. Fried, and L. Anand. *The Mechanics and Thermodynamics of Continua*. Cambridge University Press, 2009 (cit. on p. 44).

[102] U. Hiden et al. "The first trimester human trophoblast cell line ACH-3P: A novel tool to study autocrine/paracrine regulatory loops of human trophoblast subpopulations – TNF-α stimulates MMP15 expression". *BMC Developmental Biology* 7.137 (2007). DOI: `doi: 10.1186/1471-213X-7-137` (cit. on p. 42).

[117] B. Kobilka and X. Deupi. "Conformational complexity of G-protein-coupled receptors". *Trends in Pharmacological Sciences* 28.8 (2007), pp. 397–406 (cit. on pp. v, 3, 36, 48, 147, 252).

[126] A. G. Lee. *How lipids affect the activities of integral membrane proteins.* 2004. DOI: `10.1016/j.bbamem.2004.05.012` (cit. on pp. 42, 44).

[127] R. Lefkowitz. "Seven transmembrane receptors: something old, something new". *Acta Physiol* 190 (2007), pp. 9–19 (cit. on pp. v, 3, 36, 48, 147, 252).

[142] D. Marsh. "Lateral pressure profile, spontaneous curvature frustration, and the incorporation and conformation of proteins in membranes". *Biophysical journal* 93 (2007), pp. 3884–3899. DOI: `10.1529/biophysj.107.107938` (cit. on pp. 44, 45, 52).

[151] C. W. Murray and M. L. Verdonk. "The consequences of translational and rotational entropy lost by small molecules on binding to proteins". *Journal of computer-aided molecular design* 16.10 (2002), pp. 741–753. DOI: `10.1023/A:1022446720849` (cit. on p. 37).

[160] S. Ollila. *Lateral Pressure in Lipid Membranes and Its Role in Function of Membrane Proteins.* 2010, p. 96. ISBN: 9789521524806. URL: `http://urn.fi/URN:NBN:fi:tty-201011181369` (cit. on pp. 44, 52).

[210] G. Zurlo. "Material and geometric phase transitions in biological membranes". PhD thesis. Doctorate of Philosophy in Structural Engineering, University of Pisa, 2006 (cit. on pp. iii, 1, 4, 23, 25, 27, 40, 72).

60

Chapter 3

Balanced configurations of biological membranes

The aim of this Chapter is to focus the attention on the diffusive phenomena and balanced configurations of trophoblast cell membrane. In Chapter 2, the energetics of systems composed by lipid bilyers in which proteins are embedded was presented; in this Chapter this energetics will be used for looking at the set of equilibria related with the diffusion of receptors and transporters. First of all, these diffusive phenomena will be explored, and a proper model for predicting the average response of the cell is introduced. Later, the local elastic energy introduced in Chapter 1 is extended by taking into account contributions due to both adhesion and temperature. Finally, the set of equilibria are sought by employing the principle of the minimum of energy, i.e. the variational derivative of the energy functional will be computed in order to isolate configurations corresponding to stationary points of the energy itself.

3.1 Diffusive phenomena involving receptors and transporters

The time-space evolution of the density of active receptors entering in the free energy functional can be specified once their diffusion is accounted for.

Of course the cAMP transporters influence such a balance and, in turn they also must have a balanced flux. To this end, if d_ξ and d_ζ denotes the diffusivities of receptors and transporters respectively (assumed to be independent of the lipid ordering, namely on J), the following equations may be deduced:

$$-D_i\, d_\xi \xi + \xi_t = \alpha\, \zeta_t \tag{3.1a}$$

$$-D_e\, d_\zeta \zeta + \zeta_t = 0 \tag{3.1b}$$

where, roughly speaking, $\alpha\, \zeta_t$ represents a sink term in the balance of fluxes involving the active receptors due to the fraction of cAMP swept away from the cell aggregate, namely the extracellular cAMP. It is worth noting that (3.1b) is an eigenvalue problem which gives rise to suitable eigenfuntions, depending on the geometry of the domain and, eventually, on the boundary conditions. Furthermore, an expansion of (3.1a) in terms of eigenfunctions may also be considered.

The usual production process of cyclic adenosine monophosphate (cAMP) involves several cellular components, and it can be schematically depicted as shown in Figure 3.1. The pictures shows that (i) some amount of epinephrine stimulates the β2-adrenergic receptors annealed into the cellular membrane, signaling (ii) the production of intracellular cAMP; inside the cell, some of these products (iii) are degraded by the cyclic nucleotide phosphodiesterase (PDE), while others (iv) are pushed out by the multidrug-resistent protein (MRP), increasing the quantity of extracellular cAMP outside the cell. Xie et al. [205] studied this process by adopting both a two- and a three-compartment model in order to provide a mathematical description of the response of the cell, hence ODE equations governing the intracellular and extracellular compartments were provided. The key aspect of this approach is that the diffusion of the species is studied through the analysis of the products. It is worth to note that for getting information about the species itself, a proper relationship will be employed for converting such a value. Although the model employed is very simple and allows for getting qualitatively good results, the production of cAMP appear to be governed by functions only increasing in time.
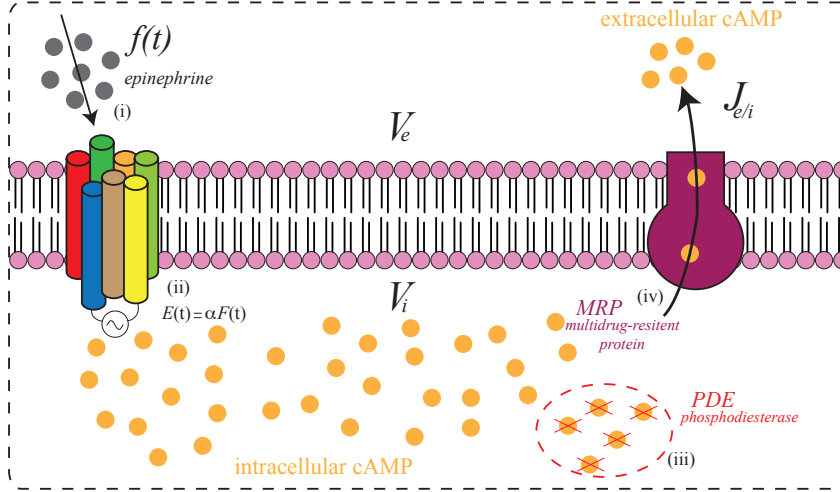
Figure 3.1: Schematic of cell processes involved in cAMP production as studied in [205].

An experiment involving the cell subject of this Thesis was recently (2010) performed by Biondi et al. [18], where cAMP efflux from human trophoblast cell lines was measured. Unlike the scheme presented above, in the experimental setup the action of PDE was inhibit; the related sketch of cAMP production involved in this experiment is displayed in Figure 3.2. For the sake of the Reader's convenience, the experiment is briefly recalled. A group of HTR-8/SVneo trophoblast cell line obtained from human first-trimester placenta ex-plant cultures were properly treated at 37°C in a controlled atmosphere. These cells were grown to confluence (2-3 days) in a 24-well plate (Figure 3.3) and then incubated for the time prescrobed by the protocol. After that, media containing approximately 250.000 cells were harvested in wells containing $C_w = 500\,\mu L$ of water and some amount of epinephrine was added. The wells were immediately frozen at -70°C until cAMP levels were measured. Intracellular and extracellular cAMP were determined by proper methods (e.g. method of Brown [22]) and the nucleotide levels were expressed as $pmoles/10^6 cells/time$ (Figure 3.4).

As an experimental result, epinephrine enhanced intracellular cAMP concentration in a dose-dependent fashion, reaching a plateau at around
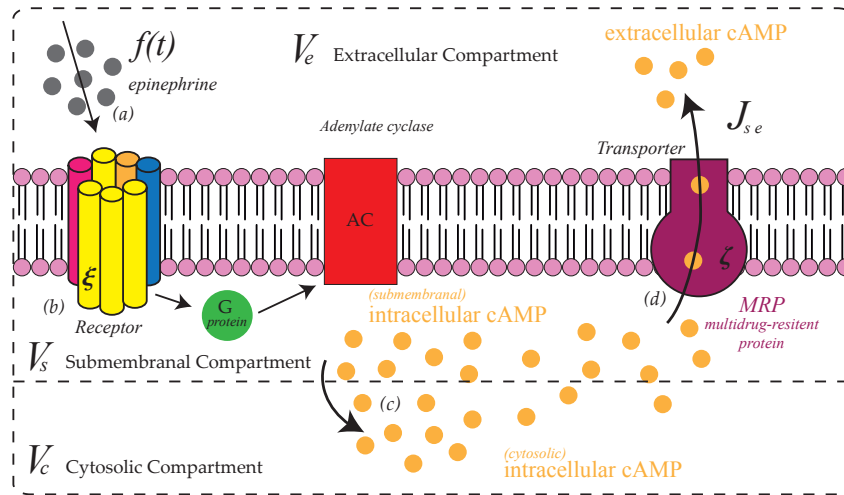
Figure 3.2: Schematic of cell processes involved in cAMP production with inhibited PDE (experimentally imposed in [18]), as assumed in this work.
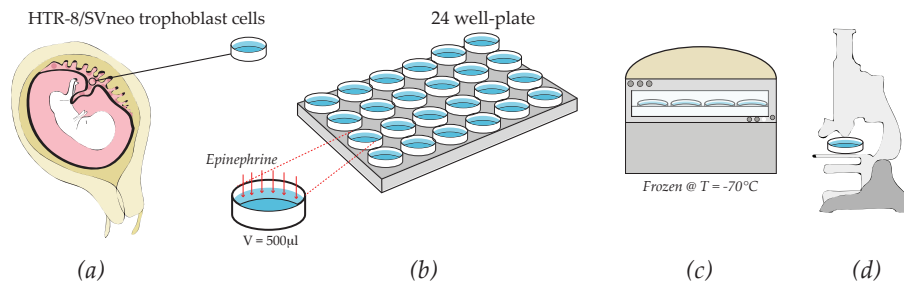
Figure 3.3: Schematic of the experiment performed in [18]: (a) trophoblast cell taken from human placenta; (b) harvesting in a 24wells plate; (c) treatment in controlled atmosphere; (d) cAMP measurement.

$10^{-4}\,M$ (Figure 3.4a). After the analysis of this *saturation* curve, the cAMP evolution over time was monitored for the fixed concentration of $10^{-6}\,M$ of epinephrine, because able to trigger a cAMP production close to the half of the maximum response (Figure 3.4b). Intracellular cAMP increased as a function of time up to about 15 min, thereafter a reduction of the nucleotide level was observed. At the same time, extracellular cAMP gradually increased in time, at least during the 60 min of observation, although this result is not showed graphically in [18]. For this specific case, when a ligand concentration $c = 1\,\mu M$ was used, the total quantity Q_e of epinephrine used in the experiment involving 10^6 cells can be then computed as:

$$Q_e = 4 \times c\,C_w = 4 \times 1\,\mu M \times 500\,\mu L = 2000\,pmol \tag{3.2}$$

3.1.1 cAMP-to-receptors relationship

The fields of active receptors density $\xi(x,t)$ and its products, namely the intracellular cAMP (i.e $S(x,t)+C(x,t)$), are intimately linked by a conversion factor, namely α_ξ, as follows:

$$cAMP_i = \alpha_\xi \left(\xi - \bar{\xi}\right) \approx \alpha_\xi\,\xi, \tag{3.3}$$

where $\alpha_\xi = 10^4$ is estimated experimentally [18]. In this Thesis, the cAMP level is referred to a population of 10^6 cells (and it is expressed in *pmol*); taking into account a parameter $c_1 = 10^6$ for switching between the population and the single cell, and $c_2 = 10^{12}$ for converting *pmol* to *mol*, the number of active receptors can be computed as follows:

$$\xi_\# = \frac{1}{c_1}\frac{1}{\alpha_\xi}\left(\frac{cAMP_i}{c_2}\right)N_A \tag{3.4}$$

where N_A is the Avogadro number. An analogue relationship holds for computing the number of transporters:

$$cAMP_e = \alpha_\zeta \left(\zeta - \bar{\zeta}\right) \approx \alpha_\zeta\zeta \tag{3.5}$$

65
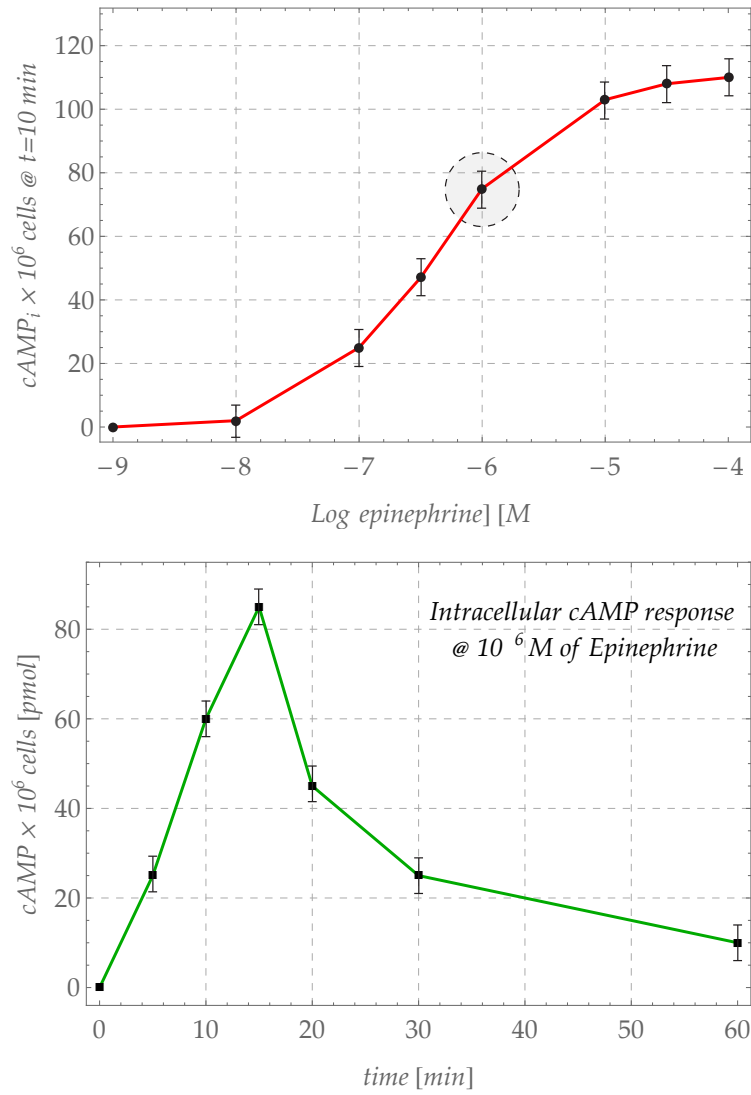
Figure 3.4: Experimental results obtained in [18]: (a) value of measured intracellular cAMP after 10 minutes depending on epinephrine concentration, (b) time evolution of measured intracellular cAMP for a fixed value of epinephrine concentration ($10^{-6}M$).

3.1.2 A model for the average diffusion

Inspired by the model developed in [205], a three-compartment model composed by a set of three ODEs is considered in order to study the *average diffusion* in terms of cAMP production:

$$\begin{cases} \dot{\hat{S}} = \omega_{11}\left(\hat{C} - \hat{S}\right) + \omega_{12}\left(\hat{Z} - \hat{S}\right) + \hat{f}(t) \\ \dot{\hat{C}} = \omega_{21}\left(\hat{S} - \hat{C}\right) \\ \dot{\hat{Z}} = \omega_{31}\left(\hat{S} - \hat{Z}\right) \end{cases} \tag{3.6}$$

and initial conditions $\hat{S}(0) = \hat{S}_0$, $\hat{C}(0) = \hat{C}_0$ and $\hat{Z}(0) = \hat{Z}_0$. Here, $\hat{S}(t)$ and $\hat{C}(t)$ denote the submembranal and cytosolic cAMP production, respectively, whereas $\hat{Z}(t)$ is related to the quantity of cAMP pulled out of the cell by transporters. The coefficients ω_{ij} are determined by means of proper ratios between flux and volume of the three considered pools (compartments), and are dimensionally expressed as $[min]^{-1}$:

$$\begin{aligned} \omega_{11} &= \frac{J_{sc}}{V_s} & \omega_{12} &= \frac{J_{se}}{V_c} \\ \omega_{21} &= \frac{J_{sc}}{V_c} & \omega_{31} &= \frac{J_{se}}{V_e} \end{aligned} \tag{3.7}$$

where V_s, V_c and V_e are the volume of submembranal, cytosolic and extracellular pool, respectively, whereas J_{sc} is the flux between submembranal and cytosolic compartment and J_{se} is the flux involved from submembranal to extracellular compartment.

The production on both intra- and extra-cellular cAMP is triggered by the bonding of a specific ligand, i.e. the epinephrine, to binding sites. It is clearly that both the formation of bindings and the triggering of cAMP production are phenomena occurring over the time, and then they depend on a rate of both precipitation of the ligand and bounds formation. For this reason, a function $f(t)$ for describing the ligand precipitation is introduced, whereas the cumulative quantity of precipitated ligand is denoted by $F(t)$:

$$F(t) = \int_0^t f(\tau)\,\mathrm{d}\tau \quad \text{and} \quad \int_0^T f(\tau)\,\mathrm{d}\tau = Q_e, \tag{3.8}$$

67

where T denotes the experiment lifetime (60 mins). It is worth noting that relationships (3.8) are suggested by phenomenological consideration. Moreover, they represent the only pragmatical choice of all the subsequent model. Immediately after the ligand is put in the well, a chemical potential $\mu_{RL} < 0$ is observed, i.e the energy difference between the binder-ligand pair in the bound and unbound states facilitates the formation of binds. This condition holds until the saturation of binding sites is reached at a certain instant, namely t_m. The chemical potential becomes then positive (i.e $\mu_{RL} > 0$) and the unbinding phenomenon is prevalent. Here, taking inspiration from [158], where an exponential form is used to model the binding/unbinding phenomena involved in the adhesive properties of fibroblasts cells, the precipitation phenomenon is assumed to be governed by the following balance equation,

$$\dot{f}(t) + k_a\, f(t) = q_a, \tag{3.9}$$

which together with the initial condition $f(0) = 0$ gives solution:

$$f(t) = \frac{q_a}{k_a}\left(1 - e^{-k_a\, t}\right). \tag{3.10}$$

Thanks to the property of the exponential function, it is clear that the ratio q_a/k_a represents the maximum value of the function $f(t)$ itself, reached after a certain saturation time. Let normalize the function $f(t)$ by means of $f_{max} := q_a/k_a$, i.e

$$f^*(t) = \frac{f(t)}{f_{max}}, \tag{3.11}$$

and assume that at time t_m, the function $f(t)$ reaches the normalized value m:

$$m := \frac{f(t_m)}{f_{max}} < 1. \tag{3.12}$$

This mathematical description follows by the consideration that at the beginning of the experiment, the rate of precipitation is increasing up to get a maximum value exactly at t_m. Under these considerations, the constant k_a, dimensionally expressed as $[T^{-1}]$, can be computed as follows:

$$f^*(t_m) = 1 - e^{-k_a\, t} = m, \tag{3.13}$$

$$k_a = -\frac{\log(1-m)}{t_m}. \tag{3.14}$$

After that, the quantity of ligand still in the solution is less than the bound quantity, hence the rate of precipitation is decelerating. Similarly to above, the differential equation governing the precipitation after the plateau is expressed as:

$$\dot{f}(t) + k_d\, f(t) = 0, \tag{3.15}$$

whose solution, assuming initial condition $f(t_m) = m\, f_{max}$, reads:

$$f(t) = f(t_m)\, e^{k_d(t-t_m)}. \tag{3.16}$$

In this case, as expected, the function $f(t)$ is decreasing in time. Let assume that at time t_f it reaches a ratio n defined as follows:

$$n := \frac{f(t_f)}{f_{max}} < \frac{f(t_m)}{f_{max}} = m. \tag{3.17}$$

Henceforth, the constant k_d is computed as follows:

$$f^*(t_f) = m\, e^{k_d(t-t_m)} = n \tag{3.18}$$

$$k_d = \frac{\log(n/m)}{t_f - t_m} \tag{3.19}$$

Finally, the piecewise normalized forcing term $f^*(t)$ (whose an example is showed in Figure 3.20) assumes the following form:

$$f^*(t) = \begin{cases} 1 - e^{-k_a t} & t \leq t_m \\ m\, e^{k_d(t-t_m)} & t > t_m \end{cases} \tag{3.20}$$

3.1.3 A model for the space-dependent diffusion

Besides the averaged diffusion over time, the diffusive phenomenon over the space is also taken into account. By considering as starting point the mathematical model for predicting the time-dependent diffusion discussed in the previous section, the diffusion over the space is considered by taking
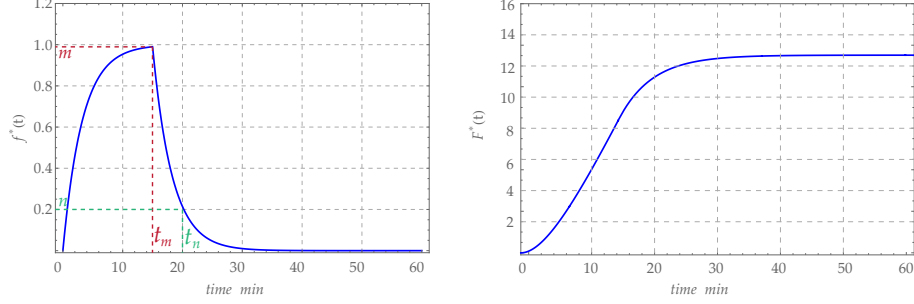
Figure 3.5: Example of normalized precipitation function $f^*(t)$, by assuming $m = 0.99$, $t_m = 15\,min$, $n = 0.2$ and $t_f = 20\,min$.

into account a term related to the Laplacian through a diffusivity coefficient, i.e.

$$
\begin{cases}
S_t = \omega_{11}\,(C - S) + \omega_{12}\,(Z - S) + d_\xi\,\Delta S + y(\hat{\Omega},\,t) \\
C_t = \omega_{21}\,(S - C) \\
Z_t = \omega_{31}\,(S - Z) + d_\zeta\Delta Z
\end{cases}
\tag{3.21}
$$

with proper initial and boundary conditions:

$$
\begin{cases}
S(\hat{\Omega}, 0) = S_0(\hat{\Omega}) \\
C(\hat{\Omega}, 0) = C_0(\hat{\Omega}) \\
Z(\hat{\Omega}, 0) = Z_0(\hat{\Omega})
\end{cases}
\tag{3.22a}
$$

$$
\begin{cases}
\nabla S(\partial\hat{\Omega},\, t) = 0 \\
\nabla C(\partial\hat{\Omega},\, t) = 0 \\
\nabla Z(\partial\hat{\Omega},\, t) = 0
\end{cases}
\tag{3.22b}
$$

where $\hat{\Omega}$ denotes a 2D domain and $\partial\hat{\Omega}$ its boundary. In equation (3.21), d_ξ and d_ζ represent receptors and transporters diffusion coefficients, respectively, and each field is a function of both space and time, i.e $S(\hat{\Omega}, t)$, $C(\hat{\Omega}, t)$ and $Z(\hat{\Omega}, t)$, whereas $y(\hat{\Omega}, t)$ is a space- and time-dependent forcing term.

For the sake of simplicity, from now on only the one-dimensional case will be considered. Also in this case, the deposition rate relationship (3.8) for describing the action of the epinephrine holds, since the time-dependent func-

tion $f(t)$ physically describes the deposition distribution of the epinephrine.

At this stage, a problem about how model the forcing term $y(x,t)$ arises. As first approach, one can imagine to find a space depending forcing term, namely $g(x)$, such that is possible to combine together effects over space and time, i.e.

$$y(x,t) = f(t)\,g(x) \tag{3.23}$$

It is possible to find reasonable shape for the function $g(x)$ (see the Section 4.4 in the sequel for more details). Although proper choices can lead to fashionable results, the used forcing term in space strongly influences the evolution of diffusion.

In order to overtake this theoretical deficiency, it is possible to relate the space diffusion to the binding/unbinding phenomenon itself. To this aim, it is worth noting that there exist locations along the membrane at which the ligand is not able to trigger cAMP production because of the lack of active receptors. Henceforth, a statistical parameter $0 \leq \beta(x,t) \leq 1$ is introduced in order to model the chance of getting bounds and, consequently, production of cAMP. With these considerations in mind, the ligand binding function $w(x,t)$ at time t is introduced as follows:

$$w(x,t) = \beta(x,t)\,F(t). \tag{3.24}$$

Henceforth, the forcing term $y(x,t)$ governing the diffusive problem arises as:

$$y(x,t) = \frac{\partial w}{\partial t} = [\beta(x,t)\,F(x,t)]_{,t} = \beta_t(x,t)\,F(t) + \beta(x,t)\,f(t). \tag{3.25}$$

since the relationship $F_t(t) = f(t)$ holds. The statistical parameter β can be also interpreted as the ratio of activated receptor over the maximum number of activable ones ξ_0, i.e.:

$$\beta := \frac{\xi(x,t)}{\xi_0}. \tag{3.26}$$

Bearing in mind the cAMP-to-receptors relationship (3.3), the statistical

71

parameter β can be also computed as follows:

$$\beta(x,t) = \frac{\xi}{\xi_0} = \frac{\xi}{\xi_0}\frac{\alpha_\xi}{\alpha_\xi} = \frac{S(x,t)+C(x,t)}{\alpha_\xi\xi_0} = \frac{S(x,t)+C(x,t)}{(S+C)_{\max}} = \frac{S(x,t)+C(x,t)}{M}$$

$$\beta(x,t) = \frac{S(x,t)+C(x,t)}{M} \tag{3.27}$$

where $S(x,t)$ is the submembranal intracellular cAMP and $C(x,t)$ is the cytosolic intracellular cAMP. The quantity $M := (\text{cAMP}_i)_{\max}$ represents the maximum value of intracellularcAMP measured experimentally by Biondi et al. [18] (see Figure 3.4a). Obviously, the following relationship holds:

$$\xi_0 = \frac{\text{cAMP}_{max}}{\alpha_\xi} \tag{3.28}$$

3.2   Stretching Energy of Cell Membranes

The local stretching energy shown in Chapter 1 has been characterized for a specific temperature of $T = 30°C$ [55, 210]. In this Section dependencies on both temperature and adhesion are considered, and an extended version of the local energy is supplied. The change in energy of the membrane is evaluated starting from the prestressed state, reached by the cell upon adhering to its substrate and prior to the insertion of the ligand into the watery solution of the surrounding medium.

3.2.1   Influence of Temperature and Adhesion

In this Thesis, cells resting on a substrate at fixed value of temperature are considered. It is known that temperature influences the behavior of lipids and, in turn, the membrane stretching energy strictly depends on this value. Indeed, experimental observations [3, 13, 38, 59, 88, 120, 164] show that the composition of the lipid membranes strongly influences the behavior of the stretching energy when the temperature changes. As an example, the compound analyzed by Goldstein and Leibler [88] is such that an increasing temperature causes the lost of the characteristic double-well shape. On the contrary, the lipids composing the membrane studied in
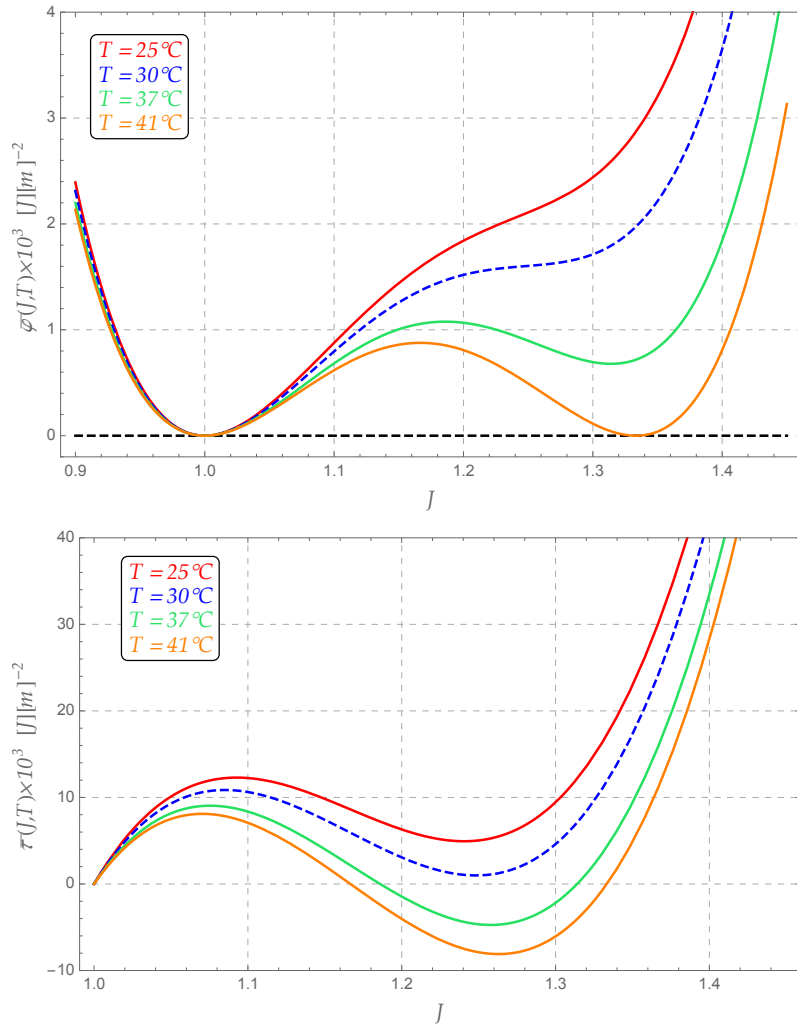
Figure 3.6: Local energy $\bar{\varphi}$ and local stress $\bar{\tau}$ depending on temperature.

this Thesis approaches a double-well energy as the temperature increases. Observations done in laboratory [18, 131] showed that the value $T \approx 41°$ can be assumed as *transition temperature* for the membrane subjected of this research. Based on these considerations, the stretching energy defined in (1.13) (and now denoted by $\varphi^*(J)$ for the sake of illustration) is modified taking into account an extra quadratic term as follows:

$$\bar{\varphi}(J, T) = \varphi^*(J) + A_T (J - 1)^2 . \tag{3.29}$$

Here the dependence on temperature is introduced through the parameter $A_T = \hat{A}(T)$. This dependence was calibrated by considering that the two characteristic wells share the same depth at the transition temperature. As result, it was found that $A_T(41°) = -0.0178 \, J/m^2$, and that the location where the second well occurs is $J = 1.333$. It is worth bearing in mind that the assumption $A_T(30°) = 0$ was done. In Figure 3.6 is shown how the temperature modifies the local stretching energy and the related stress $\bar{\tau}(J) = \bar{\varphi}'(J)$ on the basis of (3.29).

Besides the dependence on temperature, in this work also the dependence on the adhesion with the substrate is accounted for. Indeed, as shown in Figure 3.6(b), the local stress presents compression in correspondence of a stretch greater than 1, for the typical physiological range of temperature of a human body $(36° \div 3t°)$. As known, cell membranes are not able to sustain compression, suggesting that the energy $\bar{\varphi}(J, T)$ is not suitable for the purpose of this Thesis. This fact highlights the importance of introducing also a term depending on the adhesive property. Adhesion of the cells to the substrate of the well is modeled with the introduction of a specific cohesive energy, namely Γ_a, which may vary with temperature and with the stiffness of the substrate. The adhesion energy Γ_a is modeled in the same fashion of temperature dependence, i.e. by introducing a quadratic term as:

$$\Gamma_a(J, T, \hat{\Gamma}) := \frac{1}{2}\hat{\Gamma}(J - 1)^2, \tag{3.30}$$

where the values of $\hat{\Gamma}$ must be determined. The adhesion energy depends on the interaction between the membrane and substrate, and it quantifies

the energy needed to detach one of the two bodies. Sagvolden at al. [180] performed a series of experiments where the value of the adhesion force to detach the cells from the substrate was measured. However, the force-
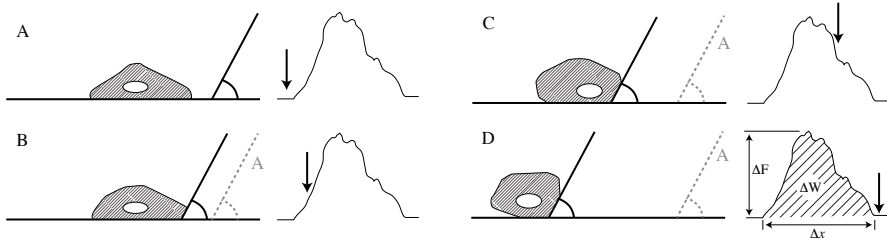
Figure 3.7: Schematic of the measured force in the experiment performed by [180] (cfr. with Figure 2 of the paper).

displacement relationship is not reported, even if the measured force is showed in Figure 3.7. As first approach, the force distribution is considered equivalent to a force acting for all the displacement Δx with half value of the peak, henceforth the adhesion energy is computed by the ratio of the work done by the adhesion force divided by the area of the cell:

$$\hat{\Gamma} = \frac{W}{A} = \frac{1}{2} \frac{F_0 \, \Delta x}{A_p \, J_p^{-2}}, \tag{3.31}$$

where A_p is the area of the membrane in the reference configuration and F_0 is the maximum value of the force applied for detaching it from the substrate. Sagvolden [180] showed that the adhesion is greater at $T = 37 \, ^\circ C$ than at $T = 23 \, ^\circ C$. On the other hand, some experiments [131] showed that adhesion decreases with temperature and it vanishes at $T \approx 40 \, ^\circ C$. Henceforth, it is reasonable to assume a triangular distribution having the higher vertex at $T = 37 \, ^\circ C$, as shown in Figure 3.8. The parameters of the adhesion for the membrane were calibrated by employing both experimental observations and data found in literature. The computed values are reported in Table 3.1.
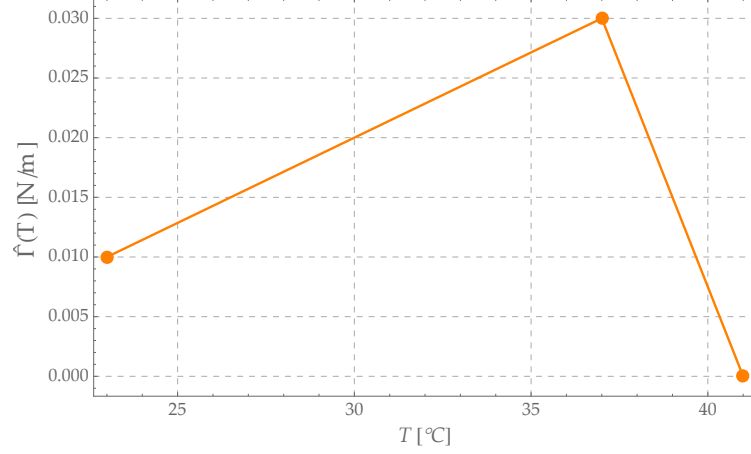
Figure 3.8: Adhesion model.

Table 3.1: Values of $\hat{\Gamma}$ (expressed in $[N/m]$) used for modeling the adhesion between a cell and its substrate.

$T = 23°$	$T = 37°$	$T = 40°$
0.01	0.03	0

3.2.2   Modified stretching energy

The *modified* stretching energy finally comes out by taking into account both the sources of influence considered above, i.e. temperature and adhesion, by means of equation (3.29) and (3.30), respectively. This modification allows the stretching energy to take the following form:

$$
\varphi_T(J, T) = \left[a_0 + A_T(T) + \frac{\hat{\Gamma}(T)}{2} \right] + \left[a_1 - 2\, A_T(T) - \hat{\Gamma}(T) \right] J +
$$
$$
+ \left[a_2 + A_T(T) + \frac{\hat{\Gamma}(T)}{2} \right] J^2 + a_3\, J^3 + a_4\, J^4
$$

$$(3.32)$$

Whenever a temperature T^* is fixed, equation (3.32) allows for computing the actual local energy $\varphi(J)$, the local stress $\tau(J)$ and the transition function $\gamma(J)$ governing the membrane equilibrium as usual:

$$\varphi(J) = \varphi_T(J, T^*) \tag{3.33a}$$

$$\tau(J) = \varphi'(J) \tag{3.33b}$$

$$\gamma(J) = -\frac{h_0^2}{12} \frac{\tau(J)}{J^3} \tag{3.33c}$$

In Figure 3.33 the energetic function (3.33) are displayed made dimensionless with respect to one tenth of Maxwell stress Σ and the square of the membrane height h_0, and at several values of temperature.

3.3 The equilibrium of the membrane

The configurations assumed by the membrane at the equilibrium are governed by the principle of the Minimum of Energy. The total potential energy is obtained as the total Helfrich free energy $\mathcal{H}$, defined by equation (2.9) minus the work $\mathcal{W}$ done by the external load, i.e

$$\mathcal{E} = \mathcal{H} - \mathcal{W}. \tag{3.34}$$

The work $\mathcal{W}$ results from the presence of two entities, a traction Σ acting against the displacement, and a hyperstress Γ acting against the gradient of the displacement, i.e.

$$\mathcal{W} = B \left[\Sigma \, u + \Gamma \, \nabla u \right]_{\partial\Omega}, \tag{3.35}$$

which in the one-dimensional case takes the form:

$$\mathcal{W} = B \left[\Sigma \, u + \Gamma \, u' \right]_{\partial\Omega}, \tag{3.36}$$

where B is the depth of the membrane patch considered.It is clear that the displacement field depends on the space, i.e. $u = \hat{u}(x)$. For the sake of illustration, the the space-dependent argument is omitted. It is worth noting that, thanks to the result addressed in Chapter 2, the change in energy due
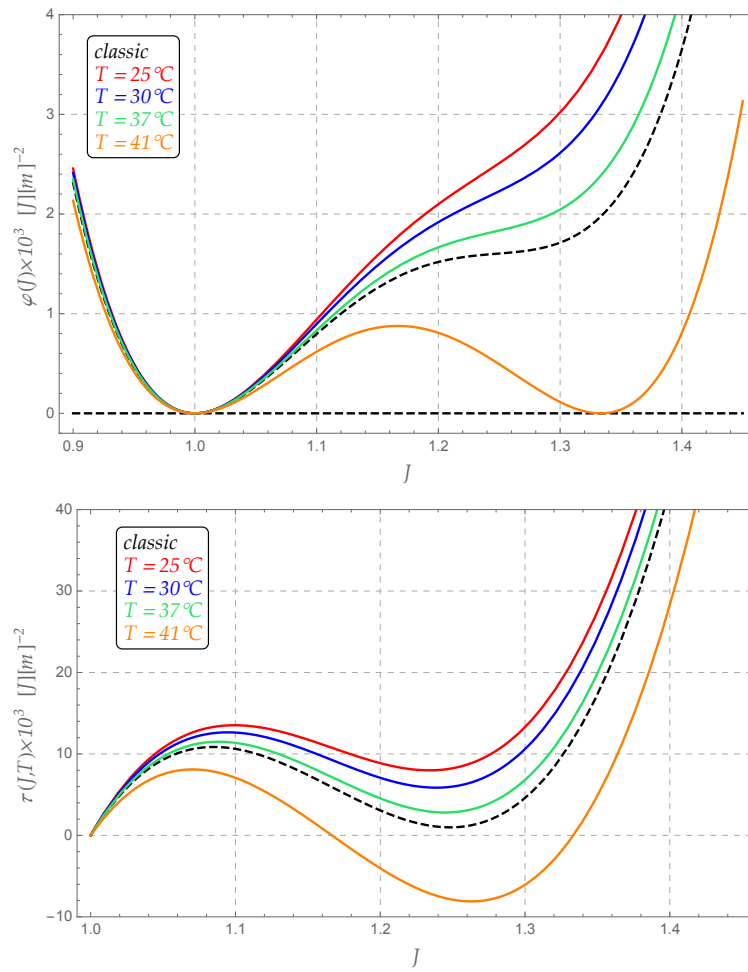
Figure 3.9: The function $\varphi(J)$, $\tau(J)$ and $\gamma(J)$ at $T = 37°C$.

to the conformational field assumes the following form:

$$-\xi\varphi_{CR} = \frac{W(J)}{K_BT}\left(\xi - \xi_0\right) = \frac{\pi d_s q\phi h_0}{K_BT}\left(\frac{1}{J} - 1\right)\left(\xi - \xi_0\right) = \frac{S(\xi)}{K_BT}\left(\frac{1}{J} - 1\right)$$

where $S = \hat{S}(\xi)$ can be interpreted as a *chemical* stress, varying along the membrane, depending on the receptor density only:

$$S(\xi) := \pi\,d_s\,q\,\phi\,h_0\,\left(\xi - \xi_0\right). \tag{3.37}$$

This quantity arises because of the presence of diffusive phenomena due to the change of receptor density. The Euler-Lagrange equation is found by employing the principle of minimum of the energy through the variational derivative in terms of the independent variable of the problem, i.e. the displacement u. For this reason, in the sequel terms not depending on the displacement u are dropped out. Bear in mind that in the 1D case the relationship $J = 1 + u'$ holds. Henceforth, the energy (3.34) in terms of displacement u reads as follows:

$$\mathcal{E} = \int_\Omega \left(\varphi(1 + u') - \frac{1}{2}\gamma(1 + u')u''^2 + S(\xi)\left(\frac{1}{1 + u'} - 1\right)\right)\mathrm{d}x + \tag{3.38}$$
$$- \left[\Sigma\,u + \Gamma\,u'\right]_{\partial\Omega}$$

The variational derivative of the energy (3.38) (see Appendix D.3) supplies the differential equation governing the equilibrium of the membrane:

$$\begin{cases} -A' = 0 & \text{in } \Omega \\ \text{either } A - \Sigma = 0 \text{ or } \delta u = 0 & \text{in } \partial\Omega \\ \text{either } \gamma\,u'' + \Gamma = 0 \text{ or } \delta u' = 0 & \text{in } \partial\Omega \end{cases} \tag{3.39}$$

where:

$$A = \varphi' + \frac{1}{2}\gamma'u''^2 + \gamma u''' - \frac{S(\xi)}{(1 + u')^2}. \tag{3.40}$$

Equation (3.39) delivers a fourth order differential equation, whose solution provides the response of the cell membrane under the specified boundary conditions. Finally, the fourth order differential equation governing the

equilibrium of the membrane assumes the following form:

$$\gamma u'''' + 2\gamma' u'' u''' + \frac{1}{2}\gamma'' u''^3 + \varphi'' u'' + \frac{2S(\xi)\,u''}{(1+u')^3} - \frac{S'(\xi)}{(1+u')^2} = 0 \quad (3.41)$$

and boundary conditions:

$$\gamma u''' + \frac{1}{2}\gamma' u''^2 + \varphi' = \Sigma + \frac{S}{(1+u')^2}. \quad (3.42)$$

Note that in equation (3.41) the prime denotes derivation with respect to the space variable.

3.4 Chemo-mechanical coupling: Kinetics of binding

Previously in this Chapter, diffusive and mechanical phenomena were modeled independently each other. For this reason, ad first approach it seems to be reasonable developing a numerical scheme in which these two physics still remain separate (see Section4.4 for details). Although the results obtained from this kind of simulations seem to be in agreement with the experimental evidence, this lack of coupling is not satisfactory.

Indeed, it would appear more natural that the diffusive evolution would be driven by association/dissociation of ligand binding. For this reason, the use of the model for the diffusion over space and time related to a statistical parameters introduced in Section 3.1.3 would be more efficient. Moreover, beside this source of influence during the time evolution, the receptor density changes because of the change in the chemical potential (2.16) μ_{RL}:

$$\frac{\mu_{RL}}{K_B T} = \frac{\mu_{RL}^0}{K_B T} + \ln\left(\frac{\xi}{\xi_0}\right) + \frac{\mathcal{W}(J)}{K_B T}.$$

A closer analysis of this relationship shows that the chemical potential itself is influenced by both the mechanics (through the current stretch J) and the receptor density ξ. It is then clear that a more sophisticated update scheme can be developed for performing reliable numerical simulations. In

this regard, it turns out be incisive the use of a kinetic relationship in the same fashion of one discussed in [158] about the kinetics of focal adhesion. By taking inspiration from this model, the following kinetic relationship is considered:

$$
\xi_t = \begin{cases} k_b\,\xi\,\left(1 - \exp\left[\dfrac{\mu_{RL}}{K_B\,T}\right]\right) & \text{if } \mu_{RL} < 0 \\[3mm] k_u\,\xi\,\mathcal{U}\left(\exp\left[-\dfrac{\mu_{RL}}{K_B\,T}\right] - 1\right) & \text{if } \mu_{RL} > 0 \end{cases}
\tag{3.43}
$$

where k_b and k_u represent the binding and unbinding constant, respectively, and U represents an unbinding chemical configurational force rate per unit of $K_B\,T$ and per unit of active receptors density. Note that the employee of relationship (3.43) is proved numerically to be an essential requirement for the right and effective evolution of the simulation (see Chapter 4). Indeed, since the forcing term is modeled by means (3.25), there would not be any chance to obtain a negative time derivative for decreasing the action of the epinephrine.

References

[3]   A. Agrawal and D. Steigmann. "Coexistent Fluid-Phase Equilibria in Biomembranes with Bending Elasticity". *Journal of Elasticity* 93.1 (2008), pp. 63–80 (cit. on pp. 1, 4, 72).

[13] T. Baumgart et al. "Membrane Elasticity in Giant Vesicles with Fluid Phase Coexistence". *Biophysical Journal* 89 (2005), pp. 1067–1080 (cit. on pp. 1, 4, 72).

[18] C. Biondi et al. "cAMP efflux from human trophoblast cell lines: a role for multidrug resistance protein (MRP) 1 transporter". *Molecular Human Reproduction* 16.7 (2010), pp. 481–91 (cit. on pp. 3, 63–66, 72, 74, 87).

[22] B. Brown, R. Ekins, and J. Albano. "Saturation assay for cyclic AMP using endogenous binding protein." *Advances in Cyclic Nucleotide Research* 2 (1972), pp. 25–40 (cit. on p. 63).

[38] S. Das, A. Tian, and T. Baumgart. "Mechanical Stability of Micropipet-Aspirated Giant Vesicles with Fluid Phase Coexistence". *The Journal of Physical Chemistry B* 112.11625Ð11630 (2008) (cit. on pp. 1, 4, 72).

[55] L. Deseri and G. Zurlo. "The stretching elasticity of biomembranes determines their line tension and bending rigidity". *Biomechanics and Modeling in Mechanobiology* 12 (2013), pp. 1233–1242. DOI: `doi: 10.1007/s10237-013-0478-z` (cit. on pp. iii, iv, 1, 4, 23–26, 30, 40, 72, 153, 154, 168, 193).

[59] M. Deserno. "Fluid lipid membranes: From differential geometry to curvature stresses". *Chemistry and Physics of Lipids* 185 (2014), pp. 11–45 (cit. on pp. iii, 4, 22, 23, 72).

[88] R. Goldstein and S. Leibler. "Structural phase transitions of interacting membranes". *Physical Review Letters A* 40.2 (1989), pp. 1025–1035 (cit. on pp. 2, 4, 25, 27, 28, 72).

[120] S. Komura et al. "Lateral phase separation in mixtures of lipids and cholesterol". *Europhysics Letters* 67.2 (2004), p. 321 (cit. on pp. 4, 27, 72).

[131] L. Lunghi et al. "Control of human trophoblast function". *Reproductive biology and endocrinology : RB&E* 5 (2007), p. 6. ISSN: 1477-7827. DOI: `10.1186/1477-7827-5-6` (cit. on pp. 3, 74, 75).

[158] J. E. Olberding et al. "The non-equilibrium thermodynamics and kinetics of focal adhesion dynamics". *PLoS ONE* 5.8 (2010), e12043 (cit. on pp. 68, 81).

[164] J. Owicki, M. Springgate, and H. McConnell. "Theoretical study of protein-lipid interactions in bilayer membranes". *PNAS* 75 (1978), pp. 1616–1619 (cit. on pp. 4, 25, 27, 72).

[180] G. Sagvolden et al. "Cell adhesion force microscopy". *PNAS* 96 (1999), pp. 471–476. URL: `http://www.ncbi.nlm.nih.gov/entrez/query.fcgi?cmd=Retrieve%5C&db=PubMed%5C&dopt=Citation%5C&list%5C_uids=9892657` (cit. on p. 75).

[205]   M. Xie et al. "Inactivation of multidrug resistance proteins disrupts
        both cellular extrusion and intracellular degradation of cAMP". *Molec-
        ular Pharmacology* 80 (2011), pp. 281–293 (cit. on pp. 62, 63, 67,
        86).

[210]   G. Zurlo. "Material and geometric phase transitions in biological
        membranes". PhD thesis. Doctorate of Philosophy in Structural En-
        gineering, University of Pisa, 2006 (cit. on pp. iii, 1, 4, 23, 25, 27, 40,
        72).

Chapter 4

Numerical simulations for getting balanced configurations

This Chapter is devoted to illustrate the numerical procedure developed for performing numerical simulations regarding the model analyzed in this Thesis. Each employed numerical scheme is reported and supplied with comments and coding remarks. For the sake of illustration, the following notation will be used in the sequel:

– bold capital letters, as $\mathbf{A}$, denote matrices;

– capital letters, as A, denote vectors;

– small letters, as $f(x)$, denote functions;

– small letters with a subscript, as f_i, denote discrete values of a function $f(x)$.

Whenever this notation is not used, it will be clearly declared.

In the sequel, the Finite Differences are employed for discretizing differential equations. Second order accurate central schemes are used in this Thesis up to the fourth derivative. Let consider a space discretization, also known as mesh, and denote with x_i the points of the mesh and with Δx the (constant) discrete difference between two neighboring points, and let be $f(x)$ a continuous function and f_i its values at meshpoints. Then, the

central finite difference schemes for computing derivatives at the generic point x_i take the forms:

$$f'(x_i) \approx \frac{1}{2\,\Delta x}\left(f_{i+1} - f_{i-1}\right) \tag{4.1a}$$

$$f''(x_i) \approx \frac{1}{\Delta x^2}\left(f_{i+1} - 2f_i + f_{i-1}\right) \tag{4.1b}$$

$$f'''(x_i) \approx \frac{1}{\Delta x^3}\left(\frac{f_{i+2}}{2} - f_{i+1} + f_{i-1} - \frac{f_{i-2}}{2}\right) \tag{4.1c}$$

$$f''''(x_i) \approx \frac{1}{\Delta x^4}\left(f_{i+2} - 4f_{i+1} + 6f_i - 4f_{i-1} + f_{i-2}\right) \tag{4.1d}$$

Relationships (4.1) allow for computing derivatives as linear operations by mean of proper matrices. In the sequel, these *differential* matrices will be denoted by the letter $\mathbf{D}$ followed by the order of differentiation, e.g. $\mathbf{D}_2$ denotes the operator for getting the second derivative of a vector representing discrete values at meshpoints of a given function. Just as example, if this vector is denoted by F, the discrete values of the second derivative at the same meshpoints are found through the linear operation $\mathbf{D}_2 \cdot F$. Obviously, these operators are more accurate as smaller is the distance Δx between two discrete points x_i. The accuracy of these operations is limited at edges: for this reason, higher order approximation are needed for preserving second order accuracy at the boundary of the domain (see Appendix E). In Matlab, a specific function called `funFD1S` is coded (see Appendix E) for computing these operators up to order 4. Note that sparse matrices are employed for optimization purposes.

4.1 Average Diffusion

In this Section the average diffusion related to the model presented in equation (3.6) is studied. The model consists of a set of three linear ODEs, representing the cAMP production and ejection between the three compartments used for modeling the cell structure (see Figure 3.2).

The action of the epinephrine is modeled by means of relationship (3.20). The values found in [205], reported in Table 4.1 were used as starting point for determining the best coefficients ω_{ij} for fitting the experimental curves

obtained from [18]. The diffusive problem is solved by coding an *implicit* scheme. Indeed, a classical forward Euler march scheme is employed for the time derivative, whereas a central finite difference scheme (see relationships (4.1)) is used for discretizing the space derivatives. Let denote with S, C and Z the variables containing discrete values of submembranal, cytosolic and extracellular cAMP over the time, respectively, with U the vector containing the unknown functions, and with F the forcing vector, i.e. $F = [f(t_i), 0, 0]^T$. Then the ODE system is solved by employing the following numerical scheme between two subsequent time steps (e.g. t_n and t_{n+1}):

$$\frac{U^{n+1} - U^n}{\Delta t} = \mathbf{K}\, U^{n+1} + F$$

$$U^{n+1}\,(\mathbf{I} - \Delta t\,\mathbf{K}) = U^n + \Delta t\,F \tag{4.2}$$

where

$$\mathbf{K} \;=\; \begin{bmatrix} (\omega_{11} + \omega_{12} + \omega_{13}) & -\omega_{12} & -\omega_{13} \\ -\omega_{21} & \omega_{21} & 0 \\ -\omega_{31} & 0 & \omega_{31} \end{bmatrix} \tag{4.3}$$

and Δt is the timestep increment of the discrete time-spanning. It is worth noting that $\mathbf{K}$ is not symmetric. Several simulations have been run by changing the values of coefficients ω_{ij} through proportional coefficients w_{ij}, in such a way the effective coefficients ODE systems are expressed as $w_{ij}\,\omega_{ij}$. The best result of this numerical simulation is shown in Figure 4.1: the experimental data taken from [18] are represented by green squares, whereas the solid curves represent the numerical solution of the cAMP diffusion. The intracellular cAMP is denoted by the color blue, and it is in good agreement with the experimental data, suggesting the well behavior of the model. The extracellular cAMP, instead, is denoted by the color red, and it is an always increasing function accordingly to the experimental result (although, as wrote in [18], no data about its values are shown in the reference paper). The influences of the *proportional* coefficients w_{ij} are shown in Figure 4.2.
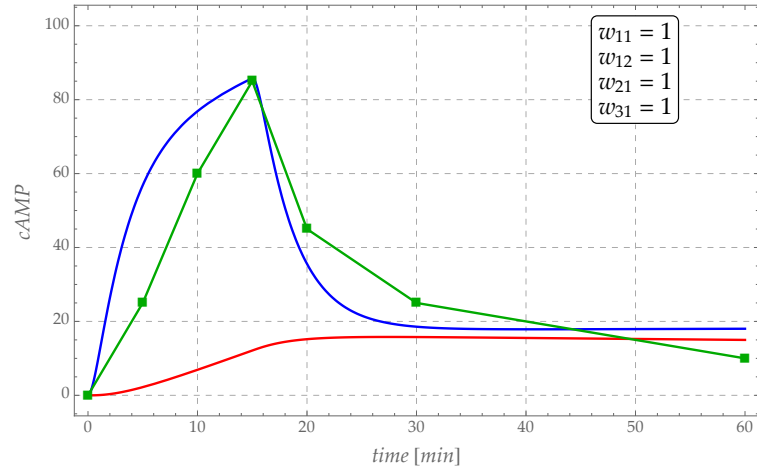
Figure 4.1: Result of numerical simulation on average diffusion.
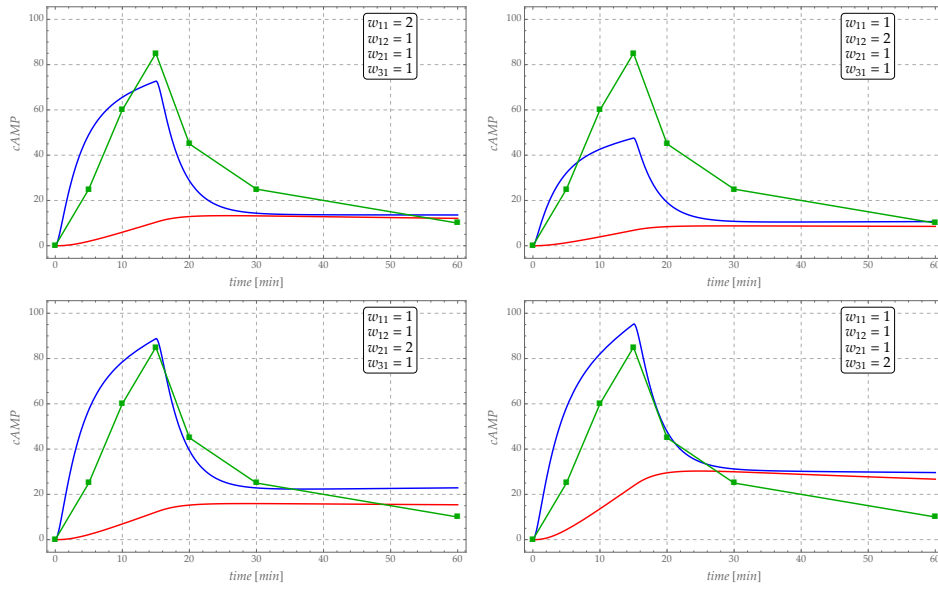
Figure 4.2: Simulation results depending on coefficients w_{ij} (see Table 4.2).

Table 4.1: Starting guess values for determining the coefficients ω_{ij} of the model in (3.6).

J_{sc}	J_{se}	V_s	V_c	V_e	ω_{11}	ω_{12}	ω_{21}	ω_{31}
$\left[\frac{pL}{min}\right]$			$[pL]$				$[min]^{-1}$	
0.006	0.03	0.02	2	2.02	0.3	1.5	3×10^{-3}	0.0148

Table 4.2: Simulation coefficients w_{ij}.

sim	w_{11}	w_{12}	w_{21}	w_{31}
Sim 1a	1	1	1	1
Sim 1b	2	1	1	1
Sim 1c	1	2	1	1
Sim 1d	1	1	2	1
Sim 1e	1	1	1	2

4.2 The equilibrium of the membrane

The membrane balanced configurations in the set of equilibria studied in this Thesis are regulated by a strongly nonlinear fourth order ODE (3.41), and it has been derived by means of the principle of the minimum energy and the variational derivative as:

$$-A = \gamma u'''' + 2\gamma' u'' u''' + \frac{1}{2}\gamma'' u''^3 + \varphi'' u'' + \frac{2S\, u''}{(1+u')^3} - \frac{S'}{(1+u')^2} = 0.$$

The solution of this governing differential equation at each discrete time during the simulation evolution allows for finding the configuration that minimize the energy and, hence, the specific profile sustaining the stress acting along the lipid membrane. The nonlinear fourth-order Euler-Lagrange equation is very hard to be solved directly, then in this Thesis two different workarounds are taken into consideration: (a) a Gradient Flow (GF) scheme and (b) a linear approximation around a known balanced configuration.

89

4.2.1 The gradient flow scheme

The basic idea beyond a gradient flow scheme is looking for a (local) minimum by following the negative direction suggested by the gradient in the *current* configuration. By employing the properties of the inner product in a specified space, a partial differential equation to be solved arises. A fake running time is employed for computing the flow until a null values is reached, i.e until relationship (3.41) is satisfied. This workaround allows for approaching the sought configuration thanks to this fictitious flow. For numerical purpose, the flow is assumed to get zero value whenever a certain tolerance *tol* is reached, i.e. $|u_t| < tol$. Two numerical schemes have been developed depending on the norm used for computing the time derivative, i.e either L_2 or H_2 norm. In literature, it has been shown [206, 207] that the latter improves the velocity of convergence and the stability of the algorithm because the possible numerical error due to 4th order derivative approximation.

■ **Norm L_2.** In order to set up the the numerical scheme in L_2 norm, a weak characterization of the energy (3.38) is imposed, i.e.

$$\langle u_t \,,\, v \rangle_{L_2} = -\langle \mathcal{E}'[u] \,,\, v \rangle \tag{4.4}$$

where $\mathcal{E}[u]$ is the energy functional written in terms of the displacement $u(x,t)$, and $\mathcal{E}'[u]$ denotes the variational derivation of the energy. Relationship (4.4) can be also represented in integral form as:

$$\int_\Omega \dot{u}\, v \,\mathrm{d}x = -\int_\Omega \frac{\delta \mathcal{E}}{\delta u}\, v \,\mathrm{d}x \qquad \forall v \in L^2 \tag{4.5}$$

Integrating by part equation (4.5), the gradient flow relationship arises in the form:

$$\dot{u} = -A' \tag{4.6}$$

Basically, the workaround strategy consists in solving the above partial differential equation. For stability purpose, the numerical scheme is developed by introducing as unknown also the second derivative with respect to the

space of the displacement field, namely $w(x)$, i.e.

$$
\begin{cases}
u'' = w \\
\dot{u} = \gamma\, w'' + 2\gamma'\, w\, w' + \frac{1}{2}\gamma''\, w^3 + \varphi''\, w + \dfrac{2S(\xi)\, w}{J^3} - \dfrac{S'(\xi)}{J^2}
\end{cases}
\tag{4.7}
$$

A semi-implicit scheme is used by means of Finite Differences and all the nonlinearities are removed by computing their values at the previous timestep. By considering two subsequent timesteps, namely t_n and t_{n+1}, the following numerical scheme was coded:

$$
\begin{bmatrix} \mathbf{I} & \mathbf{K}_{12} \\ -\mathbf{D_2} & \mathbf{I} \end{bmatrix}
\begin{pmatrix} \mathbf{U}_{n+1} \\ W_{n+1} \end{pmatrix}
= \begin{pmatrix} U_n - \Delta t\, \dfrac{\mathbf{S}_n^{(1)}}{\mathbf{J}_n^2} \\ \mathbf{0} \end{pmatrix}
\tag{4.8}
$$

and

$$
\mathbf{K}_{12} = -\,\mathbf{I} + \Delta t\left[-\,\boldsymbol{\gamma}_n^{(0)}\, D_2 - 2\boldsymbol{\gamma}_n^{(1)}\,(D_1 \cdot W_n) + \right.
$$
$$
\left. \frac{1}{2}\boldsymbol{\gamma}_n^{(2)}\, W_n^2 - \boldsymbol{\varphi}_n^{(2)} - 2\frac{\mathbf{S}_n^{(0)}}{\mathbf{J}_n^3} \right]
\tag{4.9}
$$

where the subscripts $_j$ are referred to the timestep, the apex $^{(j)}$ denotes the jth derivative of the function with respect to its own argument and Δt is the discretized fake-time increment. The energetic functions $\gamma(J)$ and $\varphi(J)$ are evaluated at the time step t_n, then $\boldsymbol{\gamma}_n^{(0)}$ denotes the vector containing the values of $\gamma(J)$ at each meshpoint by using the configuration U_n; the same notation holds for all the other functions.

■ **Norm H_2.** As shown above, also the numerical scheme employing the H_2 norm is based on finding a week formulation, i.e.

$$
\langle u_t\,,v\rangle_{H_2} = -\langle \mathcal{E}'[u]\,,v\rangle
\tag{4.10}
$$

91

or in integral form as:

$$\int_{\Omega} \left(c_0 \, \dot{u} \, v + c_1 \, \dot{u}' \, v' + c_2 \, \dot{u}'' \, v'' + \right) \mathrm{d}x = - \int_{\Omega} \frac{\delta \mathcal{E}}{\delta u} \, v \, \mathrm{d}x \qquad \forall v \in H^2 \quad (4.11)$$

where c_0, c_1 and c_2 are non-negative weights of the space derivative of the rate of change. Again, integration by parts supplies the sought partial differential equation to be solved as:

$$c_0 \dot{u} - c_1 \dot{u}'' + c_2 \dot{u}'''' = -A' \qquad (4.12)$$

The opportunity to develop a H_2-based gradient flow is due to the requirement for CFL stability of the scheme, since in presence of forward time-stepping the standard L_2 norm requires very small timestep size. The use of the H_2 norm allows for arising a fourth order terms on the LHS of (4.11) that in some sense cancels out the numerical instability due to fourth order term on the RHS. Bearing in mind the position (4.7), the discrete numerical scheme takes the form:

$$\begin{bmatrix} c_0 \, \mathbf{I} & \mathbf{K}_{12}^* \\ -\mathbf{D}_2 & \mathbf{I} \end{bmatrix} \begin{pmatrix} U_{n+1} \\ W_{n+1} \end{pmatrix} = \begin{bmatrix} c_0 \, \mathbf{I} & -c_1 \mathbf{I} + c_2 \mathbf{D}_2 \\ 0 & 0 \end{bmatrix} \begin{pmatrix} U_n \\ W_n \end{pmatrix} +$$

$$+ \Delta t \begin{pmatrix} -\dfrac{\mathbf{S}_n'(x)}{\mathbf{J}_n^2} \\ 0 \end{pmatrix} \qquad (4.13)$$

and

$$\mathbf{K}_{12}^* = -c_1 \, \mathbf{I} + c_2 \, \mathbf{D}_2 + \Delta t \Big(- \gamma_n^{(0)} \mathbf{I} \, \mathbf{D}_2 - 2(\gamma_n^{(1)} \, \mathbf{D}_1) \cdot \mathbf{I} +$$

$$- \frac{1}{2}(\gamma_n^{(2)} W_n^2) \cdot \mathbf{I} - \varphi_n^{(2)} \, \mathbf{I} - \frac{2 \, \mathbf{S}_n}{\mathbf{J}_n^3} \, \mathbf{I} \Big) \qquad (4.14)$$

4.2.2 Linearized equation

Beside the gradient flow schemes shown above, a strategy employing a linearized equation (3.41) can be very useful in terms of CPU cost and simulation time. Indeed, the focus of the simulation is the time evolution of the balanced configuration depending on the chemical processes related

to cAMP diffusion. Under the hypothesis of the minimum of the energy, it is possible to assume that the balanced geometrical configuration does not change so much between two discrete timesteps, if they are close enough. Let denote by $\overline{\Omega}$ a balanced configuration at time $\bar{t}$, and assume that the difference with the next balanced configuration at time t, namely Ω, is small enough. Then this difference can be interpreted as a perturbation, i.e.

$$\begin{cases} u = \bar{u} + v \\ J = \bar{J} + \varepsilon \end{cases}$$

where, for a 1D case, $\bar{J} = 1 + \bar{u}'$, $v = u - \bar{u}$ and $\varepsilon = v' = J - \bar{J}$. Let recall the fourth order equation (3.41) to be solved, i.e.

$$\gamma u'''' + 2\gamma' u'' u''' + \frac{1}{2}\gamma'' u''^3 + \varphi'' u'' + \frac{2S\,u''}{(1+u')^3} - \frac{S'}{(1+u')^2} = 0,$$

focus the attention on the first term of the equation and linearize it:

$$\begin{aligned} \gamma(J)u'''' &= \left(\gamma(\bar{J}) + \frac{\partial\gamma(J)}{\partial J}\Big|_{\overline{\Omega}}(J - \bar{J})\right)(\bar{u} + v)'''' \\ &= \left(\bar{\gamma} + \bar{\gamma}'\,v'\right)\left(\bar{u}'''' + v''''\right) \\ &= \bar{\gamma}\,\bar{u}'''' + \bar{\gamma}\,v'''' + \bar{\gamma}'\,\bar{u}''''\,v' + \bar{\gamma}'\,v'\,v'''' \\ &\approx \bar{\gamma}\,\bar{u}'''' + \bar{\gamma}'\,\bar{u}''''\,v' + \bar{\gamma}\,v'''' \end{aligned} \qquad (4.15)$$

At the last line the approximation symbol ($\approx$) is introduced because all the higher-order (infinitesimal) terms do not give significant contributions ans by dropping out all the nonlinearities. The same procedure can be applied to the other terms, i.e.

$$\gamma'(J)u''\,u''' = \left(\gamma'(\bar{J}) + \gamma''(\bar{J})\,v'\right)\left(\bar{u}'' + v''\right)\left(\bar{u}''' + v'''\right)$$
$$\gamma''(J)u''^3 = \left(\gamma''(\bar{J}) + \gamma'''(\bar{J})\,v'\right)\left(\bar{u}'' + v''\right)^3$$
$$\varphi''(J)u'' = \left(\varphi''(\bar{J}) + \varphi''(\bar{J})\,v'\right)\left(\bar{u}'' + v''\right)$$

93

and

$$\gamma'(J)u''\,u''' \approx \bar\gamma'\,\bar u''\bar u''' + \bar\gamma''\bar u''\bar u'''v' + \bar\gamma'\,\bar u'''\,v'' + \bar\gamma'\,\bar u''\,v''' \tag{4.17a}$$

$$\gamma''(J)u''^3 \approx \bar\gamma''\,\bar u''^3 + \bar\gamma'''\,\bar u''^3\,v' + 3\bar\gamma''\,\bar u''^2\,v'' \tag{4.17b}$$

$$\varphi''(J)u'' \approx \bar u''\bar\varphi'' + \bar\varphi'''\,\bar u''v' + \bar\varphi''v'' \tag{4.17c}$$

where bar functions denote quantities evaluated in correspondence on the previous balanced configuration $\bar\Omega$, i.e. $\gamma\left(\bar J\right) := \bar\gamma$. Let now consider the Taylor expansion around the configuration $\bar\Omega$ of the last two terms:

$$\begin{aligned}
\frac{u''}{(1+u')^3} &\approx \frac{u''}{(1+u')^3}\Big|_{\bar\Omega} + \frac{\partial}{\partial u'}\left[\frac{u''}{(1+u')^3}\right]_{\bar\Omega_0}(u'-\bar u')+ \\
&\qquad\qquad + \frac{\partial}{\partial u''}\left[\frac{u''}{(1+u')^3}\right]_{\bar\Omega}(u''-\bar u'') \\
&\approx \frac{\bar u''}{(1+\bar u')^3} - \frac{3\,\bar u''}{(1+\bar u')^4}\cdot v' + \frac{1}{(1+\bar u')^3}\cdot v''
\end{aligned} \tag{4.18}$$

$$\begin{aligned}
\frac{1}{(1+u')^2} &\approx \frac{1}{(1+u')^2}\Big|_{\bar\Omega_0} + \frac{\partial}{\partial u'}\left[\frac{1}{(1+u')^2}\right]_{\bar\Omega}(u'-\bar u') \\
&\approx \frac{1}{(1+\bar u')^2} - \frac{2}{(1+\bar u')^3}\cdot v'.
\end{aligned} \tag{4.19}$$

Finally, the (easier) linear fourth order BVP governing the balance configuration is found by considering all the linear terms obtained above:

$$\begin{cases}
b_4(x)\,v'''' + b_3(x)\,v''' + b_2(x)\,v'' + b_1(x)\,v' + b_0(x)\,v + q_0(x) = 0 \\
v(\partial\Omega) = 0 \\
v''(\partial\Omega) = 0,
\end{cases} \tag{4.20}$$

where:

$$b_4(x) = \bar{\gamma}, \tag{4.21a}$$

$$b_3(x) = 2(\bar{\gamma}'\,\bar{u}''), \tag{4.21b}$$

$$b_2(x) = 2(\bar{\gamma}'\,\bar{u}''') + \frac{1}{2}\left(3\bar{\gamma}''\,\bar{u}''^2\right) + \bar{\varphi}'' + 2\,S(x)\frac{1}{(1+\bar{u}')^3}, \tag{4.21c}$$

$$b_1(x) = \bar{\gamma}'\,\bar{u}'''' + 2(\bar{\gamma}''\bar{u}''\bar{u}''') + \frac{1}{2}\left(\bar{\gamma}'''\,\bar{u}''^3\right) + \bar{\varphi}'''\,\bar{u}'' +$$
$$- 2\,S(x)\frac{3\,\bar{u}''}{(1+\bar{u}')^4} + S'(x)\frac{2}{(1+\bar{u}')^3}, \tag{4.21d}$$

$$b_0(x) = 0 \tag{4.21e}$$

$$q_0(x) = \bar{\gamma}\,\bar{u}'''' + 2(\bar{\gamma}'\,\bar{u}''\bar{u}''') + \frac{1}{2}\left(\bar{\gamma}''\,\bar{u}''^3\right) + \bar{u}''\bar{\varphi}'' +$$
$$+ \left(\frac{2S(x)\,\bar{u}''}{(1+\bar{u}')^3} - \frac{S'(x)}{(1+\bar{u}')^2}\right). \tag{4.21f}$$

Note that the variable coefficients $b_i(x)$ are known whenever the configuration $\overline{\Omega}$ is chosen, and they depend on $\overline{\Omega}$ only. Hence, they must be computed at each timestep. The (hard) numerical solution of the nonlinear problem (3.41) is then reduced to solve the (easy) linear problem (4.20). This result implies that during the simulation only the following linear system must be solved:

$$\mathbf{M}\,U = Q \tag{4.22}$$

where Q is a vector acting as free term, and the coefficient matrix $\mathbf{M}$ is defined as follows:

$$\mathbf{M} = \mathbf{B}_4 \cdot \mathbf{D}_4 + \mathbf{B}_3 \cdot \mathbf{D}_3 + \mathbf{B}_2 \cdot \mathbf{D}_2 + \mathbf{B}_1 \cdot \mathbf{D}_1, \tag{4.23}$$

where $\mathbf{B}_i$ are matrices related to the space discretization regarding the varibale coefficients $b_i(x)$, and $\mathbf{D}_i$ are the Finite Differences operators introduced at the begin of this Chapter.

4.3 Initial Configuration

This Section is devoted to explain how each of the simulation run in the sequel has been initialized. Independently of the kind of numerical simulation procedure employed, the initial configuration is computed at the very beginning. At the initial step, namely t_0 for all simulations, diffusive phenomena are not already started, then the chemical stress is assumed to be dependent on the initial amount of receptors along the membrane only; simultaneously the mechanical stress at the edges due to the presence of the surrounding is present (and it will remain constant during all the simulation). The procedure here presented and summarized can be assumed as the **Step 0** for each simulation, i.e. how to compute the initial configuration of the membrane before that all the subsequent phenomena (receptor diffusion and evolution towards mechanical equilibrium) occur.

Just before to start, temperature and adhesive properties are chosen: in such a way, it is possible to fix stretching energy and compute all the quantities of interest, defined accordingly to notation used by Coleman [31]: the Maxwell stress Σ_M (by means of the equal-area-rule), the place of the maximum of local stress J_{max}, the place of the minimum of local stress J_{min}, the local maximum of the local stress Σ_{max} and the local minimum Σ_{min}, the places at which the Maxwell stress meets the local stress function $\tau(J)$, namely J_*, J_m and J^*, respectively. The energetic functions $\varphi(J)$ and $\gamma(J)$ are then made dimensionless by using a factor $d = \Sigma_M/10$ and a rescaling parameter $h_0^{(p)}$ of the domain is introduced (typically of order $\sqrt{10^5}$) such that

$$h_0 = h_0^{(r)} \, h_0^{(p)} \tag{4.24}$$

Dimensionless functions are used in order to get numerical stability, whereas the reason of introducing a scale parameter $h_0^{(p)}$ is to reduce the computational cost. The use of a value $h_0^{(p)} = \sqrt{10^5}$ implies that the considered domain becomes ~ 300 times smaller of the real one.

The presence of a constant mechanical stress induces the nucleation of raft, as suggested by the local energy itself. This means that the profile of the stretch $J(x)$ at time $t = 0$ is assumed to be not flat. In order to get this initial profile, a gradient flow scheme is used, using as starting stretch configuration a function profile built in such a way a perturbation is

applied to a constant value. This choice is driven by the will to move from a unstable configuration towards natural raft formation. The perturbation, namely $\mu(x)$, must satisfy the boundary conditions: therefore, both the first derivative of $\mu(x)$ and the value of the function must be zero at the edge. A function of the following form has been used:

$$\mu(x) = \frac{1}{2A_p}\left(1 - \cos\left(\pi\, n_p \frac{x - x_a}{x_b - x_a}\right)\right) \tag{4.25}$$

where A_p and n_p are parameters for governing the shape of the perturbation, and x_a and x_b are the edges of the 1D-domain (e.g. $x_a = -L/2$ and $x_b = +L/2$). It would be worth noting that $\langle\mu\rangle \neq 0$. The starting configuration $J_i(x)$ from which run the GF scheme is then chosen as:

$$J_i(x) = J_m + \mu(x) \tag{4.26}$$

where J_m is the unstable intersection between the local stress and the mechanical stress at the boundary. The second of relationship (3.39) allows for computing the stretch at the edges in terms of displacement:

$$\gamma(u')u''' + \frac{1}{2}\gamma'(u')u''^2 + \varphi'(u') = \Sigma + \frac{S(\xi)}{(1+u')^2},$$

or, in terms of stretch (for the 1D case) as:

$$\gamma(u')J'' + \frac{1}{2}\gamma'(u')J'^2 + \varphi'(u') = \Sigma + \frac{S(\xi)}{J^2},$$

where the term Σ is to be intended as the prestress at edges, i.e. $\Sigma = \Sigma_P$. Bearing in mind that the boundary conditions impose $J' = 0$ (since the hyperstress $\Gamma = 0$), the computation of the stress at edges is simplified as:

$$\gamma(J)\, J'' + \varphi'(J) = \left[\Sigma_P + \frac{S}{J^2}\right]_{\partial\Omega} \tag{4.27}$$

The stress is known, but an uncertainty remains around J''. It is easy to recognize that $J''(\partial\Omega) = \mu''(\partial\Omega)$. This observation is used for finding this unknown value. Finally, the nonlinear equation (4.27) can be solved

97

numerically at both edges, by assuming J_m as starting guess point. Whenever the value of J at edges is computed, namely J_a and J_b respectively, the *starting stretch configuration* $J_s(x)$ for the GF is computed by employing a suitable function $s(x)$ and the perturbation $\mu(x)$ itself:

$$s(x) = J_a + (J_b - J_a) \frac{1}{1 + \exp\left[-B\left(2\frac{x-X_1}{X_2-X_1} - 1\right)\right]}, \qquad (4.28a)$$

$$J_s(x) = s(x) + \mu(x). \qquad (4.28b)$$

It is worth noting that the assumption $B \geq 50$ allows for having $J'_s(\partial\Omega) \approx J''_s(\partial\Omega) \approx 0$. The *starting displacement configuration* $U_s(x)$ is instead computed by recalling the relationship between stretch and displacement in the 1D case:

$$U_s(x) = \int (J_s(x) - 1)\,\mathrm{d}x + C_0, \qquad (4.29)$$

where the constant C_0 is chosen such that $u(x_m) = 0$, and $x_m = (x_1 + x_2)/2$ is the middle point of the domain (typically $x_m = 0$).

In Figure 4.3 initial configurations obtained by spanning values of the initial (dimensionless) prestress Σ_P from $S_{\min} = 4.73$ to $S_{\max} = 15.27$, with increment of 1 unit of dimensionless stress, are shown. The initial configurations are computed by employing a gradient flow scheme. A closer analysis of the stretch profiles highlights that higher values of stress determine an higher number of rafts (oscillations) in the same reference region $\Omega = [-\frac{L}{2}, +\frac{L}{2}]$. The *numerical* statics about number of GF loops and time are shown in Figure 4.4 as decimal logarithm. As average, 88789 loops (in 455 sec) are required for determining a configuration. A closer analysis of these graphical statics show that there is a quite proportional ratio between time consumed and number of loops, although it is possible to note that the code required more time for each loop whenever the stress values is just below the Maxwell stress (`SP = 7-8`)

98

Figure 4.3: Initial configurations

99
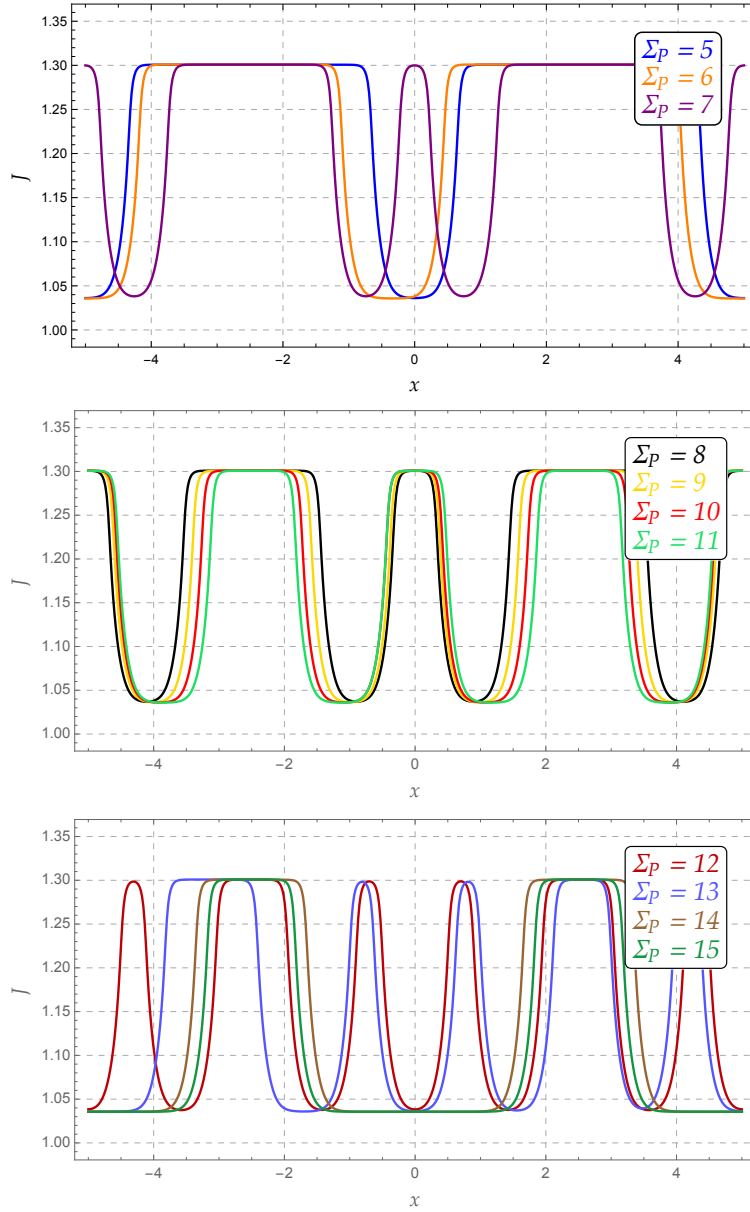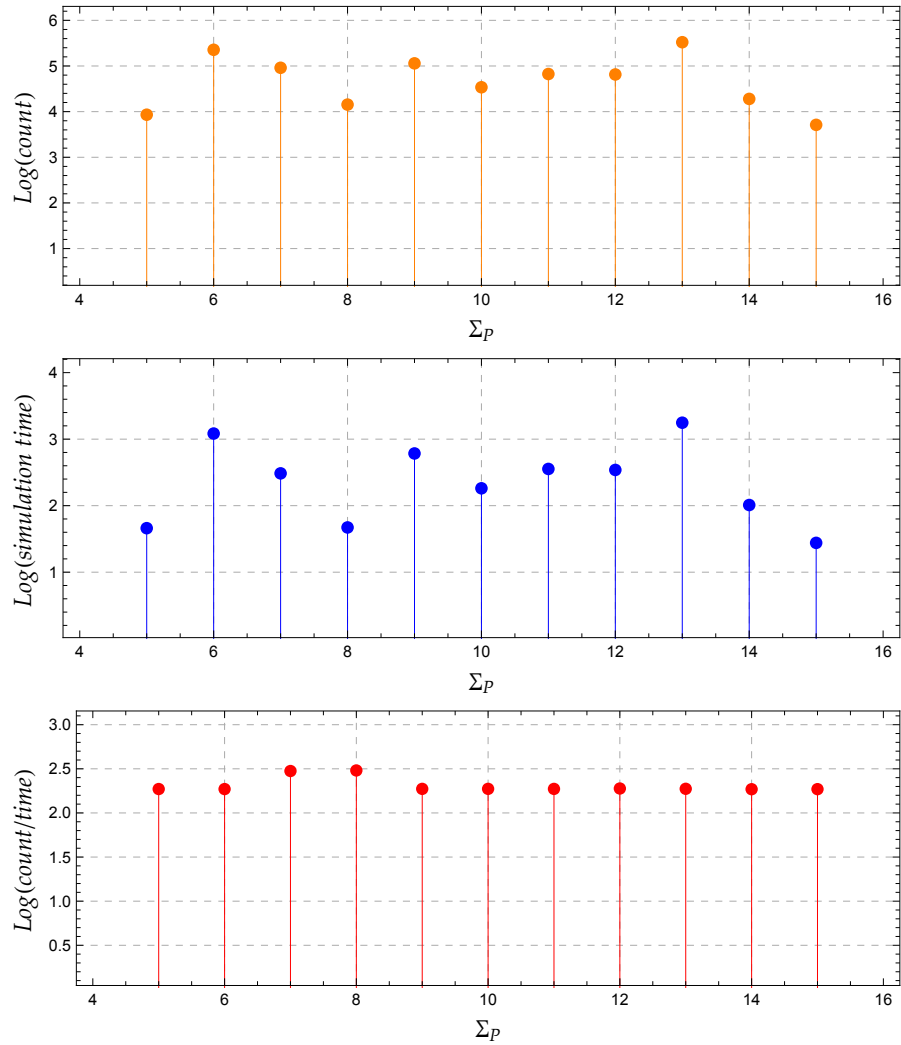
Figure 4.4: Number of GF loops (top), simulation time (middle) and time/loop ratio (bottom) taken by the code for computing the initial configurations. Both the quantities are expressed as logarithm.

4.4 "Double Step" (Uncoupled) Simulations

The presence of receptor diffusion (and related cAMP prodution) has an effect on the membrane in terms of stress. Indeed, the stress arises fed by two contributions: (i) *mechanical* stress due to the presence of the other cells in the well and (ii) *chemical* stress due to the diffusion of receptors. During the simulation, the mechanical stress is assumed to be constant during all the evolution, whereas the chemical stress is evolving together with the diffusive phenomena. As first approach, the two physics mentioned above live separately, i.e. the *first step* of the simulation is about the diffusion of receptors, while the mechanical equilibrium is studied late in the *second step*. For this reason, this kind of uncoupled numerical scheme is also called *double step* simulation.

The simulations of diffusive phenomena run autonomously from the mechanical balance, and they are driven by the choice of a proper forcing term, defined as:

$$\hat{y}(x,t) := f(t)\, g(x) \tag{4.30}$$

where the time and space influences come from different contribution. During the development of the numerical scheme, several time-dependent function $f(t)$ have been taken into account. Despite of this, for the sake of illustration in this Thesis only the result obtained by employing the form (3.20) (denoted by *type 1*). The differences in the results of the simulations shown in the sequel mainly lies in the choice of the space-component of the forcing term. In this Section several kinds of space-depending forcing term are considered: (A) sinusoidal shape higher at the center of the domain, (B) sinusoidal shape higher at the center and the edges, (C) sinusoidal shape higher at the edges, (D) sinusoidal with symmetric high concentration, (E) rectangular shape higher at the center, (F) rectangular shape higher at the edges, (G-H) random, as shown in Figure 4.5.

The work-flow procedure employed by each simulation can be summarized as follows (note that as an illustrative example, during the description only the results of **Simulation 1A** will be commented; **1A** means that time-dependent component of type "1" and space-dependent component of type "A" were used for composing the forcing term):

1. Simulate the space- and time-depending diffusion of cAMP based on

101
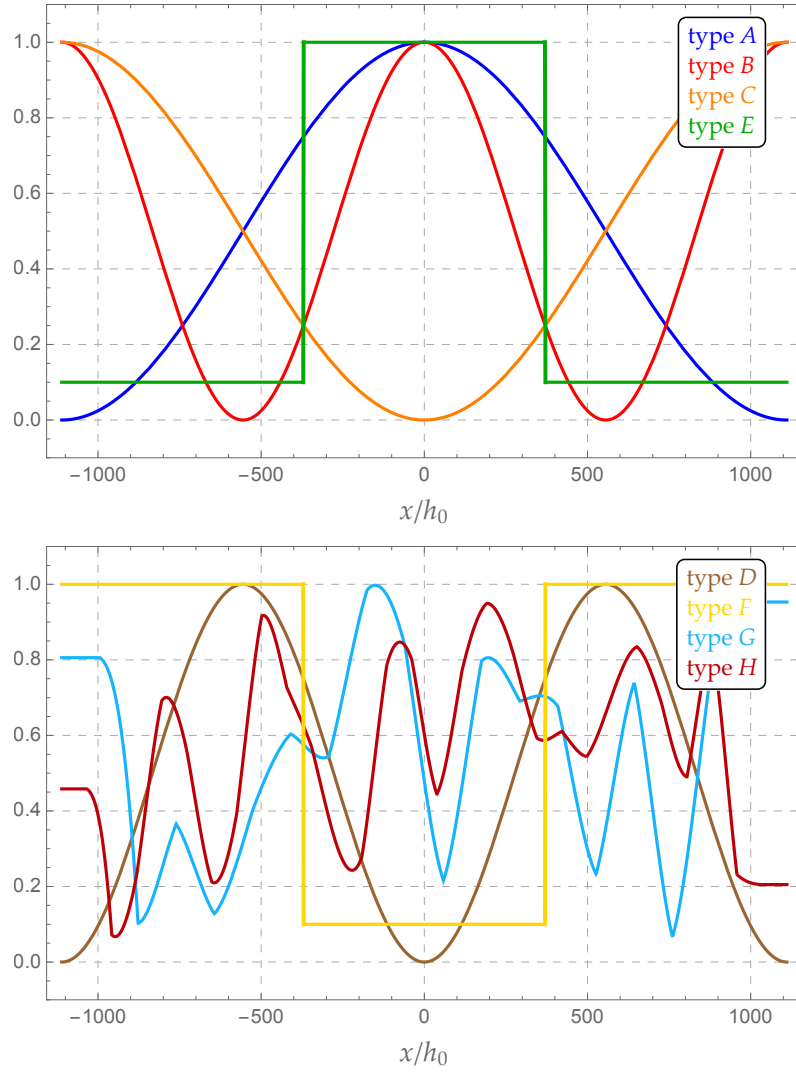
Figure 4.5: Normalized space-depending forcing term $\hat{f}(x)$.
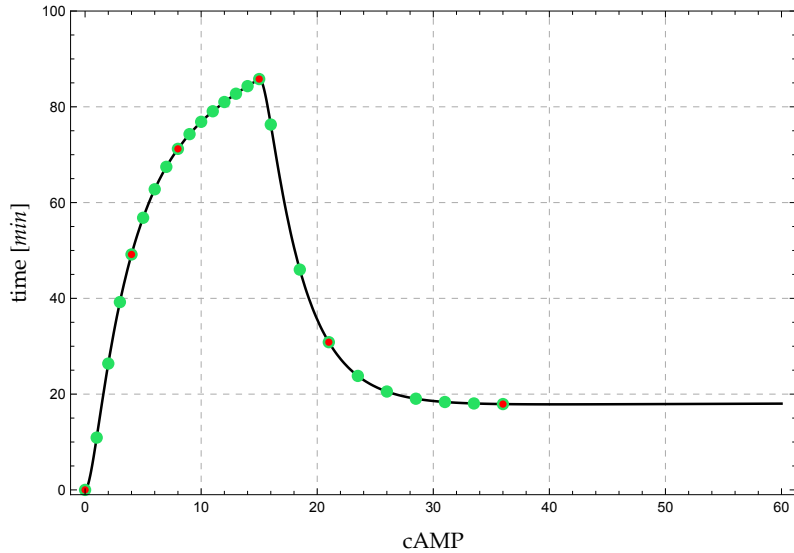
Figure 4.6: Double Step Simulation: discrete selected times.

the choice of $\hat{y}(x,t)$, as shown in Figure 4.7. Whenever the cAMP distribution is known, the receptor ratio $X = \xi/\xi_0$ is computed by means of (3.4), as shown in Figure 4.8(top). As expected, the ratio is higher at the center of the domain in correspondence of the time at which the maximum value of cAMP was measured during the experiments.

2. Because of the very huge CPU time and computational cost for integrating the PDE at each discrete timestep by means of a gradient flow scheme, only some discrete times at which solve the equation governing the equilibrium are chosen. The simulation of the average diffusion together with the experiments showed that after $30\,min$ the measure of cAMP is approximately constant. For this reason, the simulation run until $t = 36\,min$, in order to save computational time. The chosen selected discrete times are reported as green points in Figure 4.6, whereas, for the sake of illustration, the smaller red points denote the instant selected to be displayed in the Figures that the

103

Reader will meet in the sequel.

3. compute the variable chemical stress $S(\xi)$ along the membrane due to diffusion by means of (3.37) and its first derivative $\partial S/\partial x$ with respect to the space. It is worth noting that also at the time $t = 0$, when the diffusion is not started yet and $\xi(x, 0) \approx 0$ almost everywhere, a chemical stress can be found because of the presence of the term $-\xi_0$. It is worth bearing in mind that the total stress acting along the membrane, shown in Figure 4.8(middle), can be computed as:

$$\Sigma = \Sigma_P + \frac{S(\xi)}{J^2}.$$

4. Whenever the chemical stress is known, as many Gradient Flows as many are the discrete selected times run for computing the balanced configurations. The starting configuration for each GF loop is taken from the solution at the previous step. The solution allows for finding both the displacement and the stretch fields along the membrane and, consequently, also the height ratio changes $H = h/h_0 = J^{-1}$. As example, the areal stretch is shown in Figure 4.8(bottom).

A closer analysis of the results show that at the beginning of the simulation the stress acting on the membrane is constant, then spontaneously the membrane presents both ordered and disordered phase of lipids, i.e. rafts. This configuration is strictly connected with the specific form of the local energy. The analysis of the results shows that after the diffusion starts, the raft formation immediately follows the concentration of the stress.
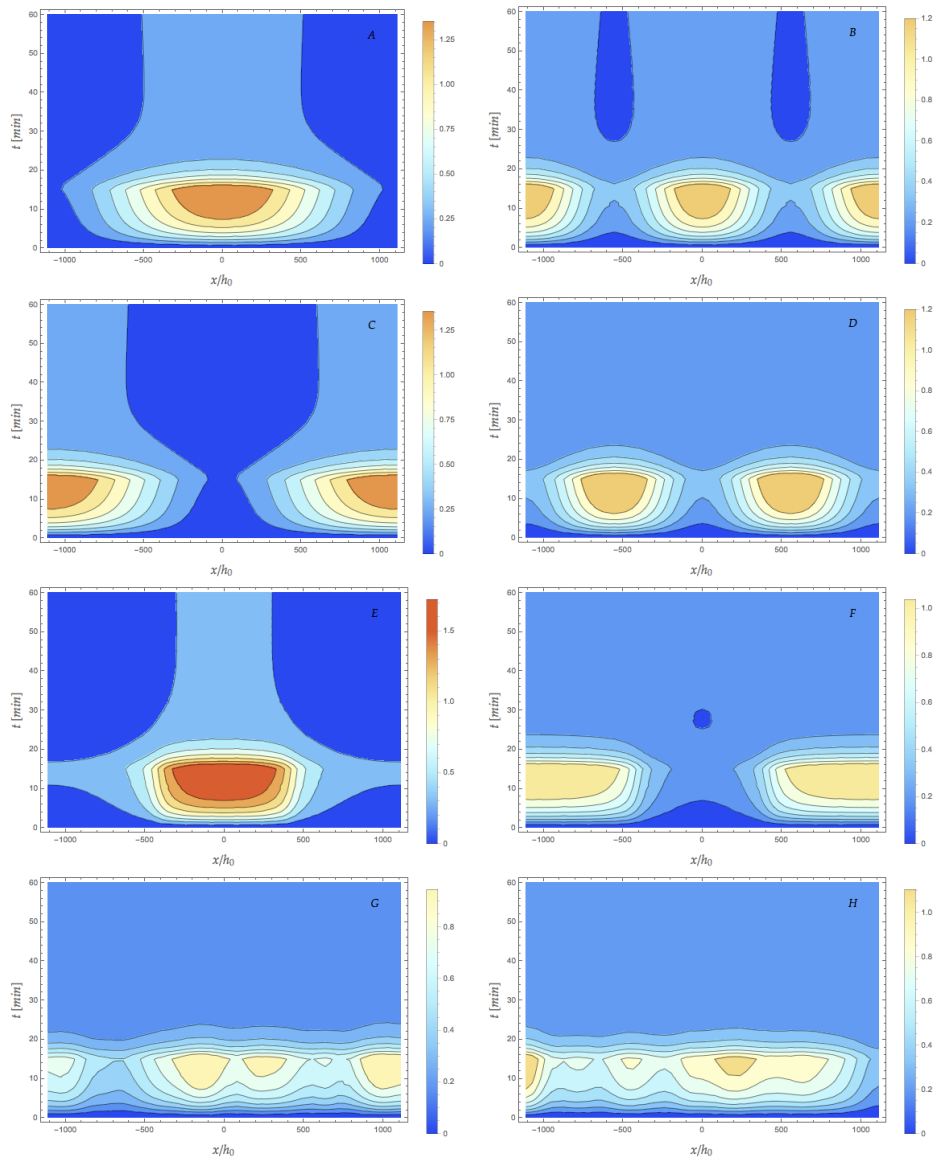
Figure 4.7: DS Simulations: diffusion over space and time.
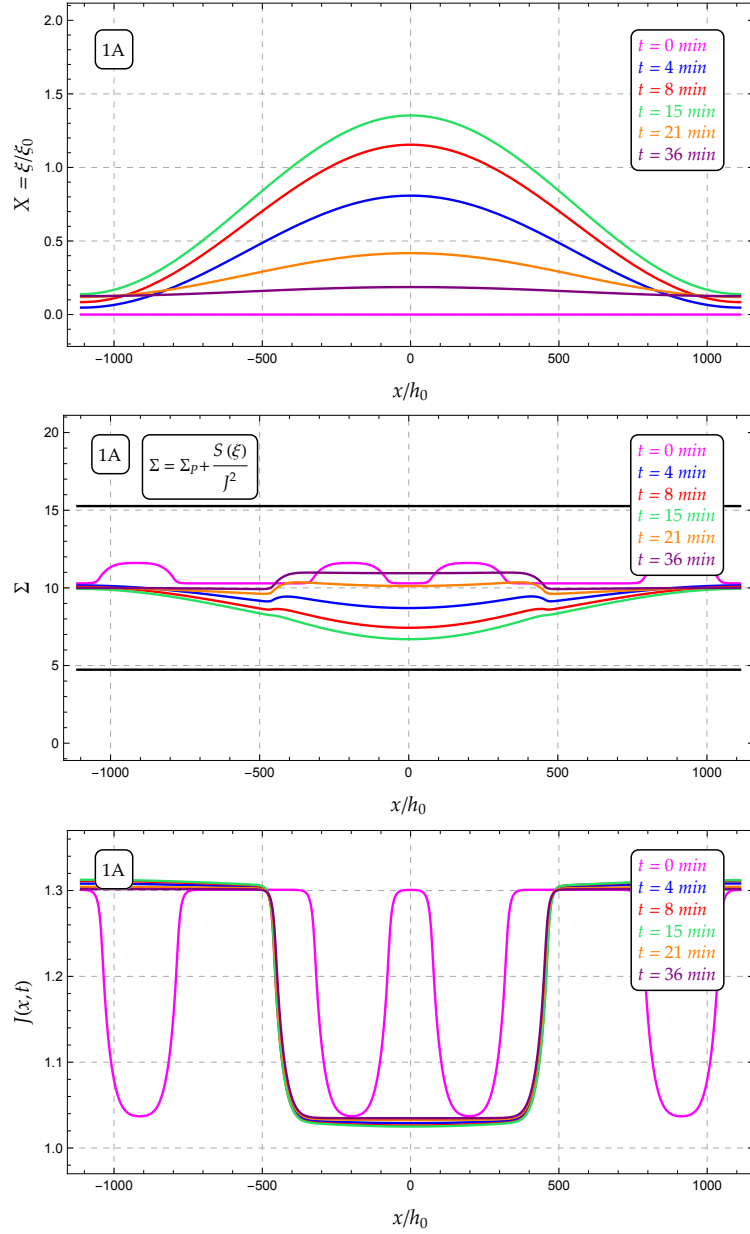
Figure 4.8: DS simulation **1A**: receptor ratio ξ/ξ_0 (top), total stress along the membrane Σ (middle) and stretch J (bottom) at discrete selected times.
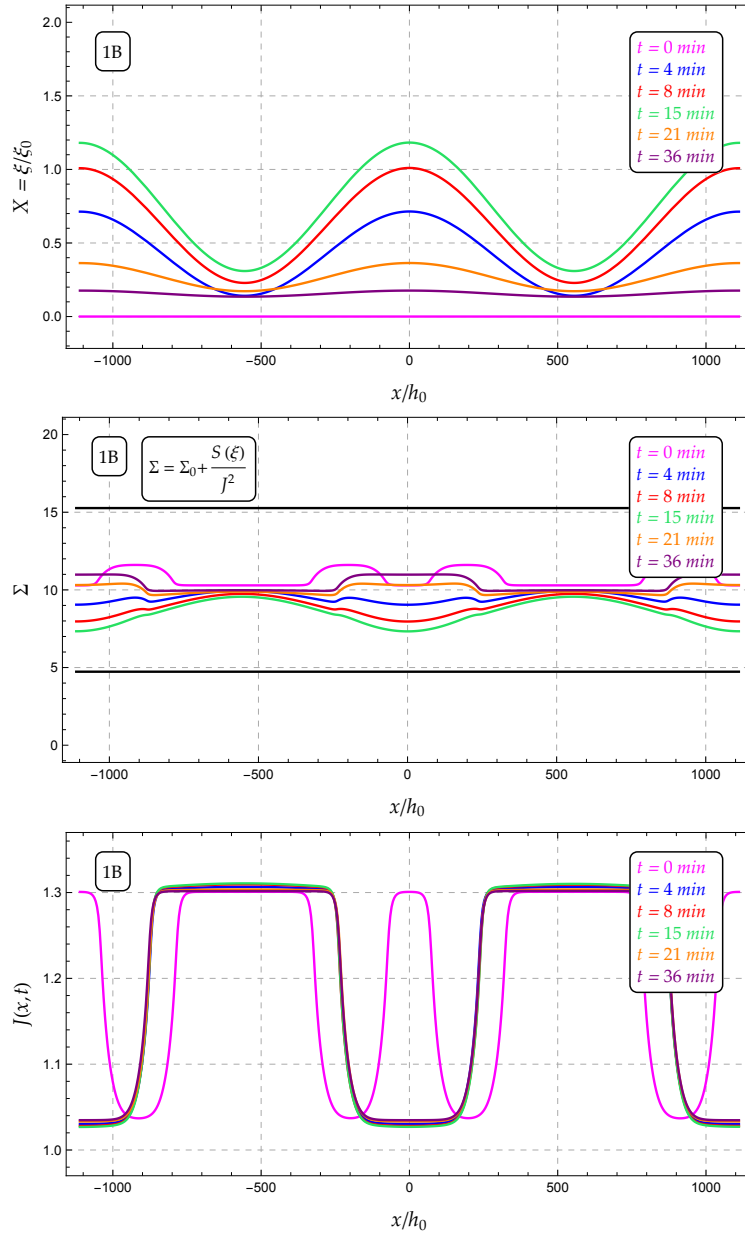
Figure 4.9: DS simulation **1B**: receptor ratio ξ/ξ_0 (top), total stress along the membrane Σ (middle) and stretch J (bottom) at discrete selected times.
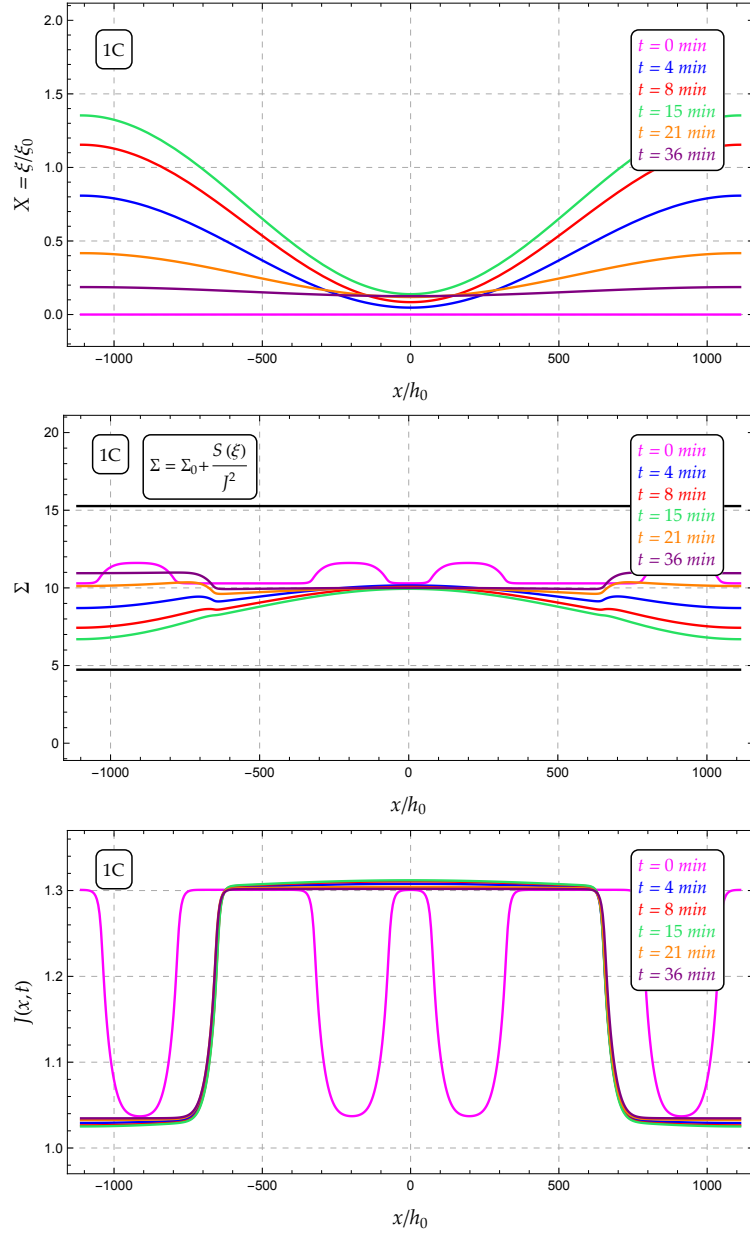
Figure 4.10: DS simulation **1C**: receptor ratio ξ/ξ_0 (top), total stress along the membrane Σ (middle) and stretch J (bottom) at discrete selected times.
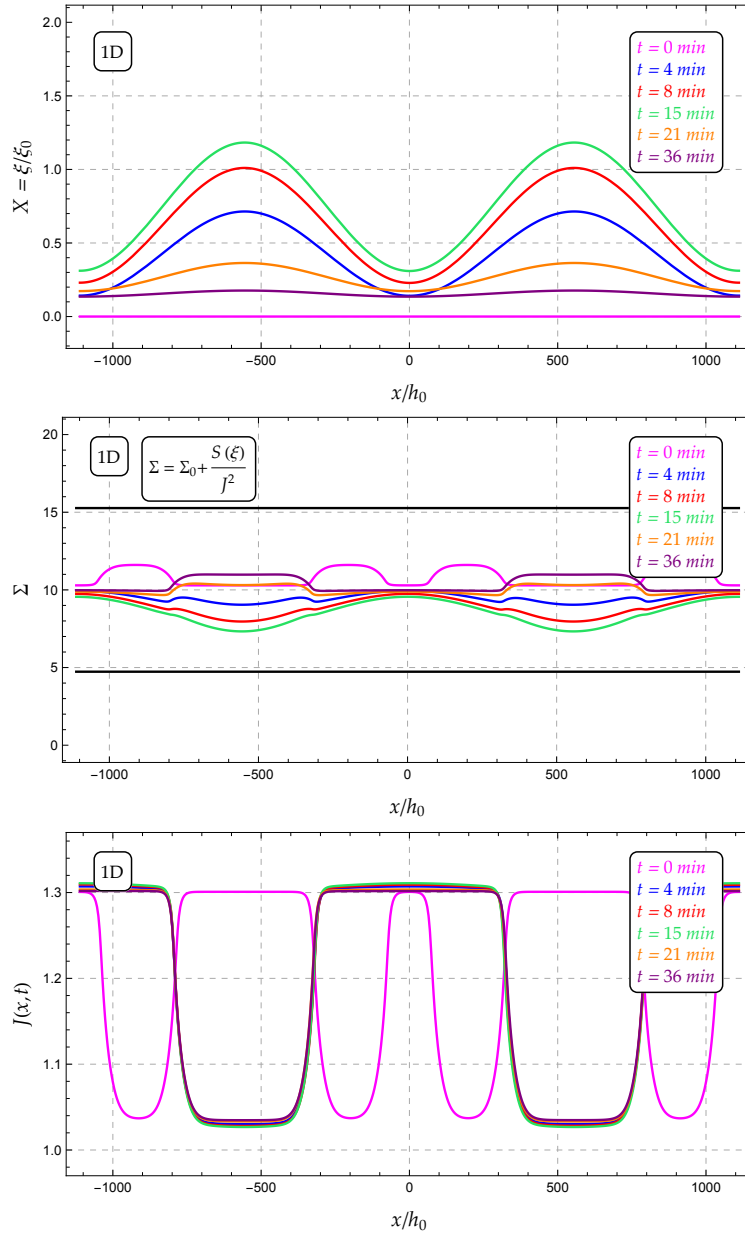
Figure 4.11: DS simulation **1D**: receptor ratio ξ/ξ_0 (top), total stress along the membrane Σ (middle) and stretch J (bottom) at discrete selected times.
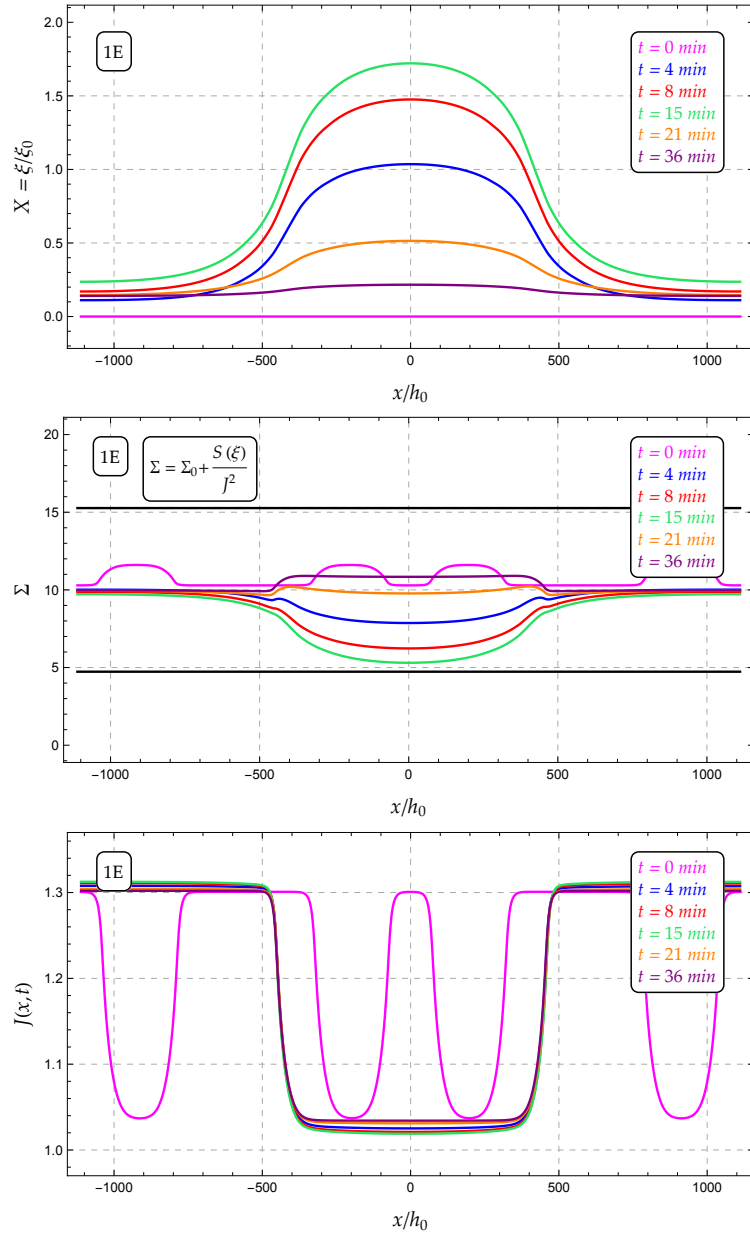
Figure 4.12: DS simulation **1E**: receptor ratio ξ/ξ_0 (top), total stress along the membrane Σ (middle) and stretch J (bottom) at discrete selected times.
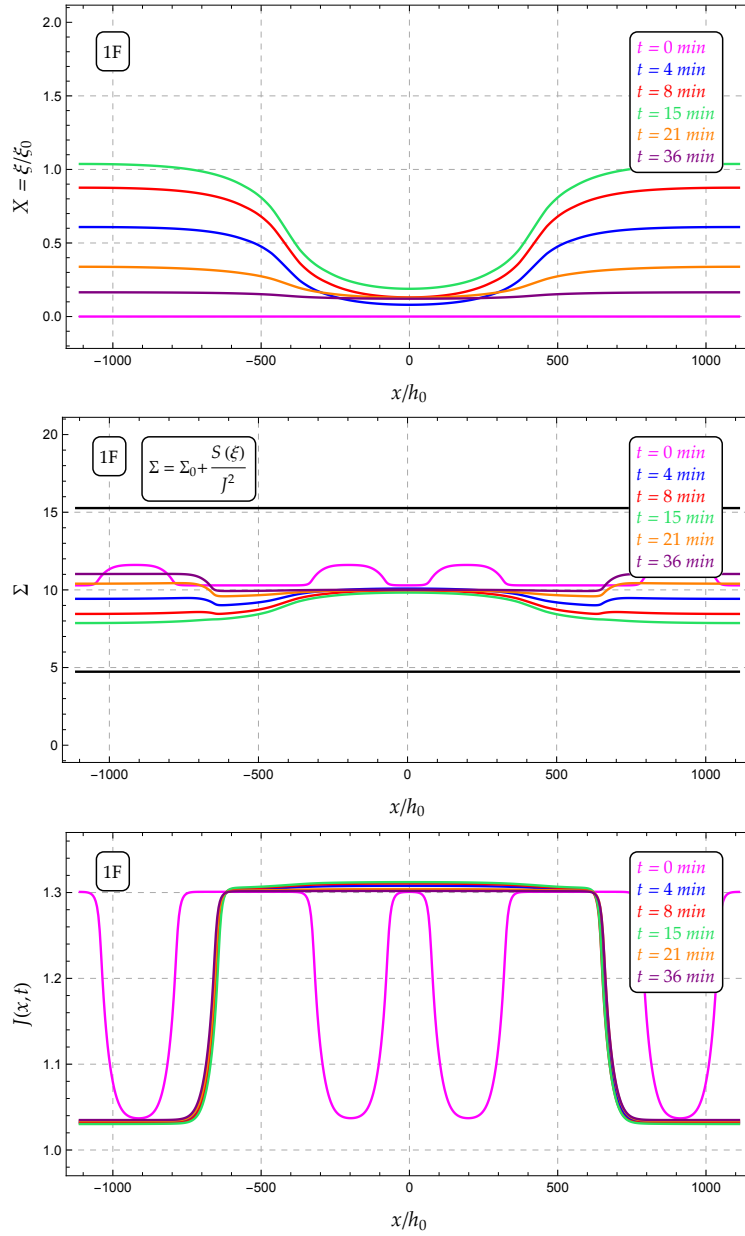
Figure 4.13: DS simulation **1F**: receptor ratio ξ/ξ_0 (top), total stress along the membrane Σ (middle) and stretch J (bottom) at discrete selected times.
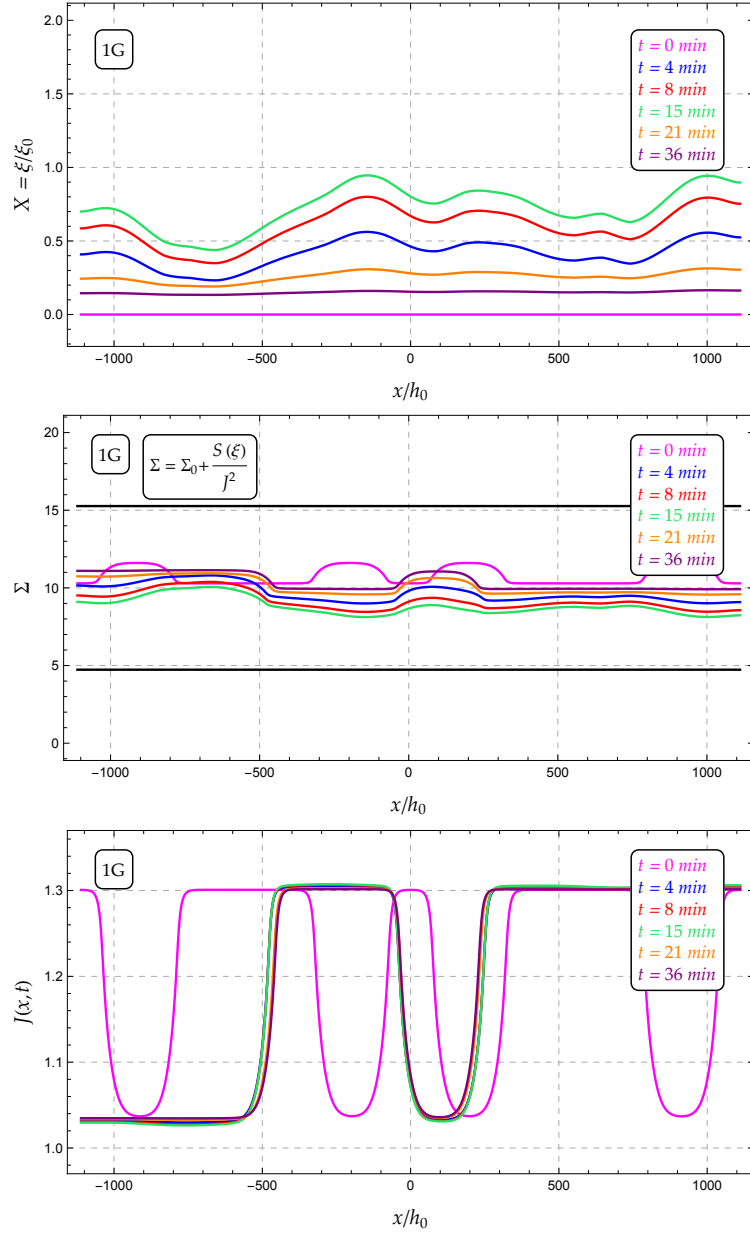
Figure 4.14: DS simulation **1G**: receptor ratio ξ/ξ_0 (top), total stress along the membrane Σ (middle) and stretch J (bottom) at discrete selected times.
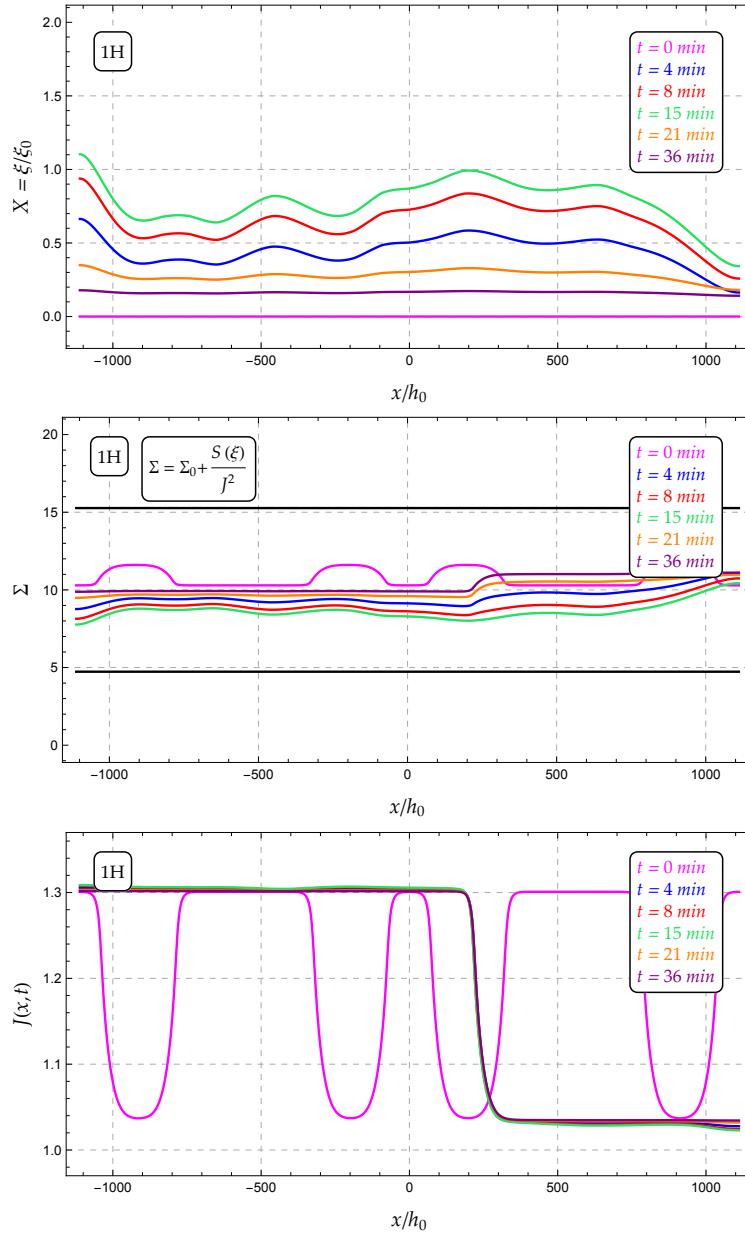
Figure 4.15: DS simulation **1H**: receptor ratio ξ/ξ_0 (top), total stress along the membrane Σ (middle) and stretch J (bottom) at discrete selected times.

113

4.5 "Double update" (Coupled) Simulations

Despite the uncoupled numerical scheme employed in Section 4.4, the mechanical and chemical phenomena are intimately linked, since they influence each other during the experimental evolution. As widely discussed in Section 3.4, this intimate coupling can be obtained by employing a forcing term of kind (3.25) and the kinetic relationship (3.43). The latter is a simple ODE that can be easily coded by means of the forward Euler Finite Difference:

$$\xi^{n+1}(\mathbf{I} - \Delta t\,\mathbf{R}) = \xi^n \tag{4.31}$$

where ξ^n and ξ^{n+1} represent the vectors of the discrete values of the receptor density at the discrete times t_n and t_{n+1}, respectively, Δt is the time increment and $\mathbf{R}$ is a diagonal matrix whose terms depend on the discrete values of the chemical potential μ_i at the meshpoints:

$$R_{i,i} = \begin{cases} k_b \left(1 - \exp\left[\dfrac{\mu_{RL}^{(i)}}{K_B\,T}\right]\right) & \text{if } \mu_{RL}^{(i)} < 0 \\[4mm] k_u\,\mathcal{U}\left(\exp\left[-\dfrac{\mu_{RL}^{(i)}}{K_B\,T}\right] - 1\right) & \text{if } \mu_{RL}^{(i)} > 0 \end{cases} \tag{4.32}$$

Based on these considerations, a numerical scheme able to catch the mutual influence of the two physics can be coded. In particular, it is possible to split each timestep into two sub-steps: during the first substep a diffusion model is employed for updating the value of the receptor density, while during the second sub-step the receptor density is updated by considering the kinetic relationship (3.43). This numerical scheme is also called "double update" scheme because of the strategy just illustrated for the chemo-mechanical coupling. The numerical procedure is coded as follows:

0. Initialize all the required quantities and load the initial configuration.

1. Do the first receptor density update, first by solving the diffusion

equation in terms of cAMP:

$$\begin{cases} S_t = \omega_{11} \left(C - S \right) + \omega_{12} \left(Z - S \right) + d_\xi \, S_{xx} + y(x,t) \\ C_t = \omega_{21} \left(S - C \right) \\ Z_t = \omega_{31} \left(S - Z \right) + d_\zeta \, Z_{xx} \end{cases}$$

As first approximation, the diffusive coefficients are set to have the same value, i.e. $d_\xi = d_\zeta$ and the guess values is roughly set to $d = 10^4 \, nm^2/s$ from Gao [81]. The solution of the ODE system allows for computing the updated value as:

$$\xi^*(x,t) = \frac{S+C}{\alpha_\xi}.$$

2. Compute the chemical potential and check at which locations x_i binding will take place, i.e where $\mu_i < 0$:

$$\frac{\mu_{RL^{(i)}}}{K_B \, T} = \frac{\mu_0}{K_B \, T} + \log \left(\frac{\xi_i^*}{\xi_m} \right) + \frac{\mathcal{W}(J_i)}{K_B \, T} < 0$$

3. Do the second receptor density update for computing ξ_i^{**} by considering the kinetic relationship (3.43).

4. Compute the chemical stress $S(\xi^{**})$ through (3.37):

$$S(\xi^{**}) = \pi \, d_s \, q \, \phi \, h_0 \left(\xi^{**} - \xi_0 \right)$$

5. Solve the Euler-Lagrange equation (3.39) by employing one of the method exposed in Section 4.2. The favorite scheme uses the *linearization method* because of the speed for getting the solution (indeed it allows for obtaining results in a reasonable time). The solution in terms of displacement U allows for computing the stretch $J = 1 + U'$ and height ratio $H = J^{-1}$.

6. Store all the variables and set them as starting values for the next loop. Note that at this step also the statistical parameter β together with its time derivative $\beta_{,t}$ are computed. The latter is evaluated by

115

considering both the updates of the current step (i.e. both ξ^* and ξ^{**}), i.e.

$$\beta_t = \frac{1}{\xi_0} \frac{\xi^{**} - \xi^*}{\Delta t}$$

Some coefficients have been introduced in the numerical code for enhancing parametric analysis. Similarly to the average case, coefficients w_{ij} have been introduced for modulating diffusion, while a coefficient d_c is used as factor in front of the diffusion coefficient, i.e:

$$\omega_{ij} = w_{ij}\, \omega_{ij}^* \tag{4.33a}$$

$$d = d_c\, d^* \tag{4.33b}$$

where the quantities on lhs denote the effective values used in the simulation, while the apex * represents guess values taken from literature. In the numerical code, the specific activation energy for the compound receptor-ligand, namely e_{RL}, is always expressed per unit of K_B, T, then it is always a dimensionless term.

In order to understand the influence of each type of parameter employed in the model, several series of simulations have been performed. After the best set of parameter was found, this *best* set has been used as reference set for comparing results obtained by performing parametric studies on varying of numerical coefficients. Time after time, only one parameter has been changed, while the others have maintained the values of the *best* set. The following series of simulation have been considered:

◇ **S00**: the simulation with the *best* set of parameters (see Figure 4.16).

◇ **Series A**, focused on the influence of `dc` (see Figure 4.17).

◇ **Series B**, focused on the influence of `eRL` (see Figure 4.18).

◇ **Series C**, focused on the influence of `w11` (see Figure 4.19).

◇ **Series D**, focused on the influence of `w12` (see Figure 4.20).

◇ **Series E**, focused on the influence of `w21` (see Figure 4.21).

◇ **Series F**, focused on the influence of `w31` (see Figure 4.22).

116

◇ **Series G**, focused on the influence of `wc` (see Figure 4.23).

◇ **Series H**, focused on the influence of `SP` (see Figure 4.24).

◇ **Series I**, focused on the influence of `tm` (see Figure 4.25).

◇ **Series L**, focused on the influence of `tf` (see Figure 4.26).

The series with the *best* set is denoted by **S00**, whereas the other are labeled by progressive order of letters. Table 4.3 collects parameter sets used in each simulation. For the sake of understanding, the varying value with respect to the basic set is highlighted by blue color.

name	SP	nx	tm	tf	m	m	eRL	dc	wc
S00	8	300	10	18	.95	.05	-6	2.3	[6 2 5 2]
SA1	8	300	10	18	.95	.05	-6	0.5	[6 2 5 2]
SA2	8	300	10	18	.95	.05	-6	1	[6 2 5 2]
SA3	8	300	10	18	.95	.05	-6	2	[6 2 5 2]
SA4	8	300	10	18	.95	.05	-6	5	[6 2 5 2]
SA5	8	300	10	18	.95	.05	-6	10	[6 2 5 2]
SB1	8	300	10	18	.95	.05	-3	2.3	[6 2 5 2]
SB2	8	300	10	18	.95	.05	+3	2.3	[6 2 5 2]
SB3	8	300	10	18	.95	.05	-4	2.3	[6 2 5 2]
SB4	8	300	10	18	.95	.05	-5	2.3	[6 2 5 2]
SB5	8	300	10	18	.95	.05	-7	2.3	[6 2 5 2]
SB6	8	300	10	18	.95	.05	-10	2.3	[6 2 5 2]
SC1	8	300	10	18	.95	.05	-6	2.3	[1 2 5 2]
SC2	8	300	10	18	.95	.05	-6	2.3	[10 2 5 2]
SC3	8	300	10	18	.95	.05	-6	2.3	[100 2 5 2]
SD1	8	300	10	18	.95	.05	-6	2.3	[6 1 5 2]
SD2	8	300	10	18	.95	.05	-6	2.3	[6 10 5 2]
SD3	8	300	10	18	.95	.05	-6	2.3	[6 100 5 2]
SE1	8	300	10	18	.95	.05	-6	2.3	[6 2 1 2]
SE2	8	300	10	18	.95	.05	-6	2.3	[6 2 10 2]
SE3	8	300	10	18	.95	.05	-6	2.3	[6 2 100 2]

117

name	SP	nx	tm	tf	m	m	eRL	dc	wc
SF1	8	300	10	18	.95	.05	-6	2.3	[6 2 5 1]
SF2	8	300	10	18	.95	.05	-6	2.3	[6 2 5 10]
SF3	8	300	10	18	.95	.05	-6	2.3	[6 2 5 100]
SG1	8	300	10	18	.95	.05	-6	2.3	[60 20 50 20]
SG2	8	300	10	18	.95	.05	-6	2.3	[.6 .2 .5 .2]
SH1	5	300	10	18	.95	.05	-6	2.3	[6 2 5 2]
SH2	11	300	10	18	.95	.05	-6	2.3	[6 2 5 2]
SH3	13	300	10	18	.95	.05	-6	2.3	[6 2 5 2]
SI1	8	300	1	18	.95	.05	-6	2.3	[6 2 5 2]
SI2	8	300	2.5	18	.95	.05	-6	2.3	[6 2 5 2]
SI3	8	300	5	18	.95	.05	-6	2.3	[6 2 5 2]
SL1	8	300	10	15	.95	.05	-6	2.3	[6 2 5 2]
SL2	8	300	10	25	.95	.05	-6	2.3	[6 2 5 2]
SL3	8	300	10	40	.95	.05	-6	2.3	[6 2 5 2]

Table 4.3: Parameters used for the Double Update (DU) Simulation.

Note that in Figures 4.16-4.24 the golden vertical lines represent t_m and t_f, respectively. On the contrary, in Figure 4.25 the line representing t_m has the same color of the relative simulation (see legend) and t_f is fixed by a golden line, while in Figure 4.26 is the opposite, t_m is highlighted by a golden line and the color of t_f changes with regard of the simulation (see legend).

First of all, the influence of the parameter dc is studied in the **Series A**. Figure 4.17 5 different values (0.5, 1, 2, 5, 10) are considered. The parameter dc influences the solution of the diffusion at the first update step (**step 1**). Increasing values determine a lower mobility of the receptors, hence relevant binding effects can not be activated. It is worth noting that the downhill of the average cAMP curve can be obtained only because of the presence of binding. Indeed, the forcing term $y(x, t)$ would be always positive. This observation becomes more clear if one pays attention to **Series B**, which is devoted to explore the role of the activation energy per unit of $K_B T$, i.e.

eRL. Positive values (bear in mind that $\mu_0 = -e_{RL} + 1$) do not allow for obtaining the typical downhill of the curve because there are not locations at which the chemical potential reaches positive values. This means that the density ratio is always increasing, then also the time derivative β_t is always positive. Indeed, a closer analysis of relationship (3.25), i.e.

$$y(x,t) = \beta_t(x,t)\,F(t) + \beta(x,t)f(t),$$

shows that the only term able to make the forcing term negative (i.e. to be a sink) is the time derivative β. This fact arises only whenever the chemical potential becomes positive and the updating relationship (3.43) imposes decreasing values of the receptor density ξ^{**}. This consideration appears as an evidence whenever one has a look to Figure 4.18. A direct inspection of the graphical results of this series shows that whenever eRL is positive (SB2, red curve), the average time evolution of cAMP appears to be always increasing; on the other hand, decreasing the values of activation energy (i.e. increasing μ_0) behaves as an advance in the starting of the downhill curve, since the condition of a positive chemical potential is reached before.

The diffusion process is of course influenced by the dimension of the pools and the flux between compartments, i.e. by the the coefficients ω_{ij} (defined in (3.7)). This dependence is examined in **Series C-G**. As expected, the results suggest the importance of two coefficients, ω_{11} and ω_{31}. The first couples the submembranal and cytosolic pool, whereas the latter is the one coupling receptors and transporters. The graphical results highlight that they are the more influential parameters of the purely diffusive process.

Beside these aspects, the value of the mechanical stress coming from the surrounding has a very important role. This aspect is studied in **Series H**. Following the results relative to the initial configuration (see Figure 4.3), three values of dimensionless prestress Σ_P have been chosen (5, 11, 13) in such a way they represent very different initial configurations. The shape of the membrane deeply influences the evolution of cAMP production, because it is strictly connected to the chemical potential and the work done by lateral pressure. The result in Figure 4.24 clearly shows the key role played by the membrane profile in this kind of evolution. Probably, different values of ligand concentration and different conditions of the surrounding environment would impose different shapes and, in turn, different behavior and response.

119

At last but not least, **Series I-L** focus the attention on the (chosen) shape of the association/dissociation relationship (3.20). Indeed, the choice of the characteristic time t_m and t_f represents the only arbitrary parameters of the model. The result in Figure 4.25 suggests that smaller values of t_m prescribe an advanced in time of the peak of the average curve; such a peak appears to be as greater as higher is the value of the chosen time t_m, probably because of its influence the diffusive phenomena. On the other hand, in Figure 4.26 it is possible to observe that moving t_f late has opposite effects: the curves appear to be more flat with decreasing value of the peak, reached at delayed time.
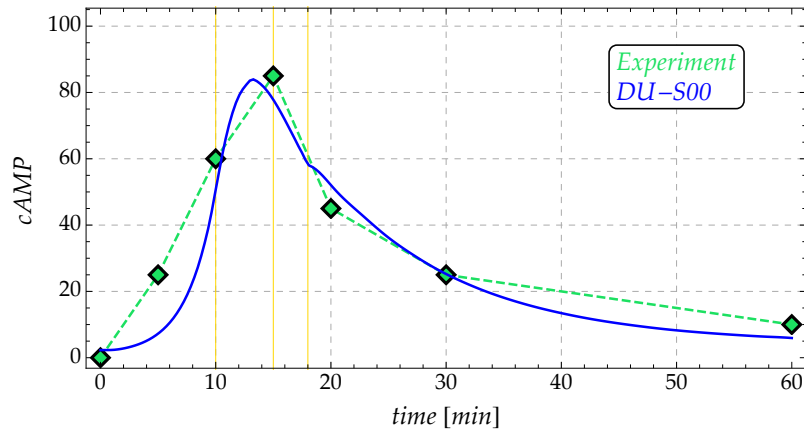
Figure 4.16: Simulation DU-S00: average evolution.
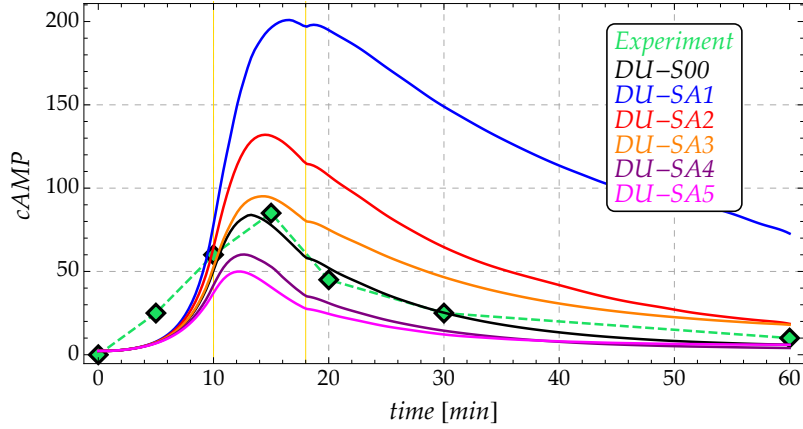
Figure 4.17: Simulation DU-Series A (influence of `dc`): average evolution.
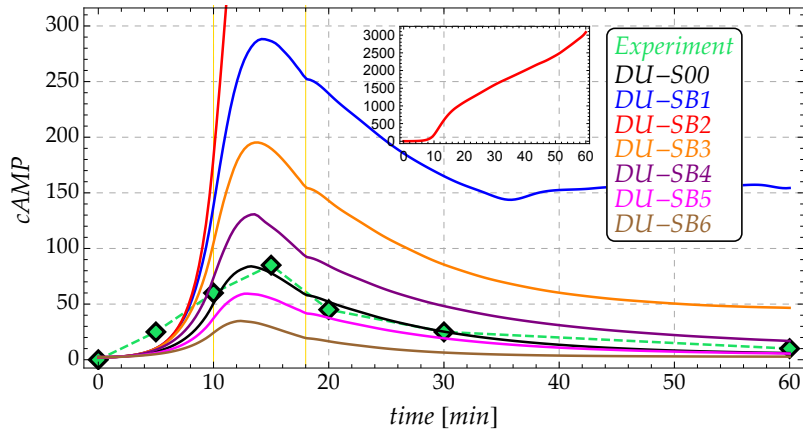
Figure 4.18: Simulation DU-Series B (influence of `eRL`): average evolution.
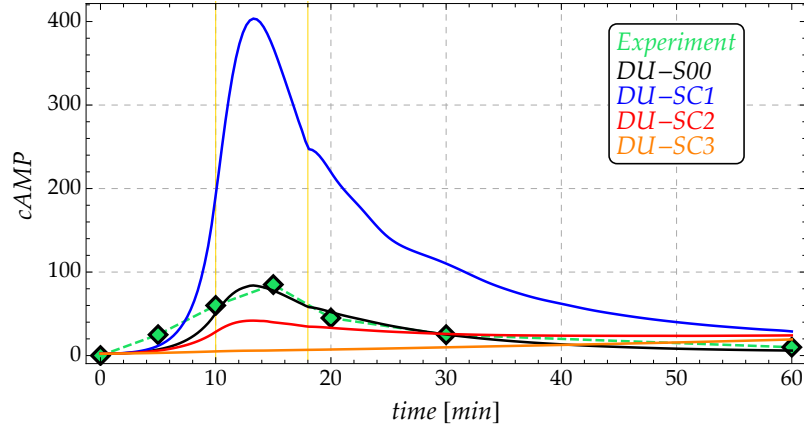
Figure 4.19: Simulation DU-Series C (influence of `w11`): average evolution.
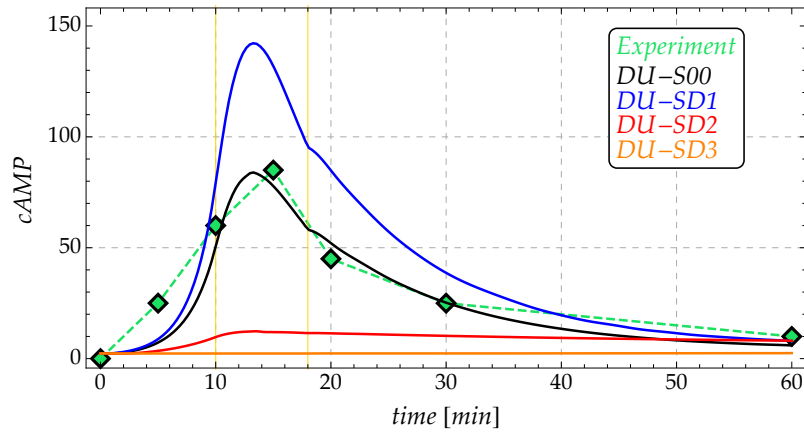
Figure 4.20: Simulation DU-Series D (influence of `w12`): average evolution.
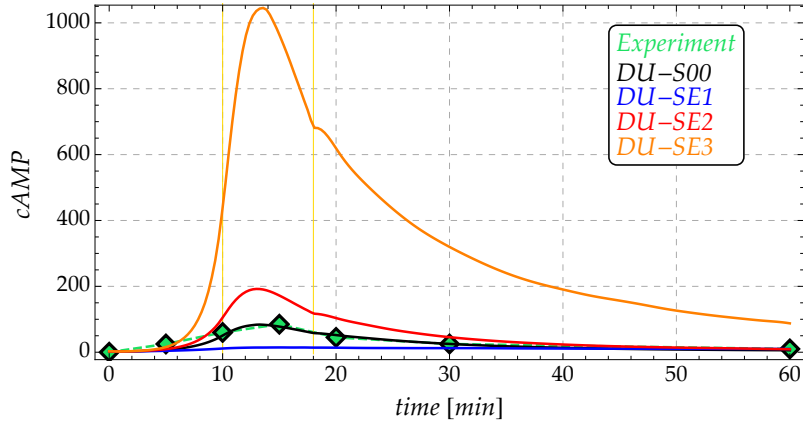
Figure 4.21: Simulation DU-Series E (influence of `w21`): average evolution.
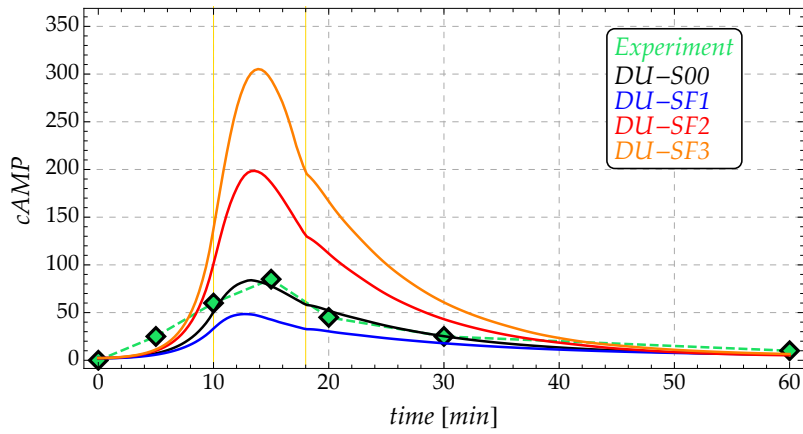
Figure 4.22: Simulation DU-Series F (influence of `w31`): average evolution.
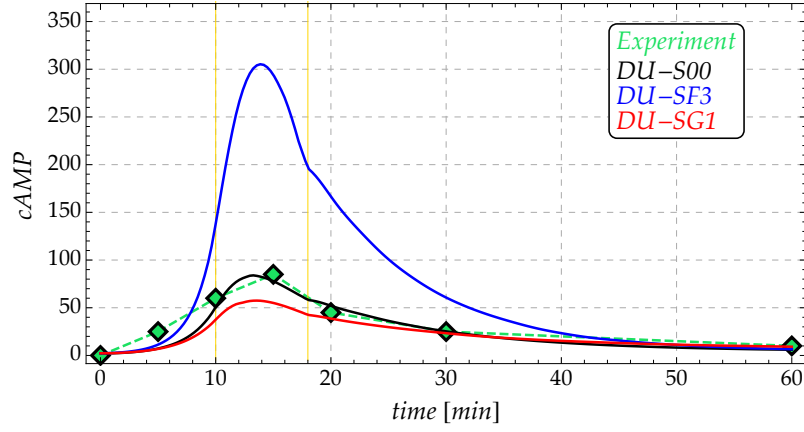
Figure 4.23: Simulation DU-Series G (influence of `wc`): average evolution.
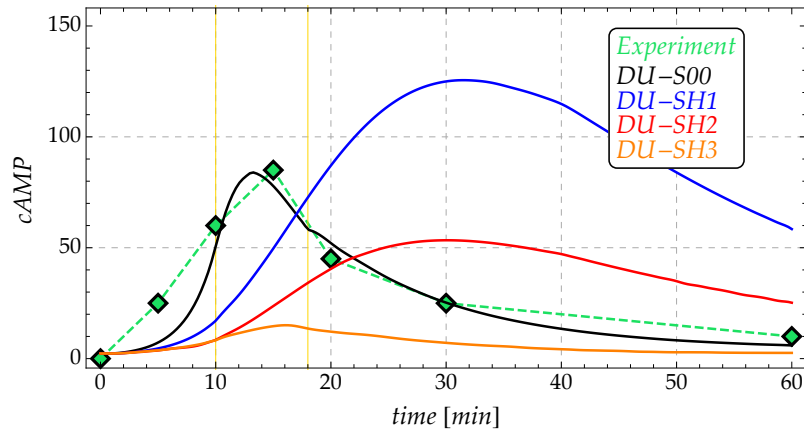
Figure 4.24: Simulation DU-Series H (influence of `SP`): average evolution.
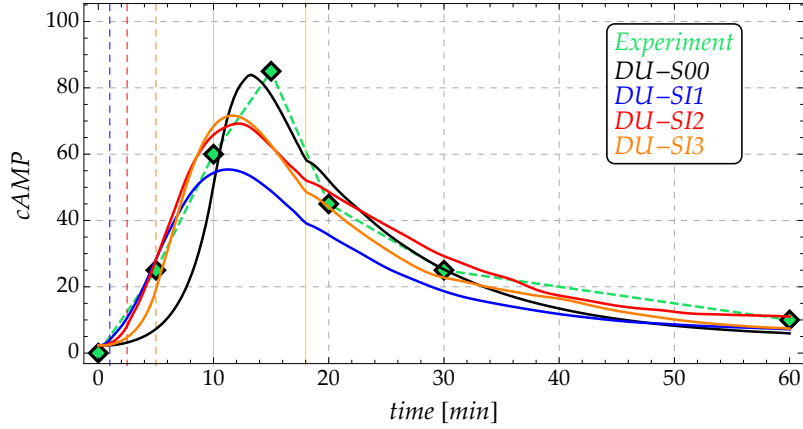
Figure 4.25: Simulation DU-Series I (influence of `tm`): average evolution.
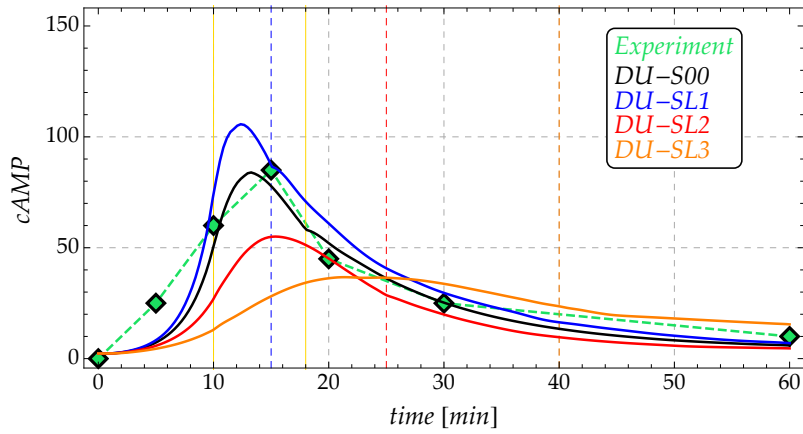
Figure 4.26: Simulation DU-Series L (influence of `tf`): average evolution.

The complete set of results regarding the simulation with the best set of parameters, namely SIMS00, is shown in Figure 4.27-4.28. The results show the strong influence of the membrane profile on the chemical potential and, in turn, on all the related quantities. The evolution of the stress over the time clearly shows that stress concentration arises in correspondence of order phases, i.e. where h/h_0 is higher and formation of rafts is observed.

Beside the results obtained by employing the *best set* of parameters, also what has been obtained in all the other simulations is shown in the sequel. The diffusive evolution over space and time is shown in Figure 4.29-4.36 as contour plot. On the right side of each plot a legend explains the relative scale. All the other quantities of interest are shown in Figures 4.37-4.45; each of these figures is relative to a specific series of simulations, as indicated in the legend, and relative to the discrete time $t = 15\,min$. Each set of results is composed by the space dependence of cAMP, the overall stress along the membrane (computed by taking into account both mechanical and chemical stress), the arising values of areal stretch obtained by solving the linearized equation for the equilibrium and the value of the chemical potential driving the evolution.
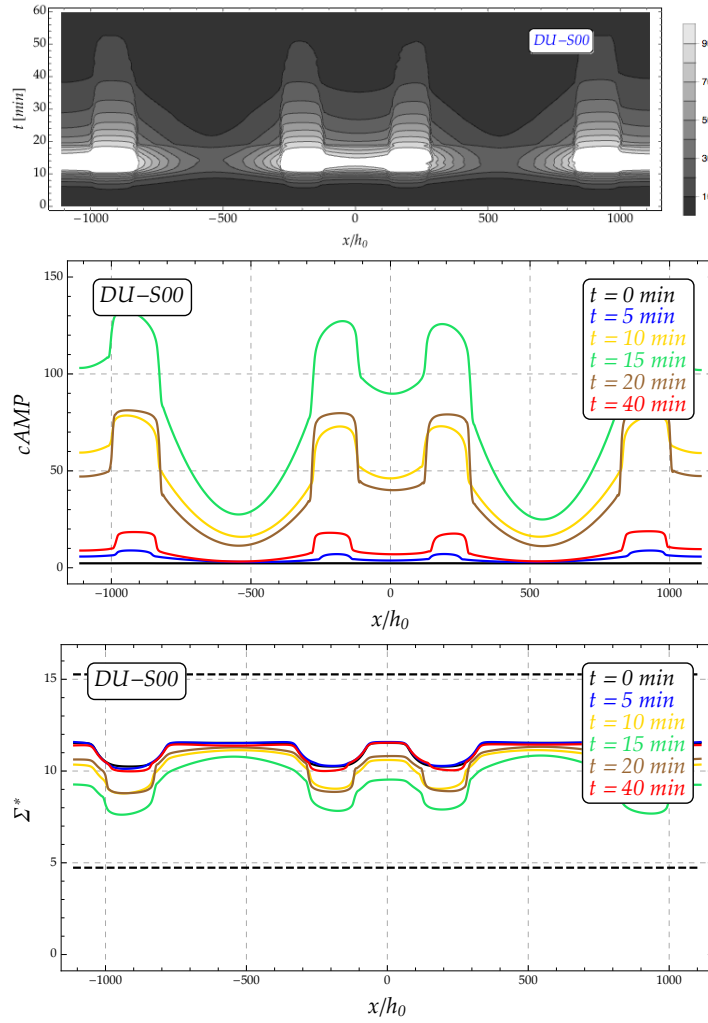
Figure 4.27: Results of simulation **DU-SIM00** (1): contour plot of the diffusion over space and time (top), values of cAMP (middle) and overall stress (bottom) along the membrane at some selected discrete times.

127
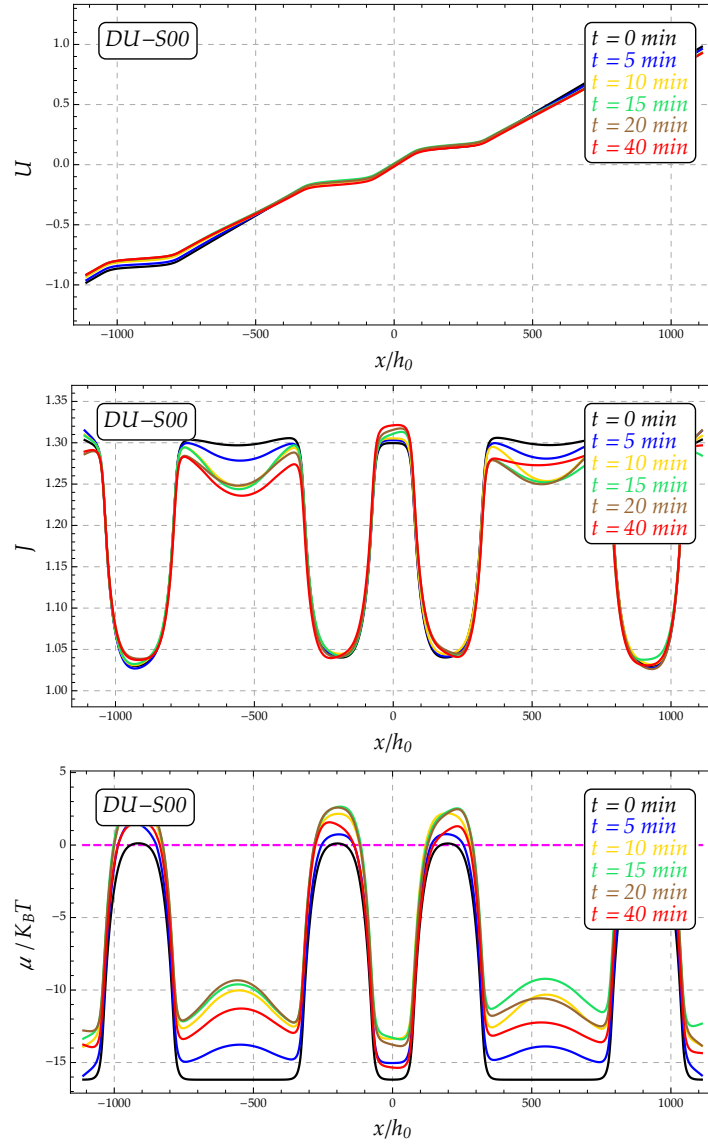
Figure 4.28: Results of simulation **DU-SIM00** (1): displacement field U (top), stretch field $J = 1 + U'$ (middle) and values of chemical potential per unit of $K_B\,T$ (bottom) along the membrane at some selected discrete times.

128
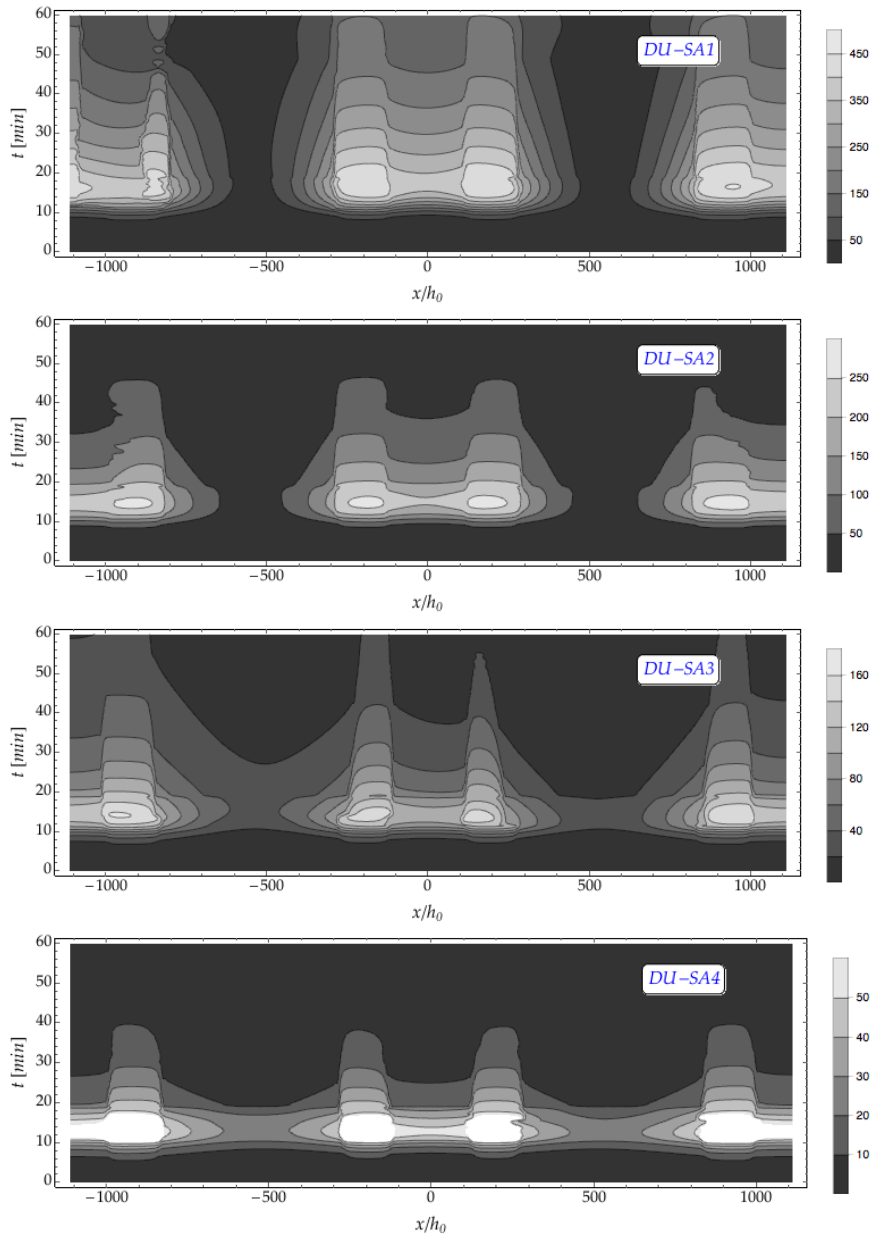
Figure 4.29: Comparison of results about diffusion: simulations DU-A1, A2, A3, A4

129
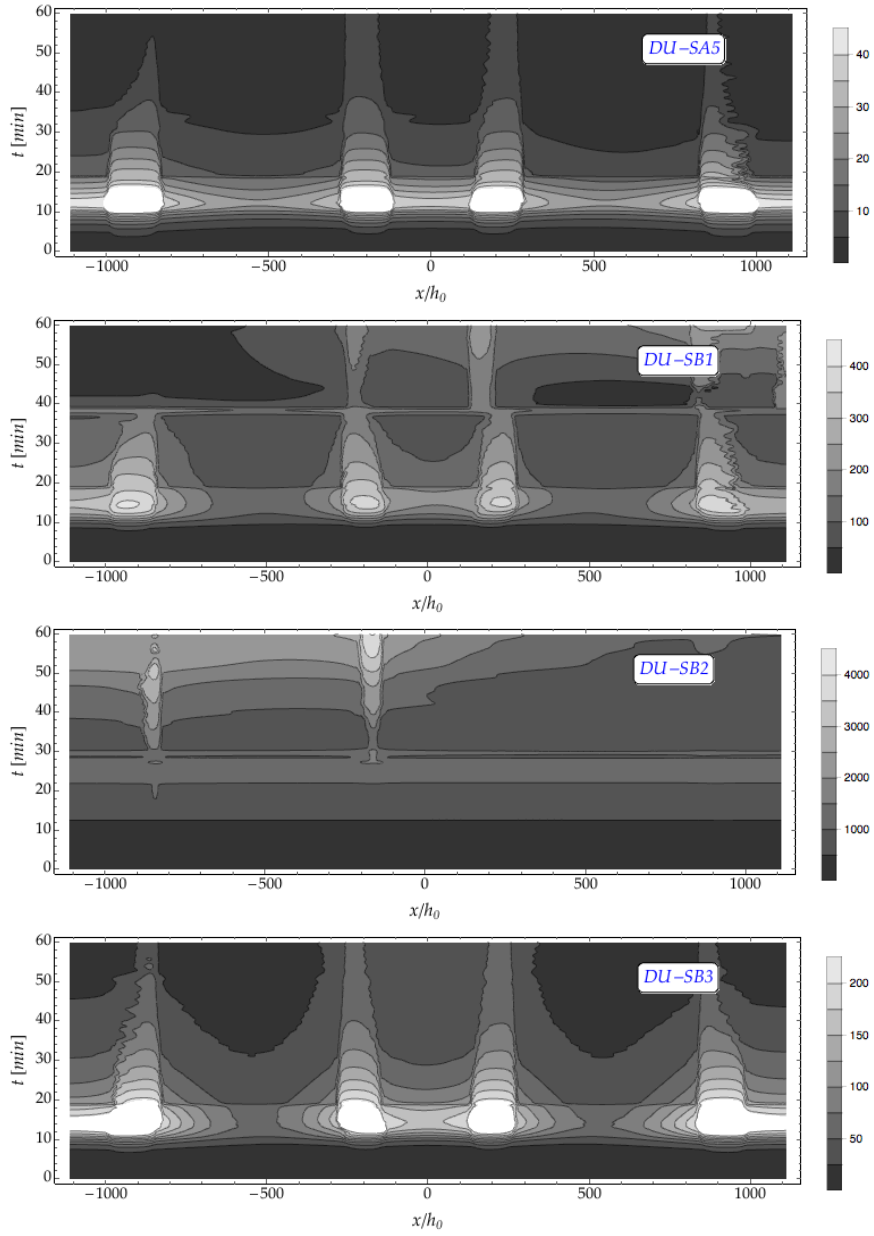
Figure 4.30: Comparison of results about diffusion: simulations DU-A1, B1, B2, B3

130
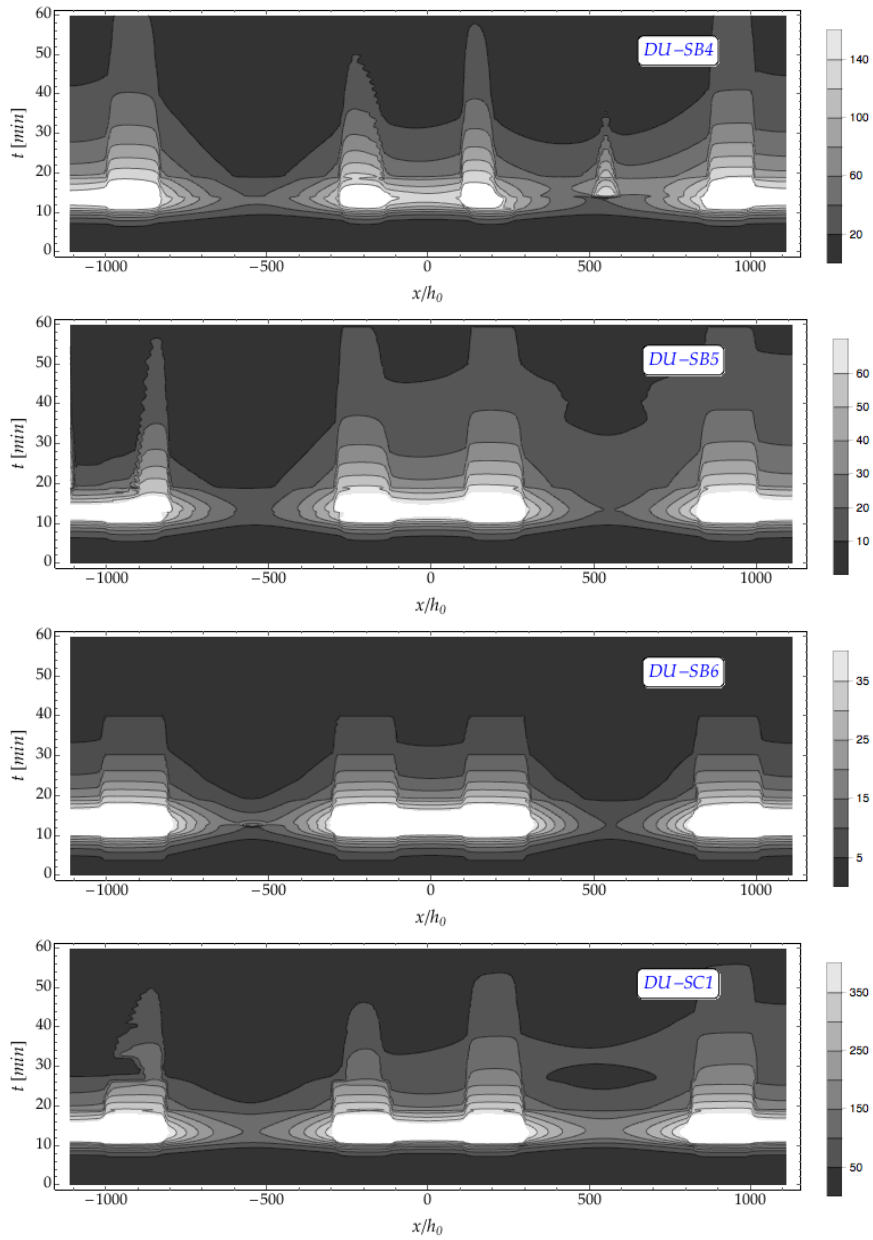
Figure 4.31: Comparison of results about diffusion: simulations DU-B4, B5, B6, C1

131
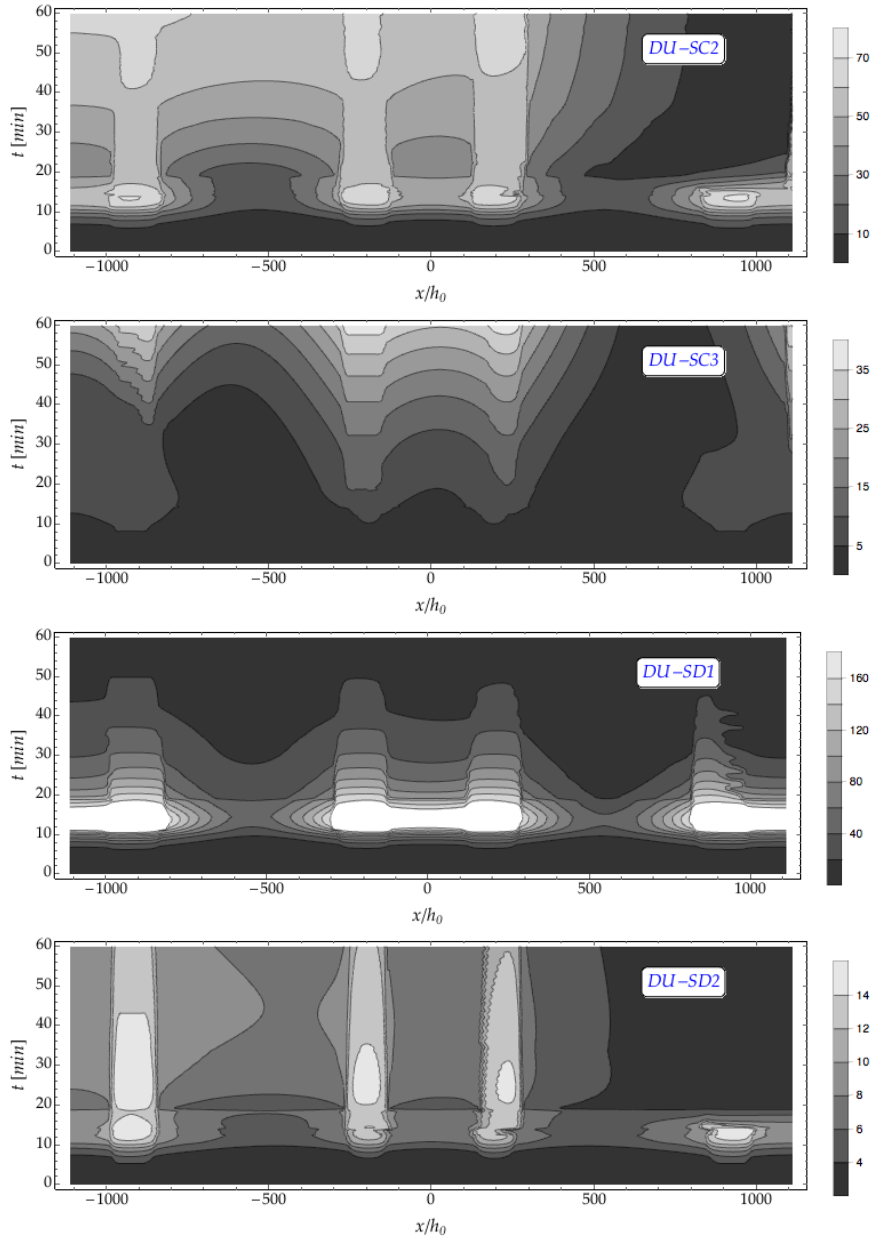
Figure 4.32: Comparison of results about diffusion: simulations DU-C2, C3, D1, D2
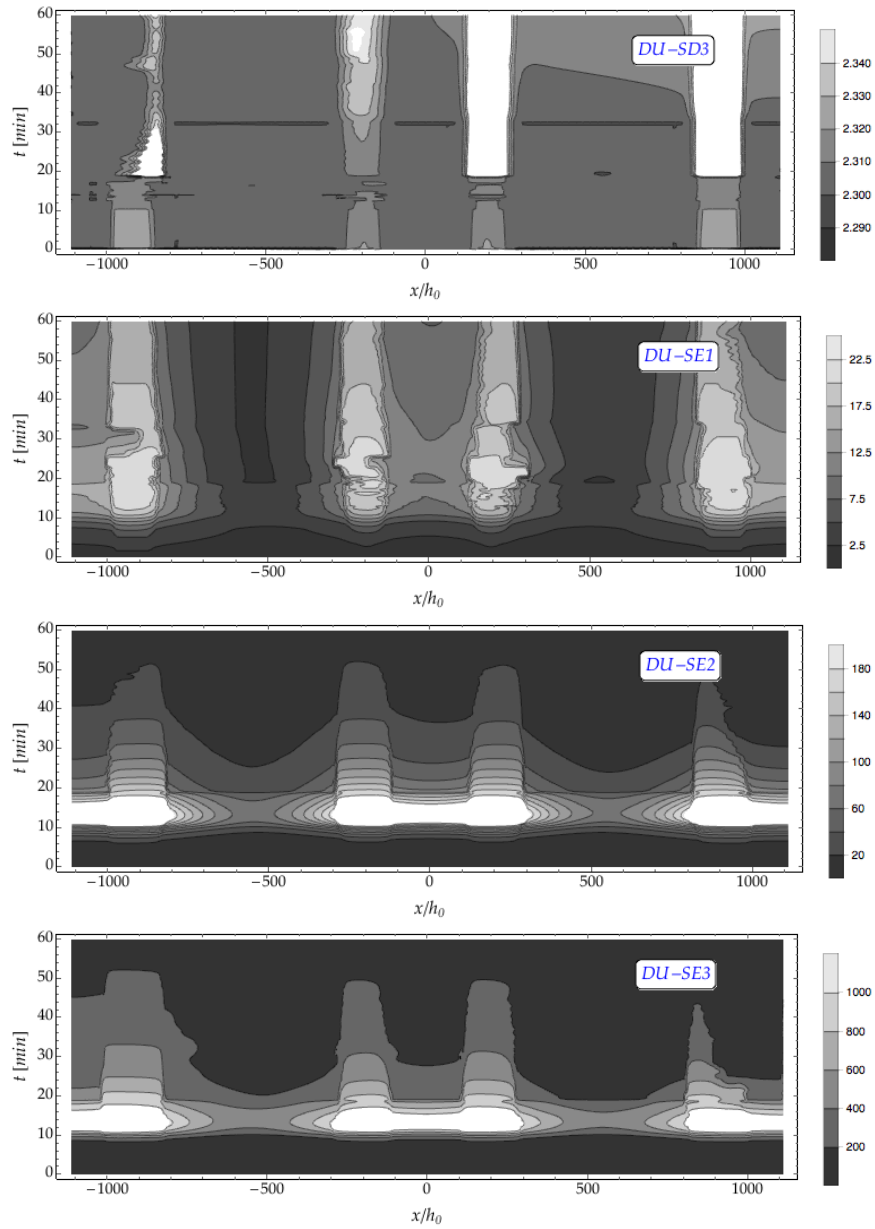
Figure 4.33: Comparison of results about diffusion: simulations DU-D3, E1, E2, E3
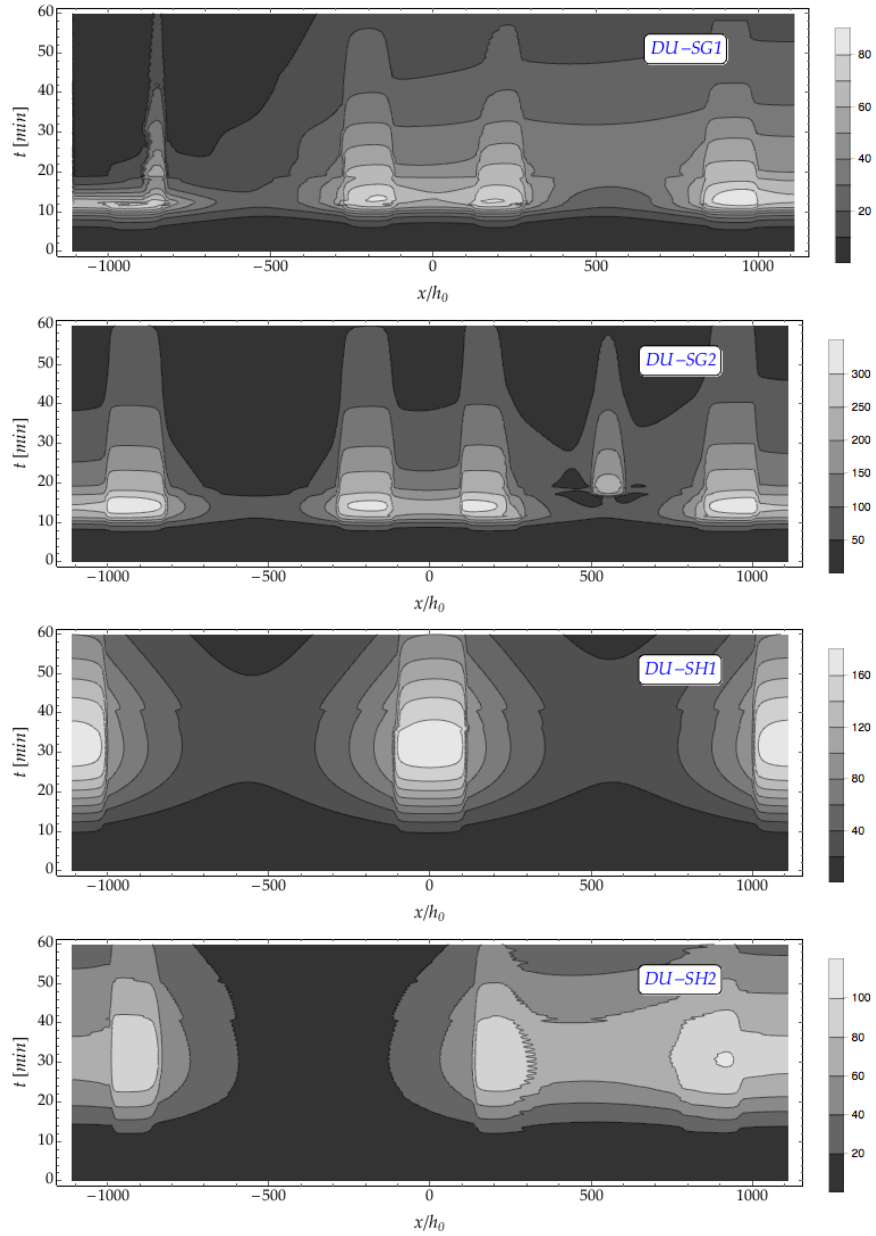
Figure 4.34: Comparison of results about diffusion: simulations DU-G1, G2, H1, H2

134
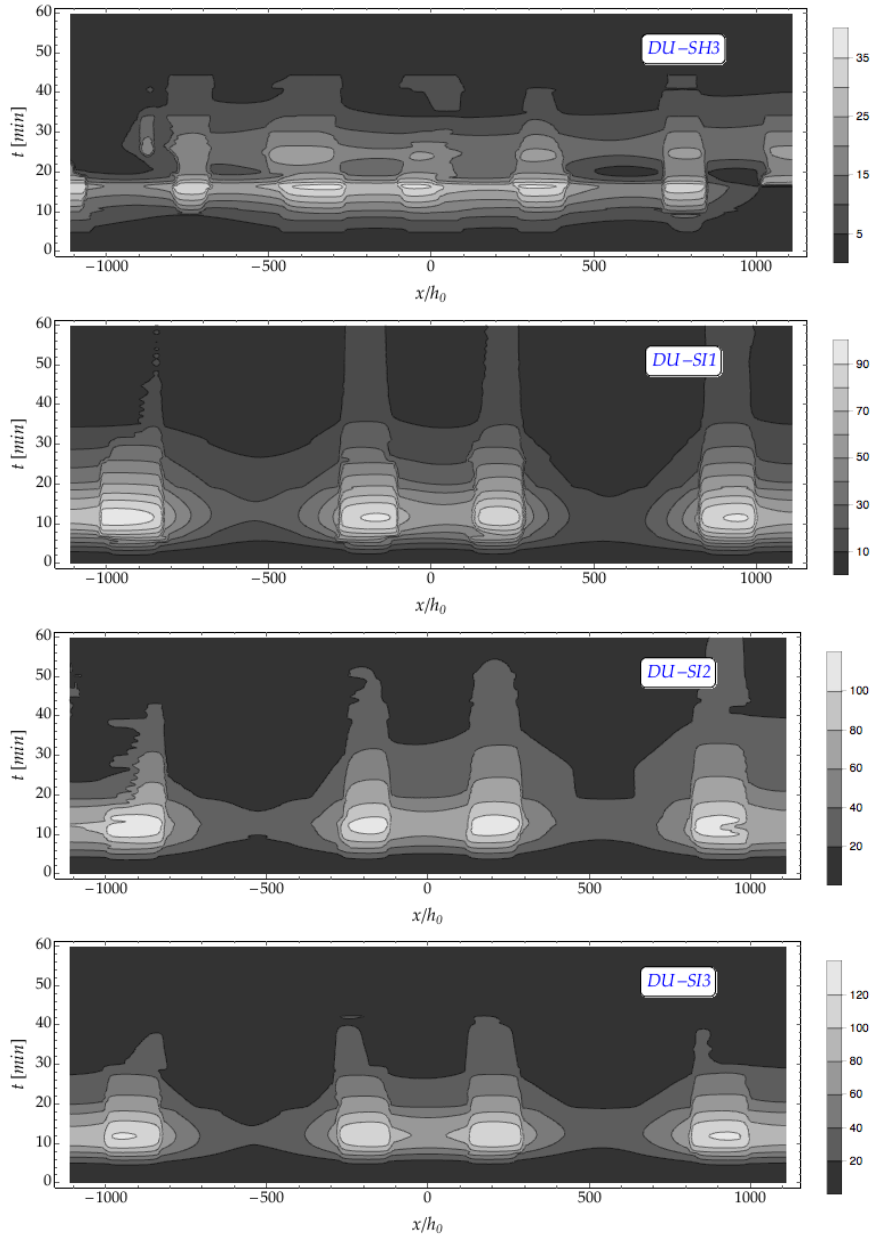
Figure 4.35: Comparison of results about diffusion: simulations DU-H3, I1, I2, I3
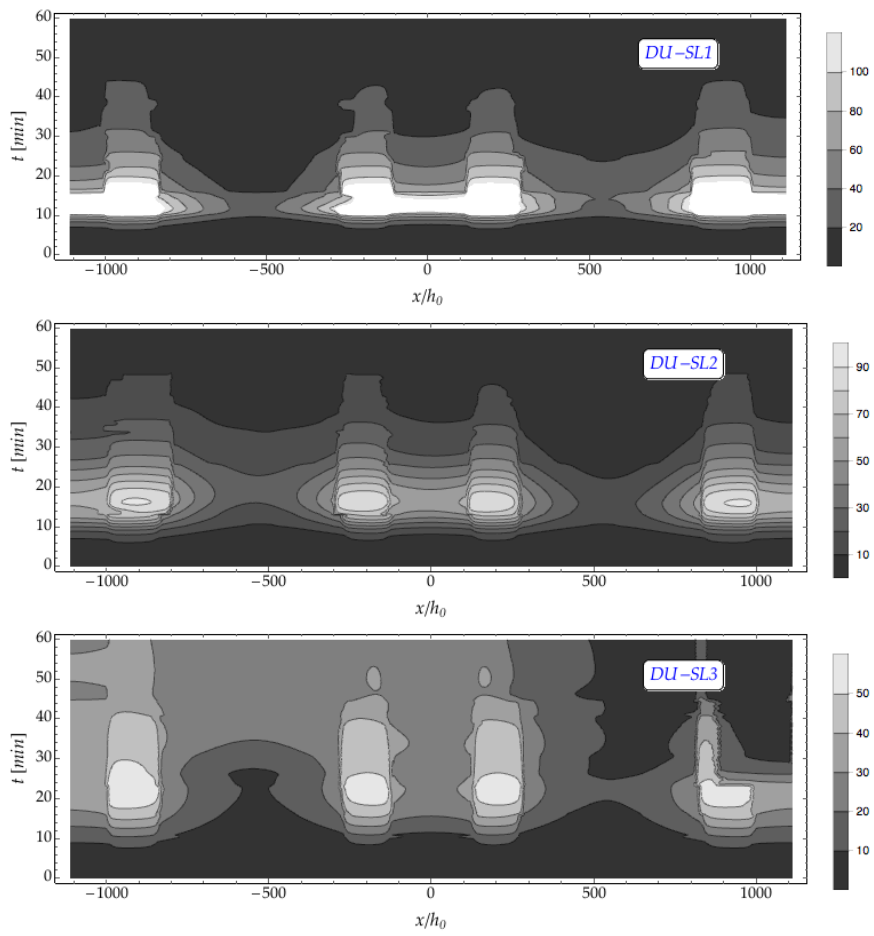
Figure 4.36: Comparison of results about diffusion: simulations DU-L1, L2, L3
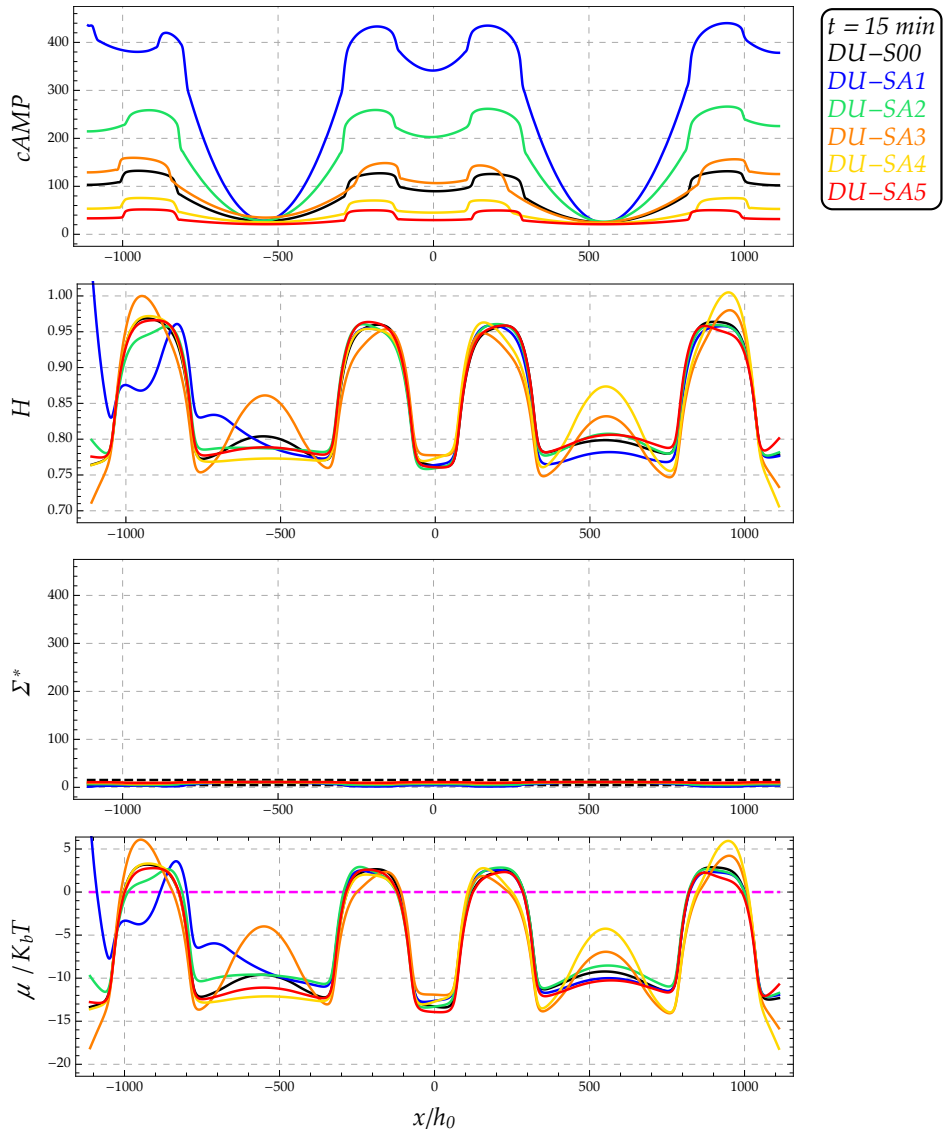
Figure 4.37: Simulation results **Series A**: cAMP, stress, stretch and chemical potential along the membrane at $t = 15\,min$.
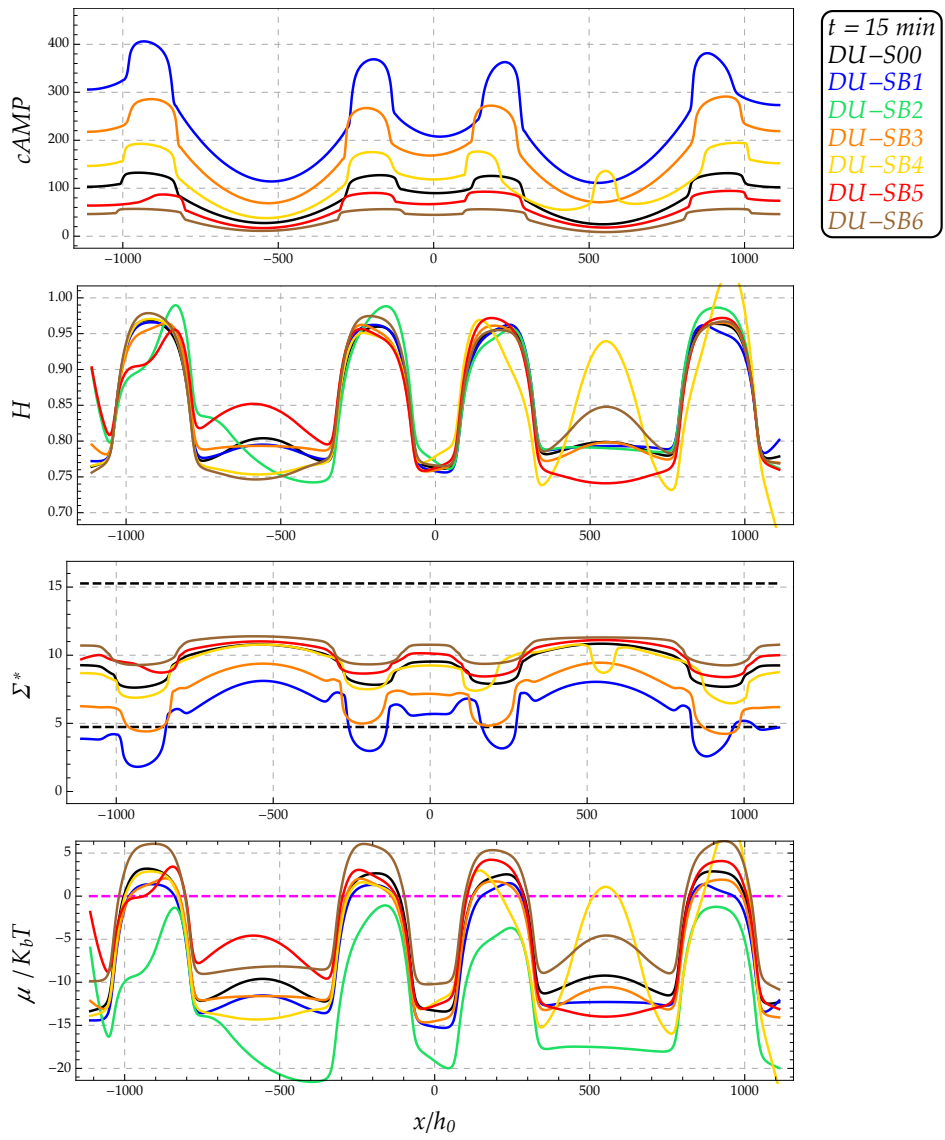
Figure 4.38: Simulation results **Series B**: cAMP, stress, stretch and chemical potential along the membrane at $t = 15\,min$.
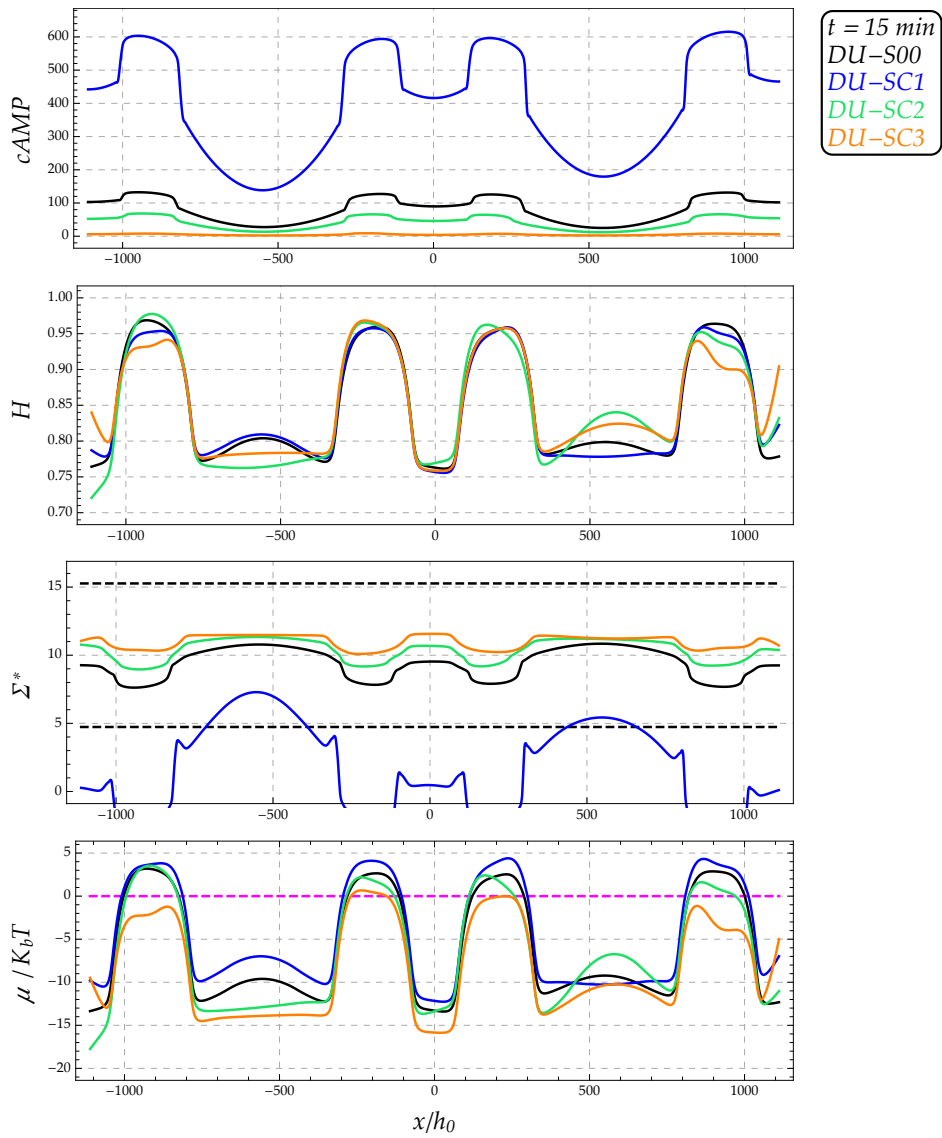
Figure 4.39: Simulation results **Series C**: cAMP, stress, stretch and chemical potential along the membrane at $t = 15\,min$.
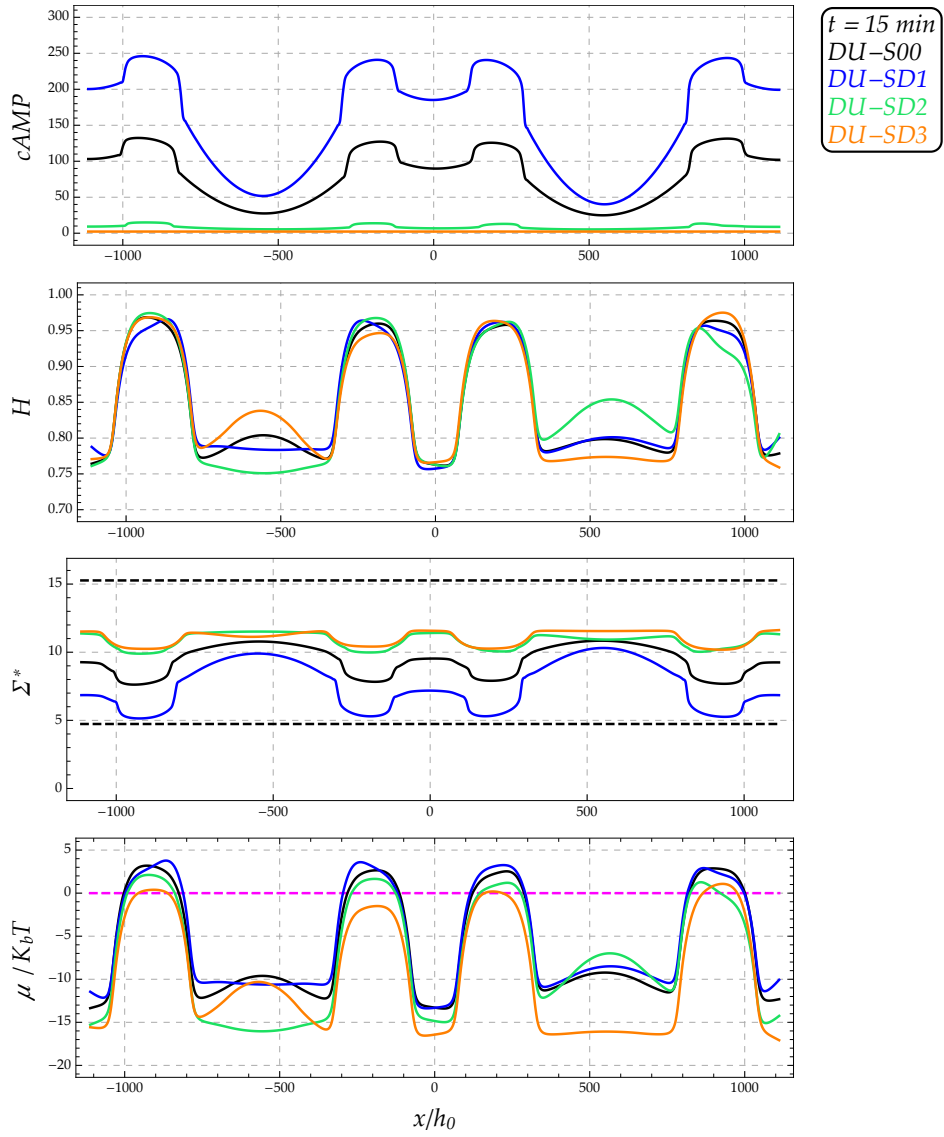
Figure 4.40: Simulation results **Series D**: cAMP, stress, stretch and chemical potential along the membrane at $t = 15\,min$.
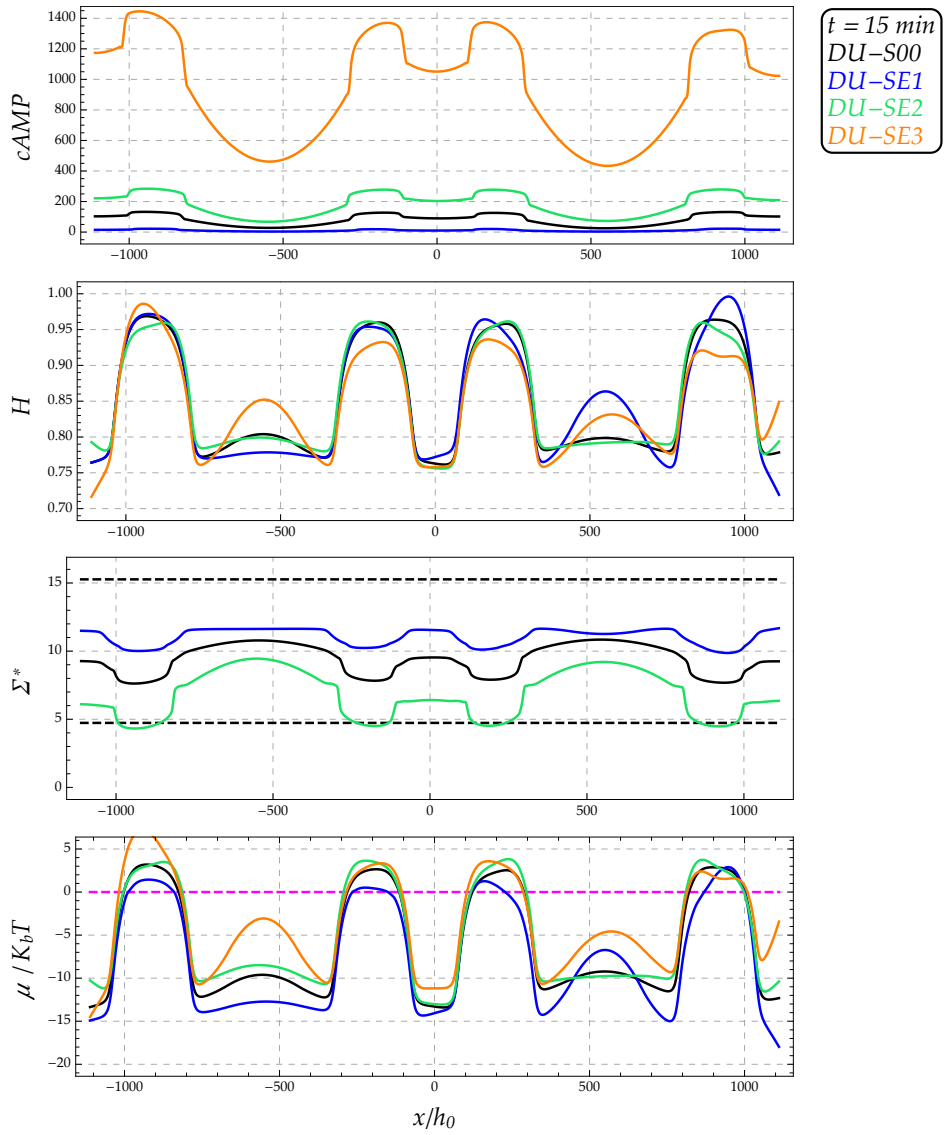
Figure 4.41: Simulation results **Series E**: cAMP, stress, stretch and chemical potential along the membrane at $t = 15\,min$.
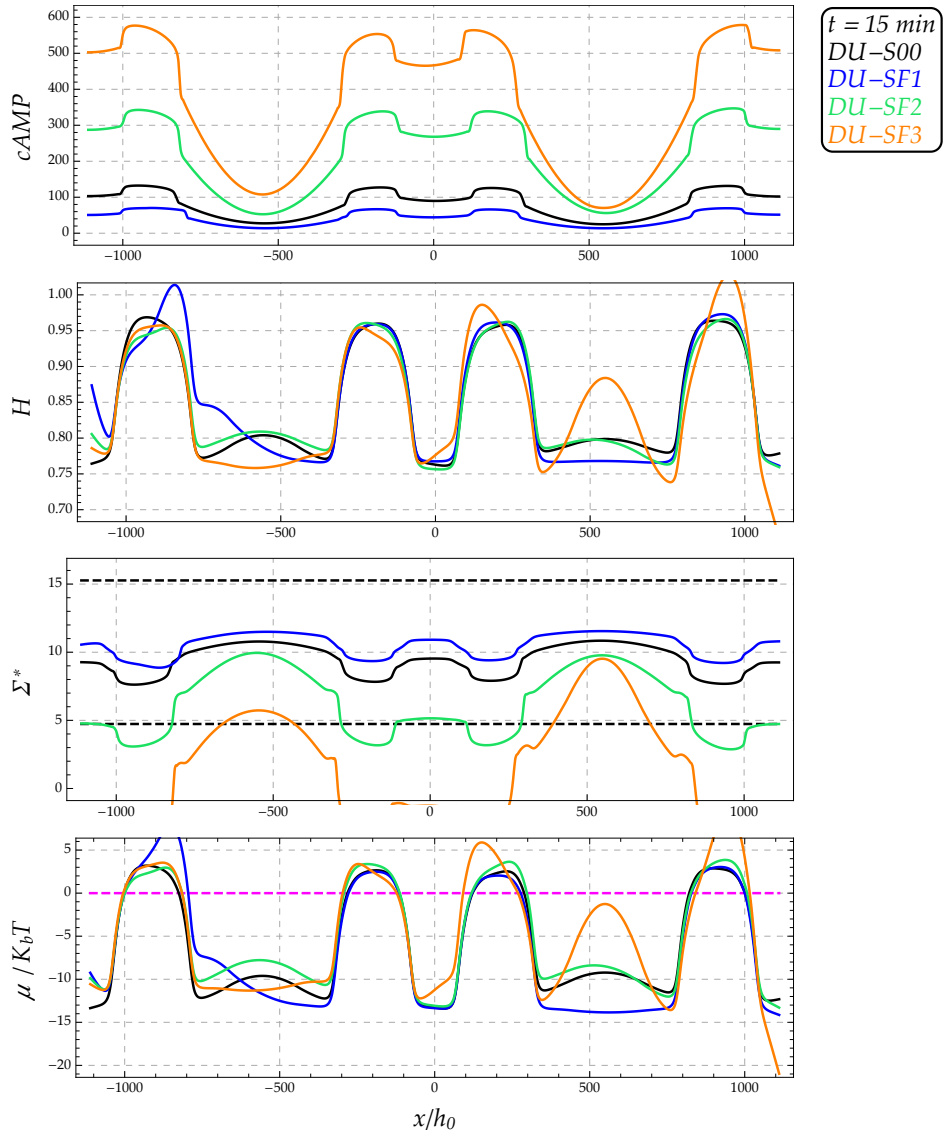
Figure 4.42: Simulation results **Series F**: cAMP, stress, stretch and chemical potential along the membrane at $t = 15\,min$.
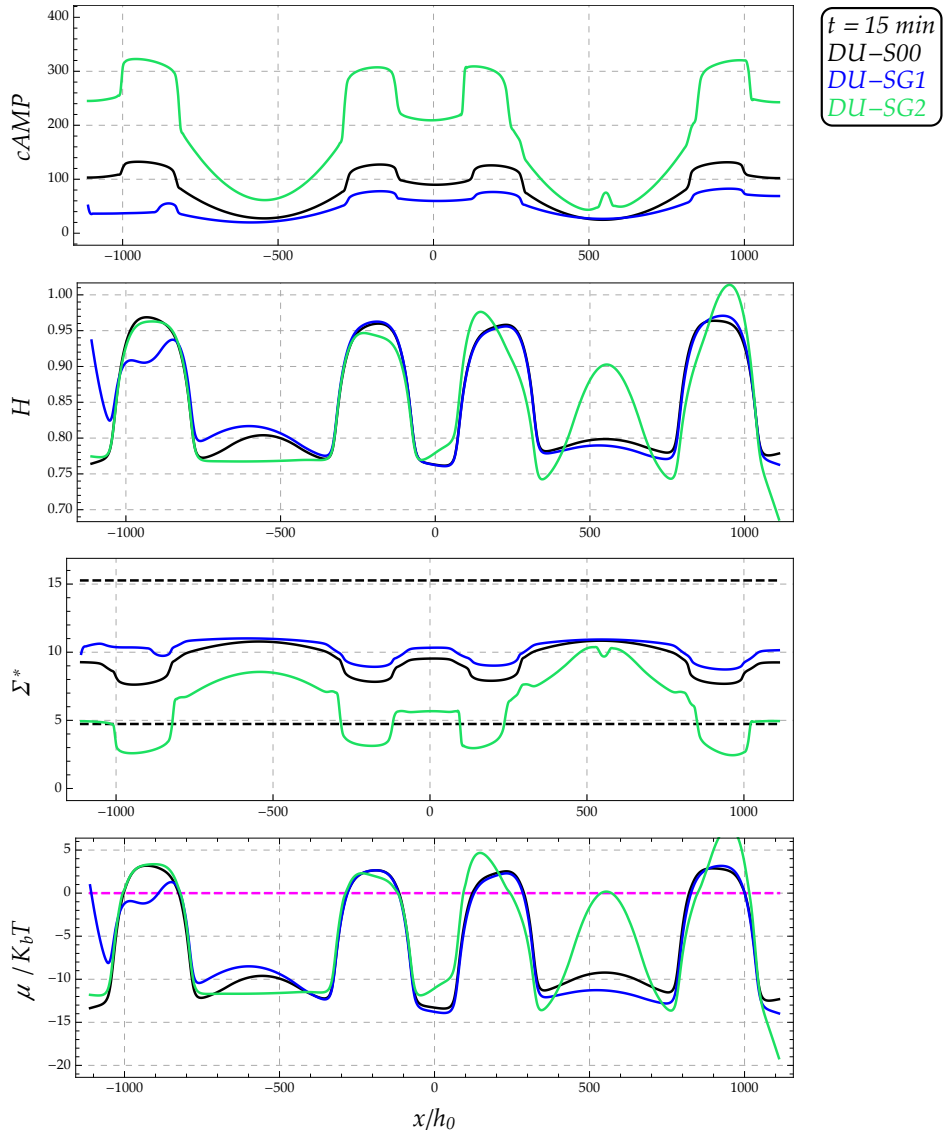
Figure 4.43: Simulation results **Series G**: cAMP, stress, stretch and chemical potential along the membrane at $t = 15\,min$.
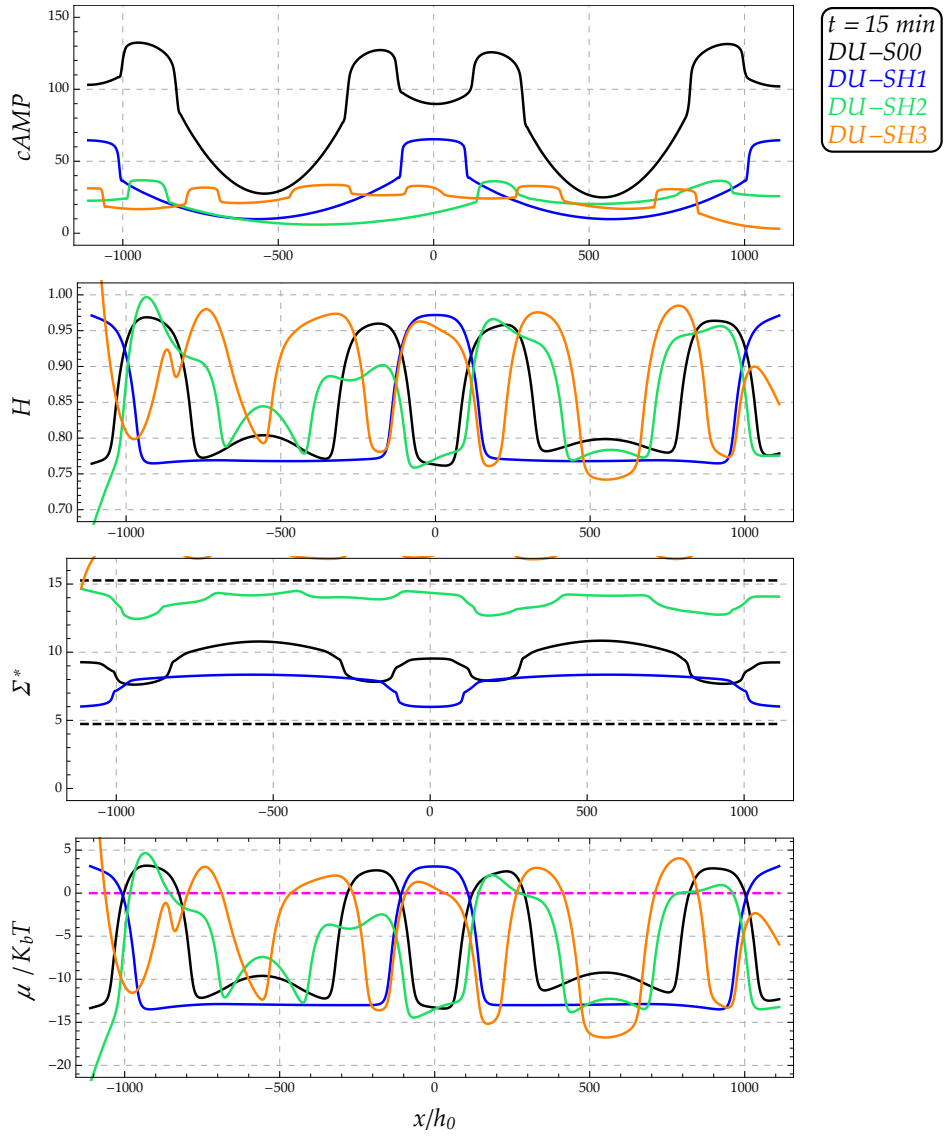
Figure 4.44: Simulation results **Series H**: cAMP, stress, stretch and chemical potential along the membrane at $t = 15\,min$.
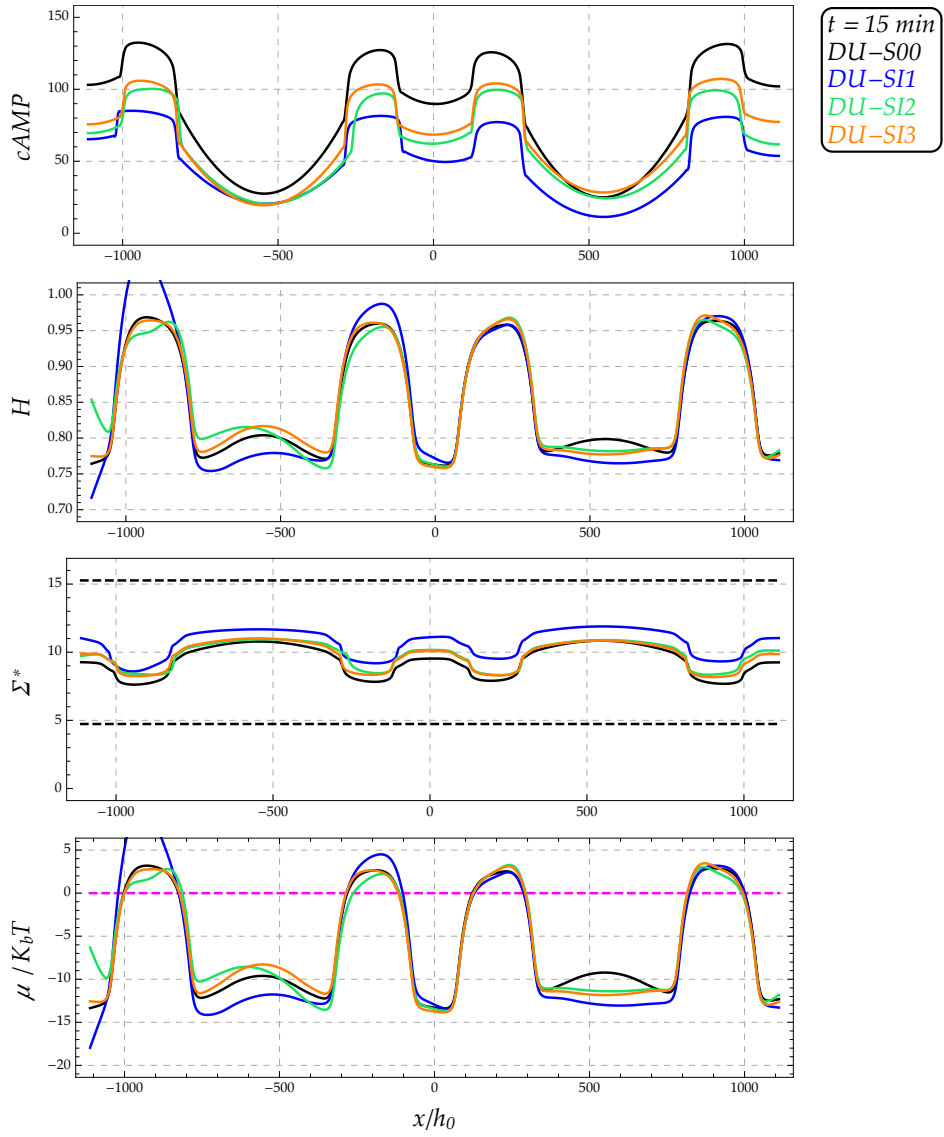
Figure 4.45: Simulation results **Series I**: cAMP, stress, stretch and chemical potential along the membrane at $t = 15\,min$.
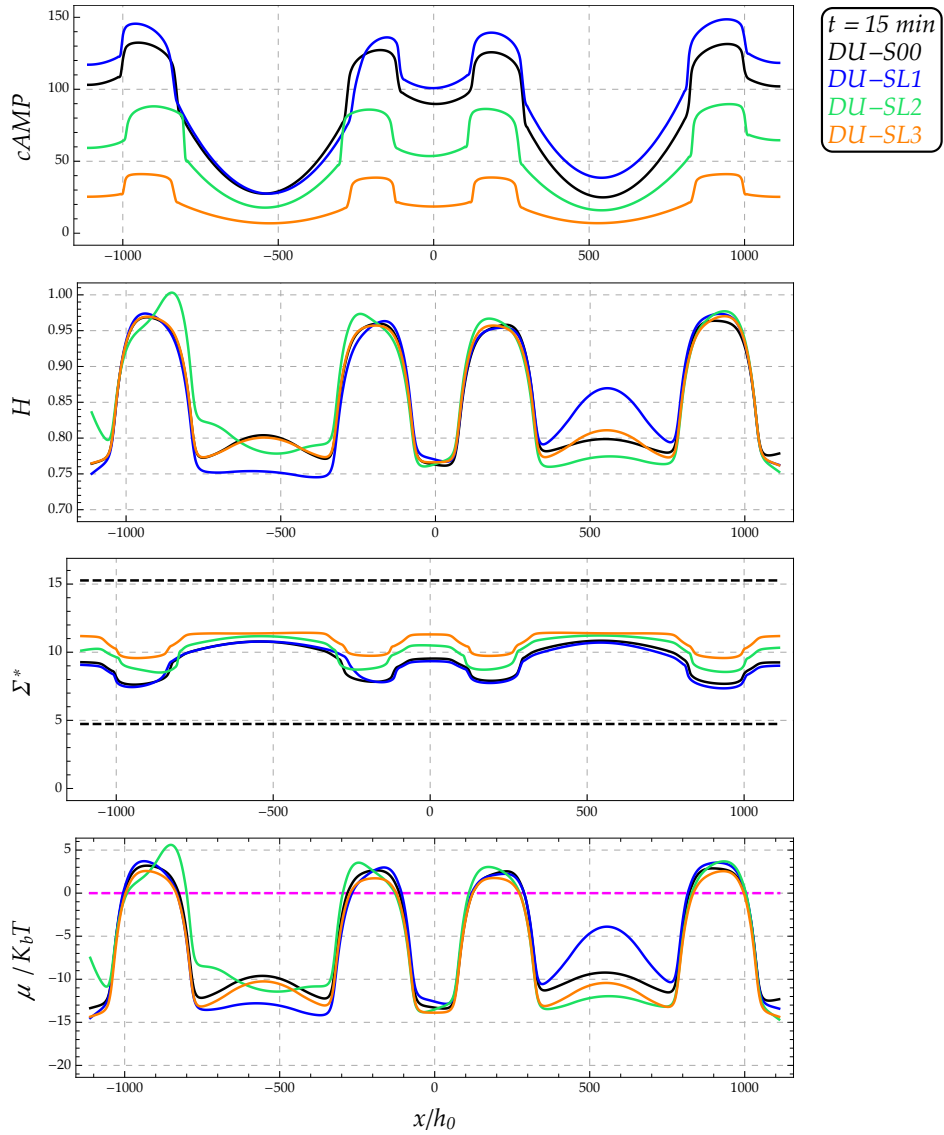
Figure 4.46: Simulation results **Series L**: cAMP, stress, stretch and chemical potential along the membrane at $t = 15\,min$.

4.6 Post-processing and Results

The aim of this Section is showing the postprocessing procedure applied for getting the final results. The more interesting analysis is focused on the exploration of the conformational field $\eta(x,t)$. The goal of these numerical simulations is exploring how the conformational field changes depending on the quantities of interest, with special regard to the change in thickness. The conformational field is computed by using the results of the simulation through the constitutive equation (2.28b), i.e.

$$\eta = \frac{1}{HK}\exp\left(-\frac{(1-H)(1-X)}{C\,X}\right),$$

derived in Chapter 2. The field $\eta(x,t)$ has been computed numerically at discrete selected times employing both the *double step* and the *double update* numerical scheme, and the results are shown in Figure 4.47 and Figure 4.48, respectively. For the sake of illustration, three different values of the constitutive parameter C have been chosen accordingly to the parametric analysis discussed in Chapter 2.3. At each instant, η can assume all the values included between the solid and the dashed line of the same color (i.e the two curves describing the field at a fixed instants). The former curve denotes the conformational change in correspondence of the minimum value of the geometrical parameter $K_{min} = 0.93$ estimated in Chapter 2.1, whereas the latter denotes the value of η related to the maximum value $K_{max} = 2.59$. The main result highlighted by these simulations is that the maximum activity is focused in correspondence of the locations where rafts take place.

Here we found, for the first time in literature at the best of the Writer's knowledge, an analytic model able to predict that the field $\eta(x,t)$ is higher where higher values of H is encountered, i.e. where formation of rafts happens, confirming the findings by Kobilka [117] and Lefkovitz [127].

A similar analysis can be done by focusing the attention on the change of the conformational field $\eta(x,t)$ at a specific location of the membrane, for instance the point on the axis of symmetry of the domain, i.e. $x = 0$, shown in Figure 4.47 and Figure 4.48. As expected, the activity is driven by the diffusion, and it is increasing until the maximum value of cAMP is

147
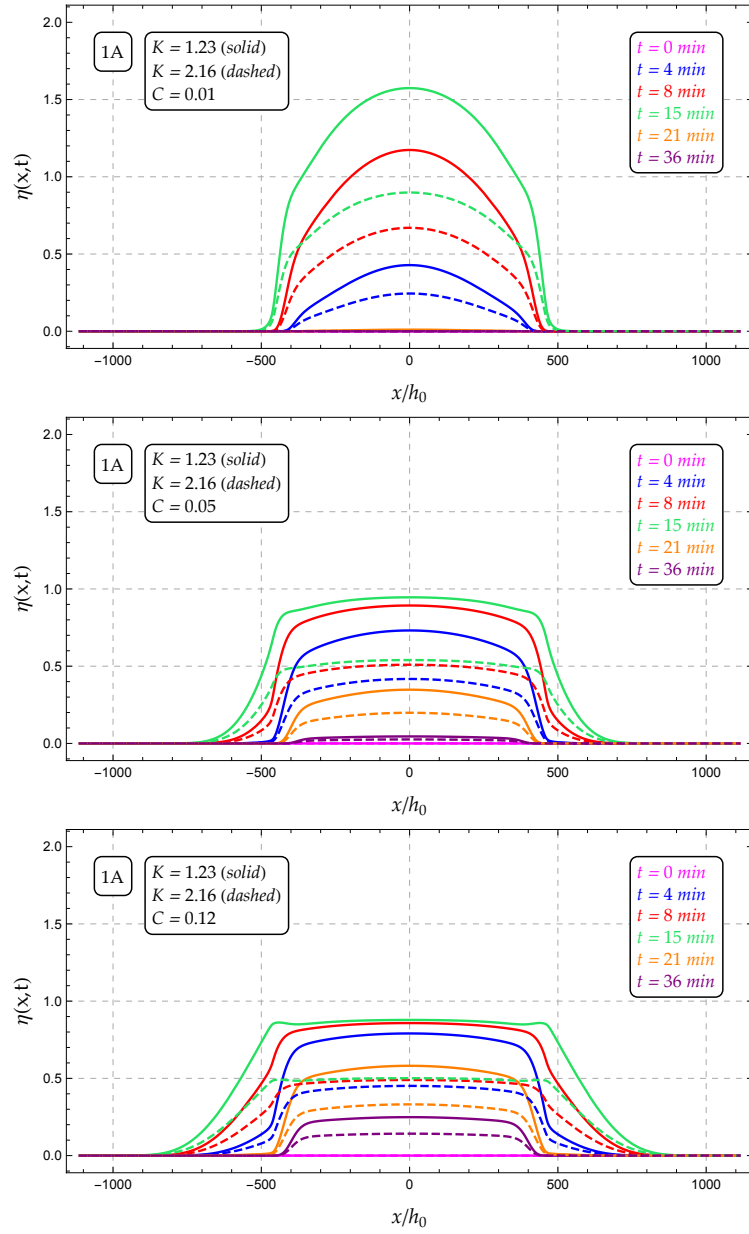
Figure 4.47: Conformational change $\eta(x,t)$ for fixed values of C (*double step* simulation).
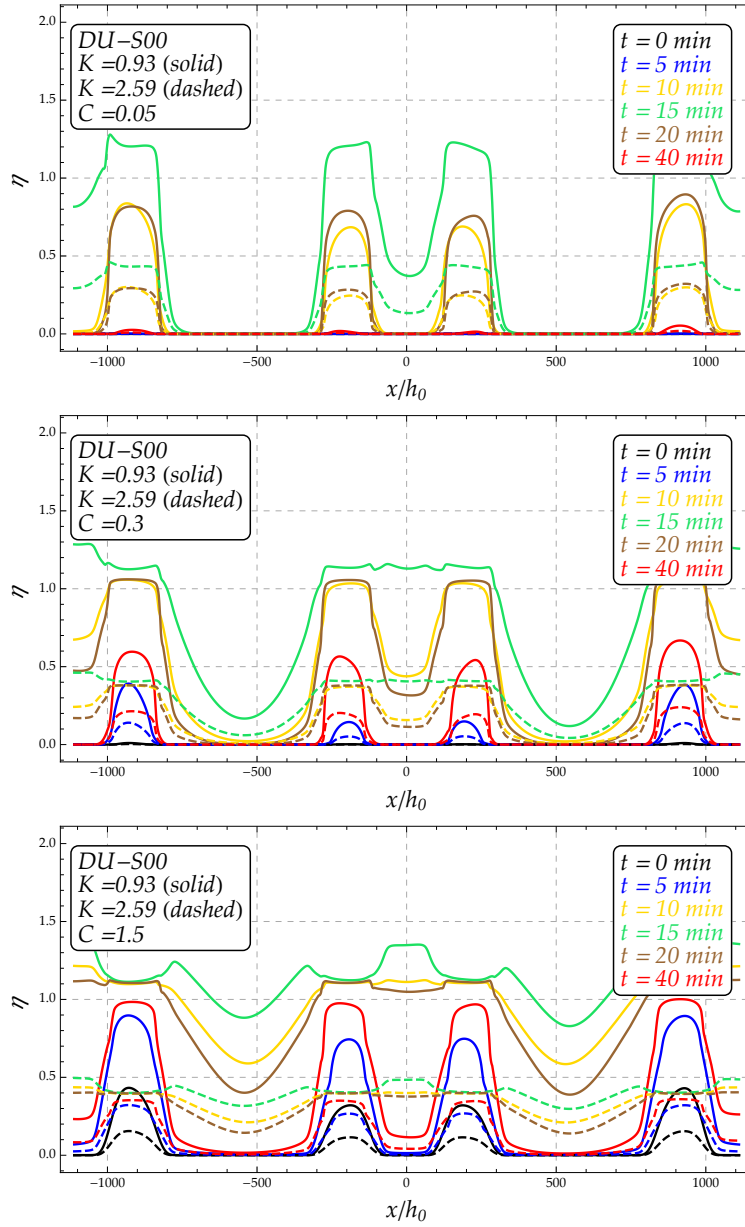
Figure 4.48: Conformational change $\eta(x, t)$ for fixed values of C (*double update* simulation).

149

measured, while it is decreasing after that point. Also in this case, three values of C are considered. The experimental results are in agreement with the experimental observations, suggesting that after some time, the receptor activity would vanish. This result is as true as smaller is the assumed value of C.
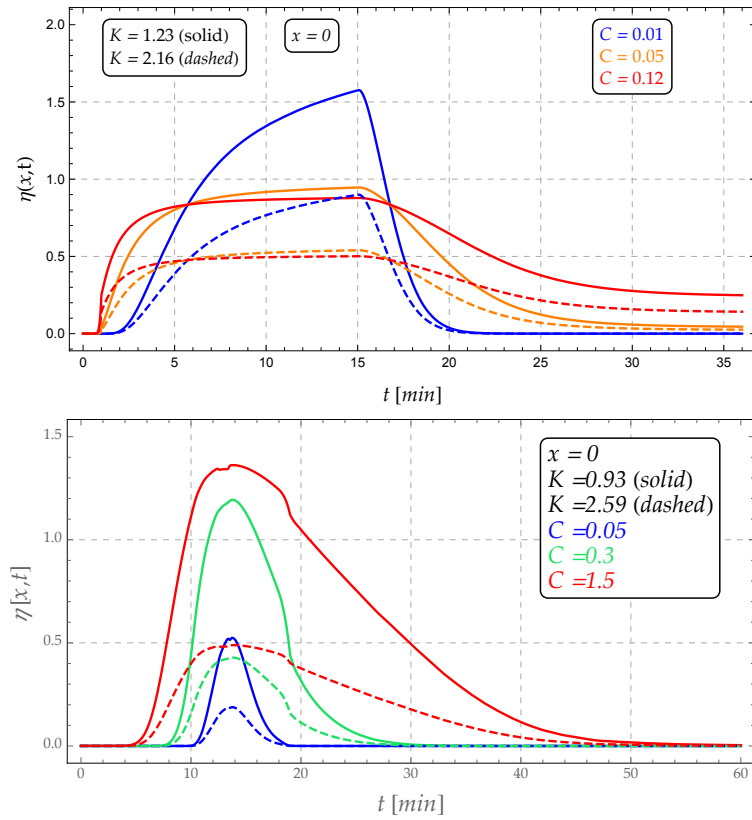
Figure 4.49: Conformational change $\eta(\bar{x}, t)$ for fixed values of C at $\bar{x} = 0$: *double step* (top) and *double update* scheme.

The analysis of the presented numerical results suggests that the more reliable value to be chosen in order to get physically reasonable results in terms of conformational changes η is $C = 0.3$. Based on this choice, in Figure 4.50 the conformational field is shown at several locations along the

membrane. The shape of the curves and the maximum reached value depend on the geometrical configuration of the receptor domain, i.e. on K: dashed curves denote the results obtained by means of K_min, whereas the solid ones are computed by using K_max. Obviously, all the region bounded by these two coupled curves (always drawn of the same color) represents possible value for η. A closer analysis of the results shows thaa after a period of about $40\,min$, the conformational activity drop to zero, independently of the studied location. This fact strengthens the choice of the parameter C.
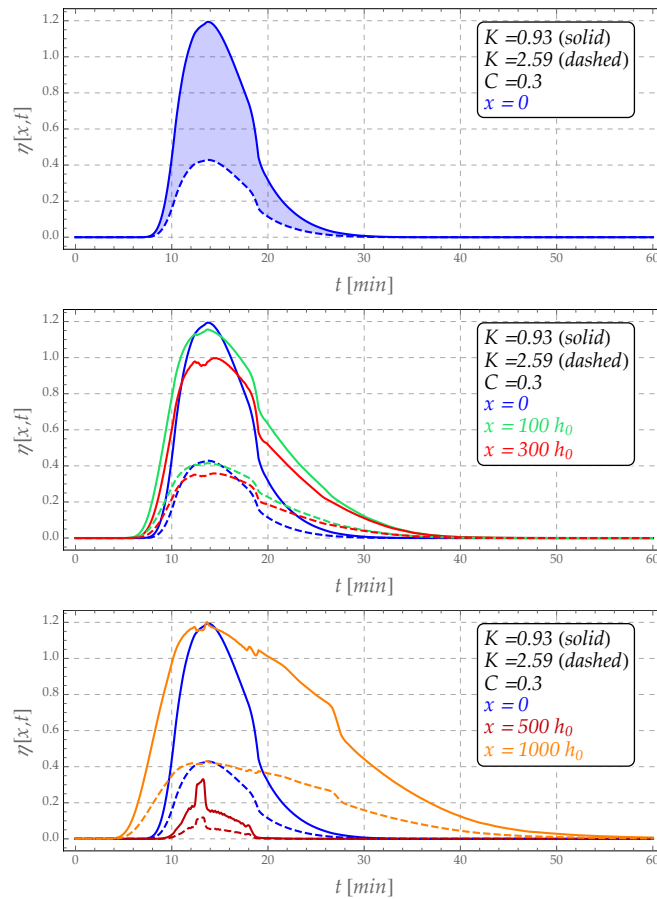
Figure 4.50: Conformational change $\eta(\bar{x}, t)$ at several fixed locations $\bar{x} = 0$.

References

[18]   C. Biondi et al. "cAMP efflux from human trophoblast cell lines: a role for multidrug resistance protein (MRP) 1 transporter". *Molecular Human Reproduction* 16.7 (2010), pp. 481–91 (cit. on pp. 3, 63–66, 72, 74, 87).

[31]   B. Coleman and D. Newman. "On the rheology of cold drawing. I.Elastic Materials". *Journal of Polymer Science: Part B: Polymer Physics* 26 (1988), pp. 1801–1822 (cit. on pp. 27, 96).

[81]   H. Gao, W. Shi, and L. Freund. "Mechanics of receptor-mediated endocytosis". *PNAS* 102.27 (2005), pp. 9469–9474 (cit. on pp. 36, 115).

[117]   B. Kobilka and X. Deupi. "Conformational complexity of G-protein-coupled receptors". *Trends in Pharmacological Sciences* 28.8 (2007), pp. 397–406 (cit. on pp. v, 3, 36, 48, 147, 252).

[127]   R. Lefkowitz. "Seven transmembrane receptors: something old, something new". *Acta Physiol* 190 (2007), pp. 9–19 (cit. on pp. v, 3, 36, 48, 147, 252).

[205]   M. Xie et al. "Inactivation of multidrug resistance proteins disrupts both cellular extrusion and intracellular degradation of cAMP". *Molecular Pharmacology* 80 (2011), pp. 281–293 (cit. on pp. 62, 63, 67, 86).

[206]   L. Yang and K. Dayal. "Free surface domain nucleation in a ferroelectric under an electrically charged tip". *Journal of Applied Physics* 111 (2012) (cit. on p. 90).

[207]   L. Yang and K. Dayal. "Microstructure and stray electric fields at surface cracks in ferroelectrics," *International Journal of Fracture* 174.1 (2012), pp. 17–27 (cit. on p. 90).

Chapter 5

Unstable behavior of lipid membranes

In this Chapter, lipid ordering phase changes arising in planar membrane bilayers is investigated both accounting for elasticity alone and for effective viscoelastic response of such assemblies. The mechanical response of such membranes is studied by minimizing the Gibbs free energy which penalizes perturbations of the changes of areal stretch and their gradients only [55]. As material instabilities arise whenever areal stretches characterizing homogeneous configurations lie inside the spinoidal zone of the free energy density, bifurcations from such configurations are shown to occur as oscillatory perturbations of the in-plane displacement. A review about the recently derived the energetics governing the thermo-chemo-mechanical behavior [4, 52, 55, 139] has been presented in Chapter 1, and it has been shown that such kind of energetics represents a powerful tool for predicting the response of biological membranes whenever specific conditions occur.

The main feature of this approach is that the energetics of the membrane can be described through one single ingredient: the in-plane membrane stretching

elasticity. This allows for describing the response with respect to local area changes on the membrane mid-surface. The principle of the minimum of energy allows for characterizing the governing equation of the mechanical response of the membrane. Both profile and the boundary layer of the disordering-ordering phenomena, i.e the change from a thicker domain (ordered phase) to a thinner one (disordered phase), and their associated rigidities have been determined.

The main feature of the energy derived in [50] is the presence of two turning points in the local stress governing the biological membrane behavior (see Figure 1.3). They are placed in a region characterized by material instabilities, i.e in a spinoidal zone. Henceforth, whenever the external conditions are such that the areal stretch, i.e. the reciprocal of the thinning, is enclosed in this region, the response may produce a rapid change of the geometry, i.e material instabilities can occur. In this work, we show that this occurrence is exhibited even when the in-plane viscosity of the lipid membrane is accounted for. In this regard, the experimental observations of lipid viscous behavior showed that the loss and storage moduli are well described by power law functions [66]. This observation suggests that the viscoelastic behavior of the biological membrane is properly described in the framework of the Fractional Hereditariness. Indeed, upon introducing an enriched kinematics accounting for in-plane shears and the exhibited in-plane power-law viscosity in a parallel contribution [53], a dimension reduction procedure analog to one shown in [52, 55] will be used for studying the fractional viscoelastic behavior mentioned above.

5.1 The linearized mechanics

In this Section linearized equation of lipid membrane under the plane strain geometry (1.20) will be derived, by starting from an homogeneous configuration $\bar{\Omega}$, such that $g_x = \bar{J}$ and $\phi = \bar{\phi}$ (hence $\phi_x = 0$). In this regard let us denote with ε the strain field perturbing uniformly the stretched configuration just described. The elastic free energy density (1.9) for the membrane is then evaluated at the perturbed configuration $J = \bar{J} + \varepsilon$, and takes the form:

$$\begin{aligned} \psi\left(\varepsilon, \varepsilon_x\right) &= \varphi\left(\bar{J} + \varepsilon\right) + \alpha(\bar{J} + \varepsilon) \|\left(\bar{J} + \varepsilon\right)_x\|^2 \\ &\approx \varphi(\bar{J}) + \varphi'(\bar{J})\,\varepsilon + \frac{\varphi''(\bar{J})}{2}\varepsilon^2 + \alpha(\bar{J})\,\|\varepsilon_x\|^2 \end{aligned} \tag{5.1}$$

where higher-order contributions in ε^2 are neglected. Then the free energy takes the form:

$$\Psi = \int_\Omega \psi(\varepsilon, \varepsilon_x)\,\mathrm{d}x, \tag{5.2}$$

154

where a domain $\Omega \in [-L/2, L/2]$ is considered and

$$\psi(\varepsilon, \varepsilon_x) = \varphi(\bar{J}) + \varphi'(\bar{J})\,\varepsilon + \frac{\varphi''(\bar{J})}{2}\varepsilon^2 + \alpha(\bar{J})\,\varepsilon_x^2. \tag{5.3}$$

As consequence of this choice, the (in-plane) displacement field is described through a perturbation v such that $u = \bar{u} + v$. Of course, $\varepsilon(x) = v_x(x)$.

It is assumed that the membrane is pulled by opposite tractions of magnitude Σ (force per reference length) at the boundary, i.e on the edges $x = \pm L/2$, although the case in which the end displacements are controlled may be treated in an analog way (see, *e.g.*, [198]). Due to the presence of nonlocal terms ε_x, it is necessary to introduce *hyper-tractions* Γ which perform work against displacement gradient v_x at the boundary [171]. Henceforth, the total energy $\mathscr{E}$ change in a neighborhood of the homogeneously deformed configuration reads as follows:

$$\mathscr{E} = B\,\Psi - \mathcal{W}(v, v_x), \tag{5.4}$$

where B denotes the width of the membrane patch and $\mathcal{W}$ is the external work of the applied tractions Σ and hypertractions Γ (see Chapter 1) defined as follows:

$$\mathscr{W}(v, v_x) = B\left[\Sigma\,(\bar{u} + v) + \Gamma\,(\bar{u}_x + v_x)\right]_{\partial\Omega}, \tag{5.5}$$

where $\bar{u} = \bar{J}_x$ is the displacement corresponding to the homogeneously stretched configuration from which bifurcations are sought. Upon substituting (5.1) and (5.4) in (5.5) the total energy change takes the following form:

$$\mathscr{E} = B\int_{\Omega}\left(\varphi + \varphi'(\bar{J})\,v_x + \frac{\varphi''(\bar{J})}{2}v_x^2 + \alpha(\bar{J})\,v_{xx}^2\right)\mathrm{d}x - B\left[\Sigma\,v + \Gamma\,v_x\right]_{\partial\Omega} + \bar{\mathscr{E}}. \tag{5.6}$$

In the sequel all the quantities with the over-bar are referred to the homogeneously stretched configuration, e.g. $\bar{\varphi} := \varphi(\bar{J})$, $\bar{\varphi}'' := \varphi''(\bar{J})$ and $\bar{\alpha} := \alpha(\bar{J})$. The variation of the energy is computed with respect to a reference value $\mathscr{E}(\bar{J})$ defined as follows:

$$\bar{\bar{\mathscr{E}}} = B\int_{\Omega}\varphi(\bar{J})dx - \left[\Sigma\,\bar{u} + \Gamma\,\bar{u}_x\right]_{\partial\Omega}. \tag{5.7}$$

In this Chapter, the unidimensional case only is considered, then the relationship $J = v'(x)$ holds. The resulting governing equation of the planar membrane is obtained by imposing the stationarity of $\mathscr{E}$, then by entering this result into the

155

energetic functional the first variation reads as follows:

$$\delta\mathscr{E} = \int_{\Omega} (\bar{\varphi}' + \bar{\varphi}''v')\,\delta v' + (2\bar{\alpha}\,v'')\delta v'' - [\Sigma\delta v + \Gamma\delta v']_{\partial\Omega}. \tag{5.8}$$

After expanding all contributions and integrating by part, the Euler-Lagrange equation with its boundary condition reads as follows:

$$\begin{cases} 2\bar{\alpha}\,v'''' - \bar{\varphi}''\,v'' = 0 & \text{in } \Omega \\ \text{either } \bar{\varphi}''\,v' - 2\bar{\alpha}\,v''' = \Sigma - \bar{\varphi} \text{ or } \delta v = 0 & \text{in } \partial\Omega \\ \text{either } 2\bar{\alpha}\,v'' = \Gamma \text{ or } \delta v' = 0 & \text{in } \partial\Omega \end{cases} \tag{5.9}$$

It is worth noting that homogeneous configurations of the membranes from which oscillatory perturbations could arise are not known. In order to find the values of $\bar{J}$ characterizing such homogeneous states and to study the solution of the boundary value problem governing bifurcated equilibria from such configurations, a parameter ω is introduced as follows:

$$\omega^2 := \begin{cases} +\dfrac{\bar{\varphi}''}{2\bar{\alpha}} & \text{if } \bar{\varphi}'' > 0 \\[3mm] -\dfrac{\bar{\varphi}''}{2\bar{\alpha}} & \text{if } \bar{\varphi}'' < 0, \end{cases} \tag{5.10}$$

where:

$$\frac{\bar{\varphi}''}{2\bar{\alpha}} = \frac{12}{h_0^2}\frac{\bar{\varphi}''}{\bar{\varphi}'}\,\bar{J}^5, \tag{5.11}$$

because of (1.10). Henceforth, equation (5.9) can be recast as:

$$\begin{cases} v'''' \mp \omega^2\,v'' = 0 & \text{in } \Omega \\ \text{either } \pm\omega^2 v' - v''' = \dfrac{\Sigma - \bar{\varphi}}{2\bar{\alpha}} \text{ or } \delta v = 0 & \text{in } \partial\Omega \\ \text{either } 2\bar{\alpha}\,v'' = \Gamma \text{ or } \delta v' = 0 & \text{in } \partial\Omega. \end{cases} \tag{5.12}$$

The choice of the boundary conditions above generate various cases. For the sake of illustration, we choose the case in which the displacement is constrained and the hypertractions are imposed at the boundary, i.e. $v = 0$ and $2\bar{\alpha}\,v'' = \Gamma$.

It is worth noting that the assumed value of ω^2 affects the quality of the solution, i.e. the onset of phase changes in the elastic membrane. In this regard some sub-cases can be identified depending upon the location of the reference condition associated to $\bar{J}$ in the stretching energy function in Figure 1.3. Indeed, because $\varphi(J)$ has at most one stationary point J_0 unless the lipid bilayer is at its

transition temperature, inspection of Figure 1.3 shows that there are four values of J besides $\bar{J}$ to be accounted for, namely $J_* \leq J_{max} \leq J_{min} \leq J^*$. Here J_{max}, J_{min} are stationarity points of $\tau(J) = \varphi'(J)$, i.e. $\varphi(J)$ changes curvature there (namely $\varphi''(J)$ changes sign, while J_* and J^* are the abscissas of the two points sharing common tangent on $\varphi(J)$. Two alternative situations may arise depending on the sign of $\bar{\varphi}''$. This depends on whether or not the configuration $\bar{J}$ is in the spinoidal (*unstable*) zone of the local energy density $\varphi(J)$.

The special form of the local stress $\tau(J) = \varphi'(J)$ shown in Figure 1.3 allows for discriminating several cases around the spinodial-zone, i.e. where the function $\tau(J)$ is an S-shaped function. Indeed, whenever $J < J_1$ and $J > J_2$ the equilibrium can be reached for only one value of J, namely $\Sigma = \tau(J)$ (see (1.23)). On the contrary, if $J_1 < J < J_2$ the configuration lies in the spinoidal-zone, and the membrane can sustain the same value of the stress by assuming three different configurations, i.e. the three intersection of the function $\tau(J)$ with the horizontal straight line representing the values of the stress at the edges. Here, the only parameter governing the membrane behavior is the areal-stretch J, henceforth, by recalling the basic idea of the instabilities of structures, the system is stable if the second derivative of the total potential energy (namely $\varphi(J)$ for an homogeneous configuration) is positive. Therefore, two different behaviors occur inside the spinoidal zone: if $J_1 < J < J_{max}$ or $J_{min} < J < J_2$ the second derivative of the energy is positive $\varphi''(J) > 0$ (i.e, the slope of $\tau(J) = \varphi'(J)$ is positive), and the behavior is stable, otherwise $J_{max} < J < J_{min}$ and the second derivative assumes negative values, namely $\varphi''(J) < 0$ and the slope of $\tau(J) = \varphi'(J)$ is negative, determining the unstable behavior.

5.1.1   Unstable zone

Let now explore the case for which $\bar{\varphi}'' < 0$ in (5.10), which happens whenever $\bar{J}$ is located in the spinoidal zone, i.e. $J_{max} < \bar{J} < J_{min}$, corresponding to a negative slope of the local stress, since $\tau(J) = \varphi'(J)$ (see Figure 1.3). Clearly, this represent the only interesting case, because the presence of the homogeneously stretched membrane[1] lying in the unstable zone, can drive unexpected evolution phenomena. The governing equation (5.12) takes the following form:

$$v_{xxxx} + \omega^2 v_{xx} = 0, \tag{5.13}$$

---

[1]At this stage, the knowledge on how the membrane got the current configuration is not of interest. It is reasonable to assume that this configuration is imposed in a experimental setup.

which admits the integral

$$v(x) = A_1 \cos(\omega\, x) + A_2 \sin(\omega\, x) + A_3\, x + A_4. \tag{5.14}$$

We explore this solution for the following boundary conditions apply:

$$v\Big|_{\partial\Omega^-} = 0 \qquad v\Big|_{\partial\Omega^+} = 0 \qquad 2\bar{\alpha}v''\Big|_{\partial\Omega^-} = \hat{\Gamma}_L \qquad 2\bar{\alpha}v''\Big|_{\partial\Omega^+} = \hat{\Gamma}_R \tag{5.15}$$

where $\hat{\Gamma}_R = \Gamma\Big|_{\partial\Omega^+}$ and $\hat{\Gamma}_L = \Gamma\Big|_{\partial\Omega^-}$. The values of the coefficients A_i in (5.14) depend on the specified boundary conditions. For the sake of convenience the positions $c = \cos(\omega\, L/2)$ and $s = \sin(\omega\, L/2)$ are assumed; henceforth, the BCs assume the following form:

$$\begin{cases} A_1\, c - A_2\, s - A_3 \dfrac{L}{2} + A_4 = 0 \\ 2\bar{\alpha}\omega^2\left(-A_1\, c + A_2\, s\right) = \hat{\Gamma}_L \end{cases} \text{ at } x = -\dfrac{L}{2}$$

$$\begin{cases} A_1\, c + A_2\, s + A_3 \dfrac{L}{2} + A_4 = 0 \\ 2\bar{\alpha}\omega^2\left(-A_1\, c - A_2\, s\right) = \hat{\Gamma}_R \end{cases} \text{ at } x = +\dfrac{L}{2}$$

$x = -L/2$	$x = +L/2$
$A_1\, c - A_2\, s - A_3 \dfrac{L}{2} + A_4 = 0$	$A_1\, c + A_2\, s + A_3 \dfrac{L}{2} + A_4 = 0$
$2\bar{\alpha}\omega^2\left(-A_1\, c + A_2\, s\right) = \hat{\Gamma}_L$	$2\bar{\alpha}\omega^2\left(-A_1\, c - A_2\, s\right) = \hat{\Gamma}_R$

In this example it is assumed $\hat{\Gamma}_L = \hat{\Gamma}_R = \hat{\Gamma}$. These assumptions lead to a simplified matrix system:

$$\begin{bmatrix} 0 & s & \frac{L}{2} & 0 \\ c & 0 & 0 & 1 \\ 0 & s & 0 & 0 \\ -2\bar{\alpha}\,\omega^2 c & 0 & 0 & 0 \end{bmatrix} \begin{pmatrix} A_1 \\ A_2 \\ A_3 \\ A_4 \end{pmatrix} = \begin{pmatrix} 0 \\ 0 \\ 0 \\ \hat{\Gamma} \end{pmatrix}, \tag{5.16}$$

whose determinant is $\bar{\alpha}\, c\, s\, L\, \omega^2$. We first study the nontrivial modes (**??**) of the system, i.e. we explore the roots of the following equation

$$\bar{\alpha}\, c\, s\, L\, \omega^2 = 0. \tag{5.17}$$

It is worth noting that, because of the definition (1.10) and $1 < J_{max} < \bar{J} < J_{min}$, we have $\bar{\alpha} > 0$ for all $\bar{J} > 1$. Then, the orthogonality of the trigonometric functions imposes that the equation is satisfied if either for $c = \cos(\omega\, L/2) = 0$ or for $s = \sin(\omega\, L/2) = 0$. Henceforth, we are left to examine two subcases.

Case 1. Let us consider the case $s = 0$ and $c = \pm 1$. This condition implies that:

$$\sin\left(\omega\,\frac{L}{2}\right) = 0 \quad\Longrightarrow\quad \omega\,\frac{L}{2} = n\,\pi \quad\Longrightarrow\quad \omega = \frac{2\,n\,\pi}{L} \qquad (5.18)$$

and a closer analysis of (5.18) shows that this case occurs whenever the following relationship holds:

$$\frac{\bar{\varphi}''}{\bar{\varphi}'}\,\bar{J}^5 = -\frac{n^2\pi^2}{3}\left(\frac{h_0}{L}\right)^2. \qquad (5.19)$$

The thinness of the membrane here enters with the ratio $(h_0/L)^2$ which is normally smaller than 10^{-8}. A large but finite number n of oscillation can certainly arise from (5.19) for J such that $\bar{\varphi}'' \to 0^-$, i.e. right after change on convexity of the local part of the strain energy density. The solution of the system allows for deducing the values of amplitude of the nth mode:

$$\begin{bmatrix} 0 & 0 & \frac{L}{2} & 0 \\ \pm 1 & 0 & 0 & 1 \\ 0 & 0 & 0 & 0 \\ \mp 2\bar{\alpha}\,\omega^2 & 0 & 0 & 0 \end{bmatrix} \begin{pmatrix} A_1 \\ A_2 \\ A_3 \\ A_4 \end{pmatrix} = \begin{pmatrix} 0 \\ 0 \\ 0 \\ \hat{\Gamma} \end{pmatrix}$$

then

$$\begin{cases} A_1 = \mp\dfrac{\hat{\Gamma}}{2\bar{\alpha}\,\omega^2} \\ A_3 = 0 \\ A_4 = \mp A_1 \end{cases}.$$

Hence, the buckled mode n has the following form:

$$v_n(x) = \pm\frac{\hat{\Gamma}}{8\,\bar{\alpha}\,n^2\,\pi^2}\left[\cos\left(2n\pi\,\frac{x}{L}\right) - 1\right] + \quad + A_2\sin\left(2n\pi\,\frac{x}{L}\right). \qquad (5.20)$$

It is worth noting that even if the hyperstress $\hat{\Gamma}$ at the boundary would vanish, equation (5.20) assures that a bifurcation always occurs with a bifurcated mode $v_n = A_2\sin\left(2n\pi\,\frac{x}{L}\right)$.

It is natural to ask if there is a reduction of energy by nucleating oscillations.

The amount of the extra energy for getting the final configuration from $\bar{J}$ is now computed. The nth buckled mode obtained in the elastic case (5.20) can be expanded as follows:

$$
\begin{aligned}
v &= \frac{\Gamma L^2}{8\pi^2\bar{\alpha}}\left[1 - \cos\left(\omega x\right)\right] + A_2 \sin\left(\omega x\right) \\
v' &= \frac{\Gamma L^2}{8\pi^2\bar{\alpha}}\,\omega\,\sin\left(\omega x\right) + A_2\,\omega\,\cos\left(\omega x\right) \\
v'' &= \frac{\Gamma L^2}{8\pi^2\bar{\alpha}}\,\omega^2\,\cos\left(\omega x\right) - A_2\,\omega^2\,\sin\left(\omega x\right)
\end{aligned}
\tag{5.21}
$$

Because the solution $v(x)$ depends on the trigonometric functions, for the sake of discussion two contributions related to the *cosine* and *sine* components, respectively, are distinguished , i.e

$$
v = v_c + v_s.
\tag{5.22}
$$

The energy stored by the membrane for getting the final configuration from the reference one can be then decomposed as follows:

$$
\begin{aligned}
\mathscr{E} &= \int_\Omega \bar{\varphi}'\,v'(x) + \frac{\bar{\varphi}''}{2}\,v'^2 + \bar{\alpha}\,v''^2 \\
&= \int_\Omega \bar{\varphi}'\left(v_c' + v_s'\right) + \frac{\bar{\varphi}''}{2}\left(v_c' + v_s'\right)^2 + \bar{\alpha}\left(v_c'' + v_s''\right)^2 \\
&= \int_\Omega \left(\bar{\varphi}'v_c' + \frac{\bar{\varphi}''}{2}v_c'^2 + \bar{\alpha}v_c''\right) + \left(\bar{\varphi}'v_s' + \frac{\bar{\varphi}''}{2}v_s'^2 + \bar{\alpha}v_s''\right) + \\
&\quad + 2\left(\frac{\bar{\varphi}''}{2}\left(v_c'v_s'\right) + \bar{\alpha}\left(v_c''v_s''\right)\right) \\
&= \mathscr{E}_s + \mathscr{E}_c + \mathscr{E}_{cs}
\end{aligned}
\tag{5.23}
$$

where the following relationships were assumed:

$$
\mathscr{E}_c = \int_\Omega \bar{\varphi}'v_c' + \frac{\bar{\varphi}''}{2}v_c'^2 + \bar{\alpha}\,v_c'',
\tag{5.24a}
$$

$$
\mathscr{E}_s = \int_\Omega \bar{\varphi}'v_s' + \frac{\bar{\varphi}''}{2}v_s'^2 + \bar{\alpha}v_s'',
\tag{5.24b}
$$

$$
\mathscr{E}_{cs} = 2\int_\Omega \frac{\bar{\varphi}''}{2}\left(v_c'v_s'\right) + \bar{\alpha}\left(v_c''v_s''\right).
\tag{5.24c}
$$

Bearing in mind that in this case $\omega^2 = -\bar{\varphi}''/2\bar{\alpha}$, it is possible to compute the

energy term by term:

$$\mathscr{E}_c = \int_\Omega \bar\varphi' \, v_c' + \frac{\bar\varphi''}{2} \, v_c'^2 + \bar\alpha v_c''^2$$

$$= \omega \, \frac{\Gamma \, L^2}{8\pi^2 \bar\alpha} \int_\Omega \bar\varphi' \, \sin\left(n\pi \frac{x}{L}\right) dx +$$

$$+ \omega^2 \left(\frac{\Gamma \, L^2}{8\pi^2 \bar\alpha}\right)^2 \int_\Omega \left[\frac{\bar\varphi''}{2} \sin\left(n\pi \frac{x}{L}\right)^2 + \bar\alpha \, \omega^2 \cos\left(n\pi \frac{x}{L}\right)^2\right] dx$$

$$= \omega^2 \left(\frac{\Gamma \, L^2}{8\pi^2 \bar\alpha}\right)^2 \frac{L}{2} \bar\alpha \left(\frac{\bar\varphi''}{2\bar\alpha} + \omega^2\right) = 0$$

and analogously

$$\mathscr{E}_s = \int_\Omega \bar\varphi' \, v_s' + \frac{\bar\varphi''}{2} \, v_s'^2 + \bar\alpha v_s''^2$$

$$= \omega \, A_2 \int_\Omega \bar\varphi' \, \cos\left(n\pi \frac{x}{L}\right) dx +$$

$$+ \omega^2 A_2^2 \int_\Omega \left[\frac{\bar\varphi''}{2} \cos\left(n\pi \frac{x}{L}\right)^2 + \bar\alpha \, \omega^2 \sin\left(n\pi \frac{x}{L}\right)^2\right] dx$$

$$= \omega^2 A_2^2 \frac{L}{2} \bar\alpha \left(\frac{\bar\varphi''}{2\bar\alpha} + \omega^2\right) = 0,$$

Finally,

$$\mathscr{E}_{cs} = \int_\Omega 2 \left(\frac{\bar\varphi''}{2} \left(v_c' v_s'\right) + \bar\alpha \left(v_c'' v_s''\right)\right) = 0$$

because of the orthogonality of the trigonometric functions. Indeed $v_s' \, v_c' \propto v_s'' \, v_c'' \propto \sin(\hat\omega \, x)\cos(\hat\omega \, x)$, and since they are orthogonal functions, the integral over a period is zero.

This result turns out that it is identically zero. This fact suggests that all the buckled configuration from $\bar J$ posses the same quantity of energy and then such buckled configuration do have the same likelihood to occur.

Case 2. Let us now consider the case $s = \pm 1$ and $c = 0$. This condition implies that:

$$\cos\left(\omega \frac{L}{2}\right) = 0 \quad \Longrightarrow \quad \omega = \frac{(1 + 2\,n)\,\pi}{L} \tag{5.25}$$

161

and

$$\frac{\bar{\varphi}''}{\bar{\varphi}'}\bar{J}^5 = -\frac{(1+2n)^2\pi^2}{12}\left(\frac{h_0}{L}\right)^2,$$
(5.26)

which has certainly roots for $\bar{J}$ such that $\bar{\varphi}'' \to 0^-$ for the reason explained in case 1. As usual, the coefficients of the mode are found by imposing the boundary conditions. We find $A_2 = A_3 = A_4 = 0$. Hence, in this case a solution is possible if and only if $\hat{\Gamma} = 0$. It follows that the buckled modes take the forms:

$$v_n(x) = A_1 \cos(\omega\,x) = A_1 \cos\left((1+2n)\pi\frac{x}{L}\right).$$
(5.27)

It is easy to recognize that also in this case the extra amount of energy needed to bifurcate from $\bar{J}$ is equal to 0.

5.1.2 Stable zone

Whenever the configuration of the membrane $\bar{J}$ is located outside of the spinoidal zone, i.e $\bar{\varphi}'' > 0$ and either $1 < \bar{J} < J_{max}$ or $\bar{J} > J_{min}$, the governing equation assumes the following form:

$$v'''' - \omega^2\,v'' = 0.$$
(5.28)

In such a case, the profile of the perturbation becomes:

$$v(x) = A_1 \cosh(\omega\,x) + A_2 \sinh(\omega\,x) + A_3\,x + A_4,$$
(5.29)

where the coefficients A_i, as in the previous analysis, depend of the specific boundary conditions.

5.1.3 Singular points

Before proceeding further some additional discussion may be withdrawn from the analysis of the singular points $\bar{J} = J_{max}$ and $\bar{J} = J_{min}$. In both cases, the first derivative of the local stress is zero, i.e $\bar{\varphi}'' = 0$: then the case $\omega = 0$ occurs. Henceforth, the governing equation appears to be simpler than in the other cases: $v'''' = 0$, whose solution reads:

$$v(x) = A_0 + A_1\,x + A_2\,x^2 + A_3\,x^3.$$
(5.30)

As an example, let us consider boundary conditions (5.15) with $\hat{\Gamma}_R = \hat{\Gamma}_L = \hat{\Gamma}$, which yields the following values for the constants:

$$A_0 = -\frac{\hat{\Gamma}\,L^2}{16\,\bar{\alpha}} \quad A_1 = 0 \quad A_2 = \frac{\hat{\Gamma}}{4\,\bar{\alpha}} \quad A3 = 0. \tag{5.31}$$

Of course no bifurcated perturbations would occur in the absence of hyperstress at the boundary.

5.1.4 Numerical Examples

Let consider a planar lipid membrane at the fixed temperature $T \sim 30°$ (see Figure 1.3). The solution of the problem in (5.12) depends on the sign of the ratio $\bar{\varphi}''/\bar{\varphi}'$, appearing in (5.11) and (5.26). We recall that bifurcations occur if $\bar{\varphi}'' < 0$, i.e. whenever the membrane stretch $\bar{J}$ lies in the unstable part of the spinoidal zone. This circumstance is highlighted in Figure 5.1 as a grey region under the orange curve which, as expected, is contained in the spinoidal zone between the two turning points for the convexity of φ, i.e. in the range $[J_{max}, J_{min}]$.
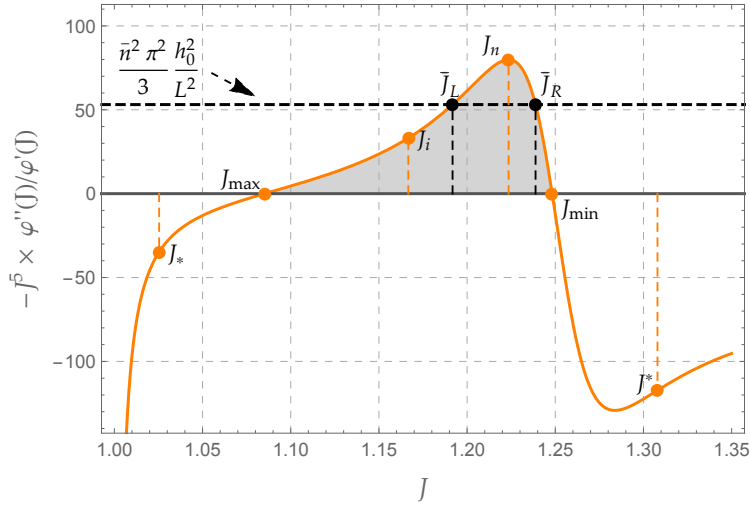
Figure 5.1: Plot of the ratio $\bar{\varphi}''/\bar{\varphi}'$ as function of the homogeneous configuration $\bar{J}$ whenever $n = 8830$, $h_0 = 4.55\,nm$ and $L = 10\,\mu m$ (see (5.19)). Courtesy of [58].

Figure 5.1 shows that for each chosen value of n, representing the index mode or "wave number", there exist two admissible solutions for (5.19). One of such

values of $\bar{J}$ lies on the left and the other one on the right branch of the curve with respect to J_n the location where the horizontal tangent is found. Moreover, this is the only location where a unique value of n is possible, i.e $J_R = J_L = J_n$. The wave number related to this location is labelled n_{max}, because (5.19) ensures that greater values of n do not allow the presence of bifurcated solutions. This value can be computed as follows:

$$ n_{max} = \frac{1}{\pi} \left(\frac{L}{h_0} \right) \sqrt{-3 \frac{\bar{\varphi}'' \bar{J}^5}{\bar{\varphi}'}} \Bigg|_{\bar{J}=J_n} . \tag{5.32} $$

The energy used for this numerical example leads to $J_n = 1.2235$ and $n_{max} = 10.832$. Each choice of n, therefore, allows for finding two configurations $\bar{J}$ from which a bifurcated mode can be nucleated. Such values are found numerically by choosing values of n from 0 up to n_{max} and computing the intersection $\bar{J}_L$ and $\bar{J}_R$ by means of equation (5.19); The results are shown in Figure 5.2. The lower blue curve
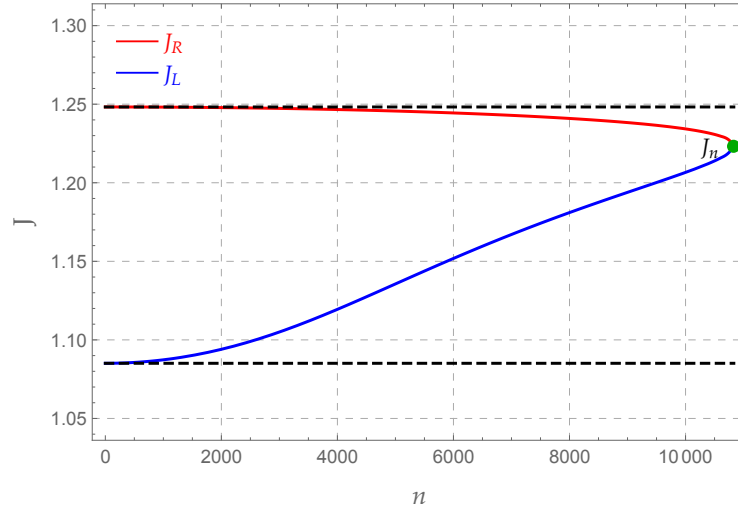
Figure 5.2: Locus of the *left* and *right* intersections as stretched balanced configurations, i.e. admissible solutions of equation (5.19). Courtesy of [58].

represents the intersection with the left branch of the curve in Figure 5.1, whereas the red curve is the intersection with the right branch. Obviously, these two curves share a common point at $J = J_n$. In order to show the behavior of the system, a value $n = 10$ is chosen for the sake of representation, then the stretch J and

the stress Σ related to this specific bifurcated configuration are computed through (1.23). Two cases are considered for illustrative purpose only, in order to show the behavior of our numerical solution: as first case, the arbitrary constant A_2 is set to 0 and the hyperstress is chosen such that $\hat{\Gamma} = \frac{\alpha(\bar{J})}{50\,L}$, whereas in the second example a case with a null hyperstress, $\hat{\Gamma} = 0$, is considered and the constant A_2 is chosen as $A_2 = \frac{1}{50}\frac{L}{2\,\pi\,n}$. Both the results are shown in Figure 5.3.

5.2 The mechanics of fractional order lipid bilayers

Available experimental data [36, 66, 94] show that lipid bilayers present a time-dependent behavior depending on the in-plane anomalous viscous behavior exhibited by various lipid molecules at different temperatures.

The aim of this Section is to introduce the governing equations of a Fractional Hereditariness capturing the evolution of the perturbations on the ordered/disordered phase transition shown by lipid bilayers. Such perturbation are predicted to occur in the lipid membrane starting from a homogenously squeezed configuration.

The problem is formulated by seeking for the values of the areal stretches for which unknown time evolving bifurcated configurations could occur. In this regard, in full analogy with the elastic case, a suitable generalization of the variational principle is invoked and the variational principle is employed. Here, the Gibbs free energy density is taken from [43], where a rheological model yields the Staverman-Schartzl free energy [39, 40, 46, 47] as the one for power-law materials.

The experimental data about lipid membrane hereditariness that can be found in literature [94] show that the case of a purely elastic membrane represents the asymptotic condition of the mechanics of the lipid bilayer under a constant uniform stress. However, this circumstance is very seldom present in the physiological conditions of living cells, for which intracellular and/or extracellular fluids contributes to change the areal membrane stretch several times during cell lifetimes. Therefore the membrane stress at a certain observation time t may be much higher than the value evaluated in the non-linear elasticity framework, it may evolve into breakage of the cell membrane or to lipid phase modification towards ceramid phase and then to cell apoptosys [36].

5.2.1 The physical description of lipid membrane hereditariness

The mechanics of lipid bilayers forming artificial and natural cytoplasmatic membranes presents a significative hereditary behavior [66]. Storage and loss moduli $G^{'}(p)$, $G^{''}(p)$ of lipid membrane depend on the type of lipids (in the membrane e.g.
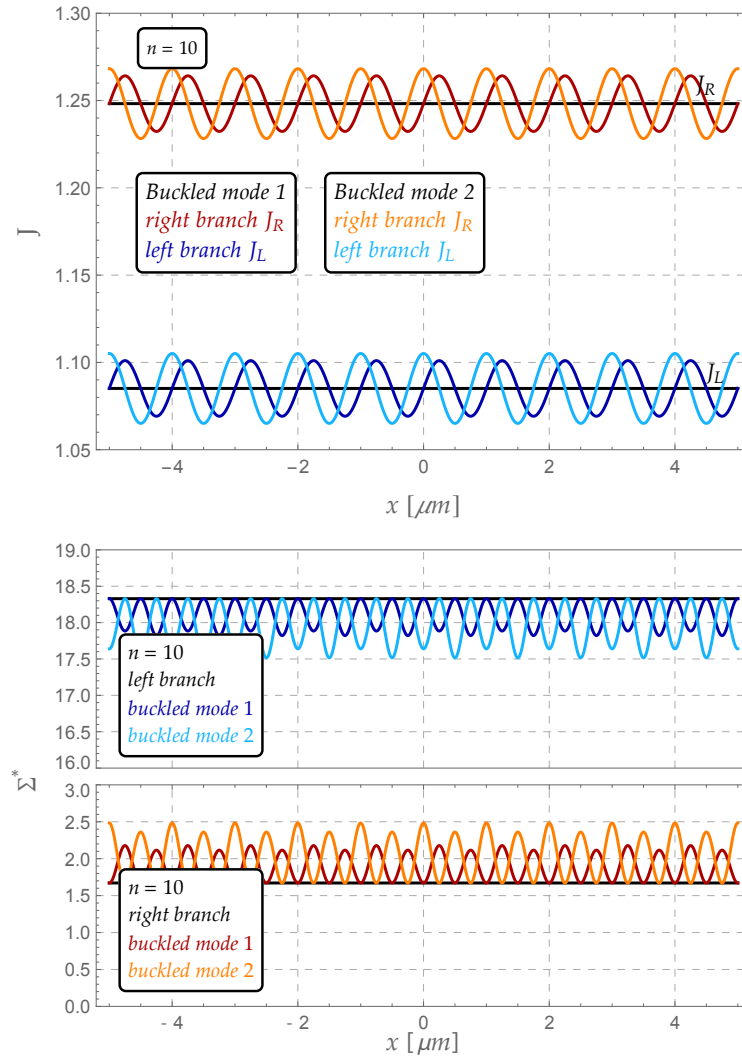
Figure 5.3: *Buckled mode 1: $A_2 = 0$ and $\hat{\Gamma} = \frac{\alpha(\bar{J})}{50\,L}$. Buckled mode 2: $A_2 = \frac{1}{50}\frac{L}{2\,\pi\,n}$ and $\hat{\Gamma} = 0$. Courtesy of [58].*

phosphatidylcholine (PODC), the sphyingomyelin (SM) based lipid chains) and on the melting temperatures of such mixtures [66]. The morphology of the lipids in the bilayers influence their viscosity. It may be either liquid-ordered or gel-phase, for temperatures over or below the melting temperatures of the PODC. For SM the liquid-disordered or the solid phase (ceramide) may be involved depending upon the temperature of the membrane.

Several experimental observations on lipid mono-and-bilayer [94] showed that the storage and loss modulus, namely $G^{'}(p)$ and $G^{''}(p)$, are proportional to the frequency through a power-law of frational order, i.e $G^{'}(p) \propto p^{\beta}$ and $G^{''}(p) \propto p^{\beta+1}$, where the exponent β depends on temperature and specific chemical composition of the biological structure.

Henceforth, the use of Maxwell rheological elements to model storage and loss moduli of the material does not provide an suitable representation for the behavior of lipid membrane. This is because Maxwell models yield $G^{'}(p) \propto p$ and $G^{''}(p) \propto p^2$, which are not observed in experimental rheology of such membranes [66].

In this context appropriate models of the hereditary behavior of the lipid membranes must contain fractional-order operators models, in which *creep* and *relaxation* are described as power-laws of real-order, such that $J(t) \propto t^{\beta}$ and $G(t) \propto t^{-\beta}$, respectively. The time evolution of small perturbations arising in lipid bilayers from homogeneous configurations describing uniform squeezing is here modeled by making use of the Boltzmann-Volterra superposition integral. In particular, this allows for measuring the stress evolution at a generic location x depending on an applied strain history $\epsilon(x, t)$ as follows:

$$\sigma(x, t) = \frac{C_{\beta}}{\Gamma[1-\beta]} \int_{-\infty}^{t} (t-\tau)^{-\beta} \, \dot{\epsilon}(x, \tau) \, d\tau; \tag{5.33}$$

the right-hand side of this expression is related to the Caputo fractional-order derivative [26, 115, 133, 169, 182], i.e.:

$$\mathcal{D}_t^{\beta} f(t) = \frac{1}{\Gamma(\beta)} \int_{-\infty}^{t} (t-\tau)^{-\beta} \dot{f}(x, \tau) d\tau. \tag{5.34}$$

A rheological model known as *springpot element* (after Scott-Blair [186]) is associated to (5.34). This represents an intermediate behavior among a linear elastic spring and a viscous dashpot that are obtained for $\beta = 0$ and $\beta = 1$, respectively.

In the next section the free energy function obtained in [43] for power-law hereditary materials is utilized. Such a free energy will be further specialized to yield the rheological description of the springpot element to handle lipid membrane

167

hereditariness.

5.2.2   The free energy of hereditary lipid bilayers

The governing equations for the evolution of small perturbations of homogeneous configuration of hereditary and planar lipid membranes is derived by employing the principle of the minimum of energy.

To this aim it is worth bearing in mind that the quadratic form of the free energy in (5.3) contains both a local perturbative term, namely $\varepsilon(x\,t)$, and a non-local contribution in term of a first order gradient $\varepsilon_x(x,\,t)$. As we observe that the free energy function of the purely elastic case is a function of the state variables $\varepsilon(x)$ and $\varepsilon_x(x)$, the free energy function in presence of material hereditariness may be assumed as the sum of different contributions related to the local and the non-local state variables (see e.g. [21, 39, 40, 44, 46, 47]).

As in the elastic case, the viscoelastic free energy has a local and a nonlocal part. There, the power at which stress and hyperstress (which performs work against changes of the displacement gradient u_x, see [55] for more details) relax could be different, as diffusion mechanisms may occur at different average speed depending on whether or nor they arise in a boundary layer between different phase or in a given phase.

By looking at purely (nonlinear) elastic contributions, in the previous section the phase transition phenomena describing areal changes of lipid membranes were obtained [52, 55]. Time evolution of small perturbation of such configurations are inferred to be modulated by the local and nonlocal stresses $\sigma_L(x,t)$ and $\sigma_N(x,t)$ respectively, i.e.

$$\sigma_L(x,t) = \int_0^t G_L(t-\tau)\dot{\varepsilon}(x,\tau)\,\mathrm{d}\tau, \tag{5.35a}$$

$$\sigma_N(x,t) = \int_0^t G_N(t-\tau)\dot{\varepsilon}_x(x,\tau)\,\mathrm{d}\tau, \tag{5.35b}$$

where G_L and G_N are the local and nonlocal relaxation moduli (relative to the configuration $\bar{J}$), respectively, defined as follows:

$$G_L(t) := \bar{\varphi}'' + f_L(t),$$
$$G_N(t) := 2\bar{\alpha} + f_N(t).$$

Here the following relationship must hold

$$\lim_{t\to\infty} f_L(t) = \lim_{t\to\infty} f_N(t) = 0, \tag{5.37}$$

168

as the elastic case has to be retrieved as limit. The specific dependence of the functions $f_L(t)$ and $f_N(t)$ on time depends on the experimental observation of the evolution of the ordered-disordered phase as well as of their transition zone. Motivated by the experimental evidence discussed in the previous Section, in this work a power law relaxation function are used for the description of the decay behavior of both local and nonlocal evolution. In particular, two different decay laws for describing both the local and the nonlocal contribution are assumed. Thus the following relaxation moduli, based on [43], are considered:

$$G_L(t) := \bar{\varphi}'' + C_L\, t^{-\lambda}, \tag{5.38a}$$

$$G_N(t) := 2\bar{\alpha} + C_N\, t^{-\nu}, \tag{5.38b}$$

where C_L and C_N represent generalized moduli of the local and nonlocal relaxations, λ and ν are the decay exponents of the relaxations (for now chosen in the range $[0, 1]$). It is worth nothing that the contributions $\bar{\varphi}''$ and $2\bar{\alpha}$ in (5.38) come from the third and fourth terms of the linearized functional in (5.6). The use of an additive relaxation form in (5.38) corresponds to the use of a fractional order rheological element introduced in (5.34).

After these considerations, the free energy function $\Psi(x,\, t)$ can be thought as composed by two distinguished contributions:

$$\Psi(x,\, t) = \Psi_{DZ}(x,\, t) + \Psi_V(x,\, t), \tag{5.39}$$

where $\Psi_{DZ}(x,\, t)$ is defined by (5.2) and represents the elastic contribution to the free energy at equilibrium (see [39]), while $\Psi_V(x,\, t)$ denotes the free energy associated to the hereditary response of the membrane. This has been shown [43] to be the Staverman-Schartzl energy [21, 39, 40]. This result and equations (5.35), (5.38) suggest that $\Psi(x,\, t)$ may be written also as:

$$\Psi(x,\, t) = \Psi_L(\varepsilon(x,\, t)) + \Psi_N(\varepsilon_x(x,\, t)), \tag{5.40}$$

where a local and nonlocal term are accounted for. The former depends on the stretch itself, while the latter on its gradient. Following [21, 43] we introduce a kernel $K(\circ, \circ)$ as a symmetric function, i.e $K(\circ, \circ) \geq 0$ and $K(\tau_1, \tau_2) = K(\tau_2, \tau_1)$.

169

The contribution above can finally be written as follows:

$$\Psi_L(x,\,t) = \frac{1}{2}K_L(0,0)\varepsilon(x,t)^2$$

$$+ \varepsilon(x,t)\int_{-\infty}^{t} \dot{K}_L(0,t-\tau)\varepsilon(x,\tau)\mathrm{d}\tau \tag{5.41a}$$

$$+ \frac{1}{2}\int_{-\infty}^{t}\int_{-\infty}^{t} \ddot{K}_L(t-\tau_1,t-\tau_2)\varepsilon(x,\tau_1)\varepsilon(x,\tau_2)\mathrm{d}\tau_1\mathrm{d}\tau_2,$$

$$\Psi_N(x,\,t) = \frac{1}{2}K_N(0,0)\varepsilon_x(x,t)^2$$

$$+ \varepsilon_x(x,t)\int_{-\infty}^{t} \dot{K}_N(0,t-\tau)\varepsilon_x(x,\tau)\mathrm{d}\tau + \tag{5.41b}$$

$$+ \frac{1}{2}\int_{-\infty}^{t}\int_{-\infty}^{t} \ddot{K}_N(t-\tau_1,t-\tau_2)\varepsilon_x(x,\tau_1)\varepsilon_x(x,\tau_2)\mathrm{d}\tau_1\mathrm{d}\tau_2,$$

where

$$K_L(t,0) := \bar{\varphi}'' + \frac{C_L}{\Gamma(1-\lambda)}(t+\delta)^{-\lambda} = G_L^{\delta}(t), \tag{5.42a}$$

$$K_N(t,0) := 2\bar{\alpha} + \frac{C_N}{\Gamma(1-\nu)}(t+\delta)^{-\nu} = G_N^{\delta}(t), \tag{5.42b}$$

where δ is a preloading time. Of course $K_L(0,t) = K_L(t,0)$ and $K_N(0,t) = K_N(t,0)$. It is worth noting that the form of equation (5.41) comes from the definition of the Staverman-Schartzl energy [21, 39, 43]. This result, together with (5.38) and the considerations addressed in equations **(17-22)** by Deseri et al. [43], allows for writing down the *final* form of the free energy as:

$$\Psi_L(x,\,t) = \frac{1}{2}G_L^{\delta}(0)\varepsilon^2(x,t) + \varepsilon(x,t)\int_{-\infty}^{t} \dot{G}_L^{\delta}(t-\tau)\varepsilon(x,\tau)\,\mathrm{d}\tau +$$

$$+ \frac{1}{2}\int_{-\infty}^{t}\int_{-\infty}^{t} \ddot{G}_L^{\delta}(2t-\tau_1-\tau_2)\varepsilon(x,\tau_1)\varepsilon(x,\tau_2)\mathrm{d}\tau_1\,\mathrm{d}\tau_2, \tag{5.43a}$$

$$\Psi_N(x,\,t) = \frac{1}{2}G_N^{\delta}(0)\varepsilon_x^2(x,t) + \varepsilon_x(x,t)\int_{-\infty}^{t} \dot{G}_N^{\delta}(t-\tau)\varepsilon_x(x,\tau)\,\mathrm{d}\tau$$

$$+ \frac{1}{2}\int_{-\infty}^{t}\int_{-\infty}^{t} \ddot{G}_N^{\delta}(2t-\tau_1-\tau_2)\varepsilon_x(x,\tau_1)\varepsilon_x(x,\tau_2)\mathrm{d}\tau_1\,\mathrm{d}\tau_2, \tag{5.43b}$$

where $\varepsilon(x,\,t) = v_x(x,\,t)$, where $v(x,\,t)$ represents the perturbation of the configuration of the lipid membranes at the location x and time t. Finally, the total (Gibbs) free energy related to the perturbation $v(x,t)$ can be computed as:

$$\mathscr{E} = \int_{t_1}^{t_2} \left(\int_{\Omega} \left[\Psi_L(x,\,t) + \Psi_N(x,\,t) \right] \mathrm{d}x \right) \mathrm{d}t - \left[\Sigma\, v(x,t) + \Gamma\, v_x(x,t) \right]_{\partial\Omega}, \quad (5.44)$$

where t_1 and $t_2 > t_1$ are two subsequent times during which the time evolution of the membrane is investigated.

5.3 Linearized evolution of lipid membranes

The governing equation for the evolution of lipid membrane is sought for v by stationarity of the functional $\mathscr{E}$ in the class of syncronous variations, i.e. $\delta v(\circ, t_1) = \delta v(\circ, t_2)$. The computation of the first variation gives:

$$\delta\mathcal{E}_L = \int_{t_1}^{t_2} \left(\int_{\Omega} \left(G_L^\delta(0)\lambda + \int_{-\infty}^{t} \dot{G}_L^\delta(t - \tau)\lambda(\tau)\mathrm{d}\tau \right) \delta\lambda \right) \mathrm{d}x\ \mathrm{d}t \qquad (5.45\mathrm{a})$$

$$\delta\mathcal{E}_N = \int_{t_1}^{t_2} \left(\int_{\Omega} \left(G_N^\delta(0)\lambda' + \int_{-\infty}^{t} \dot{G}_N^\delta(t - \tau)\lambda'(\tau)\mathrm{d}\tau \right) \delta\lambda' \right) \mathrm{d}x\ \mathrm{d}t \qquad (5.45\mathrm{b})$$

Equations (5.45) can be rewritten bearing in mind the Volterra-type integral in the following form:

$$\delta\mathcal{E}_L = \int_{\Omega} \left(\int_{-\infty}^{t} G_L^\delta(t - \tau)\dot{\lambda}(\tau)\mathrm{d}\tau \right) \delta\lambda\ \mathrm{d}x \qquad (5.46\mathrm{a})$$

$$\delta\mathcal{E}_N = \int_{\Omega} \left(\int_{-\infty}^{t} G_N^\delta(t - \tau)\dot{\lambda}'(\tau)\mathrm{d}\tau \right) \delta\lambda'\ \mathrm{d}x \qquad (5.46\mathrm{b})$$

and, after proper substitutions:

$$\delta\mathcal{E}_L = \int_{\Omega} \left(\bar{\varphi}'' \left[\lambda(x,t) - \lambda_0 \right] + C_L \mathcal{D}_t^\lambda \lambda(x,t) \right) \delta\lambda\ \mathrm{d}x \qquad (5.47\mathrm{a})$$

$$\delta\mathcal{E}_N = \int_{\Omega} \left(2\bar{\alpha} \left[\lambda'(x,t) - \lambda_0' \right] + C_N \mathcal{D}_t^\nu \lambda'(x,t) \right) \delta\lambda'\ \mathrm{d}x \qquad (5.47\mathrm{b})$$

171

Henceforth:

$$\delta\mathcal{E} = \int_{\Omega} \left(\left[\bar{\varphi}'' \left(v' - \lambda_0 \right) + C_L \mathcal{D}_t^\lambda v' \right] \delta v' + \left[2\bar{\alpha} \left(v'' - \lambda_0' \right) + C_N \mathcal{D}_t^\nu v'' \right] \delta v'' \right) \delta x +$$
$$- \left[\Sigma\, \delta v + \Gamma\, \delta v' \right]_{\partial\Omega}$$

Finally, the Euler-Lagrange equation takes the form:

$$2\bar{\alpha}\, \frac{\partial^4}{\partial x^4} \left(v + C_N^* \mathcal{D}_t^\nu v \right) - \bar{\varphi}''\, \frac{\partial^2}{\partial x^2} \left(v + C_L^* \mathcal{D}_t^\lambda v \right) = y(x), \qquad (5.48)$$

where $C_L^* = C_L/\bar{\varphi}''$ and $C_N^* = C_N/2\bar{\alpha}$ represent the normalized local and nonlocal moduli of the membrane, respectively, and the *forcing term* $y(x)$ is defined as follows:

$$y(x) = 2\bar{\alpha}\frac{\partial^4 v_0}{\partial x^4} - \bar{\varphi}''\frac{\partial^2 v_0}{\partial x^2}. \qquad (5.49)$$

Here $v_0(x)$ represents an initial perturbation displacement that can be induced on the membrane at the beginning of the observation time, and it can be thought as the initial configuration before the relaxation. The governing equation (5.48) is coupled with the following boundary conditions:

$$\begin{cases} \text{either} \\ \bar{\varphi}'' \left(v' + \bar{C}_L \mathcal{D}_t^\lambda v' \right) - 2\bar{\alpha} \left(v''' + \bar{C}_N \mathcal{D}_t^\nu v''' \right) = \Sigma + \Sigma_0 \\ \text{or} \\ \delta v = 0 \end{cases} \qquad (5.50a)$$

$$\begin{cases} \text{either} \\ 2\bar{\alpha} \left(v'' + \bar{C}_N \mathcal{D}_t^\nu v'' \right) = \Gamma + 2\bar{\alpha}\,\varepsilon_0' \\ \text{or} \\ \delta v' = 0 \end{cases} \qquad (5.50b)$$

It is worth nothing that the term $\Sigma_0 := \bar{\varphi}''\varepsilon_0 + 2\,\bar{\alpha}\,\varepsilon_0''$ can be interpreted as the *initial stress* acting on the membrane to hold it in the initially perturbed configuration. Of course, if no initial perturbation is induced on the membrane, equation (5.48) and its boundary conditions lead to an eigenvalue problem, examined in Section 5.3.3 in the sequel.

The structure of the linear partial differential equation (5.48) allows for separa-

tion of variables for the perturbation $v(x,t)$, i.e.:

$$v(x,t) = f(x)\,q(t), \tag{5.51}$$

where $q(t)$ describes the time change of the perturbation or "transfer function", and $f(x)$ describes the shape of the mode. Henceforth, the governing equation can be written in the following form:

$$\frac{2\bar{\alpha}}{\bar{\varphi}''}\frac{f^{iv}(x)}{f''(x)} = \frac{q(t) + C_L^* \, \mathcal{D}_t^\lambda q(t)}{q(t) + C_N^* \, \mathcal{D}_t^\nu q(t)} = k^2, \tag{5.52}$$

where k^2 is a constant to be determined. In this context, relationship (5.10) holds. In this work we are interested in exploring conditions from which oscillations can occur, henceforth only the case $\bar{\varphi}'' < 0$ is studied. Then:

$$-\frac{1}{\omega^2}\frac{f^{iv}(x)}{f''(x)} = \frac{q(t) + C_L^* \, \mathcal{D}_t^\lambda q(t)}{q(t) + C_N^* \, \mathcal{D}_t^\nu q(t)} = k^2, \tag{5.53}$$

as oscillatory perturbations are explored. In analogy with (5.15) the following boundary conditions are assumed for all times t:

$$\begin{cases} v\Big|_{\partial\Omega^-} = v\Big|_{\partial\Omega^+} = 0 \\ 2\bar{\alpha}\left[v'' + C_N^* \, \mathcal{D}_t^\nu v''\right]\Big|_{\partial\Omega^-} = 2\bar{\alpha}\left[v'' + C_N^* \, \mathcal{D}_t^\nu v''\right]\Big|_{\partial\Omega^+} = \hat{\Gamma} \end{cases} \tag{5.54}$$

which by (5.51) imply:

$$\begin{cases} f(x)\Big|_{\partial\Omega} = 0 \\ 2\bar{\alpha}f''\left[q(t) + C_N^* \, \mathcal{D}_t^\nu q(t)\right]\Big|_{\partial\Omega} = \hat{\Gamma} \end{cases} \tag{5.55}$$

5.3.1   Solution of the space-dependent equation

The space-dependent function $f(x)$ is found through (5.52) to obey the following ordinary differential equation:

$$f^{iv}(x) + k^2\,\omega^2 f''(x) = 0. \tag{5.56}$$

After setting

$$\zeta^2 = k^2\,\omega^2\,, \tag{5.57}$$

173

bearing in mind that $\bar{\varphi}'' < 0$, the solution of (5.56) reads as

$$f(x) = A_1 \cos\left(\zeta\, x\right) + A_2 \sin\left(\zeta\, x\right) + A_3 x + A_4. \tag{5.58}$$

As usual, the boundary conditions (5.55) must be used in order to determine the coefficients A_i, $i = 1 \div 4$. In particular, a closer analysis of the condition on the second derivative of the space-dependent function $f(x)$ yields:

$$2\bar{\alpha}\, f''\Big|_{\partial\Omega} [q(t) + C_N^* \, \mathcal{D}_t^\nu q(t)] = \hat{\Gamma} \qquad \forall\, t.$$

The latter boundary condition can be fulfilled if either $\hat{\Gamma}$ is a prescribed of of time or if it is constant. This second case is explored in the sequel. Whenever $\hat{\Gamma}$ is constant, then

$$q(t) + C_N^* \, \mathcal{D}_t^\nu q(t) = \kappa_n, \tag{5.59}$$

where κ_n is a constant. Consequently, the boundary condition is written as follows:

$$2\bar{\alpha}\, f''\Big|_{\partial\Omega} \kappa_n = \hat{\Gamma}. \tag{5.60}$$

Moreover, this condition at the edge highlights that the second derivative $v_{xx}(x,\, t)\Big|_{\partial\Omega}$ there can be zero if and only if

$$f''\Big|_{\partial\Omega} = 0 \iff \hat{\Gamma} = 0 \tag{5.61}$$

the hyperstress is zero. For such a case, equation (5.59) is irrelevant. Because in this section the attention is focused on the case $\bar{\varphi}'' < 0$, after setting $s = \sin(\zeta L/2)$ and $c = \cos(\zeta L/2)$, the boundary conditions can be written explicitly in the form:

$$
\begin{cases}
A_1\, c - A_2\, s - A_3\dfrac{L}{2} + A_4 = 0 \\[2mm]
2\bar{\alpha}\zeta^2 \left(-A_1\, c + A_2\, s\right) \kappa_n = \hat{\Gamma}
\end{cases}
\quad \text{at } x = -\dfrac{L}{2}
$$

$$
\begin{cases}
A_1\, c + A_2\, s + A_3\dfrac{L}{2} + A_4 = 0 \\[2mm]
2\bar{\alpha}\zeta^2 \left(-A_1\, c - A_2\, s\right) \kappa_n = \hat{\Gamma}
\end{cases}
\quad \text{at } x = +\dfrac{L}{2}
$$

Such a system is the analogue of (5.16):

$$
\begin{bmatrix}
0 & s & \frac{L}{2} & 0 \\
c & 0 & 0 & 1 \\
0 & s & 0 & 0 \\
-2\bar{\alpha}\,\kappa_n\zeta^2 c & 0 & 0 & 0
\end{bmatrix}
\begin{pmatrix}
A_1 \\ A_2 \\ A_3 \\ A_4
\end{pmatrix}
=
\begin{pmatrix}
0 \\ 0 \\ 0 \\ \hat{\Gamma}
\end{pmatrix}
\tag{5.62}
$$

whose nontrivial solutions can be found by studying the roots of the determinant, namely after solving:

$$
\bar{\alpha}\,c\,s\,L\,\kappa_n\,\zeta^2 = 0. \tag{5.63}
$$

Because of equation (5.60), the case $\kappa_n = 0$ implies that the hyperstress at edges is zero, and for now we do not consider this possibility to occur. Then, the quantities $\bar{\alpha}$, L and κ_n are always nonzero, and we are left to study only two cases.

Case 1. Because $\zeta^2 = k^2\,\omega^2$ with $k > 0$ (although still unknown at this stage), if $s = 0$ we have:

$$
k^2\,\omega^2 = \frac{4n^2\pi^2}{L^2}, \tag{5.64}
$$

and

$$
-\frac{\bar{\varphi}''}{\bar{\varphi}'}\bar{J}^5 = \frac{n^2\pi^2}{3\,k^2}\left(\frac{h_0}{L}\right)^2. \tag{5.65}
$$

Case 2. If $c = 0$ then $\hat{\Gamma} = 0$. As highlighted in (5.61), this happens if and only if $f''(\partial\Omega) = 0$.

5.3.2 Solution of the time-dependent equation

The time-dependent solution $q(t)$ turns out to depend on the value of the second derivative in space at the edges (see (5.60)).

Whenever in (5.55) the boundary condition on the second derivative of the displacement is nonzero , the presence of a hyperstress $\hat{\Gamma}$ at the edges implies that the time-dependent term is constant, assuring that relation (5.59) holds. This equation can be easily solved through the method of the *Laplace Transform method* (see Appendix A.2) to yield:

$$
q(t) = \frac{\kappa_n}{C_N^*}t^\nu E_{\nu,\nu+1}\left(-\frac{1}{C_N^*}t^\nu\right) + q_0 E_\nu\left(-\frac{1}{C_N^*}t^\nu\right), \tag{5.66}
$$

where $E_{\alpha,\beta}(z)$ is the Mittag-Leffler function of two parameters. At the same time, the assumption of the separation of variables dictates that (5.52) be satisfied.

175

Hence, (5.52) and (5.59) imply that the following relationship has to hold:

$$q(t) + C_L^* \, \mathcal{D}_t^\lambda q(t) = k^2 \, \kappa_n, \tag{5.67}$$

whose solution is again found by using the *Laplace Transform method*:

$$q(t) = \frac{k^2 \, \kappa_n}{C_L^*} t^\lambda E_{\lambda,\lambda+1}\left(-\frac{1}{C_L^*}t^\lambda\right) + q_0 E_\lambda\left(-\frac{1}{C_L^*}t^\lambda\right). \tag{5.68}$$

Both equations (5.66) and (5.68) give explicit analytic closed forms for the time-dependent function $q(t)$. Obviously they must be same. The trivial case in which the local and nonlocal terms have both the same relaxation exponent $\lambda = \nu$ and the same normalized material parameters $C_L^* = -C_N^*$ shows that

$$k^2 = \frac{C_L^*}{C_N^*} = 1,$$

bearing in mind that the local term $C_L^* < 0$ as it is made dimensioless dividing C_L by $\bar{\varphi}'' < 0$.

5.3.3 Complete time-dependent equation: Eigenvalues

The fact that (5.52) and (5.59) must be consistent also in the nontrivial case is studied in this section. In this regard, the complete equation coming from (5.52) and (5.59) is considered:

$$C_L^* \, \mathcal{D}_t^\lambda q(t) - C_N^* \, k^2 \, \mathcal{D}_t^\nu q(t) + (1 - k^2)q(t) = 0. \tag{5.69}$$

Equation (5.69) has the form of a Fractional Order Eigenvalue Problem, which is not easy to be solved. Indeed, very recent works show the strong effort in finding this kind of solutions [65, 101, 128, 134, 172]. In order to solve this eigenvalue problem, we make use of the right-sided Fourier transform $Q(p)$

$$Q(p) := \int_0^{+\infty} e^{-i\,p\,t} q(t) \, dt \qquad p \in \mathbb{R}. \tag{5.70}$$

By Fourier transforming both sides of (5.69) we obtain:

$$\left[C_L^* \, (-i\,p)^\lambda - C_N^* \, k^2 \, (-i\,p)^\nu + (1 - k^2) \right] Q(p) = 0. \tag{5.71}$$

176

The roots of the function inside square brackets supplies the eigenvalues of the fractional differential equation (5.69). Consider $-i = e^{-i\frac{\pi}{2}}$ and expand (5.71):

$$C_L^* \, p^\lambda \, e^{-i\frac{\pi}{2}\lambda} - k^2 C_N^* \, p^\nu \, e^{-i\frac{\pi}{2}\nu} + (1 - k^2) = 0. \tag{5.72}$$

The constant k^2 introduced in (5.52) must be a real-valued number. Solving equation (5.71) in terms of k^2 we get:

$$
\begin{aligned}
k^2 &= \frac{1 + C_L^* \, p^\lambda \, (c_\lambda - i \, s_\lambda)}{1 + C_N^* \, p^\nu \, (c_\nu - i \, s_\nu)} \\
&= \frac{\left(1 + C_L^* \, p^\lambda \, c_\lambda\right) - i \left(C_L^* \, p^\lambda \, s_\lambda\right)}{\left(1 + C_N^* \, p^\nu \, c_\nu\right) - i \left(C_N^* \, p^\nu \, s_\nu\right)} = \frac{a - i \, b}{c - i \, d} \\
&= \frac{a - i \, b}{c - i \, d} \frac{c + i \, d}{c + i \, d} = \frac{a \, c + b \, d}{c^2 + d^2} + i \frac{a \, d - b \, c}{c^2 + d^2},
\end{aligned}
$$

where we set

$$
\begin{cases} a = 1 + C_L^* \, p^\lambda \, c_\lambda \\ b = C_L^* \, p^\lambda \, s_\lambda \end{cases}
\qquad
\begin{cases} c = 1 + C_N^* \, p^\nu \, c_\nu \\ d = C_N^* \, p^\nu \, s_\nu \end{cases} ,
$$

and for the sake of convenience the positions $c_\alpha = \cos(\alpha \, \pi/2)$ and $s_\alpha = \sin(\alpha \, \pi/2)$ are used. Because of the fact that k is real, the following relationships must hold:

$$k^2 = \frac{a \, c + b \, d}{c^2 + d^2} \tag{5.73a}$$

$$a \, d - b \, c = 0. \tag{5.73b}$$

The latter of these conditions allows for characterizing the value k^2 as

$$C_N^* \, p^\nu \, s_\nu - C_L^* \, p^\lambda \, s_\lambda + C_L^* \, C_N^* \, p^{\lambda+\nu} \, (s_\nu c_\lambda - c_\nu s_\lambda) = 0.$$

Bearing in mind the transformation formulae for the difference of two angles, the relationship (5.73b) becomes:

$$
\begin{aligned}
C_N^* \, p^\nu \, \sin\left(\nu \, \frac{\pi}{2}\right) - C_L^* \, p^\lambda \, \sin\left(\lambda \, \frac{\pi}{2}\right) + \\
+ C_L^* \, C_N^* \, p^{\lambda+\nu} \, \sin\left((\nu - \lambda) \, \frac{\pi}{2}\right) = 0
\end{aligned}
\tag{5.74}
$$

177

Finally, a relationship for k^2 is found in the form:

$$k^2 = \frac{\left(1 + C_L^* \, p^\lambda \, c_\lambda\right)\left(1 + C_N^* \, p^\nu \, c_\nu\right) + \left(C_L^* \, p^\lambda \, s_\lambda\right)\left(C_N^* \, p^\nu \, s_\nu\right)}{\left(1 + C_N^* \, p^\nu \, c_\nu\right)^2 + \left(C_N^* \, p^\nu \, s_\nu\right)^2}. \tag{5.75}$$

Whenever the trivial case $\lambda = \nu$ and $C_L^* = C_N^*$ is considered, equation (5.74) has solution $p = 0$, that implies $k^2 = 1$, as noticed qualitatively above. The solution of (5.75) cannot be found in closed form. In Figure 5.4 and Figure 5.5 some numerical results are represented whenever the local modulus C_L^*, the nonlocal modulus C_N^* and both the viscoelastic exponents are known. The value of R is defined as function of the moduli ratio $C_L^*/C_N^* < 0$, showing that the eigenvalues are continuous functions, then for each choice of R is possible to find the correspondent value of k^2.

Each bifurcated configuration is characterized by a chosen value of k^2 that modifies the left and right branch of the ratio $\bar\varphi''/\bar\varphi'$, as shown in (5.65). Indeed, the elastic case (5.19) is recovered whenever $k^2 = 1$. A numerical example handling the same energy used in the elastic case is reported in Figure 5.6. A closer analysis of the curves shows that k^2 works as a rescaling parameter, increasing the magnitude of the ratio $\bar\varphi''/\bar\varphi'$ as k increases. The location of J_n is not affected by the rescaling, whereas the upper bound of the curve is deeply influenced by that. Henceforth, the value n_{max} of the spatial oscillations depends on such a rescaling, as shown in the insert in Figure 5.6. Consequently, the left and right branch change their shape, and the intersections yielding the corresponding configurations $\bar J$ are modified as shown in Figure 5.7.

5.3.4   Initial condition and Eigenvalue problem

Let consider the complete fractional differential equation (5.69) with inhomogeneous initial conditions:

$$\begin{cases} C_L^* \, \mathcal{D}_t^\lambda q(t) - C_N^* \, k \, \mathcal{D}_t^\nu q(t) + (1 - k^2)q(t) = 0, \\ q(0) = q_0. \end{cases}$$

As suggested in [169], a *Transform method* is used for solving this Fractional Differential Equation. As first step, let use the right-sided Fourier Transform on the original equation taking into account the initial condition:

$$C_L^* \left[(i\,p)^\lambda \hat Q - (i\,p)^{\lambda-1} q_0\right] - C_N^* \, k^2 \left[(i\,p)^\nu \hat Q + \right.$$
$$\left. - (i\,p)^{\nu-1} q_0\right] + \hat Q\,(1 - k^2) = 0,$$
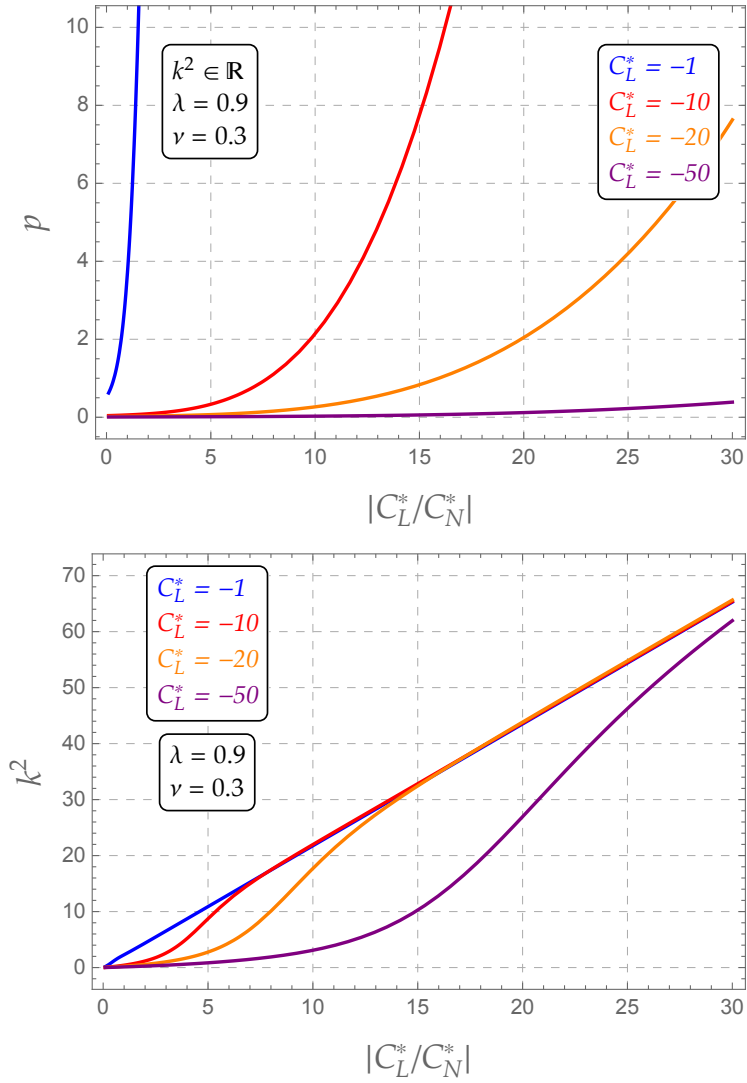
Figure 5.4: Locus of the real eigenvalues k^2 and their values as function of the ratio $R = -C_N^*/C_L^*$ whenever $\lambda = 0.9$ and $\nu = 0.3$ (see equations (5.74)-(5.75)). Courtesy of [58].
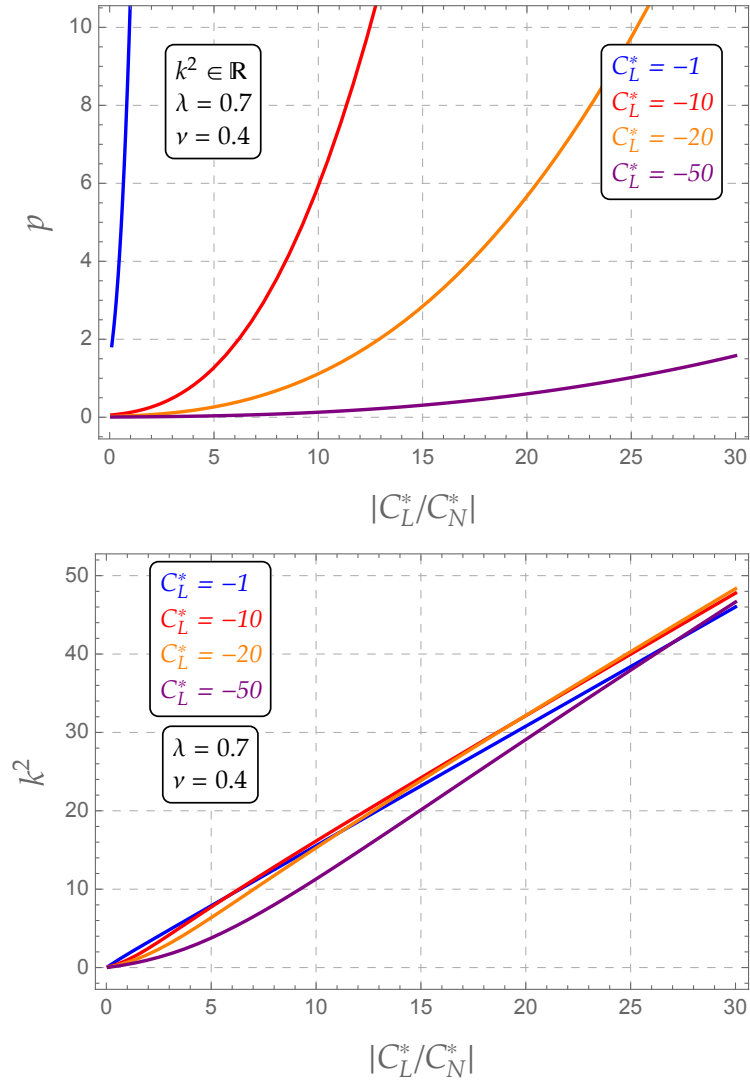
Figure 5.5: Locus of the real eigenvalues k^2 and their values as function of the ratio $R = -C_N^*/C_L^*$ whenever $\lambda = 0.7$ and $\nu = 0.4$ (see (5.74)-(5.75)). Courtesy of [58].
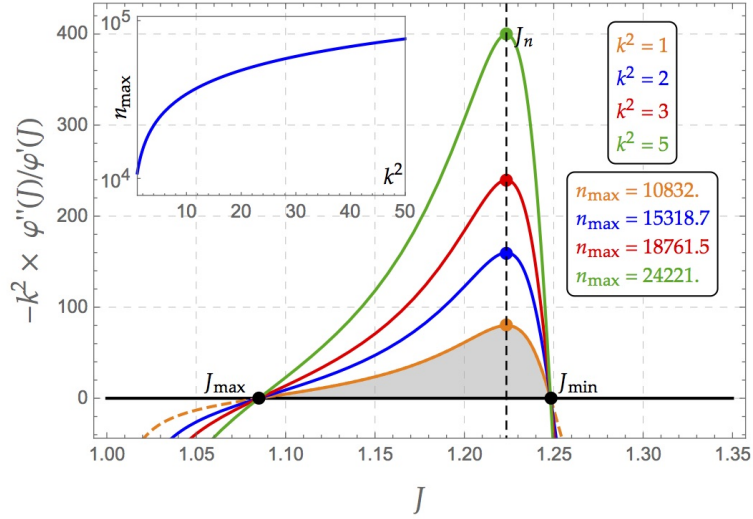
Figure 5.6: Right hand side of equation (5.65) as function of k^2. Courtesy of [58].
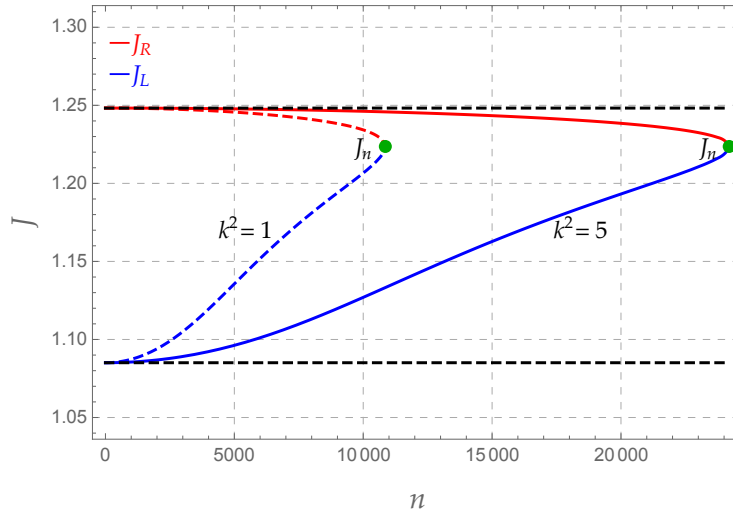
Figure 5.7: Modification of the *left* and *right* intersection depending on k^2 (see also Figure 5.2). Courtesy of [58].

181

where p is the variable in the Fourier domain; the solution of the obtained algebraic equation in term of the transformed function $\hat{Q}(p)$ reads:

$$\hat{Q}_k(p) = q_0 \frac{\left(C_L^* \,(i\,p)^{\lambda-1} - C_N^* \, k^2 \,(i\,p)^{\nu-1}\right)}{C_L^* \,(i\,p)^{\lambda} - C_N^* \, k \,(i\,p)^{\nu} + (1 - k^2)}. \tag{5.76}$$

By means of the solution displayed in [169], (eqns 5.22-5.25 pag. 155 where $a = C_L^*$, $\beta = \lambda$, $b = -C_N^* \, k^2$, $\alpha = \nu$ and $c = 1 - k^2$), the transfer function in the frequency domain of this problem reads as follows:

$$\hat{G}_k(p) = \frac{1}{C_L^* \,(i\,p)^{\lambda} - C_N^* \, k^2 \,(i\,p)^{\nu} + (1 - k^2)}. \tag{5.77}$$

It would be worth noting that the transfer function is strictly related to the eigenvalue of k^2; for this reason, we denoted $\hat{G}$ with the subscript k, in order to highlight the importance of k^2 on the transfer function. Finally, the transfer function in the real time domain if found simply by using the Inverse Fourier transform:

$$G_k(t) = \mathcal{F}^{-1}\left\{\hat{G}_k(p); t\right\} =$$
$$= \frac{1}{C_L^*} \sum_{z=0}^{\infty} (-1)^z \left(\frac{1 - k^2}{C_L^*}\right)^{z+1} t^{\lambda(z+1)-1} E_{\lambda-\nu,\lambda+z\nu}^{(z)}\left(\frac{C_N^*}{C_L^*} k^2 \, t^{\lambda-\nu}\right). \tag{5.78}$$

The transfer function $G_k(t)$ is strictly connected with the Mittag-Leffler function, and it plays a modulation role in the evolution of the membrane response in terms of both stretch and stress.

As an illustrative example, the transfer function is numerically explored in Figure 5.8 whenever two subcases of $C_L^* = -C_N^*$ are considered, by assuming several values of the exponential decay $\lambda = \nu$. Similarly, in Figure 5.9 the real and imaginary part of the transfer function are analyzed whenever different exponents of the decay $\lambda \neq \nu$ are chosen for some values of k^2. The Mittag-Leffler function drives the evolution of the membrane stretch, determining changes in the amplitude of the membrane response, as expected from the analysis with a separation of variables.

5.4   Remarks

The onset of bifurcated configurations possibly arising from homogeneous configurations characterized by an areal stretch lying in the spinoidal region has been

182
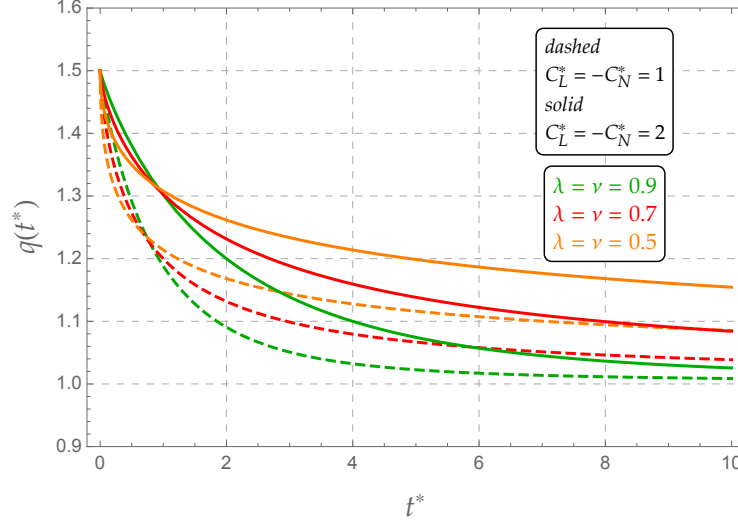
Figure 5.8: Time-dependent transfer function for two chosen values of $C_L^* = -C_N^*$ and $h_0 = 1.5$. Here $t^* = \sqrt[\nu]{\dfrac{t^\nu}{C_N^*}}$ is a dimensionless time (see equation (5.66)). Courtesy of [58].

investigated. Here the total elastic (Gibbs free) energy has been minimized in order to determine the bifurcated modes and the relationships between the number of nucleated spatial waves with the critical values of the areal stretches.

Time synchronous variations are considered for finding the boundary conditions and the field equations governing the problem. Such equations yield a non-classical eigenvalue problem to be analyzed through the method of separation of variables. Because we analyze bifurcations of the areal stretch from the spinoidal zone, the spatial modes are still found to be oscillatory. The period of oscillation is shown to decrease with the ratio of (dimensionless) generalized local and nonlocal moduli and, hence, the number of oscillation increase with respect to the elastic case. As the ratio just mentioned above increases, for a given number of oscillations the interval of stretches for which bifurcation can occur gets larger if compared with the one determined by the purely elastic behavior.

The time-dependent part of the problem leads to a non classical fractional eigenvalue problem. Upon exploring the transfer function of the governing equation for different values of the local and nonlocal relaxation power, it can be concluded

that time-decay occurs in the response. Hence, large number of spatial oscillation slowly relaxes, thereby keeping the features of a long-tail type response.

Separation of variables allows for showing how Fractional Hereditariness owes bifurcated modes with a larger number of spatial oscillations than the corresponding elastic analog. Indeed, the available range of areal stresses for material instabilities is found to increase with respect to the purely elastic case. Nevertheless, the time evolution of the perturbations solving the Euler-Lagrange equation above exhibits time-decay and the large number of spatial oscillation slowly relaxes, thereby keeping the features of a long-tail type time-response.
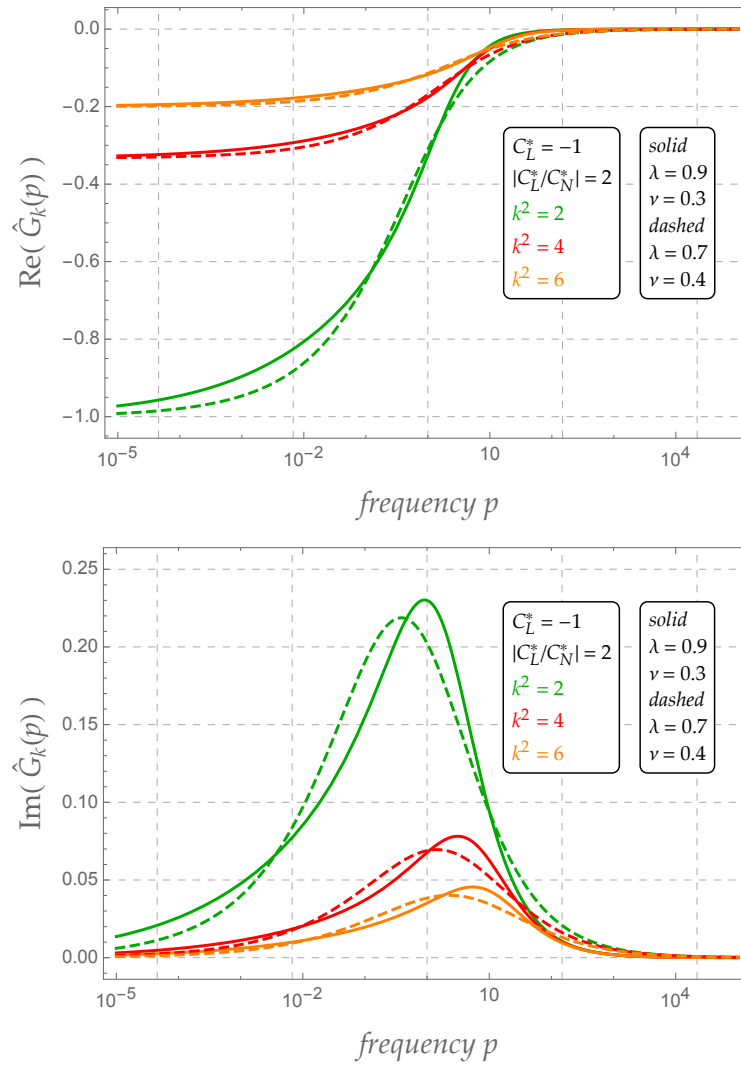
Figure 5.9: Transfer function $\hat{G}_k(p)$: real and imaginary part. Courtesy of [58].

185

References

[4]   A. Agrawal and D. Steigmann. "Modeling protein-mediated morphology in biomembranes". *Biomechanics and Modeling in Mechanobiology* 8.5 (2009), pp. 371–379 (cit. on pp. 1, 4, 153).

[21]   S. Breuer and E. Onat. "On the determination of free energies in linear viscoelastic solids". *Zeitschrift für angewandte Mathematik und Physik* 15.2 (1964), pp. 184–191 (cit. on pp. 168–170).

[26]   M. Caputo. *Elasticità e Dissipazione*. Bologna: Zanichelli, 1969 (cit. on p. 167).

[36]   D. Craiem and R. L. Magin. "Fractional order models of viscoelasticity as an alternative in the analysis of red blood cell (RBC) membrane mechanics". *Physical Biology* 7.1 (2010), p. 13001 (cit. on p. 165).

[39]   G. Del Piero and L. Deseri. "On the analytic expression of the free energy in linear viscoelasticity". *Journal of Elasticity* 43 (1996), pp. 247–278 (cit. on pp. 165, 168–170).

[40]   G. Del Piero and L. Deseri. "On the concepts of state and free energy in linear viscoelasticity." *Archive for Rational Mechanics and Analysis* 138 (1997), pp. 1–35 (cit. on pp. 165, 168, 169, 194, 195, 198, 201, 230).

[43]   L. Deseri, M. Di Paola, and M. Zingales. "Free energy and states of fractional-order hereditariness". *International Journal of Solids and Structures* 51 (2014), pp. 3156–3167 (cit. on pp. 165, 167, 169, 170).

[44]   L. Deseri, G. Gentili, and M. Golden. "An Expression for the Minimal Free Energy in Linear Viscoelasticity". *Journal of Elasticity* 54 (1999), pp. 141–185 (cit. on pp. 168, 194).

[46]   L. Deseri and M. Golden. "The Minimum Free Energy for Continuous Spectrum Materials." *SIAM Journal on Applied Mathematics* 67.3 (2007), pp. 869–892 (cit. on pp. 165, 168, 194).

[47]   L. Deseri, M. Golden, and M. Fabrizio. "The Concept of a Minimal State in Viscoelasticity: New Free Energies and Applications to PDEs". *Archive for Rational Mechanics and Analysis* 181 (2006), pp. 43–96 (cit. on pp. vi, 165, 168, 194, 195, 198, 201).

186

[50]   L. Deseri and D. R. Owen. "Submacroscopically Stable Equilibria of Elastic Bodies Undergoing Disarrangements and Dissipation". *Mathematics and Mechanics of Solids* 15.6 (2010), pp. 611–638 (cit. on pp. 37, 154, 226).

[52]   L. Deseri, M. Piccioni, and G. Zurlo. "Derivation of a new free energy for biological membranes". *Continuum Mechanics and Thermodynamics* 20.5 (2008), pp. 255–273. DOI: `10.1007/s00161-008-0081-1` (cit. on pp. iv, 1, 4, 23, 25, 26, 40, 153, 154, 168, 193).

[53]   L. Deseri and M. Zingales. "Constitutive Model of Hereditary Fluid Mosaic of Lipid Bilayers". *In preparation* (2015) (cit. on p. 154).

[55]   L. Deseri and G. Zurlo. "The stretching elasticity of biomembranes determines their line tension and bending rigidity". *Biomechanics and Modeling in Mechanobiology* 12 (2013), pp. 1233–1242. DOI: `doi: 10.1007/s10237-013-0478-z` (cit. on pp. iii, iv, 1, 4, 23–26, 30, 40, 72, 153, 154, 168, 193).

[58]   L. Deseri et al. "Fractional Hereditariness of Lipid Membranes: Instabilities and Linearized Evolution". *Journal of The Mechanical Behavior of Biomedical Materials* (2015) (cit. on pp. v, 163, 164, 166, 179–181, 183, 185).

[65]   J.-S. Duan et al. "Eigenvalue problems for fractional ordinary differential equations". *Chaos Solition Fract* 46 (2013), pp. 46–53 (cit. on p. 176).

[66]   G. Espinosa et al. "Shear rheology of lipid monolayers and insights on membrane fluidity". *PNAS* 108.15 (2011), pp. 6008–6013. DOI: `www.pnas.org/cgi/doi/10.1073/pnas.1018572108` (cit. on pp. v, 154, 165, 167).

[94]   C. W. Harland, M. J. Bradley, and R. Parthasarathy. "Phospholipid bilayers are viscoelastic". *PNAS* 107.45 (2010), pp. 19146–19150. DOI: `doi:www.pnas.org/cgi/doi/10.1073/pnas.1010700107` (cit. on pp. 165, 167).

187

[101]   J. Henderson and N. Kosmatov. "Eigenvalue comparison for Fractional Boundary Value Problems with the Caputo Derivative". *Fractional Calculus and Applied Analysis* 17.3 (2014), pp. 872–880 (cit. on p. 176).

[115]   A. A. Kilbas, H. M. Srivastava, and J. J. Trujillo. *Theory and Applications of Fractional Differential Equations.* Amsterdam, Netherlands: Elsevier, 2006 (cit. on p. 167).

[128]   J. Li and J. Qi. "Spectral problems for fractional differential equations from nonlocal continuum mechanics". *Adv Differ Equ* 85 (2014), pp. 2–12 (cit. on p. 176).

[133]   R. L. Magin. "Fractional calculus models of complex dynamics in biological tissues". *Computers & Mathematics with Applications* 59.5 (2010), pp. 1586–1593 (cit. on pp. 5, 167).

[134]   F. Mainardi. "The Fundamental Solutions for the Fractional Diffusion-Wave Equation". *Applied Mathematics Letters* 9.6 (1996), pp. 23–28 (cit. on p. 176).

[139]   M. Maleki, B. Seguin, and E. Fried. "Kinematics, material symmetry, and energy densities for lipid bilayers with spontaneous curvature". *Biomechanics and Modeling in Mechanobiology* 12.5 (2013), pp. 997–1017 (cit. on p. 153).

[169]   I. Podlubny. *Fractional Differential Equation.* Academic, New York, 1998 (cit. on pp. 167, 178, 182, 226, 257, 259–261).

[171]   G. Puglisi. "Nucleation and phase propagation in a multistable lattice with weak nonlocal interactions". *Continuum Mechanics and Thermodynamics* (2007), pp. 299–319 (cit. on p. 155).

[172]   J. Qi and S. Chen. "Eigenvalue problems of the model from nonlocal continuum mechanics". *Journal of Mathematical Physics* 52.073516 (2011) (cit. on p. 176).

[182]   S. G. Samko, A. A. Kilbas, and O. I. Marichev. *Fractional Integrals and Derivatives. Theory and Applications.* Londn - New York: Gordon & Breach Science Publishers, 1987 (cit. on pp. vi, 167).

[186] G. Scott-Blair. "Psychoreology: links between the past and the present". *Journal of the Texture Studies* 5 (1974), pp. 3–12 (cit. on p. 167).

[198] N. Triantafyllidis and S. Bardenhagen. "On Higher Order Gradient Continuum Theories in Nonlinear Elasticity Derivation from and Comparison to the Corresponding Discrete Models". *Journal of Elasticity* 33 (1993), pp. 259–293 (cit. on p. 155).

Part II

Hereditary behavior of Fractional Order Materials

Chapter 6

Notion of state for Fractional Hereditary Materials

The occurrence of time-dependent power law mechanical properties has been noticed in many materials since the first half of the twentieth century [156, 185]. Macroscopic hereditariness has indeed been detected through stress relaxation and creep mechanical tests.

As noticed in [111], the response of time-dependent systems exhibiting long tail memories would entail a very large number of approximating conventional modes, namely e.g. of exponentials, that are identifiable through classical rheological models. A more appropriate and yet precise way to handle the exhibited behavior is to account for power laws, both for creep and relaxation, leading to the occurrence of fractional hereditariness. Furthermore, the same feature is observed while monitoring complex interfaces observed experimentally in thin films formed by solutions containing surface active molecules. For instance, this is the case of lipid membranes where, often times, elasticity is taken as the only feature of the effective response (see e.g. [52, 55]). The underlying nano-structure (lipids are a

few nanometers long) determines the physical properties of such membranes, which are key constituents for cells.

A part from situations in which the experienced strains become very large and, hence, appropriate strain measures are required (see e.g. [32]), it is known that accurate descriptions of the results of experimental tests are reproduced by power-laws with real order exponents [60, 62, 83]. This elucidates the reason why linear hereditary equations are applicable to the analysis of complex materials whose behavior is time dependent, and it clarifies the confusion that sometimes is made between apparent material nonlinearity and power law behavior (see e.g. [173]). The motivations above regarding bone as an example explain why multiple scales present in many materials entail several multiple relaxation times, ultimately producing a macroscopic power-law hereditariness.

Although strong motivations for looking at such power laws have been discussed, neither they have been explicitly incorporated in general mathematical frameworks (see e.g. the ones developed in [7, 44, 46, 47, 67, 68, 132, 181] among others) nor it has been shown a direct mechanical and mathematical connection between the material properties at the submacroscopic level and the observed macroscopic power law. The latter are known to yield the Boltzmann-Volterra constitutive equations, both for creep and relaxation, in terms of fractional operators (see [9, 10, 60, 62, 111, 135–137] for their applications to viscoelasticity and [77–79, 121, 177, 178, 193, 194, 208] for applications to other mechanical contexts). This leads to refer to the constitutive properties of such media as "Fractional Hereditary Materials" (FHM).

In this Chapter, the attention is focused on the characterization of the state for such materials. The particularization of the notion of state introduced by Noll in [154] to viscoelastic materials (see [40, 47, 84, 89]), one can state that if two states are different then there must be some continuation (of arbitrary duration) of such state which produces different responses with the two states as initial ones. For viscoelastic materials the conclusion that can be drawn is that two past histories verifying this condition must correspond to the same state. Whenever the strain is taken to be the independent variable of the analysis, the material response can be described either in terms of the resulting stress (through the Boltzmann-Volterra integral (6.27a)) or in terms of the work done by the stress on any continuation (see [84]). On the other hand, for this case a notion of state has been introduced in [40] as a pair where one of the entries is an equivalence class of strain histories and the other one is the current value of the strain. The equivalence class is established through the right-hand side of (6.33) (which involves a generic relaxation function), whose solution for all non negative times characterizes equivalent histories. This notion of state, eventually called "minimal state" in [47], entails the fact that a state variable can be singled out as the residual stress measurable at any further time ($\bar{t} + \tau$ in (6.33)) after freezing and keeping the current value of the strain to zero

for any arbitrary duration τ. "Long tai" memory materials may allow for detecting such a stress for long times and this is the case for power law hereditariness. The notion of "minimality" recalled above has to do with the fact that the knowledge of such a stress is the minimum necessary information required to fully characterize the response of the material to further loadings. Obviously, the specific knowledge of the solutions of (6.33) are very useful, although very rarely they can be found explicitly.

6.1 Fractional hereditary virgin materials

It is worth recalling that two hypotheses are considered while analyzing viscoelastic materials (see e.g. [136]): 1) invariance under time translation and 2) causality. The first requirement means that time shift in the input is reflected as a same shift in the output; the second means that the material response depends on previous histories only, reflecting hereditariness of such materials. In this section we shall refer to "virgin" materials, namely either the strain or the stress are known from the very beginning of the observation of their behavior, conventionally set at $t = 0$, and hence no past histories with respect to such a time need to be taken into account. From Section 6.2 on, this requirement will be relaxed and the notion of state introduced in [40, 47] will allow for characterizing the residual stress due to unknown past histories. For the sake of illustration, the whole paper is focused on one dimensional problems.

Creep and relaxation tests are performed to detect material hereditariness [123]: in the first case, the stress is held constant and the strain is measured, whereas in the second one the strain is held constant and the stress is measured. Whenever either a unit stress or a unit strain is utilized, the creep compliance $J(\circ)$ and relaxation modulus $G(\circ)$ are found as the strain and stress response to the imposed unit stress and strain respectively, i.e.

$$\varepsilon(t) = U(t) \longrightarrow \sigma(t) = G(t) \tag{6.1a}$$

$$\sigma(t) = U(t) \longrightarrow \varepsilon(t) = J(t), \tag{6.1b}$$

where $U(\circ)$ is the unit Heaviside step function. When either the creep or the relaxation function is known, the Boltzmann superposition principle allows for writing convolution-type Riemann-Stieltjies integrals to express the relationships between σ and ε. Whenever either the strain or the stress are prescribed, the

constitutive relations for the corresponding derived quantities read as follows:

$$\sigma(t) = \int_{0^+}^{t} G(t - \tau) \, d\varepsilon(\tau), \tag{6.2a}$$

$$\varepsilon(t) = \int_{0^+}^{t} J(t - \tau) \, d\sigma(\tau). \tag{6.2b}$$

Smoothness assumptions on $\varepsilon(t)$ and $\sigma(t)$ will be discussed in the sequel.

Creep compliance and relaxation modulus are not independent. Indeed they are linked to each other by the relationship

$$\hat{J}_+(\omega)\hat{G}_+(\omega) = \frac{1}{(i\omega)^2}, \tag{6.3}$$

where the symbol ˆ denotes the right-sided Fourier transform (see Appendix A.1), equation (A.10)).

Experiments on polymeric materials performed by Nutting [156] at beginning of the twentieth century showed that their relaxation function is well fitted by power-laws, i.e.

$$G(t) = \frac{C_\beta}{\Gamma(1 - \beta)} t^{-\beta}, \tag{6.4}$$

where $\Gamma(\circ)$ is the Euler-Gamma function, C_β and β are characteristic constants of the material. The exponent β must be enclosed in the range $0 < \beta < 1$ because of thermodynamics restrictions [9, 10, 62]. At the extrema of the range, asymptotic behaviors are obtained: $\beta \to 0$ corresponds to purely elastic solid whereas $\beta \to 1$ to purely viscous fluid. The values of $0 < \beta < 1$ correspond to an intermediate behavior between elastic solid and viscous fluid, allowing for describing both complex-structured materials and soft matter. As we expect, the creep compliance of the given material can be determined through (6.3) from the relaxation modulus assumed in (6.4). Furthermore, the right Fourier transform of the relaxation function (6.4) yields

$$\hat{G}_+(\omega) = C_\beta(i\omega)^{\beta-1}, \tag{6.5}$$

and by substituting this expression in (6.3) we then obtain

$$\hat{J}_+(\omega) = \frac{1}{C_\beta(i\omega)^{\beta+1}}, \tag{6.6}$$

whose anti-transform reads as follows:

$$J(t) = \frac{1}{C_\beta \Gamma(1+\beta)} t^\beta. \tag{6.7}$$

It is worth analyzing the material behavior with the aid of normalized functions, $\overline{G}(t)$ and $\overline{J}(t)$ defined as follows:

$$\overline{G}(t) := G(t) \left(C_\beta\right)^{-1} \Gamma(1-\beta) = t^{-\beta} \tag{6.8a}$$

$$\overline{J}(t) := J(t) C_\beta \Gamma(1+\beta) = t^\beta \tag{6.8b}$$

and showed in Figure 6.1. A careful observer will notice immediately that all the curves share the common point $(1,1)$, which represents a key value. Indeed, the blue curves $(0 < \beta \leq 1/2)$ show that the elastic phase prevails on viscous one with decreasing β, whereas the red ones $(1/2 \leq \beta < 1)$ show that the viscous phase prevails on elastic one as increases as β. This consideration allows for identifying the former as *elastoviscous* (E) materials while the latter as *viscoelastic* (V) ones; the value $\beta = 1/2$ is clearly common to both kinds of materials, thus it may be obtained as a limiting case of both models described above. The corresponding rheological models, formed by proper arrangements of springs and dashpots, will be discussed in the sequel.

(a) $\overline{G}(t)$ (b) $\overline{J}(t)$
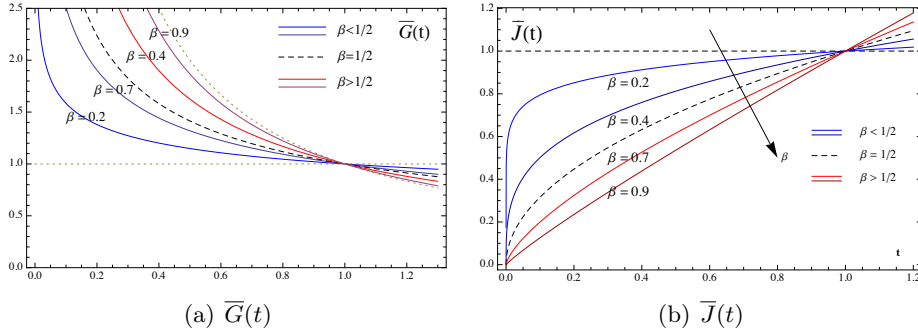
Figure 6.1: Normalized (a) relaxation and (b) creep functions. Courtesy of [54].

In order to introduce the appropriate functional setting characterizing stress and strain we start from (6.2a), i.e. when ε is assumed to be the control variable. Lemma 2.2 in [183] (p.35) assures that if $\varepsilon \in AC_{\mathrm{loc}}$, where AC_{loc} denotes the set of locally absolutely continuous functions, then the integral (6.2a) exists almost

everywhere for $0 < \beta < 1$ and takes the following form[1]:

$$\sigma(t) = \frac{C_\beta}{\Gamma(1-\beta)} \int_{0^+}^{t} \frac{\dot{\varepsilon}(\tau)}{(t-\tau)^\beta}\, d\tau.\tag{6.9}$$

Lemma 2.2 also guarantees that $\sigma \in L_{\text{loc}}^r$, where $1 \le r \le \beta^{-1}$. Nevertheless, in reality, the strain may exhibit localized jumps, i.e. strain discontinuities could be present and localized in sets of measure zero, namely in specific locations in time. Estimates regarding the properties of the generalization of (6.2a) to the tensor valued case and to $a \to -\infty$ have been provided in [40, 47]. There strains were taken in BV_{loc} and $\text{SBV}_{loc} \cup \text{L}_{\text{loc}}^2$ respectively[2]. Obviously, any absolutely continuous function has bounded total variation[3], since the following chain of inclusion holds: $\text{AC}_{\text{loc}} \subset \text{SBV}_{\text{loc}} \subset \text{BV}_{\text{loc}}$. In particular any $\varepsilon_{SBV} \in SBV_{loc}$ is such that

$$\varepsilon_{SBV}(t) = \int_{0^+}^{t} \dot{\varepsilon}_{ac}(\tau)d\tau + \varepsilon_{\mathcal{J}}(t),\tag{6.10}$$

where ε_{ac} is the absolutely continuous part of ε and the second term $\varepsilon_{\mathcal{J}}$ represents the so called jump part of ε, i.e.

$$\varepsilon_{\mathcal{J}}(t) := \sum_{t > t_i \in \mathcal{J}(\varepsilon)} [\![\varepsilon]\!](t_i)U(t-t_i),\tag{6.11}$$

where $\mathcal{J}(\varepsilon)$ is the jump set of ε, t_i are the locations of the jumps, $U(\circ - t_i)$ are unit step Heaviside functions located at t_i and $[\![\varepsilon]\!](t_i) := \varepsilon(t_i^+) - \varepsilon(t_i^-)$ is the jump experienced by ε at t_i. It is worth remarking that any $\dot{\varepsilon}_{ac} \in L_{loc}^1$. It is well known that $\varepsilon_{BV} \in BV_{loc}$ can be decomposed in the following way:

$$\varepsilon_{BV}(t) = \varepsilon_{SBV}(t) + \mathcal{C}(\varepsilon(t)),\tag{6.12}$$

where $\mathcal{C}$ represents the so called Cantor part of ε at t. Relation (6.12) is the Lebesgue decomposition of ε for BV_{loc} functions and (6.10) is its particularization to the case of $\varepsilon \in SBV_{loc}$ (see e.g. [118]). Henceforth, by considering strains in

---

[1]Here $\varepsilon(0) = 0$

[2]Here BV_{loc} and SBV_{loc} denote the sets of functions of bounded and special bounded variations on bounded sets, respectively

[3]The total variation Var of a function ε is defined as:

$$\text{Var}_{loc}(\varepsilon) := \text{Var}_{r \in (a,b)}(\varepsilon(r)) = \sup\left\{\sum_{i=1}^{n} |\varepsilon(r_i) - \varepsilon(r_{i-1})| : \{r_0, r_1, \ldots, r_n\} \in (a,b)\right\}$$

such space, the stress can still be computed by means of (6.9), by understanding that the following representation holds for the strain rate:

$$\dot{\varepsilon}(\tau) = \dot{\varepsilon}_{ac}(\tau) + \sum_{t > t_i \in \mathcal{J}(\varepsilon)} [\![\varepsilon]\!](t_i)\delta(t - t_i), \qquad (6.13)$$

where $\delta(\circ - t_i)$ are Dirac delta masses located at $t_i \in \mathcal{J}(\varepsilon)$. Because $\varepsilon \in SBV_{loc}$ its total variation $\underset{loc}{\mathrm{Var}}(\varepsilon)$ is finite, and hence the strain measure[4] $d\varepsilon = \dot{\varepsilon}(t)dt$, with $\dot{\varepsilon}(t)$ as in (6.13), is bounded from above by $\underset{loc}{\mathrm{Var}}(\varepsilon)$. It is worth noting that the power law relaxation function (6.4) is such that $\dot{G} \in L^1_{loc/\{0\}}$ and that $G(0)$ is unbounded (for thermodynamic restriction about such function see [87]). Henceforth, as long as $t = 0$ is excluded, estimates of the stress (see Section 6.2 in the sequel) can be done by using the fact that (6.2a) is a Riemann-Stieltjies integral and hence (see Theorem 2 in [118] p. 368) the following inequality holds, i.e.

$$\left| \int_a^t G(t - \tau)d\varepsilon(\tau) \right| \leq \sup_{r \in (a,b)} |G(t - r)| \underset{r \in (a,b)}{\mathrm{Var}}(\varepsilon(r)) \quad \forall a \neq 0, \forall t \leq b. \qquad (6.14)$$

Finally, we recognize that relation (6.9) may be recast in terms of the Caputo fractional derivative of order β of ε (see Appendix A), i.e.

$$\sigma(t) = C_\beta \left({}_C\mathrm{D}_{0^+}^\beta \varepsilon \right)(t). \qquad (6.15)$$

This notation must be interpreted bearing in mind that every straining $\dot{\varepsilon}$ appearing in (6.9) has the representation (6.13); in the sequel of this section the contribution of the Dirac delta masses to the stress will be singled out. Whenever σ is assumed as control variable (6.2b) must be considered. By substituting relation (6.7) in (6.2b) we get:

$$\varepsilon(t) = (C_\beta\Gamma(1 + \beta))^{-1} \int_{0^+}^t (t - \tau)^\beta \dot{\sigma}(\tau)d\tau. \qquad (6.16)$$

A simple integration by parts yields the following representation formula:

$$\varepsilon(t) = \frac{1}{C_\beta} \left(\frac{\sigma(0)t^\beta}{\Gamma(1 + \beta)} + \left(\mathrm{I}_{0^+}^\beta \sigma \right)(t) \right) \qquad (6.17)$$

---

[4]It is worth noting that $d\varepsilon$ can be seen as a Radon measure and, hence, (6.13) represents the Radon-Nykodim derivative of $\varepsilon(t)$ with respect to the one-dimensional Lebesgue measure dt.

after setting

$$\left(\mathrm{I}_{0^+}^{\beta}\sigma\right)(t) := \frac{1}{C_\beta\Gamma(1-\beta)}\int_{0^+}^{t}(t-\tau)^{\beta-1}\sigma(\tau)\,\mathrm{d}\tau; \qquad (6.18)$$

this defines the Riemann-Liouville fractional integral of order β of the stress. It is worth noting that this is well defined since $\sigma \in L_{loc}^r$, $1 \le r \le \beta^{-1}$, $0 < \beta < 1$. Furthermore, the fact that σ is at least L_{loc}^1 is a necessary and sufficient condition for the resulting ε to be AC_{loc} (see Theorem 2.3 in [183] p. 43).

Moreover, Theorem 2.4 in [183] (p.44) ensures that if σ is represented through (6.15), where $\dot\varepsilon$ is replaced by $\dot\varepsilon_{ac}$, because $\dot\varepsilon_{ac} \in L_{loc}^1$ then

$$\mathrm{I}_{0^+}^{\beta}\left(\mathrm{D}_{0^+}^{\beta}\varepsilon_{ac}\right)(t) = \varepsilon_{ac}(t). \qquad (6.19)$$

The jump part $\varepsilon_{\mathcal{J}}$ defined in (6.11) of ε must then be treated separately. By denoting with $\sigma_{\mathcal{J}}(t)$ the contribution to the stress $\sigma(t)$ of $\varepsilon_{\mathcal{J}}(t)$, the direct evaluation of (6.9) (or (6.15)) can be done bearing in mind that

$$\dot\varepsilon_{\mathcal{J}}(t) := \sum_{t>t_i\in\mathcal{J}(\varepsilon)} [\![\varepsilon]\!](t_i)\delta(t-t_i). \qquad (6.20)$$

Such a contribution to the total stress reads as follows

$$\sigma_{\mathcal{J}}(t) = \frac{C_\beta}{\Gamma(1-\beta)}\sum_{t>t_i\in\mathcal{J}(\varepsilon)}\frac{[\![\varepsilon]\!](t_i)}{(t-t_i)^\beta}. \qquad (6.21)$$

We are now in the position to check whether or not the analog result for ε_{ac}, granted by Theorem 2.4 in [183], holds also for $\varepsilon_{\mathcal{J}}$. In other words, we conjecture that the relationship (6.19) above holds in the form

$$\left(\mathrm{I}_{0^+}^{\beta}\sigma_{\mathcal{J}}\right)(t) = \varepsilon_{\mathcal{J}}(t). \qquad (6.22)$$

Actually, the fact that this may be the case follows from the property of $\sigma_{\mathcal{J}}$ in (6.21) which is certainly L_{loc}^1. Henceforth, Theorem 2.4 in [183] applies. Nevertheless, a direct proof of the validity of relation (6.22) can be obtained by substitution of (6.21) into (6.18). Indeed, a direct inspection shows that the fractional integral at the left hand side of (6.22) can be written as follows:

$$\left(\mathrm{I}_{0^+}^{\beta}\sigma_{\mathcal{J}}\right)(t) = \frac{(C_\beta)}{\Gamma(\beta)\Gamma(1-\beta)}\sum_{t>t_i\in\mathcal{J}(\varepsilon)}[\![\varepsilon_{\mathcal{J}}]\!](t_i)\int_{t_i}^{t}(t-\tau)^{\beta-1}(\tau-t_i)^{-\beta}d\tau \qquad (6.23)$$

Each integral on the right hand side may be easily evaluated by setting $\alpha := 1 - \beta$ and by making use of procedure highlighted in [183] (p.29) namely:

$$\int_{t_i}^{t} (t - \tau)^{-\alpha} (\tau - t_i)^{\alpha - 1} d\tau = B(\alpha, 1 - \alpha), \qquad (6.24)$$

where $B(z, w)$ is the Euler Beta function defined as follows:

$$B(z, w) = \int_0^1 x^{z-1} (1 - x)^{w-1} dx. \qquad (6.25)$$

By noting that $\Gamma(\beta)\Gamma(1 - \beta) = B(\beta, 1 - \beta)$ and $B(\beta, 1 - \beta) = B(1 - \beta, \beta)$, the solution of (6.23) may be recast in the following form:

$$\left(I_{0^+}^{\beta} \sigma_{\mathcal{J}} \right)(t) = C_\beta \sum_{t > t_i \in \mathcal{J}(\varepsilon)} [\![\varepsilon_{\mathcal{J}}]\!](t_i) U(t - t_i) \qquad (6.26)$$

This result shows that (6.19) holds true even when jumps are present in the strain ε as long as $\varepsilon \in SBV_{loc}$.

6.2 The state of pre-stressed fractional hereditary materials

In [40, 47, 132] a definition of state introduced by Noll [154] has been established for viscoelastic materials whenever the strain is the control variable. This allows for defining equivalence classes of past-strain histories which, together with the current value of the strain, characterize the state in such context. Two histories are equivalent if any arbitrary continuation (often called either process or segment) of finite arbitrary duration yields to the same response. The latter can be either measured in terms of the stress or through the work done on processes [132].

On the other hand, whenever the stress is assumed to be the control variable, then the response is measured in terms of the strain. Here an equivalence class of stress histories could be singled out for the given material so that its state can be expressed in terms of any representative of such a class and of the current value of the stress (this belongs to a work in progress [56], although the logic followed in [40, 47, 132] applies with appropriate substitutions and considerations). In either case, here we completely characterize the state of FHM by making use of the analog of

(6.2a) and (6.2b), both extended to $(-\infty, t)$, i.e.

$$\sigma(t) = \int_{-\infty}^{t} G(t-\tau)d\varepsilon(\tau) = \frac{C_\beta}{\Gamma(1-\beta)} \int_{-\infty}^{t} \frac{\dot{\varepsilon}(\tau)}{(t-\tau)^\beta} d\tau = C_\beta \left({}_C\mathrm{D}_+^\beta \varepsilon \right)(t),$$
(6.27a)

$$\varepsilon(t) = \int_{-\infty}^{t} J(t-\tau)d\sigma(\tau) = \frac{(C_\beta)^{-1}}{\Gamma(1+\beta)} \int_{-\infty}^{t} (t-\tau)^\beta \dot{\sigma}(\tau)d\tau = \frac{1}{C_\beta} \left(\mathrm{I}_+^\beta \sigma \right)(t),$$
(6.27b)

where $\dot{\varepsilon}$ in (6.27a) and $\dot{\sigma}$ in (6.27b) make sense because of the smoothness assumptions listed above. We bear in mind that $\sigma(-\infty) = 0$ and, hence, by extending (6.16), (6.17) and (6.18) when 0^+ is replaced by $-\infty$ we get (6.27b). We start by considering (6.27a) and two functions $\dot{\varepsilon}_{(i)}$, $i = 1, 2$ to be defined as follows:

$$\dot{\varepsilon}_{(i)}(r) := \dot{\varepsilon}_{(i)}^*(r) + U(r - \bar{t})\dot{\varepsilon}^p(r) \quad i = 1, 2 \text{ and } r \in (-\infty, t)$$
(6.28)

where:
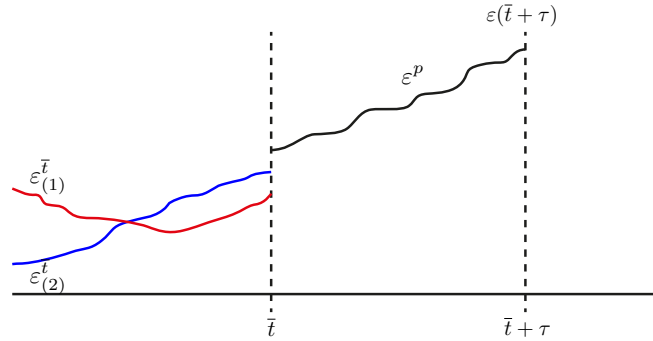
Figure 6.2: Past histories $\varepsilon_{(1)}^{\bar{t}}$, $\varepsilon_{(2)}^{\bar{t}}$ and deformation process ε^p. Courtesy of [54].

$$\dot{\varepsilon}_{(i)}^*(r) := \begin{cases} \dot{\varepsilon}_{(i)}^{\bar{t}}(\tau) & r \in (-\infty, \bar{t}) \\ 0 & r \in [\bar{t}, \bar{t}+\tau) \end{cases} \quad i = 1, 2$$
(6.29)

represents the null extension of $\dot{\varepsilon}_{(i)}^{\bar{t}}(\circ)$ and where

$$\dot{\varepsilon}_{(i)}^{\bar{t}}(r) := \dot{\varepsilon}_{(i)}(\bar{t} - r) \quad i = 1, 2.$$
(6.30)

The latter represent two past straining histories with respect to the initial observa-

tion time (conventionally labeled with $\bar{t}$), namely the instant in which the common straining continuation $\dot{\varepsilon}^p$ is applied. In the sequel we shall refer to $\varepsilon^*_{(i)}$, $i = 1, 2$, as *extended histories*, namely the null extensions of finite duration, τ, of the given histories $\varepsilon^{\bar{t}}_{(i)}$. Henceforth, by substituting (6.30) in (6.29) and the result in (6.28) and, finally, by evaluating the stress response through (6.27a) of both $\dot{\varepsilon}_{(i)}$ $i = 1, 2$ we have:

$$
\begin{aligned}
\sigma_{(i)}(\bar{t} + \tau) &:= \int_{-\infty}^{\bar{t}} G(\tau + \bar{t} - r)\dot{\varepsilon}^{\bar{t}}_{(i)}(r)dr + \int_0^{\tau} G(t - r')\dot{\varepsilon}^p(r')dr' \\
&= \int_{-\infty}^{\bar{t}+\tau} G(\tau + \bar{t} - r)\dot{\varepsilon}^*_{(i)}(r)dr + C_\beta\left({}_C D_{0+}^\beta \varepsilon^p\right)(\tau) \\
&= C_\beta\left(\left({}_C D_+^\beta \varepsilon^*_{(i)}\right)(\bar{t} + \tau) + \left({}_C D_{0+}^\beta \varepsilon^p\right)(\tau)\right) \quad i = 1, 2
\end{aligned}
\tag{6.31}
$$

where ε^p represents the prescribed strain during the interval $[0, \tau]$. Following the definition of state given above, we say that $\dot{\varepsilon}^*_{(1)}$ and $\dot{\varepsilon}^*_{(2)}$ are equivalent if

$$
\sigma_{(1)}(\bar{t} + \tau) = \sigma_{(2)}(\bar{t} + \tau) \quad \forall \tau \geq 0
\tag{6.32}
$$

on any process ε^p. In other words, this condition implies that

$$
\int_{-\infty}^{\bar{t}+\tau} G(\bar{t} + \tau - r)\dot{\varepsilon}^*(r)dr \equiv C_\beta\left({}_C D_+^\beta \varepsilon^*\right)(\bar{t} + \tau) = 0 \quad \forall \tau \geq 0
\tag{6.33}
$$

where $\varepsilon^* := \varepsilon^*_{(2)} - \varepsilon^*_{(1)}$. Henceforth, an equivalence class on the set of extended histories may be considered. The state of the material at the time $\bar{t} + \tau$ may be determined by any of such extended histories, say e.g. ε^*, in the equivalence class characterized by (6.33) together with the current value of the strain $\varepsilon(\bar{t} + \tau)$.

It is worth noting that a more realistic condition for (6.33) is when we impose that such a relationship holds for all $\tau > 0$ which, in practice, would imply that there is always a nonzero unloading time. In order to show that the equivalence class of extended histories does not contain the zero strain only we need to study the solutions of (6.33). This may not be done directly, but rather by constructing a one parameter family of strains approximating such a solutions. For this purpose, it may also be considered the function ${}_a\varepsilon^*(\circ)$ as the restriction of $\varepsilon^*(\circ)$ to the domain $[a, \bar{t} + \tau)$ namely (see Figure 6.2):

$$
{}_a\varepsilon^*(r) := \begin{cases} 0 & r < a \\ \varepsilon(r) & a \leq r < \bar{t} \\ 0 & \bar{t} \leq r < \bar{t} + \tau . \end{cases}
\tag{6.34}
$$

203

where a is finite time. In this case relation (6.33) yields:

$$\left({}_C\mathrm{D}_{a^+}^{\beta}\varepsilon^*\right)(\bar{t}+\tau) = 0 \quad \forall \tau > 0, \tag{6.35}$$

where

$$\left({}_C\mathrm{D}_{a^+}^{\beta}\varepsilon^*\right)(\bar{t}+\tau) = \frac{1}{\Gamma(1+\beta)}\int_a^{\bar{t}+\tau}\frac{\dot{\varepsilon}(r)}{(\bar{t}+\tau-r)^{\beta}}\,\mathrm{d}r. \tag{6.36}$$

The result 2.27 in [183] (p.36) may be useful; its translation to the current notation allows for stating that solution of (6.35) are such that

$$\varepsilon_{(2)}^*(\bar{t}+\tau) - \varepsilon_{(1)}^*(\bar{t}+\tau) = \frac{\varepsilon_0}{(\bar{t}+\tau-a)^{1-\beta}}. \tag{6.37}$$

It is worth noting that whenever (A.3b) (see Appendix A) is considered, the
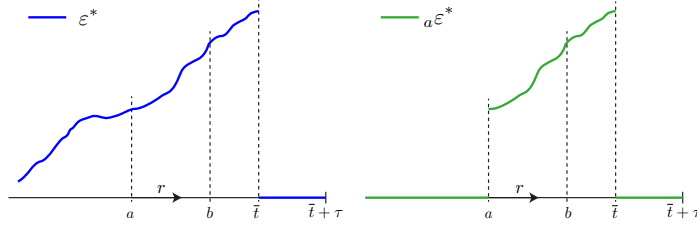
Figure 6.3: Restriction ${}_a\varepsilon^*$ to a prescribed domain of the strain ε^*. Courtesy of [54].

relationship (6.36) may be rewritten in the form

$$\left({}_C\mathrm{D}_{a^+}^{\beta}\varepsilon^*\right)(\bar{t}+\tau) = \left(\mathrm{D}_{a^+}^{\beta}\varepsilon^*\right)(\bar{t}+\tau) - \frac{\varepsilon^*(a)}{\Gamma(1-\beta)(\bar{t}+\tau-a)^{\beta}} \tag{6.38}$$

where $\left(\mathrm{D}_{a^+}^{\beta}\varepsilon^*\right)(\bar{t}+\tau)$ is the Riemann-Lioville fractional integral defined in (A.2b) (Appendix A).

In order to show that the left-hand side of (6.35) approximates (6.33) we first show that the stress response associated with ${}_a\varepsilon^*$ approximates the stress caused by ε^*. To this end we consider relations (6.27a) and (6.29) yielding the following

expression for the stress at $\bar{t} + \tau$:

$$\sigma(\bar{t} + \tau) = -G(t)\varepsilon(\bar{t}) + \int_b^{\bar{t}} G(\tau + \bar{t} - r)\dot{\varepsilon}(r)\,\mathrm{d}r + \int_a^b G(\tau + \bar{t} - r)\dot{\varepsilon}(r)\,\mathrm{d}r +$$
$$+ \int_{-\infty}^a G(\tau + \bar{t} - r)\dot{\varepsilon}(r)\,\mathrm{d}r,$$

(6.39)

where b is such that $a < b < \bar{t}$ is a fixed arbitrary time. The stress ${}_a\sigma(\bar{t} + \tau)$ corresponding to ${}_a\varepsilon^*$ defined by (6.34) is obtained from (6.39) by neglecting the last integral, i.e.

$${}_a\sigma(\bar{t} + \tau) = G(\tau + \bar{t} - a)\varepsilon(a) - G(\tau)\varepsilon(\bar{t}) + \int_b^{\bar{t}} G(\tau + \bar{t} - r)\,\mathrm{d}\varepsilon(r) +$$
$$+ \int_a^b G(\tau + \bar{t} - r)\,\mathrm{d}\varepsilon(r).$$

(6.40)

By computing the difference between (6.39) and (6.40) we obtain:

$$\sigma(\bar{t} + r) - {}_a\sigma(\bar{t} + r) = \int_{-\infty}^a G(\tau + \bar{t} - r)\,\mathrm{d}\varepsilon(r) - G(\tau + \bar{t} - a)\varepsilon(a),$$

(6.41)

whose magnitude may be estimated as follows

$$\left|\sigma(\bar{t} + r) - {}_a\sigma(\bar{t} + r)\right| \le \left|G(\tau + \bar{t} - a)\right||\varepsilon(a)| + \sup_{r \in (-\infty, a]} |G(\tau + \bar{t} - r)|\mathrm{Var}_{r \in (-\infty, a)}(\varepsilon(r)).$$

(6.42)

The following extension of (6.14)

$$\left|\int_{-\infty}^a G(\tau + \bar{t} - r)\,\mathrm{d}\varepsilon(r)\right| \le \sup_{r \in (-\infty, a)}|G(\tau + \bar{t} - r)| \quad \mathrm{Var}_{r \in (-\infty, a)}(\varepsilon(r))$$

(6.43)

holds true since, by inspection of (6.4), it can be shown that $G(\tau + \bar{t} - \circ)$ is absolutely continuous and, hence, bounded in $(-\infty, a)$. Indeed, because of relation (6.4), if we let $\delta > 0$ there exists at least an a_δ for which if we chose an $a < a_\delta$ we have that $G(\tau + \bar{t} - a)C_\beta^{-1} = \Gamma(1 - \beta)^{-1}(\tau + \bar{t} - a)^{-\beta} < \delta$. Finally, by extending $\varepsilon \in SBV_{(-\infty, a)}$ we can find an $M > 0$ such that $\mathrm{Var}_{r \in (-\infty, a)}(\varepsilon(r)) < M$, so that $\left|\sigma(\bar{t} + r) - {}_a\sigma(\bar{t} + r)\right| < M\delta$. Hence

$$\lim_{a \to \infty} {}_a\sigma(\bar{t} + \tau) = \sigma(\bar{t} + \tau),$$

(6.44)

205

in other words the stress $_a\sigma$ converges to σ in L^∞. Obviously the same conclusions could have been drawn starting from (6.31) written for ε^* and for its restriction $_a\varepsilon^*$ instead of $\varepsilon^*_{(i)}$ and by setting $\varepsilon^p = 0$.

It is worth noting that the integral appearing in (6.41) represents the residual stress at time $\bar{t} + \tau$ caused by past strain histories truncated at the time a

$$\mathcal{I}^a(\tau + \bar{t}) := \int_{-\infty}^{a} G(\tau + \bar{t} - r) d\varepsilon(r). \tag{6.45}$$

If one considers the difference

$$\varepsilon^*_a := \varepsilon^* - {}_a\varepsilon^* \tag{6.46}$$

then (6.45) can be expressed as follows:

$$\mathcal{I}^a(\tau + \bar{t}) = C_\beta \left({}_C\mathrm{D}^\beta_+ \varepsilon^*_a\right)(\tau + \bar{t}). \tag{6.47}$$

Upon considering the intermediate arbitrary time $b \in (a, \bar{t})$ introduced in (6.39) and the equality:

$$_a\mathcal{I}^b(\tau + \bar{t}) := \int_{a}^{b} G(\tau + \bar{t} - r)\,\mathrm{d}\varepsilon(r) - G(\tau + \bar{t} - b)\varepsilon(b) + G(\tau + \bar{t} - a)\varepsilon(a), \tag{6.48}$$

the reasoning leading to (6.44) allows for proving that (6.48) approximates the state variable (6.45), i.e.

$$\lim_{a \to -\infty} {}_a\mathcal{I}^b(\tau + \bar{t}) = \mathcal{I}^b(\tau + \bar{t}). \tag{6.49}$$

As a first step, we may consider the stresses $_b\sigma(\bar{t} + \tau)$ and $_a\sigma(\bar{t} + \tau)$ whenever $_b\varepsilon$ and $_a\varepsilon$ defined by (6.34) are assumed to be experienced at the material point; the difference between such stresses reads as follows:

$$_b\sigma(\bar{t}+\tau) - {}_a\sigma(\bar{t}+\tau) = G(\tau+\bar{t}-b)\varepsilon(b) - G(\tau+\bar{t}-a)\varepsilon(a) - \int_{a}^{b} G(\tau+\bar{t}-r)\,\mathrm{d}\varepsilon(r). \tag{6.50}$$

An estimate of the magnitude of such a difference may be delivered by noting that:

$$\left|{}_b\sigma(\bar{t}+\tau) - {}_a\sigma(\bar{t}+\tau)\right| \le \left|G(\tau+\bar{t}-b)\varepsilon(b) - G(\tau+\bar{t}-a)\varepsilon(a)\right| +$$
$$+ \left|\int_{a}^{b} G(\tau+\bar{t}-r)\,\mathrm{d}\varepsilon(r)\right|. \tag{6.51}$$

Henceforth, we also note that whenever $\delta > 0$ is given such that there exists at least a $\Delta_\delta > 0$ for which if $|b - a| < \Delta_\delta$ we have $\left| G(\tau + \bar{t} - b) - G(\tau + \bar{t} - a) \right| < \omega \frac{C_\beta}{\Gamma(1-\beta)} \Delta_\delta$, with $\omega > 0$ and $\underset{r \in (a,b)}{\mathrm{Var}}(\varepsilon(r)) < \delta$, hence we obtain

$$\left| G(\tau + \bar{t} - b)\varepsilon(b) - G(\tau + \bar{t} - a)\varepsilon(a) \right| < \frac{C_\beta}{\Gamma(1-\beta)} \left((\tau + \bar{t})^{-\beta}\delta + \omega \left| \varepsilon(a) \right| \Delta_\delta \right)$$

(6.52)

and

$$\left| \int_a^b G(\tau + \bar{t} - r)\, \mathrm{d}\varepsilon(r) \right| \leq \left| G(\tau + \bar{t} - a) \right| \delta < \frac{C_\beta}{\Gamma(1-\beta)(\tau + \bar{t})^\beta}\, \delta.$$

(6.53)

Therefore it turns out that the following result holds

$$\lim_{b \to a} \, {}_b\sigma(\bar{t} + \tau) = \, {}_a\sigma(\bar{t} + \tau).$$

(6.54)

Of course the stress ${}_a\sigma(\bar{t} + \tau)$ may be expressed in terms of a fractional derivative, simply by recalling relation (6.34) for ${}_a\varepsilon^*$, which allows for writing

$$_a\sigma(\bar{t} + \tau) = \frac{C_\beta}{\Gamma(1-\beta)} \left(\frac{\varepsilon(a)}{(\bar{t} + \tau - a)^\beta} - \frac{\varepsilon(\bar{t})}{\tau^\beta} + \left({}_C\mathrm{D}^\beta_{a+} \, {}_a\varepsilon^* \right)(\bar{t} + \tau) \right).$$

(6.55)

On the other hand the stress response evaluated for ε^* (see (6.31) with $\varepsilon^*_{(i)}$ replaced by ε^* and $\varepsilon = 0$) reads as follows

$$\sigma(\bar{t} + \tau) = C_\beta \left({}_C\mathrm{D}^\beta_+ \varepsilon^* \right)(\bar{t} + \tau) - \frac{C_\beta \varepsilon(\bar{t})}{\Gamma(1-\beta)\tau^\beta}.$$

(6.56)

By comparing the procedures used for showing that (6.44) and (6.54) hold, it is not difficult to show that the approximation formula (6.49) for the state variable holds. Hence (6.37) allows for providing an approximation to equivalent histories for FHMs. Physically, if a in (6.37) is interpreted as the instant in which the virgin material can bear loading, then (6.37) gives the exact characterization of the state of the material, in terms of histories that can equivalently bring the material to the same stress.

6.3 Rheological models for fractional hereditariness

The design of novel materials is strictly related to the capability to obtain the desired behavior at the macroscale starting from both the knowledge of mechanical properties of basic constituents and their proper arrangement at the nano-to-microscale. Often times real materials have intermediate behavior between elastic materials and viscous fluids, showing hereditary features. Micromechanics provides a way, to deliver macroscopic properties starting from basic elements at the submacroscopic level. For this reason, a rheological model explaining fractional hereditariness is required.

In this regard, the exact mechanical model of fractional hereditary materials was recently proposed in [62]. The authors separated the behavior of elasto-viscous material from visco-elastic one: both are ruled by β-order differential equation, but in the former case $0 < \beta < 1/2$ while in the latter $1/2 \leq \beta < 1$. The different range of fractional-order involved in constitutive equations is linked to a different mechanical model. In this section we show two different mechanical arrangements to describe the material behavior.
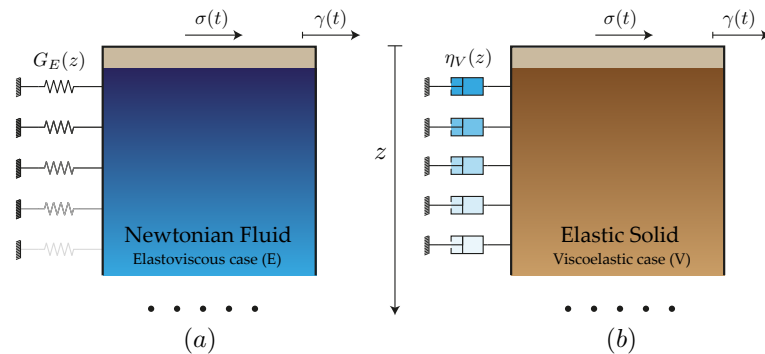
Figure 6.4: Rheological continuum models: (a) elastoviscous (E) and (b) viscoelastic (V). Courtesy of [54].

The rheological scheme of *Elasto-Viscous* material (E) is represented by an indefinite massless plate resting on a column of Newtonian fluid supported on a side by a "bed" by way of independent elastic springs, whereas the model of *Visco-Elastic* material (V) is represented by an indefinite massless plate resting on a column of elastic solid linked to a rigid support through independent viscous dashpots, as depicted in Figure 6.4. In both cases, we consider a cross-section with area A; moreover, we assume that the material elastic modulus $k(z)$ and viscous

coefficient $c(z)$ spatially decay with a power-law, resembling a functionally graded microstructure. Thus, in the case of elastoviscous material, they read as follows:

$$k_E(z) = AG_E(z) = A\frac{G_0}{\Gamma(1+\alpha)}z^{-\alpha} \tag{6.57a}$$

$$c_E(z) = A\eta_E(z) = A\frac{\eta_0}{\Gamma(1-\alpha)}z^{-\alpha} \quad , \tag{6.57b}$$

whereas in the case of viscoelastic material they become:

$$k_V(z) = AG_V(z) = A\frac{G_0}{\Gamma(1-\alpha)}z^{-\alpha} \tag{6.58a}$$

$$c_V(z) = A\eta_V(z) = A\frac{\eta_0}{\Gamma(1+\alpha)}z^{-\alpha}. \tag{6.58b}$$

In equations (6.57), (6.58) the subscripts E and V indicate Elastoviscous and Viscoelastic case, respectively, and $0 \leq \alpha \leq 1$ is the decay parameter. In these models the equilibrium is governed by a differential equation in the following form:

$$(EV): \quad \frac{\partial}{\partial z}\left[c_E(z)\frac{\partial \dot{\gamma}}{\partial z}\right] = k_E(z)\gamma(z,t) \tag{6.59a}$$

$$(VE): \quad \frac{\partial}{\partial z}\left[k_V(z)\frac{\partial \gamma}{\partial z}\right] = c_V(z)\dot{\gamma}(z,t), \tag{6.59b}$$

where $\gamma(z,t)$ represent the transverse displacement imposed to the shear layer at depth z and $\dot{\gamma}(z,t) := \frac{\partial}{\partial t}\gamma(z,t)$ is its time rate of change. In order to solve the problems above, we make use of the boundary conditions related to mechanical schemes in Figure 6.4, expressed in the form of limits as follows:

$$\begin{cases} \lim_{z\to 0} \gamma(z,t) = \gamma(t) \\ \lim_{z\to\infty} \gamma(z,t) = 0. \end{cases} \tag{6.60}$$

By using such boundary conditions in [62] it is shown that (6.59a) (or (6.59b)) delivers a relationship between the force σ arising in the top layer in both models and the Caputo fractional derivative of displacement γ, i.e.

$$\sigma(t) = C_\beta \left({}_C\mathrm{D}_{0^+}^\beta \gamma\right)(t) \tag{6.61}$$

209

where we assumed the parameters as:

$$C_\beta := C_\beta^E = \frac{G_0 \Gamma(\beta)}{\Gamma(2 - 2\beta)\Gamma(1 - \beta)2^{1-2\beta}} \left(\tau_\alpha^{(E)}\right)^\beta \tag{6.62a}$$

$$\tau_\alpha^{(E)} = \frac{\eta_0}{G_0} \frac{\Gamma(1 + \alpha)}{\Gamma(1 - \alpha)} \tag{6.62b}$$

and $\alpha = 1 - 2\beta$ for the EV material, whereas:

$$C_\beta := C_\beta^V = \frac{G_0 \Gamma(1 - \beta)}{\Gamma(2 - 2\beta)\Gamma(\beta)2^{2\beta-1}} \left(\tau_\alpha^{(V)}\right)^\beta \tag{6.63a}$$

$$\tau_\alpha^{(V)} = \frac{\eta_0}{G_0} \frac{\Gamma(1 - \alpha)}{\Gamma(1 + \alpha)} \tag{6.63b}$$

and $\alpha = 2\beta - 1$ for the VE material. The terms $\tau_E(\alpha)$, $\tau_V(\alpha)$ are relaxation times. The result expressed by (6.61) highlights that these rheological models are capable to yield a force on the top layer relaxing with a power-law, ultimately resembling the macroscopic material behavior. In this respect, the boundary of such rheological models reproduces the material response.

6.4 Overall response from the rheological model: *micro* and *macro* state

The forces $\sigma_m^{(E)}(z, t)$ exerted either on the springs (E model) or $\sigma_m^{(V)}(z, t)$ on the dashpots (V model) at z may be computed as follows:

$$\sigma_m^{(E)}(z, t) = k(z)\, \gamma^{(E)}(z, t), \tag{6.64a}$$

$$\sigma_m^{(V)}(z, t) = c(z)\, \dot{\gamma}^{(V)}(z, t). \tag{6.64b}$$

By denoting by $\gamma^{(E)}$ and $\gamma^{(V)}$ the solution of the field equations (6.59a) and (6.59b), the knowledge of transfer functions $H^{(E)}(z, \circ)$ and $H^{(V)}(z, \circ)$, relative to (6.59a) and (6.59b) yield the following representation formulas:

$$\gamma^{(E)}(z, t) = \int_{-\infty}^{t} H^{(E)}(z, t - r)\gamma(r)\, \mathrm{d}r, \tag{6.65a}$$

$$\gamma^{(V)}(z, t) = \int_{-\infty}^{t} H^{(V)}(z, t - r)\gamma(r)\, \mathrm{d}r, \tag{6.65b}$$

where

$$H^{(E)}(z,t) = \mathcal{F}_+^{-1}\left[\hat{H}^{(E)}(z,\circ)\right](t) \tag{6.66a}$$

$$H^{(V)}(z,t) = \mathcal{F}_+^{-1}\left[\hat{H}^{(E)}(z,\circ)\right](t) \tag{6.66b}$$

and

$$\hat{H}^{(E)}(z,\omega) = \frac{G_0}{\Gamma(1-\beta)\Gamma(2-2\beta)2^{-\beta}}\left(\tau_\alpha^E i\omega\right)^{\frac{\beta}{2}} z^\beta \, \mathrm{K}_\beta\left(\frac{z}{\sqrt{\tau_\alpha^E i\omega}}\right) \tag{6.67a}$$

$$\hat{H}^{(V)}(z,\omega) = \frac{G_0}{\Gamma(\beta)\Gamma(2-2\beta)2^{\beta-1}}\left(\tau_\alpha^V i\omega\right)^{\frac{1+\beta}{2}} z^{1-\beta} \, \mathrm{K}_{1-\beta}\left(z\sqrt{\tau_\alpha^V i\omega}\right). \tag{6.67b}$$

Let us assume that the displacement of the rigid top plate of both models (E) and
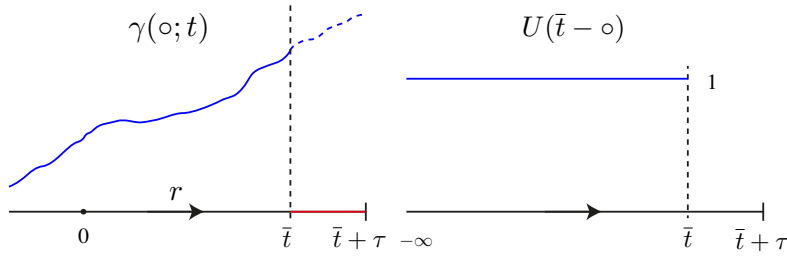
Figure 6.5: Displacement at the rigid top plate. Courtesy of [54].

(V) is prescribed up to the time $\bar{t}$ and it is held constant to zero (Figure 6.5), i.e.

$$\gamma(r;\bar{t}) := \gamma(r)U(\bar{t}-r). \tag{6.68}$$

In other words, the prescribed displacement history for the top plate is continued by the null process (see Figure 6.5). The displacement recorded at z in the rheological model at time $\tau+\bar{t}$ ($\tau>0$) is simply calculated through (6.65a) and (6.65b) respectively by setting $t = \tau+\bar{t}$:

By substituting the resulting expressions in (6.64a) and (6.64b) respectively, the "micro" stresses $\sigma_m^{(E)}$, $\sigma_m^{(V)}$ are recovered. In both cases the resultants of those forces can be evaluated by integrating the equation across the semi-infinite sequence

of springs and dashpots respectively. Such resultants read as follows:

$$\int_0^\infty \sigma_m^{(E)}(z, \tau + \bar{t})dz = \int_{-\infty}^{\tau + \bar{t}} \int_0^\infty k(z)H^{(E)}(z, \tau + \bar{t} - r)\,\gamma(r)\;\mathrm{d}z\;\mathrm{d}r \qquad (6.69a)$$

$$\int_0^\infty \sigma_m^{(V)}(z, \tau + \bar{t})dz = \int_{-\infty}^{\tau + \bar{t}} \int_0^\infty c(z)H^{(V)}(z, \tau + \bar{t} - r)\,\dot{\gamma}(r)\,\mathrm{d}z\;\mathrm{d}r, \qquad (6.69b)$$

where the order of integration has been interchanged thanks to Fubini's Theorem. The upper limit on the integrals in r can be truncated at $\bar{t}$ because of (6.68), although it is kept as it is for the sake of convenience. For the purpose of obtaining the overall response of the two rheological models there is no need to produce (6.66a) and (6.66b). We may indeed evaluate the right Fourier transforms of (6.69a) and (6.69b), and make use of (6.67a) and (6.67b) respectively in order to perform the explicit calculations. Upon introducing

$$\hat{\sigma}_m^{(E)}(z, \omega) := \mathcal{F}_+ \left\{ \sigma_m^{(E)}(z, \circ) \right\}(\omega) \qquad (6.70a)$$

$$\hat{\sigma}_m^{(V)}(z, \omega) := \mathcal{F}_+ \left\{ \sigma_m^{(V)}(z, \circ) \right\}(\omega), \qquad (6.70b)$$

and

$$\hat{\gamma}^{(E)}(z, \omega) := \mathcal{F}_+ \left\{ \gamma^{(E)}(z, \circ) \right\}(\omega) \qquad (6.71a)$$

$$\hat{\gamma}^{(V)}(z, \omega) := \mathcal{F}_+ \left\{ \gamma^{(V)}(z, \circ) \right\}(\omega), \qquad (6.71b)$$

(6.69a) and (6.69b) yield

$$\int_0^{+\infty} \hat{\sigma}_m^{(E)}(z, \omega)dz = \int_0^{+\infty} k_E(z)\hat{\gamma}^{(E)}(z, \omega)\,\mathrm{d}z$$
$$= \frac{k_0 \left(\tau_\alpha^{(E)}\,i\omega\right)^{\frac{\beta-1}{2}}}{\Gamma(2-2\beta)\Gamma(1-\beta)2^{-\beta}} \int_0^{+\infty} z^\beta \mathrm{K}_{1-\beta}\left(\frac{z}{\sqrt{\tau_\alpha^{(E)}i\omega}}\right)\,\mathrm{d}z\;\hat{\gamma}(\omega) \qquad (6.72a)$$

$$\int_0^{+\infty} \hat{\sigma}_m^{(V)}(z, \omega)dz = i\omega \int_0^{+\infty} c_V(z)\hat{\gamma}^{(V)}(z, \omega)\,\mathrm{d}z$$
$$= \frac{k_0 \left(\tau_\alpha^{(V)}\,i\omega\right)^{\frac{\beta+2}{2}}}{\Gamma(2-2\beta)\Gamma(\beta)2^{\beta-1}} \int_0^{+\infty} z^{1-\beta} \mathrm{K}_\beta\left(z\sqrt{\tau_\alpha^{(V)}i\omega}\right)\,\mathrm{d}z\;\hat{\gamma}(\omega). \qquad (6.72b)$$

6.4.1 Direct evaluation of the microstresses

The displacement functions along the depth of the continuum column of the mechanical models displayed in Figure 6.4 (see [62] for more details) analyzed in

the right Fourier domain assume the following forms

$$\hat{\gamma}^{(E)}(z,\omega) = \hat{\gamma}(\omega)\frac{(\tau_\alpha^{(E)}i\omega)^{-\frac{\overline{\beta}}{2}}}{\Gamma(\overline{\beta})2^{\overline{\beta}-1}}z^{\overline{\beta}}\mathrm{K}_{\overline{\beta}}\left(\frac{z}{\sqrt{\tau_\alpha^{(E)}i\omega}}\right) \tag{6.73a}$$

$$\hat{\gamma}^{(V)}(z,\omega) = \hat{\gamma}(\omega)\frac{(\tau_\alpha^{(V)}i\omega)^{\frac{\beta}{2}}}{\Gamma(\beta)2^{\beta-1}}z^{\beta}\mathrm{K}_{\beta}\left(z\sqrt{\tau_\alpha^{(V)}i\omega}\right), \tag{6.73b}$$

for the (E) and (V) case respectively, where $\hat{\gamma}(\omega)$ is the right Fourier transform of the imposed displacement at the top plate, $\mathrm{K}_\nu(\circ)$ is the modified Bessel function of the second kind of order ν, $\tau_\alpha^{(E)}$ and $\tau_\alpha^{(V)}$ have been defined in (6.62b) and (6.63b) respectively and $\overline{\beta} = 1 - \beta$. The relationships above are preparatory to enable us evaluating $\hat{\sigma}_m^{(E)}$ and $\hat{\sigma}_m^{(V)}$, namely the time-(right)-Fourier transforms of the microstress, arising in the external devices for both models.

Bearing in mind that $\overline{\alpha} = 2\overline{\beta} - 1$, the right-Fourier Transform of the microstress related to the external springs for the (E) case may be written as follows:

$$\begin{aligned}
\hat{\sigma}_m^{(E)}(z,\omega) &= \frac{1}{A}k_E(z)\hat{\gamma}^{(E)}(z,\omega) \\
&= \frac{G_0}{\Gamma(1+\overline{\alpha})}z^{-\overline{\alpha}}\ \hat{\gamma}(\omega)\frac{(\tau_\alpha^{(E)}i\omega)^{-\frac{\overline{\beta}}{2}}}{\Gamma(\overline{\beta})2^{\overline{\beta}-1}}z^{\overline{\beta}}\mathrm{K}_{\overline{\beta}}\left(\frac{z}{\sqrt{\tau_\alpha^{(E)}i\omega}}\right) \\
&= \hat{\gamma}(\omega)\frac{G_0(\tau_\alpha^{(E)}i\omega)^{\frac{\beta-1}{2}}}{\Gamma(2-2\beta)\Gamma(1-\beta)2^{-\beta}}z^{\beta}\mathrm{K}_{1-\beta}\left(\frac{z}{\sqrt{\tau_\alpha^{(E)}i\omega}}\right).
\end{aligned} \tag{6.74}$$

The resultant of such quantities can be computed as the integral across the external devices (the springs for the (E) case). In order to evaluate this quantity, we recall that following result holds for a modified Bessel function of second kind integral:

$$\int_0^\infty z^{\mu-1}\mathrm{K}_\nu(Az)\,dz = 2^{\mu-2}A^{-\mu}\Gamma\left(\frac{\mu-\nu}{2}\right)\Gamma\left(\frac{\mu+\nu}{2}\right). \tag{6.75}$$

By assuming $\mu - 1 = \beta$ and $\nu = 1 - \beta$ in (6.75) and with the aid of (6.74), the resultant of the right-Fourier Transform of the microstress for the (E) case arises

213

in the following form:

$$
\begin{aligned}
\int_0^\infty \hat{\sigma}_m^{(E)}(z,\omega)dz &= \hat{\gamma}(\omega)\frac{G_0\left(\tau_\alpha^{(E)}i\omega\right)^{\frac{\beta-1}{2}}}{\Gamma(2-2\beta)\Gamma(1-\beta)2^{-\beta}}\int_0^\infty z^\beta \mathrm{K}_{1-\beta}\left(\frac{z}{\sqrt{\tau_\alpha^{(E)}i\omega}}\right)dz \\
&= \hat{\gamma}(\omega)\frac{G_0\left(\tau_\alpha^{(E)}i\omega\right)^{\frac{\beta-1}{2}}}{\Gamma(2-2\beta)\Gamma(1-\beta)2^{-\beta}}\,2^{\beta-1}\left(\frac{1}{\tau_\alpha^{(E)}i\omega}\right)^{-\frac{(\beta+1)}{2}}\Gamma(\beta) \\
&= \hat{\gamma}(\omega)\underbrace{\frac{G_0\left(\tau_\alpha^{(E)}\right)^\beta\Gamma(\beta)}{\Gamma(2-2\beta)\Gamma(1-\beta)2^{1-2\beta}}}_{C_\beta^E}(i\omega)^\beta\left(\frac{i\omega}{i\omega}\right) \\
&= (i\omega)\hat{\gamma}(\omega)\,C_\beta^E(i\omega)^{\beta-1}.
\end{aligned}
$$
(6.76)

Hence, by taking the inverse right-Fourier transform of both sides and by using Fubini's Theorem on the left-hand side, we have:

$$
\int_0^\infty \sigma_m^{(E)}(z,t)dz = \int_{-\infty}^t G(t-\tau)\dot{\gamma}(\tau)d\tau,
$$
(6.77)

since the right Fourier transform of the assumed relaxation function in (6.4) takes the form:

$$
\mathcal{F}_+\left\{\frac{C_\beta}{\Gamma(1-\beta)}t^{-\beta}\right\}(\omega) = C_\beta(i\omega)^{\beta-1}.
$$
(6.78)

Similarly, whenever it is assumed that $\alpha = 2\beta - 1$ the microstress for the external dashpots for the (V) case can be evaluated as follows:

$$
\begin{aligned}
\hat{\sigma}_m^{(V)}(z,\omega) &= \frac{1}{A}c_V(z)(i\omega)\hat{\gamma}^{(V)}(z,\omega) \\
&= \frac{\eta_0}{\Gamma(1+\alpha)}z^{-\alpha}\,(i\omega)\hat{\gamma}(\omega)\frac{\left(\tau_\alpha^{(V)}i\omega\right)^{\frac{\beta}{2}}}{\Gamma(\beta)2^{\beta-1}}z^\beta \mathrm{K}_\beta\left(z\sqrt{\tau_\alpha^{(V)}i\omega}\right) \\
&= \frac{G_0\tau_\alpha^{(V)}}{\Gamma(1+\alpha)}\frac{\Gamma(1+\alpha)}{\Gamma(2-2\beta)}\,(i\omega)\hat{\gamma}(\omega)\frac{\left(\tau_\alpha^{(V)}i\omega\right)^{\frac{\beta}{2}}}{\Gamma(\beta)2^{\beta-1}}z^{1-\beta}\mathrm{K}_\beta\left(z\sqrt{\tau_\alpha^{(V)}i\omega}\right) \\
&= \hat{\gamma}(\omega)\frac{G_0\left(\tau_\alpha^{(V)}i\omega\right)^{\frac{\beta+2}{2}}}{\Gamma(\beta)\Gamma(2-2\beta)2^{\beta-1}}z^{1-\beta}\mathrm{K}_\beta\left(z\sqrt{\tau_\alpha^{(V)}i\omega}\right)
\end{aligned}
$$
(6.79)

where equation (6.63b) has been used in the following form:

$$\tau_\alpha^{(V)} = \frac{\eta_0}{G_0} \frac{\Gamma(1-\alpha)}{\Gamma(1+\alpha)} \quad \Longrightarrow \quad \eta_0 = \tau_\alpha^{(V)} G_0 \frac{\Gamma(1+\alpha)}{\Gamma(2-2\beta)}. \tag{6.80}$$

The use of (6.79) and the assumptions $\mu - 1 = 1 - \beta$ and $\nu = \beta$ in (6.75) allow for writing the overall microstress for the (V) case in the following form:

$$
\begin{aligned}
\int_0^\infty \hat{\sigma}_m^{(V)}(z,\omega)dz &= \hat{\gamma}(\omega) \frac{G_0 \left(\tau_\alpha^{(V)} i\omega\right)^{\frac{\beta+2}{2}}}{\Gamma(\beta)\Gamma(2-2\beta)2^{\beta-1}} \int_0^\infty z^{1-\beta} \mathrm{K}_\beta \left(z\sqrt{\tau_\alpha^{(E)} i\omega}\right) dz \\
&= \hat{\gamma}(\omega) \frac{G_0 \left(\tau_\alpha^{(V)} i\omega\right)^{\frac{\beta+2}{2}}}{\Gamma(\beta)\Gamma(2-2\beta)2^{\beta-1}} \, 2^{-\beta} \left(\tau_\alpha^{(V)}\right)^{\frac{\beta-2}{2}} \Gamma(1-\beta) \\
&= \hat{\gamma}(\omega) \underbrace{\frac{G_0 \left(\tau_\alpha^{(V)}\right)^\beta \Gamma(1-\beta)}{\Gamma(\beta)\Gamma(2-2\beta)2^{2\beta-1}}}_{C_\beta^V} (i\omega)^\beta \left(\frac{i\omega}{i\omega}\right) \\
&= (i\omega)\hat{\gamma}(\omega) \, C_\beta^V \, (i\omega)^{\beta-1}.
\end{aligned}
\tag{6.81}
$$

Now, proceeding like in (6.77) we get:

$$\int_0^\infty \sigma_m^{(V)}(z,t)dz = \int_{-\infty}^t G(t-\tau)\dot{\gamma}(\tau)d\tau \tag{6.82}$$

The results addressed by (6.76)-(6.77) and (6.81)-(6.82) show that it is possible to compute the resultant of the microstresses in both models without knowing explicitly the transfer function $H(z,t)$ in the time domain.

6.4.2 *Micro* and *macro* state

It is not difficult to show that, thanks to the results addressed in Secion 6.4.1, the integrals in (6.72a) and (6.72b)) can take the form:

$$\int_0^{+\infty} \hat{\sigma}_m^{(E)}(z,\omega)dz = \frac{k_0 \left(\tau_\alpha^{(E)}\right)^\beta}{2^{1-2\beta}} \frac{\Gamma(\beta)}{\Gamma(2-2\beta)\Gamma(1-\beta)} (i\omega)^{\beta-1} i\omega\hat{\gamma}(\omega)$$
$$= \int_0^{+\infty} e^{-i\omega(\bar{t}+\tau)} \int_{-\infty}^{\bar{t}+\tau} G^{(E)}(\bar{t}+\tau-r)\dot{\gamma}(r)\,dr\,\,d\tau \tag{6.83a}$$

$$\int_0^{+\infty} \hat{\sigma}_m^{(V)}(z,\omega)dz = \frac{k_0 \left(\tau_\alpha^{(V)}\right)^\beta}{2^{2\beta-1}} \frac{\Gamma(1-\beta)}{\Gamma(\beta)\Gamma(2-2\beta)} (i\omega)^{\beta-1} i\omega\hat{\gamma}(\omega)$$
$$= \int_0^{+\infty} e^{-i\omega(\bar{t}+\tau)} \int_{-\infty}^{\bar{t}+\tau} G^{(V)}(\bar{t}+\tau-r)\dot{\gamma}(r)\,dr\,\,d\tau. \tag{6.83b}$$

Henceforth, the inverse right Fourier transform of the relations above yield that (6.69a) and (6.69b) read as follows:

$$\int_0^{+\infty} \sigma_m^{(E)}(z,\bar{t}+\tau)dz = \int_{-\infty}^{\bar{t}+\tau} G^{(E)}(\bar{t}+\tau-r)\dot{\gamma}(r)dr \tag{6.84a}$$

$$\int_0^{+\infty} \sigma_m^{(V)}(z,\bar{t}+\tau)dz = \int_{-\infty}^{\bar{t}+\tau} G^{(V)}(\bar{t}+\tau-r)\dot{\gamma}(r)dr \tag{6.84b}$$

From the latter relations, we can conclude that no matter what rheological model is considered, their overall response, i.e. the resultant of the "microforces", namely of the forces on the lateral springs (for the (E)-model) or dashpots (for the (V)-model), match exactly the force arising at the "macrolevel", i.e. the force acting on the top plate.

Once more this is a confirmation of the fact that the detected "macroscopic" stress response, governed by a power-law relaxation function, is completely determined by constitutive properties of the submacroscopic structure which, in this case, is resembled by the rheological models (E) and (V).

The achieved result is consistent with what is encountered in micromechanics, where a displacement (in this case γ) is prescribed on the boundary (namely the top plate) of a representative volume element of heterogeneous material and a boundary value problem is solved in the interior of such an element. The latter is essentially provided by the procedure followed in [62]: there it was found that the response of the top plate, upon which a time varying displacement was prescribed, was precisely given by the convolution between the rate of change pf the imposed displacement

and the relaxation function $G^{(E)}(\circ)$ or $G^{(V)}(\circ)$ for (E) or (V) respectively.

Nevertheless, (6.84a) and (6.84b) from (E) and (V), respectively, can be interpreted by invoking the balance of forces arising on each system. In particular, the free body diagrams displayed in Figure 6.6 are self explanatory about the fact that for each if the two models balance of forces yields that the following relation must hold

$$\sigma(t) = \int_0^\infty \sigma_m(z,t)dz \qquad (6.85)$$

where $\sigma(t)$ is given by (6.61) and $\sigma_m(z,t)$ represents either (6.64a) and (6.64b).
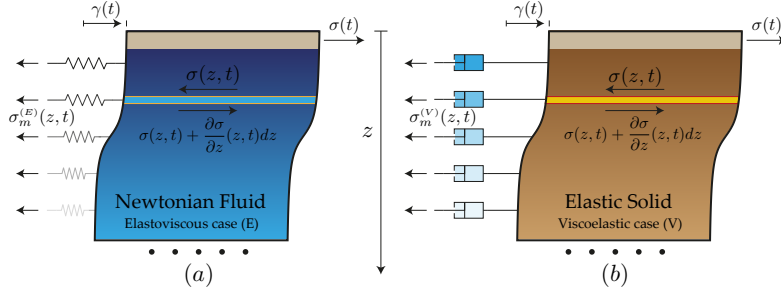
Figure 6.6: Elastoviscous (E) and Viscoelastic (V) deformed models and related external microstresses. Courtesy of [54].

Since (6.61) is nothing but the representation in terms of (Caputo) fractional derivative of either $G^{(E)}(\circ)$ or $G^{(V)}(\circ)$, (6.85) reproduces exactly (6.84a) and (6.84b). Evidently, a third way to achieve the same result provided by the latter equation is that (6.59a) and (6.59b) deliver the balance of linear momentum of an arbitrary slab (of unitary width) in between the depths z and $z + dz$, i.e.

$$\frac{\partial\tau(z,t)}{\partial z} = \sigma_m(z,t) \qquad (6.86)$$

where τ is the shear stress inside the column and the pair (τ, σ_m) for (E) and (V) agrees with $\left(c_{(E)}(z)\frac{\partial\dot\gamma(z,t)}{\partial z},\ \sigma_m^{(E)}\right)$, $\left(k_{(V)}(z)\frac{\partial\gamma(z,t)}{\partial z},\ \sigma_m^{(V)}\right)$ respectively. Henceforth, the simple integration of (6.86) across the depth of the column yields

$$\tau(0,t) = -\int_0^\infty \sigma_m(z,t)dz. \qquad (6.87)$$

It is not difficult to check that a direct evaluation of the left-hand side for each of

217

the two rheological models yield (6.84a) and (6.84b) back again.

Ultimately, the knowledge of the time history of the displacement of the top plates determines:

(i) the overall response of the system, no matter what rheological model is used;

(ii) the values of the displacement "at the microlevel" $\gamma^{(E)}(z,t)$, $\gamma^{(V)}(z,t)$ for (E) and (V) respectively (e.g. (6.65a) and (6.65b)) ultimately leading to the "microstresses" $\sigma_m^{(E)}(z,t)$ and $\sigma_m^{(V)}(z,t)$ through (6.64a) and (6.64b) respectively.

Physically it is unlikely to know the whole past strain history of a viscoelastic material, whereas residual stresses may be detectable. As remarked in Sect. 3 before defining $\mathcal{I}^{t_1}(t_2)$ with (6.45) (here t_1 and t_2 denote two arbitrary times), this variable represents such a stress at time t_2 for not necessarily known strain histories acting from the far past up to the initial observation time $t_1 < t_2$.

The approximation formulas (6.49) and (6.37) allow us to state that although (approximately) equivalent histories differ by a power-law strain, the knowledge of $\mathcal{I}^{t_1}(t_2)$ at any $t_1 < t_2$ allows for uniquely determining (i) and (ii).

Unlike (i), which has been treated in [62], (ii) needs to be clarified. If we set

$$_a\varepsilon_b^*(r) := \begin{cases} _a\varepsilon^*(r) & a \leq r < b \\ 0 & b \leq r < \bar{t} + \tau \end{cases} \tag{6.88}$$

then relation (6.48) delivering the corresponding residual stress at $\bar{t} + \tau$ reads as follows

$$_a\mathcal{I}^b(\tau + \bar{t}) = \left(_C D_{a+}^\beta \, _a\varepsilon_b^*\right)(\tau + \bar{t}) - \frac{\varepsilon(b)}{(\bar{t} + \tau - b)^\beta} + \frac{\varepsilon(a)}{(\bar{t} + \tau - a)^\beta}. \tag{6.89}$$

This allows for obtaining representatives of the equivalence class of histories by computing the fractional integrals I_{a+}^β of order β of both sides of such a relationship.

As far as the rheological models are concerned, we can state that, instead of prescribing the displacement history of the top plate, the knowledge of the associated residual stress $_a\mathcal{I}^b(\tau + \bar{t})$ allows for evaluating

$$\left(I_{a+}^\beta \, _a\mathcal{I}^b\right)(\tau + \bar{t}) = \frac{1}{\Gamma(\beta)} \int_{a+}^{\tau + \bar{t}} \, _a\mathcal{I}^b(r)(t - r)^{\beta - 1} dr. \tag{6.90}$$

This (besides the terms depending on $\varepsilon(b)$ and $\varepsilon(a)$, where the latter vanishes in the limit for $a \to -\infty$) divided by C_β permits to replace γ in (6.84a) and (6.84b) and hence allows for determining the overall response of the rheological models. In this sense, we may state that the "state at the microlevel", namely the knowledge

218

of $\sigma_m^{(E)}(z,t)$ (or $\gamma^{(E)}(z,t)$), $\sigma_m^{(V)}(z,t)$ (or $\gamma^{(V)}(z,t)$) is fully determined through the knowledge of the "macroscopic" state.

6.5 Remarks

In this Chapter, at first the attention has been focused on "virgin" materials characterized by power law relaxation (and hence creep) functions, it has been considered absolutely continuous strain functions in time, for which the Boltzmann-Volterra integral relation can be recast in terms of a Caputo fractional derivative, whose order matches the power encountered in the relaxation function (besides its sign). Such derivative is characterized by a hyper-singular integral, whose convergence is guaranteed whenever the strain is absolutely continuous in time (see [183], Lemma 2.2, p.35). In this case, the resulting stress is at least locally integrable and its representation formula enjoys its inverse in terms of the Riemann-Liouville integral of the same order of the derivative above. This result has been generalized here to strains which are locally of Special Bounded Variations (SBV_{loc}) in time. This has been done by first evaluating the contribution to the stress of the jump part of the strain, which can be represented through its Lebesgue decomposition (see e.g. [118]). It has been proved, both through the use of Theorem 2.4 in [183] and also by direct calculation, that the corresponding stress turns out to be invertible as well as the one associated with the absolutely continuous part of the strain. This has allowed for reconstructing any strain in SBV_{loc} starting from the associated stress.

The state for a "non-virgin", namely prestressed (or prestrained), FHM has been then treated in Section 6.2. Whenever the strain is assumed as the independent variable, the equivalence of two past histories is recast in terms of the Caputo fractional derivative of their difference ε^* (see equation (6.33)). An approximation of this equation has been considered and its solution has generated a one parameter family of strains producing a corresponding family of stresses converging in L^∞ to the response related to ε^*. In turn, it has been shown that this procedure permits to single out the explicit expression of the residual stress obtained by freezing the strain to zero for any arbitrary duration starting from a conventional observation time, $\bar{t}$, before which the experienced past history is not known. For such a variable an approximation formula has been provided in analogy with the one discussed above.

Two rheological models derived in [62] yielding power law creep and relaxation have been discussed in Section 6.4. The first one conveys the idea of having a functionally graded submacroscopic structure, labelled with the letter (V), formed by a continuous elastic layer supported on one of its sides by a continuous sequence

of dashpots whose stiffness and viscosity both decrease with depth. The second model, labelled with (E), is somehow the dual of the previous one, since it is obtained by considering a viscous layer supported on continuous springs both characterized by viscosity and stiffness decreasing with depth, respectively. In both cases the two systems are driven by an indefinite massless rigid plate on which a displacement time history is prescribed. The initial boundary value problems corresponding to both systems have been summarized, whose solutions (6.61) arise in terms of the fractional derivative of the imposed time history, leading to the force (stress) arising at the rigid plate.

On the other hand, Section 6.4 has provided newer insights on the models introduced above. Indeed, the "microstresses", namely the "forces" arising in the continuous distributions of dashpots (model (V)) and springs (model (E)) have been evaluated.The overall responses of both systems has been shown to match the force arising at the rigid plate. This is motivated a-posteriori by exploring the balance of forces in both rheological models and it also shown how the knowledge of the state of the top plate determines the microstresses in both systems.

References

[7]   G. Amendola, M. Fabrizio, and M. J. Golden. *Thermodynamics of materials with memory: Theory and applications.* ISBN: 978-1-4614-1691-3. Springer, 2002 (cit. on p. 194).

[9]   R. Bagley and P. Torvik. "Fractional Calculus - A different Approach to the Analysis of Viscoelastically Damped Structures". *The American Institute of Aeronautics and Astronautics Journal* 21.5 (1983), pp. 741–748 (cit. on pp. 194, 196).

[10] R. Bagley and P. Torvik. "On the Fractional Calculus Model of Viscoelastic Behavior". *Journal of Rheology* 30.1 (1986), pp. 135–155 (cit. on pp. 194, 196).

[32] B. Coleman and D. Newman. "On the rheology of cold drawing II. Viscoelastic materials". *Journal of Polymer Science: Part B: Polymer Physics* 30 (1992), pp. 25–47 (cit. on p. 194).

[40] G. Del Piero and L. Deseri. "On the concepts of state and free energy in linear viscoelasticity." *Archive for Rational Mechanics and Analysis* 138 (1997), pp. 1–35 (cit. on pp. 165, 168, 169, 194, 195, 198, 201, 230).

[44] L. Deseri, G. Gentili, and M. Golden. "An Expression for the Minimal Free Energy in Linear Viscoelasticity". *Journal of Elasticity* 54 (1999), pp. 141–185 (cit. on pp. 168, 194).

[46] L. Deseri and M. Golden. "The Minimum Free Energy for Continuous Spectrum Materials." *SIAM Journal on Applied Mathematics* 67.3 (2007), pp. 869–892 (cit. on pp. 165, 168, 194).

[47] L. Deseri, M. Golden, and M. Fabrizio. "The Concept of a Minimal State in Viscoelasticity: New Free Energies and Applications to PDEs". *Archive for Rational Mechanics and Analysis* 181 (2006), pp. 43–96 (cit. on pp. vi, 165, 168, 194, 195, 198, 201).

[52] L. Deseri, M. Piccioni, and G. Zurlo. "Derivation of a new free energy for biological membranes". *Continuum Mechanics and Thermodynamics* 20.5 (2008), pp. 255–273. DOI: `10.1007/s00161-008-0081-1` (cit. on pp. iv, 1, 4, 23, 25, 26, 40, 153, 154, 168, 193).

[54] L. Deseri, M. Zingales, and P. Pollaci. "The State of Fractional Hereditary Materials (FHM)". *Discrete and Continuous Dynamical Systems B* 19.7 (2014), pp. 2065–2089 (cit. on pp. v, 5, 197, 202, 204, 208, 211, 217).

[55] L. Deseri and G. Zurlo. "The stretching elasticity of biomembranes determines their line tension and bending rigidity". *Biomechanics and Modeling in Mechanobiology* 12 (2013), pp. 1233–1242. DOI: `doi: 10.1007/s10237-013-0478-z` (cit. on pp. iii, iv, 1, 4, 23–26, 30, 40, 72, 153, 154, 168, 193).

[56] L. Deseri et al. "Hereditary creep: state and free energy". *In preparation* () (cit. on p. 201).

[60] M. Di Paola, F. P. Pinnola, and M. Zingales. "A discrete mechanical model of fractional hereditary materials". *Meccanica* (Jan. 2013). DOI: `DOI10.1007/s11012-012-9685-4` (cit. on pp. 194, 234).

[62] M. Di Paola and M. Zingales. "Exact mechanical models of fractional hereditary materials". *Journal of Rheology* 56.5 (2012), pp. 983–1004 (cit. on pp. 194, 196, 208, 209, 212, 216, 218, 219, 226, 230–232, 241, 243, 246).

[67]   M. Fabrizio and M. J. Golden. "Minimum free energies for materials with finite memory". *Journal of Elasticity,* 72 (2003), pp. 121–143 (cit. on p. 194).

[68]   M. Fabrizio and A. Morro. "Mathematical problems in linear viscoelasticity". *SIAM Philadelphia* (1992) (cit. on p. 194).

[77]   A. P. G. Mishuris and E. Radi. "Steady-state propagation of a Mode III crack in couple stress elastic materials". *International Journal of Engineering Science* (2012), pp. 112–128 (cit. on p. 194).

[78]   L. Galuppi and G. R. Carfagni. "Laminated beams with viscoelastic interlayer". *International Journal of Solids and Structures* 49 (2012), pp. 2637–2645 (cit. on p. 194).

[79]   L. Galuppi and G. R. Carfagni. "The design of laminated glass under time-dependent loading". *International Journal of Mechanical Sciences* 68 (2013), pp. 67–75 (cit. on p. 194).

[83]   A. Gemant. "A method of analyzing experimental results obtained from elasto-viscous bodies". *Physics* 7 (1936), pp. 311–317 (cit. on p. 194).

[84]   G. Gentili. "Maximum recoverable work, minimum free energy and state space in linear viscoelasticity". *Quarterly of Applied Mathematics* 60 (2002), pp. 153–182 (cit. on p. 194).

[87]   C. Giorgi and A. Morro. "Viscoelastic solids with unbounded relaxation function". *Continuum Mechanics and Thermodynamics* 4 (1992), pp. 151–165 (cit. on p. 199).

[89]   D. Graffi and M. Fabrizio. "Sulla nozione di stato per materiali viscoelastici di tipo "rate"". *Atti Accademia dei Lincei, Rendiconti di Fisica,* 83 (1989), pp. 201–208 (cit. on p. 194).

[111] A. Jaishankar and G. H. McKinley. "Power-law rheology in the bulk and at the interface: quasi-properties and fractional constitutive equations". *Proceedings of the Royal Society A* 469 (2013). DOI: `doi: 10.1098/rspa.2012.0284` (cit. on pp. 5, 193, 194).

[118] A. N. Kolmogorov and S. V. Fomin. *Introductory Real Analysis.* Prentice Hall, 1970 (cit. on pp. 198, 199, 219).

[121]   G. M. L. Morini A. Piccolroaz and E. Radi. "On fracture criteria for a crack propagating in couple stress elastic materials". *International Journal of Engineering Science* 71 (2013), pp. 45–61 (cit. on p. 194).

[123]   R. Lakes. *Viscoelastic materials.* Cambridge University Press, 2009 (cit. on p. 195).

[132]   G. G. M. Fabrizio and M. J. Golden. "The minimum free energy for a class of compressible viscoelastic fluids". *Differential and Integral Equations* 7 (2002), pp. 319–342 (cit. on pp. 194, 201).

[135]   F. Mainardi. "Fractals and Fractional Calculus in Continuum Mechanics". Wien: Springer Verlag, 1997. Chap. Fractional calculus: Some basic problems in continuum and statistical mechanics, pp. 291–348 (cit. on p. 194).

[136]   F. Mainardi. *Fractional Calculus and Waves in Linear Viscoelasticity.* Imperial College Press, 2010 (cit. on pp. 194, 195, 226).

[137]   F. Mainardi and G. Spada. "Creep, relaxation and viscosity properties for basic fractional models in rheology". *The European Physical Journal* 193 (2011), pp. 133–160. URL: `arXiv:1110.3400` (cit. on p. 194).

[154]   W. Noll. "A new mathematical theory of simple materials". *Archive for Rational Mechanics and Analysis,* 48 (1972), pp. 1–50 (cit. on pp. 194, 201).

[156]   P. Nutting. "A new general law of deformation". *Journal of The Franklin Institute* 191 (1921), pp. 679–685 (cit. on pp. 5, 193, 196).

[173]   V. Quaglini, V. La Russa, and S. Corneo. "Nonlinear stress relaxation of trabecular bone". *Mechanics Research Communications* 36 (2009), pp. 275–283 (cit. on pp. 194, 226, 228, 229).

[177]   S. S. Ray, B. P. Poddar, and R. K. Bera. "Analytical solution of a dynamic system containing fractional derivative of order one-half by Adomian decomposition method". *Journal of Applied Mechanics* 72.2 (2005), pp. 290–295. DOI: `doi:10.1115/1.1839184` (cit. on p. 194).

[178]   F. Riewe. "Mechanics with fractional derivatives". *Physical Review E* 55 (1997), pp. 3581–3592 (cit. on p. 194).

[181] S. Sakakibara. "Relaxation properties of fractional derivative viscoelasticity models". *Nonlinear Analysis* 47 (2001), pp. 5449–5454 (cit. on p. 194).

[183] S. G. Samko, A. A. Kilbas, and O. I. Marichev. *Fractional Integrals and Derivatives. Theory and Applications*. Londn - New York: Gordon & Breach Science Publishers, 1987 (cit. on pp. 197, 200, 201, 204, 219, 226, 257, 258, 260).

[185] G. Scott Blair. "The role of psychophysics in rheology". *Journal of Colloid Science* 2 (1947), pp. 21–32 (cit. on pp. 5, 193, 230).

[193] M. K. Suchorsky and R. H. Rand. "A pair of van der Pol oscillators coupled by fractional derivatives". *Nonlinear Dynamics* 69 (2012), pp. 313–324. DOI: `doi:10.1007/s11071-011-0266-1` (cit. on p. 194).

[194] M. R. Sunny et al. "A modified fractional calculus approach to model hysteresis". *Journal of Applied Mechanics* 77 (2010). DOI: `doi:10.1115/1.4000413` (cit. on p. 194).

[208] P. Yang, Y. C. Lam, and K. Zhu. "Constitutive equation with fractional derivatives for generalized UCM model". *Journal of Non-Newtonian Fluid Mechanics* 165 (2010), pp. 88–97. DOI: `doi:http://dx.doi.org/10.1016/j.jnnfm.2009.10.002` (cit. on p. 194).

Chapter 7

Power-law hereditariness of herarchical fractal bones

    In this Chapter, the attention is focused on the mechanical behavior of bone tissues because as highly functionalized tissues because of its important in biomedical engineering. Indeed, the main feature that biomedical devices must possess have high compatibility with directly interacting biological tissues. For natural and artificial bone-like structures, this feature involves similar stiffness, strength and toughness among in vivo and artificial devices. The bones can grow, change their form during their life and self-heal after a fracture, renewing through a remodeling process. All these processes are regulated by mechanical, hormonal and physiological signals. In particular osteocytes basic remodelling is mainly led by mechanical transduction through strain/energy density in bone tissue [23, 35, 143, 168, 196] and, henceforth, the hereditariness of mineralized biological tissue is a crucial aspect to detect the speed of bone reformations as well as to predict its interactions with artificial devices.

    Here, it will shown that relaxation/creep functions of trabecular and compact

bones are well captured by real-order power-laws t^β $(0 < \beta \le 1/2)$ yielding a rheological model in term of real-order differintegral operators [136, 169, 183]. This behavior has been associated to the anomalous Euclidean scaling of bone specimen geometry as in ordinary fractal analysis. This observation provides a relation among the Hausdorff dimension of the geometry scaling and the decay of the power-law. Indeed, stiffness and viscosity coefficients of the fractance decay of power-law with the observation scale have exponent related to the observed dependence of both the creep and relaxation functions [62].

7.1 Bone hereditariness: The power-law rheological model

Mineralized biological tissues as bones, tendons and ligaments are very sophisticated and highly specialized engineered materials. Macroscopic observations of trabecular bone tissue show that its architecture is built upon a complex network of beams and platelets forming a three-dimensional geometric structure. Spaces among the mineralized tissues are filled by bone marrow, a fluid-like material formed by fat cells, water and proteins. The biphasic nature of the trabecular bone is the main reason why its macroscopic mechanical behavior fades out stress peaks due to high frequency and impulsive loads. Mathematical models of the macroscopic behavior of biphasic trabecular bones make wide use of the Biot's poroelasticity [33, 98–100, 168], although a more modern treatment of such media may be found through the theory of Structured Deformations [49–51].

Despite the macroscopic behavior of trabecular bones, the rheological description of mineralized biological tissues deserves careful considerations. Indeed load capacity and ultimate strength of bones, as well as stiffness, depend on the mechanical properties of the solid-like phase. However several pathological diseases such as osteoporosis and/or osteosynthesis affect, specifically, the nano-micro scale structure of the mineralized tissue modifying, primarily, its rheological properties [145, 192, 204]. In this regard, it is well known that the structure of bones is self-organized in a hierarchic sequence repeating its fundamental elements in different stacking at different resolution scales [122]. The overall behavior of the mineralized tissue is detected through macroscale relaxation tests from several authors [1, 173, 203] and is displayed in Figure 7.2 In the pictures, dots represent the experimental data whereas solid lines are the fitting relaxation curves chosen in the following class:

$$G(t) := \frac{C_\beta}{\Gamma(1-\beta)} t^{-\beta} \qquad \beta \in [0,1] \tag{7.1}$$

where $G(t)$ and $\Gamma(1-\beta)$ are the relaxation function and the Euler-Gamma function
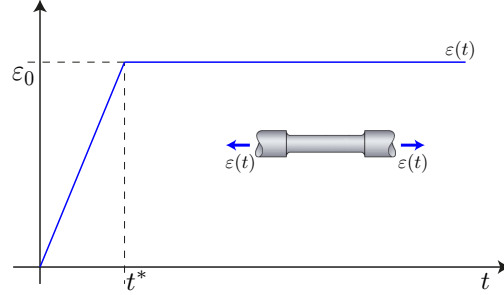
Figure 7.1: Schematic representation of relaxation test: after the initial ramp, the strain is held constant. Courtesy of [57].

evaluated at t and at $1 - \beta$ respectively and $[C_\beta] = FT^\beta/L^2$ is an anomalous *force* coefficient of the material. Inspection of Figure 7.2 shows that the fitting curves in (7.1) are in good agreement with experimental results for different kinds of bones undergoing to relaxation tests (schematically represented in Figure 7.1). The viscoelastic behavior of collagen is then shown to agree with our choice of the class of relaxation functions, even if a closer analysis of data seems to require an additional constant elastic term to model the equilibrium response. Indeed, the hereditary feature causes continuum stress relaxation in time depending on an exponent near to 0 (see Table 7.1). Henceforth the stress value fades out in a very long time. Experimental tests are performed in a limited time frame, so that the proposed model approximates very well the experimental data in the given time-range [34, 82, 170]. The results of best-fitting procedure, collected in Table 7.1, show that the power-law exponent depends on the anatomical location of the considered specimen [149]. This observation is in good agreement with several bone microscopies showing that the mineralized tissue architecture changes upon the anatomic location as the result of a material optimization procedure. In the context of linear hereditariness and in the absence of past histories, the Boltzmann-Volterra superposition principle may be used to provide the stress response as well as the strain evolution for prescribed strain γ (stress σ) processes:

$$\sigma(t) := \int_0^t G(t - \tau)\dot{\gamma}(\tau)\,\mathrm{d}\tau \tag{7.2a}$$

$$\gamma(t) := \int_0^t J(t - \tau)\dot{\sigma}(\tau)\,\mathrm{d}\tau. \tag{7.2b}$$

As the model parameters have been obtained from the best-fitting of experimental data on stress relaxations, the creep function $J(t)$ may be obtained from the relaxation function $G(t)$ in (7.1) by mean of the well-known relation in the Laplace domain, i.e.

$$\tilde{G}(s)\tilde{J}(s) = \frac{1}{s^2} \implies J(t) = \frac{1}{C_\beta\Gamma(1+\beta)}t^\beta \tag{7.3}$$

where the symbol $\tilde{\ }$ denotes the Laplace transform.
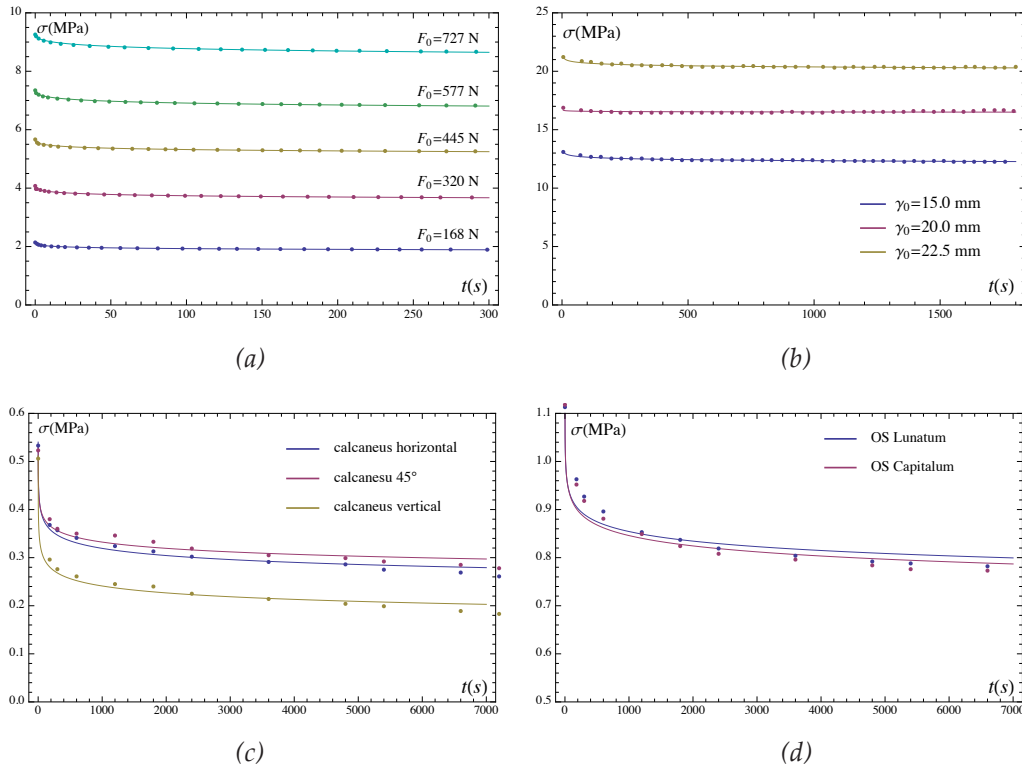
Figure 7.2: Fitting of relaxation experimental data from several authors: a) [173]; b) [203]; c) and d) [1]. Courtesy of [57].

By inspection of the last term in the equality chains in (7.2) through the definitions reported in Appendix A, it is shown that assuming a power-law expression of the relaxation/creep function of the material results into rheological expressions:

Table 7.1: Parameters from best-fitting procedure on curve in Figure 7.2.

		β	C_β $\left[\dfrac{N}{mm^2}s^\beta\right]$	Notes
(a) [173]	$F_0 = 168\ N$	0.0194	71.17	
	$F_0 = 320\ N$	0.0171	71.52	
	$F_0 = 445\ N$	0.0128	71.58	bovine femoral head
	$F_0 = 577\ N$	0.0139	72.13	
	$F_0 = 727\ N$	0.0136	72.56	
(b) [203]	$\varepsilon_0 = 1.143\%$	0.0690	46.99	human calcaneus horizontal
	$\varepsilon_0 = 0.678\%$	0.0575	75.61	human calcaneus 45°
	$\varepsilon_0 = 0.478\%$	0.0886	98.53	human calcaneus vertical
	$\varepsilon_0 = 0.480\%$	0.0341	229.95	os lunatum
	$\varepsilon_0 = 0.707\%$	0.0372	158.22	os capitalum
(c) [1]	$u_0 = 0.15\ mm$	0.0104	88.99	
	$u_0 = 0.20\ mm$	0.0015	83.50	bovine femur
	$u_0 = 0.25\ mm$	0.0069	84.09	

$$\sigma(t) = \frac{C_\beta}{\Gamma(1-\beta)} \int_0^t (t-\tau)^{-\beta} \dot{\gamma}(\tau) \, d\tau = C_\beta \left({}_C D_{0+}^\beta \gamma \right)(t) \qquad (7.4a)$$

$$\gamma(t) = \frac{1}{C_\beta \Gamma(1+\beta)} \int_0^t (t-\tau)^\beta \dot{\sigma}(\tau) \, d\tau = \frac{1}{C_\beta} \left(I_{0+}^\beta \sigma \right)(t) \qquad (7.4b)$$

containing the well-known Caputo and Riemann-Liouville differential and integral operators. For "non-virgin" materials, i.e. materials whose state at the very beginning of observation is characterized by prestressed (or prestrained) configuration, equation (7.2) would be supplemented by state variables [40, 45]. The use of fractional operators in the context of rheological material modeling has been proved to be a key tool to predict the hereditariness of stresses and strains in organic polymers [74–76]. The rheological description of the hereditary features of bone tissues has been shown in Figure 7.2, where the material parameters have been estimated by a best fitting procedure for different kinds of trabecular bone tissues. The stress-strain behavior in (7.4) may be fruitfully explained by making use of a rheological device, called *springpot* [185]. The springpot has an intermediate behavior between a linear spring, whose constitutive equations reads as $\sigma = E\gamma$, and a Newtonian dashpot with constitutive law relation $\sigma = \eta \dot{\gamma}$ (Figure 7.3). Limiting

$$\sigma(t) = E(D^0 \gamma)(t) = E\gamma(t) \qquad (\beta = 0)$$

$$\sigma(t) = C_\beta (D^\beta \gamma)(t) \qquad (0 < \beta < 1)$$

$$\sigma(t) = \eta (D^1 \gamma)(t) = \eta \dot{\gamma}(t) \qquad (\beta = 1)$$
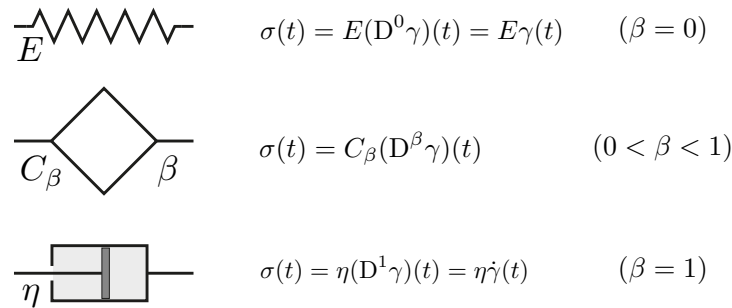
Figure 7.3: The mechanical *devices*: (a) spring, (b) springpot, (c) dashpot. Courtesy of [57].

values of the order of differentiation $\beta \to 0$ or $\beta \to 1$ yield springs and dashpot devices, respectively. The fairly limited use of fractional-order derivatives in the context of mechanics is related to the lack of a clear mechanical description of the associated rheological devices. An efficient and exact representation of springpot devices has been recently obtained [61, 62].

230

7.2 The mechanical model of bone fractional-order hereditariness

An exact mechanical model of fractional hereditary materials was recently proposed in [62], where two different mechanical representations of fractional hereditary material (FHM) depending on the mathematical range of the exponent β are reported. The mechanical description of *Elasto-Viscous* (EV) materials ($0 \leq \beta \leq 1/2$) is represented by an indefinite massless viscous shear fluid externally restrained by a bed of independent elastic springs. *Visco-Elastic* (VE) materials ($1/2 \leq \beta \leq 1$) are represented instead by an indefinite elastic shear layer externally restrained by independent linear dashpots (Figure 7.4).
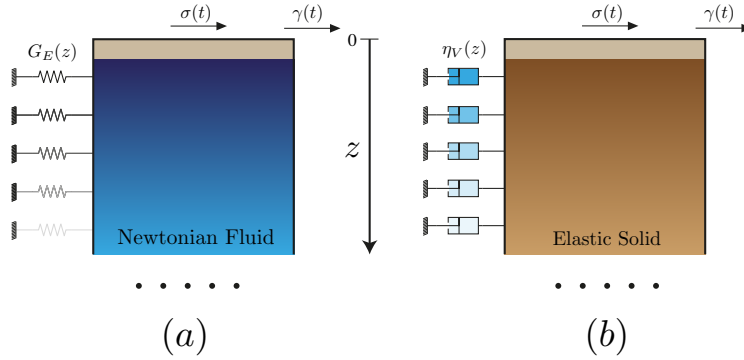
Figure 7.4: Continuum fractional models: (a) elastoviscous (EV) and (b) viscoelastic (VE) cases.

It is assumed that the mechanical parameters of the model, namely the elastic modulus $k(z)$ and the viscosity coefficient $c(z)$ decay with power-law with the axial coordinate z as:

$$k_E(z) := AG_E(z) = A\frac{G_0}{\Gamma(1+\alpha)}z^{-\alpha} \tag{7.5a}$$

$$c_E(z) := A\eta_E(z) = A\frac{\eta_0}{\Gamma(1-\alpha)}z^{-\alpha}, \tag{7.5b}$$

for EV materials (denoted by subscript E), whereas for VE materials (denoted by

subscript V) they read as follows:

$$k_V(z) := AG_V(z) = A\frac{G_0}{\Gamma(1-\alpha)}z^{-\alpha} \tag{7.6a}$$

$$c_V(z) := A\eta_V(z) = A\frac{\eta_0}{\Gamma(1+\alpha)}z^{-\alpha} \tag{7.6b}$$

where $0 \leq \alpha \leq 1$, A is the cross-sectional area and G_E, G_V and η_E, η_V represent the elastic modulus and the viscosity coefficient per unit of area for both cases respectively (see [62] for more details). In the following it is assumed a unit area ($A = 1$) so that $k_{E,V}(z) = G_{E,V}(z)A = G_{E,V}(z)$ and $c_{E,V}(z) = \eta_{E,V}(z)A = \eta_{E,V}(z)$. In these circumstances the balance of linear momentum of the model reads:

$$(\mathrm{EV}): \quad \frac{\partial}{\partial z}\left[c_E(z)\frac{\partial\dot\gamma}{\partial z}\right] = k_E(z)\gamma(z,t) \tag{7.7a}$$

$$(\mathrm{VE}): \quad \frac{\partial}{\partial z}\left[k_V(z)\frac{\partial\gamma}{\partial z}\right] = c_V(z)\dot\gamma(z,t), \tag{7.7b}$$

where $\gamma(z,t)$ is the transverse displacement of the shear layer at depth z and $\dot\gamma(z,t) = \frac{\partial\gamma(z,t)}{\partial t}$. Boundary conditions associated to the mechanical model in Figure 7.4 are provided in the form:

$$\begin{cases} \lim_{z\to 0}\gamma(z,t) = \gamma(t) \\ \lim_{z\to\infty}\gamma(z,t) = 0. \end{cases} \tag{7.8}$$

Upon solving the boundary value problem, the stress arising at the top surface turns out to be related to the transverse displacement $\gamma(t)$ by the following relation:

$$\sigma(t) = C_\beta\left({}_C\mathrm{D}_{0^+}^\beta\gamma\right)(t), \tag{7.9}$$

where:

$$C_\beta := C_\beta^E = \frac{G_0\Gamma(\beta)}{\Gamma(2-2\beta)\Gamma(1-\beta)2^{1-2\beta}}\left(\tau_E(\alpha)\right)^\beta \tag{7.10a}$$

$$\tau_E(\alpha) = -\frac{\eta_0}{G_0}\frac{\Gamma(\alpha)}{\Gamma(-\alpha)} \tag{7.10b}$$

and $\alpha = 1 - 2\beta$ for the EV material, whereas:

$$C_\beta := C_\beta^V = \frac{G_0 \Gamma(1 - \beta)}{\Gamma(2 - 2\beta)\Gamma(\beta)2^{2\beta - 1}} \left(\tau_V(\alpha)\right)^\beta \tag{7.11a}$$

$$\tau_V(\alpha) = -\frac{\eta_0}{G_0} \frac{\Gamma(-\alpha)}{\Gamma(\alpha)} \tag{7.11b}$$

and $\alpha = 2\beta - 1$ for the VE material, where the terms $\tau_E(\alpha)$, $\tau_V(\alpha)$ are dimensionally a relaxation time. This result shows that the mechanical models analyzed above and formed by a proper arrangement of springs and dashpots with mechanical parameters decaying with power-law provides exactly a rheological model in terms of fractional derivatives.

It is worth noting, with the aid of the normalized creep function $\overline{J}(t) = J(t)C_\beta \Gamma(1+\beta) = t^\beta$ (see Figure 7.5), that the value $\beta = 1/2$ of the derivation order separates two different ranges for the material behavior. In the range $1/2 \leq \beta \leq 1$ the viscosity prevails, the elastic phase decreases with increasing β and then it is appropriate to define such materials as VE. The corresponding mechanical model is composed by an elastic indefinite column undergoing shearing and resting on a bed of linear dashpots. The second behavior is characterized by $0 \leq \beta \leq 1/2$ in which the elastic phase prevails with decreasing β, and then it is appropriate to define these materials as EVs. The corresponding mechanical model is described as an unbounded column of viscous fluid resting on a bed of linearly independent springs.

The critical value of the fractional derivation order $\beta = 1/2$ may be also obtained as a limit case for the two different models described above.
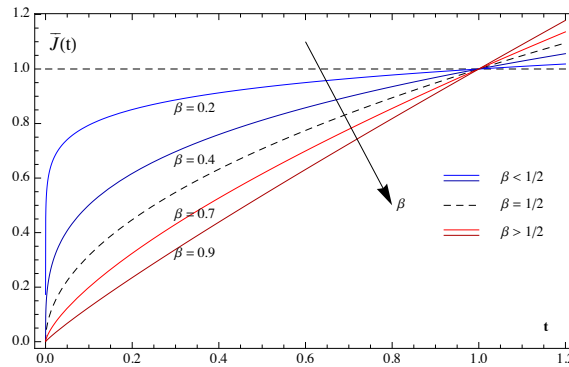
Figure 7.5: Normalized creep function $\overline{J}(t)$ (curves with different β). Courtesy of [57].

7.3 The discrete equivalent representation of FHM

Validation and challenges of the mechanical equivalent representation of FHM have been discussed in previous papers [60, 61] for EV ($0 \leq \beta \leq 1/2$) and VE ($1/2 \leq \beta \leq 1$) materials. To this aim the continuum mechanical model has been discretized into a mechanical fractance. Introducing a finite discretization grid of the $z-$axis into point $z_j = (j-1)\Delta z$, $j = 1, 2, \dots, n$, with step $\Delta z = h/n$ where h is the spatial extension of the fractance.
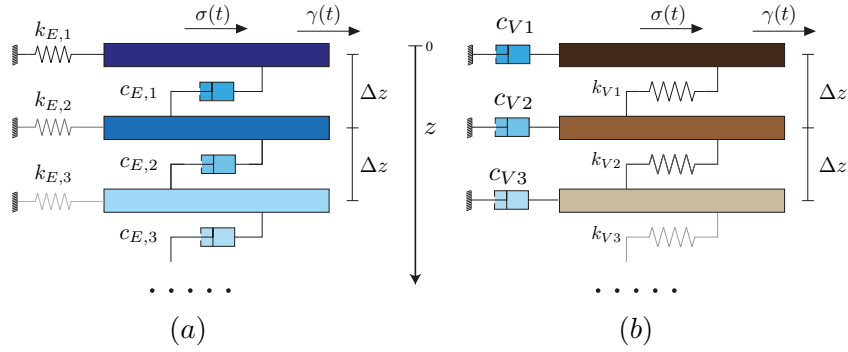
Figure 7.6: Fractional mechanical model: discrete counterpart of (a) EV and (b) VE materials. Courtesy of [57].

The introduction of $z-$axis discretization yields discrete mechanical fractances both for EV and VE cases (Figure 7.6) with stiffness and damping coefficients that for EV case read:

$$k_{E,j} = G_E(j\Delta z)\Delta z = \frac{\eta_0}{\Gamma(1+\alpha)}(j\Delta z)^{-\alpha}\ \Delta z \qquad (7.12a)$$

$$c_{E,j} = \frac{\eta_E(j\Delta z)}{\Delta z} = \frac{G_0}{\Gamma(1-\alpha)}\frac{(j\Delta z)^{-\alpha}}{\Delta z}. \qquad (7.12b)$$

Hence, the equilibrium equations are provided in the following form:

$$\begin{cases} \sigma(t) = k_0\gamma_1 - c_0\Delta\dot{\gamma}_0 \\ k_j\gamma_j - c_j\Delta\dot{\gamma}_j + c_{j-1}\Delta\dot{\gamma}_{j-1} = 0 \end{cases} \qquad (7.13)$$

where $\Delta\dot{\gamma}_{j+1} = \dot{\gamma}_{j+1} - \dot{\gamma}_j$. May be shown that as $\Delta z \to 0$ and $h \to \infty$ (7.13) reverts to the governing equation in (7.7b). Similar considerations hold for VE

models as we select the spring coefficient of the model in (7.6) as follows:

$$k_{V,j} = \frac{G_v(z)}{\Delta z} = \frac{G_0}{\Gamma(1-\alpha)} j^{-\alpha} \frac{\Delta z^{-\alpha}}{\Delta z} \tag{7.14a}$$

$$c_{V,j} = \eta_v(z)\Delta z = \frac{\eta_0}{\Gamma(1+\alpha)} j^{-\alpha} \Delta z^{-\alpha} \; \Delta z, \tag{7.14b}$$

while the equilibrium equation are:

$$\begin{cases} \sigma(t) = c_0\dot{\gamma}_0 - k_0\Delta\gamma_1 \\ c_j\dot{\gamma} - k_j\Delta\gamma_j + k_{j-1}\Delta\gamma_{j-1} = 0 \end{cases} \tag{7.15}$$

where $\Delta\gamma_{j+1} = \gamma_{j+1} - \gamma_j$.

The discretized version of the equilibrium equations may be cast in a compact form for EV and VE, namely:

$$p_E\mathbf{A}\dot{\boldsymbol{\gamma}} + q_E\mathbf{B}\boldsymbol{\gamma} = \mathbf{v}\sigma(t) \tag{7.16a}$$

$$p_V\mathbf{B}\dot{\boldsymbol{\gamma}} + q_V\mathbf{A}\boldsymbol{\gamma} = \mathbf{v}\sigma(t), \tag{7.16b}$$

where p and q are constant coefficients only depending on discretization increment Δz, $\boldsymbol{\gamma}$ is the vector of displacement at each layer of discretization, $\mathbf{v}\sigma(t)$ is the vector of applied stress, and:

$$p_E := \frac{\eta_0}{\Gamma(1-\alpha)}\Delta z^{-(1+\alpha)} \qquad p_V := \frac{\eta_0}{\Gamma(1+\alpha)}\Delta z^{1-\alpha} \tag{7.17a}$$

$$q_E := \frac{G_0}{\Gamma(1+\alpha)}\Delta z^{1-\alpha} \qquad q_V := \frac{G_0}{\Gamma(1-\alpha)}\Delta z^{-(1+\alpha)} \tag{7.17b}$$

$$\boldsymbol{\gamma} = [\gamma_1 \quad \gamma_2 \dots \gamma_n]^T \qquad \mathbf{v} = [1 \quad 0 \dots 0]^T, \tag{7.17c}$$

Here the matrices $\mathbf{A}$ and $\mathbf{B}$ are defined as follows:

$$A_{i,j} = \begin{cases} (i-1)^{-\alpha} + i^{-\alpha} & i = j \\ -i^{-\alpha} & (j-i) = 1 \text{ with } j > i \\ -j^{-\alpha} & (i-j) = 1 \text{ with } i > j \\ 0 & other \end{cases}$$

235

$$\mathbf{A} = \begin{bmatrix} 1^{-\alpha} & -1^{-\alpha} & 0 & \dots & 0 \\ 1^{-\alpha} & 1^{-\alpha} + 2^{-\alpha} & 2^{-\alpha} & \dots & 0 \\ 0 & 2^{-\alpha} & 2^{-\alpha} + 3^{-\alpha} & \dots & 0 \\ \vdots & \vdots & \vdots & \ddots & \vdots \\ 0 & 0 & 0 & \dots & (n-1)^{-\alpha} + n^{-\alpha} \end{bmatrix} \tag{7.18}$$

$$B_{i,j} = \begin{cases} i^{-\alpha}, & i = j \\ 0, & i \neq j \end{cases}$$

$$\mathbf{B} = \begin{bmatrix} 1^{-\alpha} & 0 & 0 & \dots & 0 \\ 0 & 2^{-\alpha} & 0 & \dots & 0 \\ 0 & 0 & 3^{-\alpha} & \dots & 0 \\ \vdots & \vdots & \vdots & \ddots & \vdots \\ 0 & 0 & 0 & \dots & n^{-\alpha} \end{bmatrix} \tag{7.19}$$

It is worth noting that $\mathbf{B}$ is actually positive difinite and, hence, invertible. In the sequel we will report analysis and solutions for both elastoviscous and viscoelastic materials.

Let now focus the attention on EV case. The solution of the system of differential equations in (7.16a) will be obtained introducing the following change of coordinate:

$$\mathbf{x} = \mathbf{B}^{\frac{1}{2}} \boldsymbol{\gamma} \tag{7.20}$$

By left-multiplying both sides of (7.16a) by $\mathbf{B}^{-\frac{1}{2}}$, we obtain:

$$p_E \mathbf{D} \dot{\mathbf{x}} + q_E \mathbf{I} \mathbf{x} = \mathbf{B}^{\frac{1}{2}} \mathbf{v} \sigma(t), \tag{7.21}$$

where $\mathbf{D} = \mathbf{B}^{-\frac{1}{2}} \mathbf{A} \mathbf{B}^{-\frac{1}{2}}$ is the dynamical matrix, and it is symmetric and positive and $\mathbf{I}$ is the identity operator. This equation may be studied by making use of $\boldsymbol{\Phi}$ (where each column is an eigenvector of $\mathbf{D}$), which has the following properties:

$$\boldsymbol{\Phi}^T \mathbf{D} \boldsymbol{\Phi} = \boldsymbol{\Lambda} \tag{7.22a}$$

$$\boldsymbol{\Phi}^T \boldsymbol{\Phi} = \mathbf{I}, \tag{7.22b}$$

where $\boldsymbol{\Lambda}$ is the diagonal matrix of the eigenvalues $\lambda_i > 0$ of $\mathbf{D}$. In order to obtain a decoupled set of equations, the modal transformation $\mathbf{x} = \boldsymbol{\Phi} \mathbf{y}$ is performed; henceforth by left-multiplicating for $\boldsymbol{\Phi}^{-1} = \boldsymbol{\Phi}^T$, the following modal equation

236

arises:

$$p_E \mathbf{\Lambda} \dot{\mathbf{y}} + q_E \mathbf{y} = \mathbf{\Phi}^T \mathbf{v} \, \sigma(t) \tag{7.23}$$

where $\mathbf{B}^{\frac{1}{2}} \mathbf{v} = \mathbf{v}$ for the special form both of $\mathbf{B}$ and $\mathbf{v}$.

Following the same steps with the same assumptions the governing equation for VE discrete model read as follows:

$$p_V \dot{\mathbf{y}} + q_V \mathbf{\Lambda} \mathbf{y} = \mathbf{\Phi}^T \mathbf{v} \, \sigma(t). \tag{7.24}$$

In the modal space, the jth equation of each model takes the following form:

$$\dot{y}_j + \frac{q_E}{p_E \lambda_j} y_j = \frac{\phi_{1,j}}{p_E \lambda_j} \sigma(t) \tag{7.25a}$$

$$\frac{p_V}{q_V \lambda_j} \dot{y}_j + y_j = \frac{\phi_{1,j}}{q_V \lambda_j} \sigma(t), \tag{7.25b}$$

where $\phi_{1,j}$ is the first element of the jth eigenvector of the dynamical matrix $\mathbf{D}$. Equations (7.25) are analog to the ones governing the evolution of a generic Kelvin-Voigt element with viscous coefficient $a_E := 1$ ($a_V := p_V/(q_V \lambda_j)$, elastic spring $b_E := q_E/(p_E \lambda_j) > 0$ ($b_V := 1$), and forced by $\sigma_j := f_j \sigma(t)$:

$$a_j \dot{y}_j + b_j \, y_j = f_j \sigma(t) \quad j = 1, \, 2, \ldots, \, n; \tag{7.26}$$

the previous statement allows for detecting the relaxation time of each level as the ratio $\tau_j = b_j/a_j$. In equation (7.26) the magnitude modal-load coefficients are defined as follows:

$$f_j := \begin{cases} f_E = \dfrac{\phi_{1,j}}{p_E \lambda_j} & \text{EV} \\[2mm] f_V = \dfrac{\phi_{1,j}}{q_V \lambda_j} & \text{VE} \end{cases} . \tag{7.27}$$

Setting the initial condition properly as

$$\mathbf{y}(0) = \mathbf{\Phi}^T \mathbf{B}^{\frac{1}{2}} \boldsymbol{\gamma}(0) \tag{7.28}$$

the complete solution of differential equation of Kelvin-Voigt model in the modal space reads:

$$y(t) = y_j(0) \varepsilon^{-\frac{b_j}{a_j} t} + \frac{f_j}{a_j} \int_0^t \varepsilon^{-\frac{b_j}{a_j}(t-\tau)} \sigma(\tau) d\tau, \tag{7.29}$$

where $y_j(0)$ is the jth element of initial values vector $\mathbf{y}(0)$; yielding the displacement
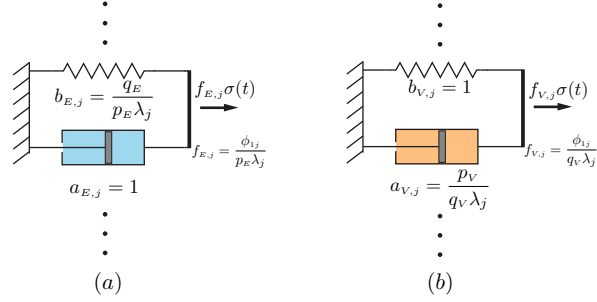
Figure 7.7: The jth EV (a) and VE (b) Kelvin-Voigt resolution model in modal space. Courtesy of [57].

vector of the fractance as:

$$\boldsymbol{\gamma}(t) = \mathbf{B}^{-\frac{1}{2}} \boldsymbol{\Phi} \mathbf{y}(t). \tag{7.30}$$

The displacement at the top of the mechanical model is provided by the first element of the solution vector $\boldsymbol{\gamma}(t)$. In order to separate such a displacement from the rest of the response, one can make use of the vector $\mathbf{v}$ defined before, i.e. $\gamma(t) = \mathbf{v}^T \boldsymbol{\gamma}(t)$.

Inspection of (7.25) shows that the dynamical system in the modal space is described by a set of decoupled, linear, one-degree of freedom system with different relaxation times τ_j. Such a consideration shows that the continuous spectrum relaxation function of FHM may be properly discretized in a set of spectral rows corresponding to relaxation times τ_j, $(j = 1, 2, \ldots, n, \ldots)$.

The capability of the model may be shown for EV and VE forced by a constant force $\sigma(t) = \sigma_0 = U(t)$. The solution of generic Kelvin-Voigt for a quiescent system at its starting time (i.e. the initial conditions are zero for each layer) in modal space reads as follows:

$$y_j(t) = f_j \sigma_0 \left(1 - \varepsilon^{-\frac{b_j}{a_j} t} \right)$$

In particular, Figure 7.8a shows the influence of the number of layer n (using $\beta = 0.4$ and $\Delta z = 0.001$). Figure 7.8b shows the influence of Δz (using $\beta = 0.4$ and $n = 500$). It may be observed that as soon as more layers are considered the solution converges towards the exact expression of a fractional integral. At last, the exact and discrete solutions are compared for several values of β studying both EV case ($n = 1500$, $\Delta z = 0.001$) and VE case ($n = 1500$, $\Delta z = 0.02$), as depicted in Figure 7.8c and Figure 7.8d respectively. It is interesting to note that the predicted

238

response for VE needs a lower discretization step to match the exact one.

The mechanical model presented yields a power-law creep function and that the discretized model involves a discretized time spectrum. In this regard we may consider that FHM as a continuum counterpart of 1D linearly independent n degree of freedom system with decaying stiffness and viscosity. This behavior will be used in Section 5 to address bone hereditary response.

(a) Influence of the number of layers n

(b) Influence of discretization parameter Δz

(c) Discrete solution for creep test (EV model)

(d) Discrete solution for creep test (VE model)
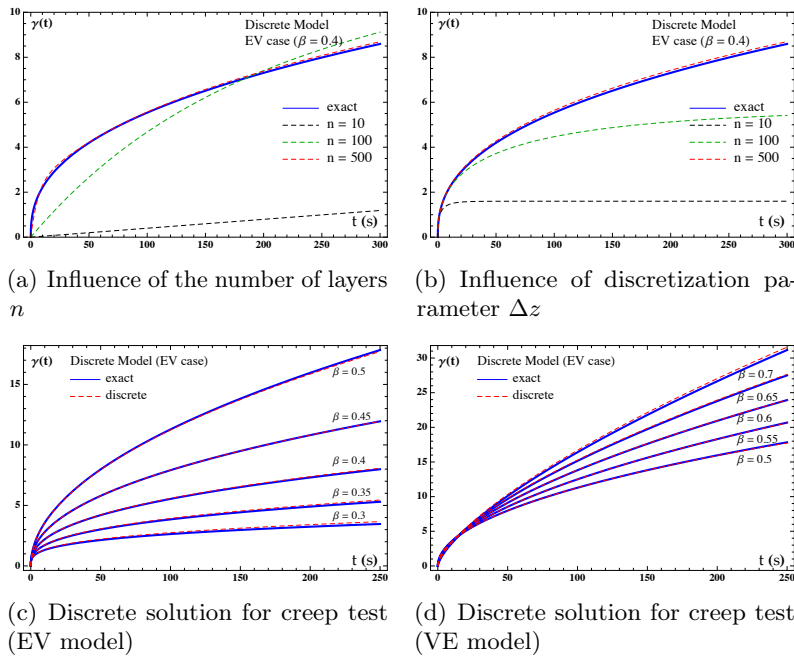
Figure 7.8: The influence of parameters on discrete solution and its match with exact values for several values of β ($\eta_0 = 1$, $G_0 = 1$, $\sigma_0 = 1$, $\gamma_0 = 0$). Courtesy of [57].

7.4 Power-law hereditariness of fractal models of bones

The mechanical picture of power-law hereditariness of FHM that showed Section 7.3 does not correspond to the material organization of bone.

In this Section it will be provided a fractal geometrical model of material specimen that corresponds to a power-law creep/relaxation function. A relation among the fractal geometric dimension of the material specimen and the exponent of the power-law is obtained. Details about fractal geometry and fractal dimension has been reported in Appendix B.

To this aim let us consider a material specimen of length measure L_0 and squared cross section of side length b_0 at the macroscopic observation scale. Let us assume, moreover, that material specimen involves several, self-similar, scale-dependent microstructures that appear with the refinement of the observation scale. Each microstructure is constituted by a bundle of longitudinal fibers of length $L_j = L_0/\varepsilon_j$, with ε_j the resolution factor, $j = 1, 2, ...$ the resolution level, and $\Delta\varepsilon$ the resolution interval. Let us assume that the the cross-sectional area measure of the self-similar microstructure is scale-invariant and that it presents more and more details with the refinement of the observation scale. As a consequence, more and more detailed cross-section is present for the microstrucure observed for the ε_{j+1} resolution with respect to the microstructure appearing at the ε_j scale.

The requirement of self-similarity, scale-invariance measure in conjunction with the presence of more details of the microstructured cross-section yields that it must belong to a more general class of geometrical sets with respect to the Euclidean objects. An example of such class are the lacunar-type fractal sets. In Figure 7.9 we reported the geometrical architecture of a Sierpinski carpet, a specific precursor of fractals of side b_0. According to the definition of fractal dimension and fractal measure, the Sierpinski carpet has measure equal to $b_0^d/\Gamma(d-1)$, with $1 \le d = \frac{\log(8)}{\log(3)} \le 2$ which denotes the anomalous Hausdorff dimension. The case $d = 2$ corresponds to the well-known Euclidean set with measure b_0^2. As we increase the observation scale of a fractal $\varepsilon_j = j\Delta\varepsilon$, where $j = 1, 2, \ldots$ and $\Delta\varepsilon$ is the resolution interval, the fractal cross-section shows a smaller self-similar geometrical architecture still maintaining the same overall measure of the fractal cross-section area $b_0^d/\Gamma(d-1)$. In this context, as we refine the resolution scale of a factor ε_j to observe the jth microstructure, we identify geometric elements with measure $(b/\varepsilon_j)^d = b_0^d\varepsilon_j^{-d}/\Gamma(d-1)$.

It is assumed that the microstructure fibers are composed by a two-phase material: i) a purely elastic, Hookean solid phase with Young modulus E_0 and; ii) a purely viscous, Newtonian fluid phase with viscosity coefficient η_0. Let us assume that the dense space around singular points of the fractal support is occupied by the viscous phase, whereas the pores of the cross-sections are filled by the elastic phase. Since the cross-section of the material specimen possesses anomalous dimension, a scale-dependent damping coefficient c_j and stiffness of the jth microstructure, is involved. Indeed, as we refine the observation scale of factor ε_j and we measure the cross-section area at this new resolution, we must rescale the length measure of

a factor ε_j^{-d} to maintain the same overall measure. This geometrical consideration yields that the scaling law of stiffness and dampig coefficients of the material read (see [62] for details):

$$c_j = \frac{\eta_d b_0^d \varepsilon_j^{-d}}{L_j \Gamma(d-1)} = \frac{\eta_0}{L_0} \frac{b_0^d \varepsilon_j^{1-d}}{\Gamma(1-d)} \tag{7.31a}$$

$$k_j = \frac{E_d}{L_0} b_0^d \frac{\varepsilon_j^{1-d}}{\Gamma(d)} = \frac{E_0}{L_0} \frac{b_0^d \varepsilon_j^{1-d}}{\Gamma(1-d)} \tag{7.31b}$$

where $\eta_d = \eta_0 b^{2-d} \Gamma(d-1)/\Gamma(1-d)$ and $E_d = E_0 b^{2-d} \Gamma(d-1)/\Gamma(1-d)$ is the anomalous viscosity coefficient.
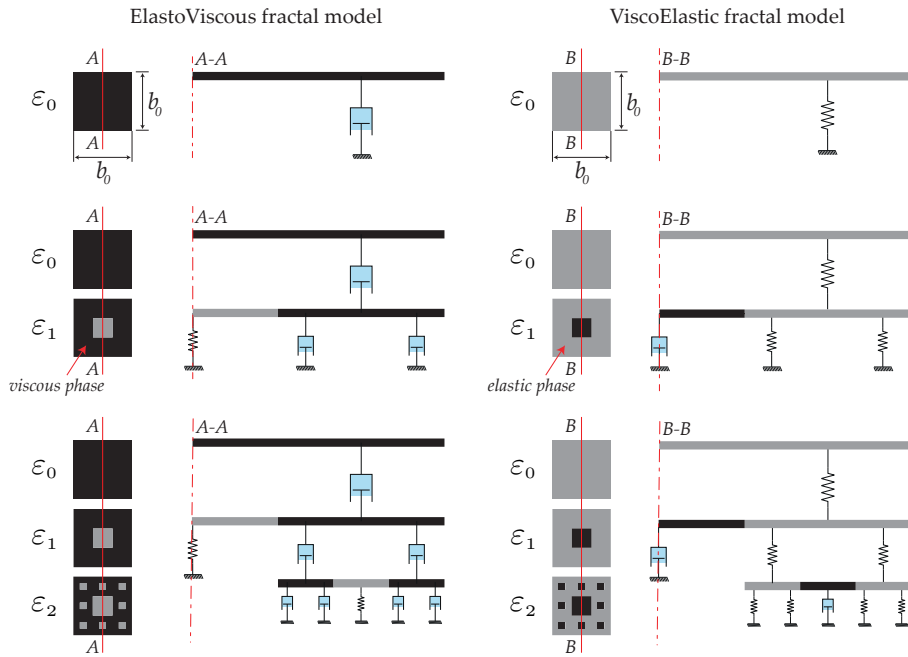
Figure 7.9: Fractal mechanical representation of the elastic and viscous phase of the material microstructure. Courtesy of [57].

The presence of a material microstructure that is maintained, as we refine the observation scale, togheter with a new microstructure appearing at smaller scales involves a connection among the different microstructures as observed by

241

the mechanical fractance in Figure 7.9. To this aim we reported in Figure 7.9 the micromechanical fractal tree corresponding to section A-A of the Sierpinsky carpet modelling the EV and VE Material, respectively. The elastic (for VE material), as well as the viscous (for EV material), phase are distributed among scales in a self-similar fashion, filling pores with an Hookean or Newtonian material, respectively.

It must be remarked that, as we consider the presence of self-similar microstructures appearing at different observation scales, still maintaining previously observed microstructures, is not corresponding to the classical mechanical discussions on fractal sets. Indeed the introduced material model is not equivalent to the analysis of a fractal-like solid that involves, instead different microstructures at different scales without any interaction among the scales.

The kinematic degrees of freedom of the microstructure observed at different scales are defined as u_j and, in this regard, the mechanical fractance is fully equivalent to a mechanical hierarchical assembly of viscous dashpots with damping coefficients c_j externally restrained by linear springs with stiffness coefficients k_j as reported in Figure 7.10:

The balance of linear momentum involves contributions from the $j-1$ and $j+1$ observation scales and, the system of differential equation ruling the time-evolution of the microstructure displacements may be written as:

$$
\begin{aligned}
F &= c_1 \left(\dot{u}_1 - \dot{u}_2 \right) + k_1 u_1 \\
c_1 \frac{(\dot{u}_1 - \dot{u}_2)}{\Delta \varepsilon} &= c_2 \frac{(\dot{u}_2 - \dot{u}_3)}{\Delta \varepsilon} + k_2 u_2 \Delta \varepsilon \\
c_2 \frac{(\dot{u}_2 - \dot{u}_3)}{\Delta \varepsilon} &= c_3 \frac{(\dot{u}_3 - \dot{u}_4)}{\Delta \varepsilon} + k_3 u_3 \Delta \varepsilon \\
&\vdots \\
c_{j-1} \frac{(\dot{u}_{j-1} - \dot{u}_j)}{\Delta \varepsilon} &= c_j \frac{(\dot{u}_j - \dot{u}_{j+1})}{\Delta \varepsilon} + k_j u_j \Delta \varepsilon \\
&\vdots
\end{aligned}
\tag{7.32}
$$

The use of the Laplace transform allows for solving the system reported in (7.32) in the following form:

$$
\tilde{u}_1(s) = \frac{\tilde{F}(s)}{k_1} \frac{1}{f_1} - \frac{\tilde{\tau}_1 \tilde{\tau}_2}{f_2} - \frac{\tilde{\tau}_2 \tilde{\tau}_3}{f_3} - \cdots \frac{\tilde{\tau}_{j-1} \, \tilde{\tau}_j}{f_j} - \cdots
\tag{7.33}
$$

where the symbol denoting the continued fractions was used (see Appendix C for more details). In (7.33) we defined the quantities $\tilde{\tau}_j = s \, \overline{c}_j / \overline{k}_j$, $f_j = 1 + r_j + \tilde{\tau}_j$ and $r_j = s \, \overline{c}_{j-1} / \overline{k}_j$ in order to get a compact form of the expression, where $\overline{k}_j = k_j \Delta \varepsilon$
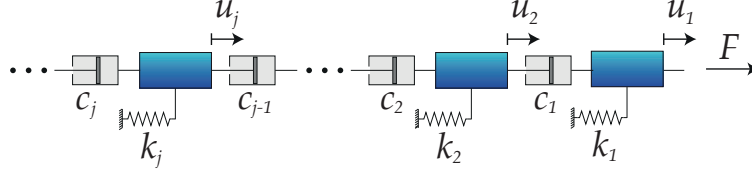
Figure 7.10: The mechanical hierarchy of the microstructure at the jth observation scale. Courtesy of [57].

and $\bar{c}_j = c_j/\Delta\varepsilon$. Moreover, the quantity $\tilde{\tau}_j$ represent the relaxation time at the jth observation scale. The substitution in (7.32) of the stiffness k_j and the viscosity c_j using (**??**) and (**??**), respectively, and replacing Δz with $\Delta\varepsilon$ yields the following differential equation as $\Delta\varepsilon \to 0$:

$$\frac{E_0}{\Gamma(1-d)}\varepsilon^{1-d}u(\varepsilon,t) = \frac{\partial}{\partial\varepsilon}\left[\frac{\eta_0}{\Gamma(1-d)}\varepsilon^{1-d}\frac{\partial\dot{u}(\varepsilon,t)}{\partial\varepsilon}\right] \tag{7.34}$$

with boundary conditions stated as:

$$u(\infty,t) = 0 \tag{7.35a}$$

$$F = \lim_{\varepsilon\to 0}\frac{\eta_0}{\Gamma(1-d)}b^d\frac{\partial\dot{u}}{\partial\varepsilon}\varepsilon^{1-d}, \tag{7.35b}$$

(see Sect. IV in [62] for an analog derivation). The observation of ((7.34),(7.35)) shows that assuming $\alpha = d - 1$, the solution for $\varepsilon \to 0$ yields a displacement-force rheological relation as:

$$F_0 = C_\beta\left(\mathrm{D}_{0^+}^\beta u\right)(t) \tag{7.36}$$

with a relation among the decaying coefficient β, the proportionality coefficient C_β and the fractal dimension of the cross-section area that reads:

$$\beta = \frac{(1-\alpha)}{2} = \frac{(2-d)}{2}, \qquad C_\beta = \frac{G_0\Gamma(\frac{2-d}{2})}{\Gamma(d)\Gamma(d/2)2^{d-1}}\left(\tau_E(\alpha)\right)^{\frac{(2-d)}{2}} \tag{7.37}$$

with $\tau_E(\alpha) = -\frac{\eta_0}{G_0}\frac{\Gamma(d-1)}{\Gamma(1-d)}$. We observe that, as $d = 2$, the Euclidean dimension of the cross-section yields a perfectly elastic material. In case $d = 1$, instead a fractional hereditary material at critical state, that is with exponent $\beta = 1/2$, is obtained.

The case involving VE material, i.e. with $1/2 \leq \beta \leq 1$ may be dealt with similar arguments yielding a relation among the power-law exponent and the fractal

dimension as $\beta = d/2$. More details about the fractal representation of material hereditariness will be reported in a forthcoming paper [63].

It is interesting to observe that by introducing a fractal geometric description of the microstructure of material specimen, a relation among the power-law exponent of creep/relaxation function and the fractal dimension of the geometric cross-section may be obtained.

As the relation among Hausdorff dimension and power-law exponent has been established the application may be devoted to a fractal model of the bone tissue hereditariness. Indeed in Figure 7.11 c we reported the Hausdorff dimension of a rat femural cross-section trabecular structure at resolution scales $(cm - \mu m)$.

The fractal dimension have been obtained, by an isthological specimen of bone tissue of a bone head after a period in fornaline for 24 hours. Bone specimen have been then decalcified in EDTA with an acid tampon and, furthermore reconditioning have been performed with Phosphate Buffered Saline (PBS). The specimen have been also immersed in alchoolical solutions with different concentrations, left in xilene solution, and immersed in paraffine at 60 °C for two hours.

The observation of the prepared bone tissue specimen have been performed on an optical microscope after coloration of the bone marrow with emathossiline-eosin and observed in the range from 10x to 40x with a Leica DM 5000 B with camera CCD Leica 3000 F as in Figure 7.11a. The observed images have been then recomposed to cover the entire rat femoural head and the evaluation of the fractal dimension of the bone head has been performed on a binary image conversion as in Figure 7.11b). The fractal dimension have been obtained by means of the box-counting method (see Appendix B for more details) obtaining, for the different specimen analized, fractal dimension in the range $\Delta_r = 1.70 - 1.83$. A representation of the fractal dimension has been reported in the Log-Log representation in Figure 7.11c

With the estimated values of Hausdorff dimension Δ_r we may conclude that the cross-sectional area of a bone head is not Euclidean and, by recalling previous arguments, a relation among the fractal dimension and the creep/relaxation exponent may be provided (with $\Delta_r = 1.83$) as $\beta = (2 - d)/2 = (2 - \Delta_r)/2 = 0.085$. This value is very close to the estimated one for β, obtained from macroscopic mechanical experimental tests as reported in Section 7.1 on different bone tissues specimens.

However, it may be observed that the bone tissue has a hierarchical self-organization and that, at different resolution scales, different geometric structures may be observed [122]. Indeed, bones are not true fractal since they do not posses a self-similar organization at every resolution scale and, therefore, a fractal model of bone tissue may be only a rough approximation.

In this regard, we observe that the lack of self-similarity of real bone is limited

244

(a)   (b)   (c)
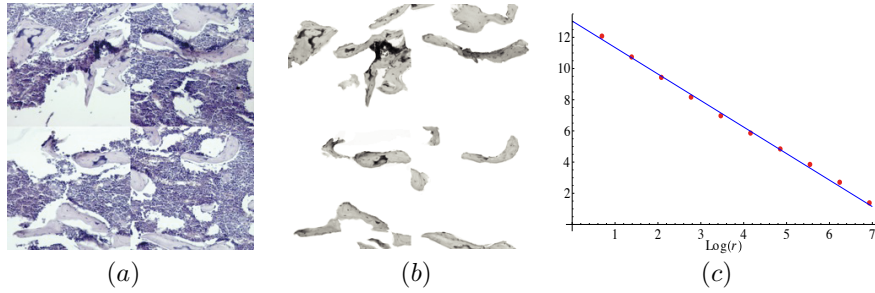
Figure 7.11: (a) High resolution image of a cross-section of a health rat bone proximis femural epiphisis after chemical treatment (as deffatting). (b) Image elaboration oriented to highlight the resistant section. (c) Evaluation of the fractal dimension using the box-counting method. Courtesy of [57].

to the difference among observed hierarchic levels of bone tissue (see Figure 7.12). However, for each element of the hierarchy a specific value of the fractal dimension

lamellae   collagen fibers   collagen fibrils
(10 μm)   (1 μm)   (100 nm)
(a)   (b)   (c)
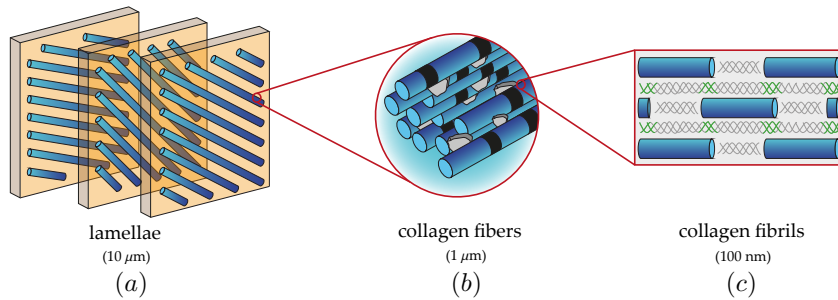
Figure 7.12: (a) Bone Lamellae scale. (b) Collagen fibers scale. (c) Collagen fibrils scale. Courtesy of [57].

Δ_k, with $k = 1, 2, \ldots, N$ (N represents the number of level of the hierarchy), may be identified. As we observe that for each level of the hierarchy an elastic and a viscous phase exists and more details in their separation may be obtained increasing the resolution scale, within the range of the observed hierarchical structure a relation as $\beta_k = (2 - \Delta_k)/2$ may be provided. In this case a model involving linear combinations of power-laws with $C_{\beta_1} t^{\beta_1} + C_{\beta_2} t^{\beta_2} + \ldots$ may be build providing a better estimate of creep and relaxation functions. Details about this possibility to model material behavior will be reported elsewhere.

245

It is interesting to observe that the FHM model with a single power-law with exponent $\overline{\beta}$ may represent the creep/relaxation of a multiple hierarchic fractal geometry with averaged dimension $\overline{\Delta} = \left(\sum_{k=1}^{N} p_k \Delta_k \right) / N$ with $0 \le \beta_k \le 1$ and $p_k, \, k = 1, 2, ..., N$ weighting coefficients $0 \le p_k \le 1$ useful to provide the influences of the jth scale to the overall hereditariness of material specimen. In this latter case the value of the exponent of the power-law creep/relaxation may be obtained as $\overline{\beta} = (2 - \overline{d})/2$.

7.5   Remarks

In this Chapter, a hierarchic fractal model to describe bone hereditariness has been introduced. Indeed, experimental data of stress relaxation or creep functions obtained by compressive/tensile tests have been proved to be fit by power-law with real exponent $0 \le \beta \le 1$. The rheological behavior of the material has therefore been obtained, using the Boltzmann-Volterra superposition principle, in terms of real order integrals and derivatives (fractional-order calculus). It has been also shown that the power-laws describing creep/relaxation of bone tissue may be obtained introducing a fractal description of bone cross-section and the Hausdorff dimension of the fractal geometry is then related to the exponent of the power-law.

The presence of a power-law with $0 < \beta \le 1/2$ has been justified with a mechanical model represented by a Newtonian viscous material resting on a bed of independent spring [62]. The presence of such mechanical model, however, is not observed in bone tissue and, henceforth a fractal description of bone cross-section has been introduced. In this regard it has been shown that the specimen cross-section at any level of hierarchy has a non-Euclidean dimension. As it is assumed that this dimension is identical at several observation scale of the bone, as in fractal set, a relation among the the power-law and the fractal dimension has been found.

References

[1]   A. Abdel-Wahab, K. Alam, and V. Silberschmidt. "Analysis of anisotropic viscoelastoplastic properties of cortical bone tissues". *Journal of The Mechanical Behavior of Biomedical Materials* 4 (2011), pp. 807–820 (cit. on pp. 226, 228, 229).

[23] E. H. Burger. "Bone Mechanics Handbook". Ed. by S. C. Cowin. Second Edition. New York: CRC Pres, 2001. Chap. Experiments on cell mechanosensitivity: bone cells as mechanical engineers (cit. on p. 225).

[33] S. C. Cowin. "Bone poroelasticity". *Journal of Biomechanics* 32 (1999), pp. 217–238 (cit. on p. 226).

[34] S. C. Cowin and S. B. Doty. *Tissue Mechanics*. New York: Springer, 2007 (cit. on p. 227).

[35] S. C. Cowin, L. Moss-Salentijn, and M. L. e Moss. "Candidates for the mechanosensory system in bone". *Journal of Biomechanical Engineering* 113.2 (1992), pp. 191–197 (cit. on p. 225).

[40] G. Del Piero and L. Deseri. "On the concepts of state and free energy in linear viscoelasticity." *Archive for Rational Mechanics and Analysis* 138 (1997), pp. 1–35 (cit. on pp. 165, 168, 169, 194, 195, 198, 201, 230).

[45] L. Deseri, M. J. Golden, and M. Fabrizio. "The Concept of a Minimal State in Viscoelasticity: New Free Energies and Applications to PDEs." *Archive for Rational Mechanics and Analysis* 181 (2006), pp. 43–96 (cit. on p. 230).

[49] L. Deseri and D. R. Owen. "Toward a field theory for elastic bodies undergoing disarrangements". *Journal of Elasticity* 70.I (2003), pp. 197–236 (cit. on pp. 37, 226).

[50] L. Deseri and D. R. Owen. "Submacroscopically Stable Equilibria of Elastic Bodies Undergoing Disarrangements and Dissipation". *Mathematics and Mechanics of Solids* 15.6 (2010), pp. 611–638 (cit. on pp. 37, 154, 226).

[51] L. Deseri and D. R. Owen. "Moving interfaces that separate loose and compact phases of elastic aggregates: a mechanism for drastic reduction or increase in macroscopic deformation". *Continuum Mechanics and Thermodynamics* 25 (2012), pp. 311–341. DOI: `10.1007/s00161-012-0260-y` (cit. on pp. 37, 226).

247

[57] L. Deseri et al. "Power-law hereditariness of hierarchical fractal bones". *International Journal for Numerical Methods in Biomedical Engineering* 29.12 (2013), pp. 1338–1360 (cit. on pp. v, 5, 6, 227, 228, 230, 233, 234, 238, 239, 241, 243, 245).

[60] M. Di Paola, F. P. Pinnola, and M. Zingales. "A discrete mechanical model of fractional hereditary materials". *Meccanica* (Jan. 2013). DOI: `DOI10.1007/s11012-012-9685-4` (cit. on pp. 194, 234).

[61] M. Di Paola, F. Pinnola, and M. Zingales. "Fractional differential equations and related exact mechanical models". *Computers and Mathematics with Applications* In press (2012) (cit. on pp. 230, 234).

[62] M. Di Paola and M. Zingales. "Exact mechanical models of fractional hereditary materials". *Journal of Rheology* 56.5 (2012), pp. 983–1004 (cit. on pp. 194, 196, 208, 209, 212, 216, 218, 219, 226, 230–232, 241, 243, 246).

[63] M. Di Paola and M. Zingales. "Fractal bodies hereditariness: The power-laws". *Journal of Rheology* (submitted) (cit. on p. 244).

[74] C. Friedrich. "Relaxation and retardation functions of the Maxwell model with fractional derivatives". *Rheologica Acta* 30.2 (1991), pp. 151–158 (cit. on p. 230).

[75] C. Friedrich. "Mechanical stress relaxation in polymers: Fractional integral model versus fractional differential model". *Non-Newtonian Fluid Mechanics* 46 (1993), pp. 307–314 (cit. on p. 230).

[76] C. Friedrich and H. Braun. "Linear viscoelastic behaviour of complex polymeric materials: A fractional mode representation". *Colloid & Polymer Science* 272 (1994), pp. 1536–1546 (cit. on p. 230).

[82] A. Gautieri et al. "Hierarchical Structure and Nanomechanics of Collagen Microfibrils from the Atomistic Scale Up". *American Chemical Society Nano Letters* 11 (2011), pp. 757–766 (cit. on p. 227).

[98] C. Hellmich, D. Celundov, and F. J. Ulm. "Multiporoelasticity of hierarchically structured materials: micromechanical foundations and application to bone." *Journal of Engineering Mechanics* 135.5 (2009), pp. 382–394 (cit. on p. 226).

[99]   C. Hellmich and F. Ulm. "Microporodynamics of Bones: Prediction of the "Frenkel-Biot" Slow Compressional Wave". *Journal of Engineering Mechanics* 131.9 (Sept. 2005), pp. 918–927 (cit. on p. 226).

[100]   C. Hellmich and F. J. Ulm. "Drained and undrained poroelastic properties of healthy and pathological bone: a poro-micromechanical investigation." *Transport in Porous Media* 58 (2005), pp. 243–268 (cit. on p. 226).

[122]   R. Lakes. "Materials with structural hierarchy". *Nature* 361 (1993), pp. 511–515 (cit. on pp. vii, 6, 226, 244).

[136]   F. Mainardi. *Fractional Calculus and Waves in Linear Viscoelasticity.* Imperial College Press, 2010 (cit. on pp. 194, 195, 226).

[143]   T. J. Martin and E. Seeman. "Bone remodelling: its local regulation and the emergence of bone fragility". *Best Practice & Research Clinical Endocrinology & Metabolism* 22.5 (2008), pp. 701–722 (cit. on p. 225).

[145]   K. McDonald et al. "Development of a multi-scale finite element model of the osteoporotic lumbar vertebral body for the investigation of apparent level vertebra mechanics and micro-level trabecular mechanics". *Medical Engineering & Physics* 32 (2010), pp. 653–661 (cit. on p. 226).

[149]   E. F. Morgan, H. H. Bayraktar, and T. M. Keaveny. "Trabecular bone modulus–density relationships depend on anatomic site". *Journal of Biomechanics* 36 (2003), pp. 897–904 (cit. on p. 227).

[168]   P. Pivonka et al. "Model structure and control of bone remodeling: A theoretical study". *Bone* 43 (2008), pp. 249–263 (cit. on pp. 225, 226).

[169]   I. Podlubny. *Fractional Differential Equation.* Academic, New York, 1998 (cit. on pp. 167, 178, 182, 226, 257, 259–261).

[170]   A. A. Poundarik et al. "Dilatational band formation in bone". *PNAS* (2012), pp. 19178–19183. DOI: `www.pnas.org/cgi/doi/10.1073/pnas.1201513109` (cit. on p. 227).

[173]   V. Quaglini, V. La Russa, and S. Corneo. "Nonlinear stress relaxation of trabecular bone". *Mechanics Research Communications* 36 (2009), pp. 275–283 (cit. on pp. 194, 226, 228, 229).

[183]   S. G. Samko, A. A. Kilbas, and O. I. Marichev. *Fractional Integrals and Derivatives. Theory and Applications.* Londn - New York: Gordon & Breach Science Publishers, 1987 (cit. on pp. 197, 200, 201, 204, 219, 226, 257, 258, 260).

[185]   G. Scott Blair. "The role of psychophysics in rheology". *Journal of Colloid Science* 2 (1947), pp. 21–32 (cit. on pp. 5, 193, 230).

[192]   M. S. Stein et al. "Bone size and mechanics at the femoral diaphysis across age and sex". *Journal of Biomechanics* 31 (1998), pp. 1101–1110 (cit. on p. 226).

[196]   J. S. Thomsen et al. "Stochastic simulation of vertebral trabecular bone remodeling". *Bone* 15.6 (1994), pp. 655–666 (cit. on p. 225).

[203]   Y. Wang et al. "Experimental study on the viscoelastic properties of cancellous bone of the os calcaneus, os lunatum and os capitalum]". *Journal of Biomedical Engineering* 20.3 (Sept. 2003), pp. 434–438 (cit. on pp. 226, 228, 229).

[204]   H. J. Werner et al. "The loss of stiffness as osteoporosis progresses". *Medical Engineering & Physics* 18.7 (1996), pp. 601–606 (cit. on p. 226).

Conclusion

The main result obtained in this Thesis is the novel constitutive model presented in Chapter 2. The analysis of the cell membrane behavior has allowed for extrapolating three main contributions to the Helmholtz free energy: (1) diffusion of receptors and transporters embedded in the lipid membrane; (2) conformational changes of the receptors; (3) membrane elasticity. As widely done in literature, the areal stretch J, defined as the inverse of the thick stretching, has been employed as coarse-grained parameter. Moreover, a proper conformational field η has been introduced. First of all, a proper energetics has been constructed based on experimental data and pragmatical observations. A dependence on temperature and adhesive properties have been taken into account for developing a reliable model. The total energy has been finally derived by coupling the energy of receptor-ligand bonds, the energy due to loss of diffusional entropy of the activated GPRCs, and the newly deduced energy due to conformational changes in the transmembranal (TM) domains in the current configuration. This energy has allowed for determining the chemical potential of the receptor-ligand compound through the variational derivative. Beside this, the interplay between TM conformational changes and lateral pressure of the lipid membrane against such TMs has been introduced and compared with the one calculated by accounting for the work done by the lateral pressure. Thank to this comparison, a relationship between the conformational field, the mechanical field (interpreted as either the thickness change or the areal change) and the distribution of the compound receptor-ligand has been found. In order to get more insights into this newly constitutive relationship, a deeper parametric analysis has been done for characterizing the unknown quantities arisen during the study (namely C, A, a).

In Chapter 3 the balanced configurations of the membrane in the set of equilibria have been sought. This has be done with special regard to an existing experiments involving HTR-8/SVneo cells and β2AR. Diffusive phenomena, both in time and space, have been considered and a proper chemo-mechanical coupling has been introduced through the kinetics of ligand bindings. The model has been numerically tested in Chapter 4. At first, it has been assumed that diffusive phenomena and

mechanical equilibrium would be independent, while later the full coupled problem has been faced. These two approaches have given rise to two different numerical schemes, called Double Step (DS) and Double Update (DU), respectively.

The analysis of the resulting constitutive equations among conformational field, receptor density and areal stretch has shown that the reason why ligand-GPRCs compounds prefer to live on lipid rafts is the consequence of the interplay between the work performed by the lateral pressure and the need of TMs to change their conformation during ligand binding. Moreover, the results are strengthened by the numerical results obtained by means of numerical simulations. The analytic model presented and discussed in this Thesis is able, for the first time in literature at the best of the Writer's knowledge, to predict that the field $X = \xi(x,t)/\xi_0$ of active receptors is higher where higher values of $H = h/h_0$ are encountered, i.e. where formation of rafts happens, confirming the findings by Nobel Prize 2012 Kobilka [117] and Lefkovitz [127].

Because of the characteristic double-well energy, lipid membranes can also experience material instability. This topic has been analyzed in Chapter 5, both in the linear and viscoelastic framework, by employing a linearization of the energy around an unstable configuration. A flat prismatic membrane with constant thickness has been assumed as reference configuration. The value of the thickness is chosen in such a way the initial homogeneous stretch lies in the unstable region of the energy (i.e. the spinoidal zone of the local stress). This occurrence allows for studying the set of equilibria by introducing a small perturbation. By assuming two sets of boundary conditions, it has been shown that this perturbation drives the nucleation of bifurcated shapes, forcing the separation of the phases and determining natural lipid ordering. First this occurrence has been studied in the asymptotic elastic case. By employing the variational principle, it has been shown that the bifurcated modes appear to be oscillatory, with periods larger than the reference thickness of the bilayer. Beside this, the viscoelastic behavior of lipid membrane has been taken into account through their exhibited power-law in-plane viscosity. As in the elastic case, the set of equilibria has been sought by a variational principle, in order to find the minimum of the energy in the class of synchronous perturbations. The resulting Euler-Lagrange equation is a Fractional Order PDE yielding a non-classical eigenvalue problem. The strategy employed for solving the fractional PDE is the separation of variables, then the mode (spatial dependence) and transfer (time dependence) functions are determined. It has been shown that the characteristic modes of the viscoelastic case, namely ζ^2, are still oscillatory, and appear to be amplified by a factor (k^2) with respect to the elastic counterpart. The time-dependent part of the differential equation is a non classical fractional eigenvalue problem, and leads to an anomalous time long-tail of the

252

response. The ratio of (dimensionless) generalized local and nonlocal moduli drives this amplification, and it has been shown that the viscoelastic case is characterized by a larger (if compared with the elastic case) range os stretches at which instabilities (namely bifurcations) can occur. The time decay is strongly influenced by the factor k^2 and, in turn, is by local and local modulus. In Figure 5.8 has been shown the specific case in which the same power-law describes both the local and the nonlocal response. All the other cases are studied in Figure 5.9, where both the real and imaginary part of the transfer function are shown, revealing always the occurrence of a fading memory in time.

The treatise presented in Chapter 6 is strongly motivated by the revitalized interest on the hereditariness of biological and bioinspired substructured materials exhibiting macroscopic power-law behavior. The aim of the discussion is to frame the study of Fractional Hereditary Material in a proper framework. In order to achieve this result, first of all the stress and the strain response are mathematically characterized in the broader functional setting of strains in SBV_{loc}. It has been shown how the very long-tail memory of prestressed FHM can be studied by means of power-law hereditariness. Starting from the notion of state for general linear viscoelastic materials, it has been found a new relationship for the class of the equivalent past strain histories in terms of the Caputo fractional derivative. A simplifies analysis has been considered for deriving the explicit expression of the state variable, i.e. the residual stress living in the material after a prescribed past history of arbitrary duration. Two rheological models, composed by proper arrangement of springs and dashpots, for modeling the FHMs have been presented. A direct connection between the microstress along the depth of the model and the arising macrostress has been established, and it has been shown that it can be expressed in terms of the Caputo fractional derivative of the macroscopic strain history. It is worth noting that the imposed strain history is not known *a priori*. It has been shown that the use of the balance of linear momentum justifies the equality between macrostresses, and a relationship between macro and micro stress has been derived in terms of fractional operators.

Among several biological structures owing the properties above, a special attention must be paid to mineralized biological tissues like bones, tendons and ligaments, because of their importance in biomedical engineering. The aim of Chapter 7 has been to face this problem in the advanced framework of fractal geometry and fractional-order calculus. These tools allow for employing fractional derivatives (i.e. convolution integral having power-law kernel) for describing the relaxation and creep functions as hereditary features. In the case of a bone, this function is well described by power-law function, and well justified by assuming

a fractal scaling of the cross-section. The presence of both a purely elastic and a purely viscous phase can be modeled as a proper arrangement of spring an dashpots. The use of a proper self-repetition of these devices at the microlevel captures the arising anomalous scaling properties, and it has be shown to be natural the presence of fractional-differentiation order relationships. In order to construct a solid base for these observations, several experiments found in literature have been analyzed and it has been shown that a relation among the fractional-order derivation index and the fractal dimension of bone model there exist. It is worth noting that the value of fractal dimension computed is very close to the value obtained from the analysis of the experimental tests.

Part III

Appendices

Appendix A

Basic concepts on Fractional Calculus

Fractional calculus may be considered the extension of the ordinary differential calculus to non-integer powers of derivation orders (e.g. see [169, 183]). In this Appendix we address some basic notions about this mathematical tool.

The Euler-Gamma function $\Gamma(z)$ may be considered as the generalization of the factorial function since, as z assumes integer values as $\Gamma(z+1) = z!$ and it is defined as the result of the integral as follows:

$$\Gamma(z) = \int_0^\infty e^{-x} x^{z-1} dx. \tag{A.1}$$

The Riemann-Liouville fractional integrals and derivatives with $0 < \beta < 1$ of functions defined on the entire real axis $\mathbb{R}$ have the following forms:

$$\left(\mathrm{I}_+^\beta f \right)(t) = \frac{1}{\Gamma(\beta)} \int_{-\infty}^t \frac{f(\tau)}{(t-\tau)^{1-\beta}} d\tau \tag{A.2a}$$

$$\left(\mathrm{D}_+^\beta f \right)(t) = \frac{1}{\Gamma(1-\beta)} \frac{d}{dt} \int_{-\infty}^t \frac{f(\tau)}{(t-\tau)^\beta} d\tau. \tag{A.2b}$$

The Riemann-Liouville fractional integrals and derivatives with $0 < \beta < 1$ of functions defined over intervals of the real axis, namely $f(t)$ such that $t \in [a, b] \subset \mathbb{R}$,

have the following forms:

$$\left(I_a^\beta f \right)(t) = \frac{1}{\Gamma(\beta)} \int_a^t \frac{f(\tau)}{(t-\tau)^{1-\beta}} d\tau \tag{A.3a}$$

$$\left(D_a^\beta f \right)(t) = \frac{f(a)}{\Gamma(1-\beta)(t-a)^\beta} + \frac{1}{\Gamma(1-\beta)} \int_a^t \frac{f'(\tau)}{(t-\tau)^\beta} d\tau. \tag{A.3b}$$

The relation (A.3b) is a direct consequence of Corollary of Lemma 2.1 in [183] (p.32). Beside Riemann-Liouville fractional operators defined above, another class of fractional derivative that is often used in the context of fractional viscoelasticity is represented by Caputo fractional derivatives defined as:

$$\left(_C D_{a^+}^\beta f \right)(t) := I_{a^+}^{m-\beta} \left(D_{a^+}^m f \right)(t) \quad m-1 < \beta < m \tag{A.4}$$

and whenever $0 < \beta < 1$ it reads as follows:

$$\left(_C D_{a^+}^\beta f \right)(t) = \frac{1}{\Gamma(1-\beta)} \int_a^t \frac{f'(\tau)}{(t-\tau)^\beta} d\tau. \tag{A.5}$$

A closer analysis of (A.3b) and (A.5) shows that Caputo fractional derivative coincides with the integral part of the Riemann-Liouville fractional derivative in bounded domain. Moreover, the definition in (A.4) implies that the function $f(t)$ has to be absolutely integrable of order m (e.g. in (A.5) the order is $m = 1$). Whenever $f(a) = 0$ Caputo and Riemann-Liouville fractional derivatives coalesce.

Similar considerations hold true also for Caputo and Riemann-Liouville fractional derivatives defined on the entire real axis. Caputo fractional derivatives may be consider as the interpolation among the well-known, integer-order derivatives, operating over functions $f(\circ)$ that belong to the class of Lebesgue integrable functions $(f(\circ) \in L^1)$ as a consequence, they are very useful in the mathematical description of complex system evolution.

A.1 Notes on fractional calculus and Fourier transforms

It is worth introducing integral transforms for fractional operators. In this regard, it is useful to recall that the Laplace and Fourier integral transforms are defined as

follows:

$$\mathcal{L}[f(t)] = \int_0^\infty f(t)\mathrm{e}^{-st}dt \tag{A.6a}$$

$$\mathcal{F}[f(t)] = \int_{-\infty}^{+\infty} f(t)\mathrm{e}^{-i\omega t}dt. \tag{A.6b}$$

Similarly to classical calculus, the Laplace integral transform $\mathcal{L}(\circ)$ is defined in the following forms:

$$\mathcal{L}\left[\left(\mathrm{D}_{0+}^\beta f\right)(t)\right] = s^\beta \mathcal{L}[f(t)] = s^\beta \tilde{f}(s) \tag{A.7a}$$

$$\mathcal{L}\left[\left(\mathrm{I}_{0+}^\beta f\right)(t)\right] = s^{-\beta}\mathcal{L}[f(t)] = s^{-\beta}\tilde{f}(s). \tag{A.7b}$$

In the same way, the Fourier integral transform $\mathcal{F}(\circ)$ assumes the following forms:

$$\mathcal{F}\left[\left(\mathrm{D}_+^\beta f\right)(t)\right] = (-i\omega)^\beta \mathcal{F}[f(t)] = (-i\omega)^\beta \hat{f}(\omega) \tag{A.8a}$$

$$\mathcal{F}\left[\left(\mathrm{I}_+^\beta f\right)(t)\right] = (-i\omega)^{-\beta}\mathcal{F}[f(t)] = (-\omega)^{-\beta}\hat{f}(\omega). \tag{A.8b}$$

Obviously, the right-Fourier Transform of both Caputo fractional derivative and Riemann-Liouville fractional integral are defined as follows:

$$\mathcal{F}_+\left\{\left(\mathrm{I}_+^\beta f\right)(\circ)\right\}(\omega) = (-i\omega)^{-\beta}\hat{f}_+(\omega) \tag{A.9a}$$

$$\mathcal{F}_+\left\{\left({}_C\mathrm{D}_+^\beta f\right)(\circ)\right\}(\omega) = (-i\omega)^\beta \hat{f}_+(\omega) \tag{A.9b}$$

where

$$\mathcal{F}_+\left\{f(\circ)\right\}(\omega) := \hat{f}_+(\omega) := \int_0^\infty f(t)\mathrm{e}^{-i\omega t}dt. \tag{A.10}$$

These mathematical tools may be very useful to solve systems of fractional differential equations, which *appear more and more frequently in various research areas and engineering applications* [169]. The research on electrical circuits (especially on semiintegrating circuits) was one of the first fields of application of differential equations of fractional order [159]. As example we consider the following differential equation of order $\beta = 1/2$:

$$\left(\mathrm{D}_0^{\frac{1}{2}}f\right)(t) + af(t) = 0 \tag{A.11}$$

with the following initial condition

$$C = \left[\left(\mathrm{D}_0^{-\frac{1}{2}} f \right)(t) \right]_{t=0}. \tag{A.12}$$

The use of the Laplace integral transform allows for writing the solution in the Laplace domain as follows:

$$\tilde{f}(s) = \frac{C}{s^{1/2} + a}. \tag{A.13}$$

Whenever the time domain is restored, the solution has the following form:

$$f(t) = Ct^{-\frac{1}{2}} E_{\frac{1}{2}, \frac{1}{2}} \left(-a\sqrt{t} \right) \tag{A.14}$$

where $E_{\alpha, \beta}(z)$ is the Mittag-Leffler function, defined as follows:

$$E_{\alpha, \beta}(z) = \sum_{k=0}^{\infty} \frac{z^k}{\Gamma(\alpha k + \beta)} \qquad \alpha > 0 \ , \ \beta > 0. \tag{A.15}$$

In his textbook, Podlubny showed [169] (p. 21) an expression for the Laplace transform can be found in the following form

$$\mathcal{L} \left[t^{\frac{k-1}{2}} E_{\frac{1}{2}, \frac{1}{2}}^{(k)} \left(a \pm \sqrt{t} \right) \right] = \frac{k!}{\left(\sqrt{s} \mp a \right)^{k+1}} \tag{A.16}$$

where the notation $^{(k)}$ denotes the kth-derivative. We recognize that in (A.13) $k = 0$, henceforth the time domain solution reads has the form reported in (A.14).

The curious reader can find several procedures and examples on differential equations of fractional order in the complete textbooks by Podlubny [169] and Samko [183].

A.2 Solution of a Fractional Ordinary Differential Equation

As an example, let us solve the following Fractional Order Differential Equation:

$$a \mathcal{D}_t^{\alpha} h(t) + b \, h(t) = c, \tag{A.17}$$

and denote with h_0 the initial condition. The Laplace Transform of (A.17) takes the form:

$$(ap^\alpha + b) H = \frac{c}{p} + a\, p^{\alpha-1} h_0 \tag{A.18}$$

For the sake of convenience, we distinguish to contribution to the transformed function H:

$$\begin{cases} H_1 = \dfrac{c\, p^{-1}}{ap^\alpha + b} = \dfrac{c}{a} \dfrac{p^{-1}}{p^\alpha + \frac{b}{a}} \\[3mm] H_2 = \dfrac{a\, p^{\alpha-1} h_0}{ap^\alpha + b} = h_0 \dfrac{a}{a} \dfrac{p^{-1}}{p^\alpha + \frac{b}{a}} \end{cases} \tag{A.19}$$

Let us recall the *Laplace Transform of the Mittag-Leffler function* (see Podlubny pag 21, eqn 1.80 [169])

$$\mathcal{L}\left\{ t^{\alpha^* k + \beta^* - 1} E_{\alpha^*,\beta^*}^{(k^*)}\left(\pm a^* t^{\alpha^*} \right) ; t; p \right\} = \frac{k^*!\, p^{\alpha^* - \beta^*}}{\left(p^{\alpha^*} \mp a^* \right)^{k^*+1}}, \tag{A.20}$$

and look for the Anti-transform of each term. For the first term we get recognize that $k^* = 0$, $\alpha^* - \beta^* = -1$, $\alpha^* = \alpha$, $a^* = b/a$, then:

$$h_1(t) = \frac{c}{a} t^\alpha E_{\alpha,\alpha+1}\left(-\frac{b}{a} t^\alpha \right), \tag{A.21}$$

whereas for the second one $k^* = 0$, $\alpha^* - \beta^* = \alpha - 1$, $\alpha^* = \alpha$, $a^* = b/a$, then

$$h_2(t) = h_0 t^0 E_{\alpha,1}\left(-\frac{b}{a} t^\alpha \right). \tag{A.22}$$

Finally, the sought solution takes the following form:

$$h(t) = \frac{c}{a} t^\alpha E_{\alpha,\alpha+1}\left(-\frac{b}{a} t^\alpha \right) + h_0 E_\alpha\left(-\frac{b}{a} t^\alpha \right). \tag{A.23}$$

Appendix B

Basic concepts on Fractal Geometry

The *fractal geometry* (from the Latin word *fractus*, extremely divided) was introduced by Mandelbrot [140] at the end of the seventies in order to give scholars a new mathematical tool to describe *real* objects. The notions stated by Mandelbrot have spread in several field of research, such as chaos and financial theories [124, 141]

The particular property of the fractal objects is the self-similarity. This property means, roughly speaking, that the object may be defined as the union of smaller, self-similar copies of itself. Such a property of fractal objects may also be used to define fractals by means of self-similar transformations of the parent object. This feature has to be understood rigorously for mathematical fractals only, whereas it has to be interpreted in a statistical sense for real objects.

The measure of fractal objects as well as their dimension are the main differences with respect to their Euclidean description. The classical Euclidean objects are characterized by *integer* dimension which identifies the degrees of freedom of the object in the related Euclidean space. On the contrary, the dimension of the fractal objects is different from one of the Euclidean space which encloses them; whenever the dimension of the fractal object is greater than the one of the Euclidean space it is defined *lacunar*, otherwise it is *invasive*.

Several authors [69] tried to provide a mathematical definition of fractal dimensions. The most used definitions have been addressed by Mandelbrot [140], Hausdorff and Besikovitch [95] and Minkowski [147]. The first is related to the invariance property under change of observation scale of fractal objects, whereas the latter ones depend on the coverage density of fractal object by Euclidean covers.

The Mandelbrot's dimension Δ is strictly related to the Mandelbrot's fundamental relation as follows:

$$Nr^{\Delta} = L_0^{\Delta} \quad \implies \quad \Delta = \frac{\log N}{\log \frac{L_0}{r}} \tag{B.1}$$

where N is the number of self-similar copies when the observation scale changes, L_0 is the length of the parent object and r is the length of the ruler.

In order to define the Hausdorff-Besikovitch dimension, it is worth to introduce the concept of Hausdorff-measure. Let U be a non-empty set enclosed in $\mathbb{R}^n$. The diameter of this set is defined as the greater distance between two any points belonging to it, i.e. $|U| = \sup\{|x - y| : x, y \in U\}$. The δ-cover of a fractal subset F depends on the parameter δ as follows:

$$F \subset \bigcup_{i=1}^{\infty} U_i \quad |U|_i \leq \delta \tag{B.2}$$

where δ represents the greater diameter allowed. Let α be a non-negative real number. For all $\delta \geq 0$, the Hausdorff measure is defined in the following form:

$$\mathcal{H}_{\delta}^{\alpha} = \lim_{\delta \to 0} \inf \left\{ \sum_{i=1}^{\infty} |U|_i^{\alpha} : |U|_i \text{ is a } \delta\text{-cover of } F \right\}. \tag{B.3}$$

The value of the limit defined in (B.3) is either 0 or ∞, except for a specific

Figure B.1: The Hausdroff-Besikovitch dimension of a fractal object $\mathcal{H}^{\alpha}(F)$.
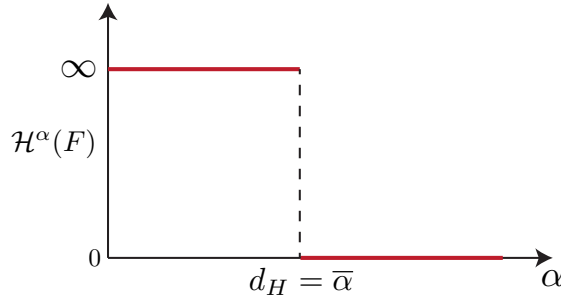
choice of $\overline{\alpha}$ in correspondence to which the curve $\mathcal{H}^{\alpha}(F)$ have a jump (see Figure B.1). The Hausdorff-Besikovitch dimension d_H of a fractal object F is defined as the smaller value of α such that the Hausdorff measure of F has zero value

or, equivalently, the greater value of α such that the Hausdorff measure of F has infinite value :

$$d_H(F) = \overline{\alpha} = \sup\{\alpha : \mathcal{H}^\alpha(F) = \infty\} = \inf\{\alpha : \mathcal{H}^\alpha(F) = 0\}. \qquad \text{(B.4)}$$

The Hausdorff dimension is an integer number for the Euclidean objects whereas it is a real number for the fractal ones.

The last definition of dimension uses the covering definition by Minkowski [140] and it was studied by Bouligand [20] and Kolomogorov [69]. The observer selects a proper coverage box (e.g. a range, a square and a cube for 1D, 2D and 3D Euclidean spaces respectively) and computes how many objects need to completely cover the fractal object when the amplitude of the cover decreases. The computation of the slow of the best fitting straight-line in the bi-logarithmic plane allows for calculating the fractal dimension as follows:

$$d_{MB} = \lim_{\delta \to 0} \left[D - \frac{\log F(\delta)}{\log \delta} \right] \qquad \text{(B.5)}$$

where D is the dimension of the Euclidean space in which the object is enclosed, δ is the dimension of the cover and $F(\delta)$ is the overall coverage (union of all covers of the object). This procedure is the most used since it is easily enforced in numerical codes.

Appendix C

Fundamentals of Continued Fraction

The continued fractions give an exact mathematical representation of rational and irrational numbers. For instance, the exact representation of $67/29$ reads as:

$$\frac{67}{29} = 2 + \cfrac{1}{3 + \cfrac{2}{9}}. \tag{C.1}$$

The use of this powerful mathematical tool is strictly related to need to find a better mathematical representation of the decimal one. The *general* definition of continued fraction can be expressed in the following form:

$$f = b_0 + \cfrac{a_1}{b_1 + \cfrac{a_2}{b_2 + \cfrac{a_3}{b_3 + \ddots}}} \tag{C.2}$$

where a_n and b_n, namely the *elements* of the continued fraction, are complex numbers and $a_m \neq 0$ for all m. The numbers a_m and b_m are called m^{th} *partial numerator* and *partial denominator*. Whenever $a_m = 1$ for all m, equation (C.2) is defined *simple* continued fraction. A more convenient form for (C.2) can be written as follows:

$$f = b_0 + \frac{a_1}{b_1} + \frac{a_2}{b_2} + \frac{a_3}{b_3} + \dots . \tag{C.3}$$

Let $\{a_m\}_{m\in\mathbb{N}}$ and $\{b_m\}_{m\in\mathbb{N}}$ an ordered pair of complex numbers, where $\mathbb{N}_0$ and $\mathbb{N}$ are the set of the positive integer including or not the 0 respectively. It is possible to define a linear fractional transformation as follows:

$$s_0(w) := b_0 + w \qquad s_n(w) := \frac{a_n}{b_n + w} \qquad n = 1, 2, 3, \ldots \qquad \text{(C.4)}$$

$$S_0(w) := s_0(w) \qquad S_n(w) := S_{n-1}\left(s_n(w)\right) \qquad n = 1, 2, 3, \ldots \qquad \text{(C.5)}$$

The form assumed by (C.5) for a generic value of w is the following:

$$S_n(w) = b_0 + \cfrac{a_1}{b_1 + \cfrac{a_2}{b_2 + \cfrac{a_3}{b_3 + \cfrac{\ddots}{\cfrac{a_n}{b_n + w}}}}} \qquad \text{(C.6)}$$

Whenever the number f is rational the elements of the continued fraction coalesce with the Euclidean algorithm and they are finite; otherwise if f is irrational the continued fraction is composed by an infinite number of elements. The nth approximation of an irrational number can be written as follows:

$$f_n = b_0 + \frac{a_1}{b_1 +} \frac{a_2}{b_2 +} \frac{a_3}{b_3 +} \cdots + \frac{a_n}{b_n}. \qquad \text{(C.7)}$$

Every rational number has an essentially unique continued fraction representation.

The continued fraction have been used to give more accurate description of several mathematical functions (such as exponential, power-law, trigonometric, hyperbolic, error, Bessel functions and many other) and constants (Euler's number, Euler's constant, golden ratio and many other) and also in the eigen-analysis. The curious reader can find more details are deeply treated in the complete *Handbook of Continued Fractions for Special Function* [37].

Appendix D

Some Calculations

This Appendix is devoted to simply collect explicit calculations of some results presented in this Thesis.

D.1 Work done by lateral pressure

With respect to Figure 2.5, the profile of lateral pressure is approximated by the following (symmetric) piecewise function:

$$
\pi(\boldsymbol{x},\, z) := \begin{cases}
-p & 0 < z < \dfrac{h}{2} - \phi \\[2ex]
\dfrac{q}{\phi_L/4}\left[z - \left(\dfrac{h}{2} - \dfrac{\phi_L}{2}\right)\right] & \dfrac{h}{2} - \phi < z < \dfrac{h}{2} - \dfrac{\phi}{2} \\[2ex]
q - \dfrac{\bar{q}}{\phi_L/4}\left[z - \left(\dfrac{h}{2} - \dfrac{\phi_L}{4}\right)\right] & \dfrac{h}{2} - \dfrac{\phi}{2} < z < \dfrac{h}{2}
\end{cases}
$$

or equivalently bearing in mind that $\phi = \phi_L/2$:

$$
\pi(\boldsymbol{x},\, z) := \begin{cases}
-p & 0 < z < \dfrac{h}{2} - \dfrac{\phi_L}{2} \\[2ex]
\dfrac{q}{\phi_L/4}\left[z - \left(\dfrac{h}{2} - \dfrac{\phi_L}{2}\right)\right] & \dfrac{h}{2} - \dfrac{\phi_L}{2} < z < \dfrac{h}{2} - \dfrac{\phi_L}{4} \\[2ex]
q - \dfrac{\bar{q}}{\phi_L/4}\left[z - \left(\dfrac{h}{2} - \dfrac{\phi_L}{4}\right)\right] & \dfrac{h}{2} - \dfrac{\phi_L}{4} < z < \dfrac{h}{2}
\end{cases}
$$

269

where q denotes the value of the pressure arising between of the contrast of the lipid head against the domain of receptor protein, and p is the value of the pressure along the lipid tail arising fol self-balancing the pressure profile. Indeed, because of the force balance, the following relationship must hold:

$$2 \cdot p \left(\frac{h}{2} - \phi \right) = 4 \cdot \frac{q \cdot \phi/2}{2}.$$

This balance allows for finding a relationship between p and q in the form:

$$p = \frac{q}{2} \frac{\phi}{\frac{h}{2} - \phi} \quad \text{or} \quad p = \frac{q}{2} \frac{\phi_L}{h - \phi_L}.$$

Let now compute the work done by this lateral pressure:

$$\mathcal{W} = \pi \, d_s \, h \, \mathcal{W}^*$$

where $\mathcal{W}^*$ denotes the work done per unit of area. After setting

$$\theta = z - \left(\frac{h}{2} - \frac{\phi_L}{2} \right) \qquad \text{and} \qquad \theta' = z - \left(\frac{h}{2} - \frac{\phi_L}{4} \right)$$

the quantity $\mathcal{W}^*$ can be evaluated as follows:

$$\mathcal{W}^* = \int_{-h/2}^{+h/2} \pi(\boldsymbol{x}, z, t) \, J(\boldsymbol{x}, z, t) \, dz = 2 \int_0^{\frac{h}{2}} \pi(\boldsymbol{x}, z, t) \, J(\boldsymbol{x}, z, t) \, \mathrm{d}z$$

$$= 2 \left(- p \int_0^{\frac{h}{2} - \frac{\phi_L}{2}} J(\boldsymbol{x}, z, t) \, \mathrm{d}z + \underbrace{q \frac{4}{\phi_L} \int_0^{\frac{\phi_L}{4}} \theta \, \tilde{J}(\boldsymbol{x}, \theta, t) \, \mathrm{d}\theta}_{a} + \left(q \frac{\phi_L}{4} \right) + \right.$$

$$\left. - \underbrace{q \frac{4}{\phi_L} \int_0^{\frac{\phi_L}{4}} \theta' \, \hat{J}(\boldsymbol{x}, \theta', t) \, \mathrm{d}\theta'}_{a} \right)$$

$$\approx 2 \left[q \frac{4}{\phi_L} - p \int_0^{\frac{h}{2} - \frac{\phi_L}{2}} [J(\boldsymbol{x}, 0, t) + z \, J_z(\boldsymbol{x}, 0, t)] \, \mathrm{d}z \right]$$

$$= 2 \left[q \frac{4}{\phi_L} - p \left(\frac{h}{2} - \frac{\phi_L}{2} \right) J + 0 \right] = 2 \left[p \left(\frac{h}{2} - \frac{\phi_L}{2} \right) - p \left(\frac{h}{2} - \frac{\phi_L}{2} \right) J \right]$$

$$= p \left(h - \phi_L \right) \left(1 - J \right)$$

Finally, the work done the lateral pressure is computed as:

$$\mathcal{W} = \pi \, d_s \, h \, \mathcal{W}^* \approx \pi \, d_s \, h \, \bar{p} \, (h - \phi_L) \, (1 - J)$$

$$= \pi \, d_s \, \bar{p} \, h \, (h - \phi_L) \left(1 - \frac{h_0}{h} \right) = \pi \, d_s \underbrace{\bar{p} \, (h - \phi_L)}_{\bar{q}\phi_L/2} (h - h_0) = \frac{\pi \, d_s \, \bar{q} \, \phi_L}{2} (h - h_0) =$$

$$= \frac{\pi \, d_s \, \bar{q} \, \phi_L}{2} h_0 \left(\frac{1}{J} - 1 \right) = \frac{\pi \, d_s \, \bar{q} \, \phi_L}{2} h_0 \left(\frac{1}{J} - 1 \right)$$

Finally:

$$\mathcal{W} = \pi \, d_s \, \phi \, \bar{q} \, (h - h_0) \leq 0$$

Moreover, bearing in mind that the surface tension γ_{RL} is related to the lateral pressure as

$$q = \gamma_{RL}/d_s$$

where d_s denotes the diameter of a single receptor domain, a more compact relationship can be written as follows:

$$\mathcal{W} = \pi \, \phi \, \gamma_{RL} \, (h - h_0) \leq 0$$

D.2 Chemical Potential

Integration of (2.17) supplies the following result

$$-\xi \varphi_{CR} = \frac{\mathcal{W}(J)}{K_B T} \xi + d(J),$$

where the constant $d(J)$ must be determined. This is done by assuming that in reference state, denoted by the subscript 0, the value of the conformational field has zero-value. Hence, the constant is found as:

$$0 = \frac{\mathcal{W}(J)}{K_B T} \xi_0 + d(J) \implies d(J) = -\frac{\mathcal{W}(J)}{K_B T} \xi_0.$$

This result allows for obtaining a relationship for the conformational field in the form

$$-\varphi_{CR} = \frac{\mathcal{W}(J)}{K_B T} \left(1 - \frac{\xi_0}{\xi} \right)$$

A comparison of this result (reported in the main text as equation (2.19)) with the previous one obtained in (2.5) yields the following relationship:

$$-A \log\left(K\frac{\eta}{J}\right) = \frac{\mathcal{W}(J)}{K_B T}\left(1 - \frac{\xi_0}{\xi}\right)$$

$$\left(\frac{\xi}{\xi_0}\right)^{-1} = 1 + \frac{A\,K_B T}{\mathcal{W}}\log\left(K\frac{\eta}{J}\right) = 1 + \frac{A\,K_B T}{\pi d_s q \phi h_0 \left(\frac{1}{J} - 1\right)}\log\left(K\frac{\eta}{J}\right) =$$

$$= 1 + \frac{A\,K_B T}{\pi d_s q \phi h_0}\frac{J}{1 - J}\log\left(K\frac{\eta}{J}\right) = 1 - \frac{A\,K_B T}{\pi d_s q \phi h_0}\frac{J}{J - 1}\log\left(K\frac{\eta}{J}\right)$$

$$\left(\frac{\xi}{\xi_0}\right)^{-1} = 1 - \frac{C\,J}{J - 1}\ln\left(K\frac{\eta}{J}\right),$$

where

$$a := \frac{\pi h_0 \phi_L \gamma_{RL}}{K_B T}$$

$$C := \frac{K_B T\,A}{\pi h_0 \phi_L \gamma_{RL}} = \frac{A}{a}.$$

See Chapter 2.3 in the text for the strategy employed for determining the parameters C, A and a.

D.3 First variation of the energy functional

Let consider the one-dimensional energy functional in (3.38) written in term of the displacement field $u(x)$. Then, by consider a virtual perturbation δu, the first variation with respect the field variable reads as follows (note that the integration is done along the onedimensional domain Ω, and that the explicit differential dx is omitted for simplicity of writing, since it is clear that each term is function of x):

$$\delta\mathcal{E} = \int_\Omega \varphi\,\delta u' - \frac{1}{2}\left(\gamma' u''^2 \delta u' + 2\gamma u'' \delta u''\right) - \frac{S}{(1+u')^2}\delta u' - \left(\Sigma'\delta u + \Sigma\delta u' + \Gamma'\delta u' + \Gamma du''\right)$$

$$= \int_\Omega -\left(\gamma u'' + \Gamma\right)\delta u'' + \left(\varphi' - \frac{1}{2}\gamma' u''^2 - \frac{S}{(1+u')^2} - \Sigma - \Gamma'\right)\delta u' - \Sigma'\delta u$$

$$= -\left[\left(\gamma u'' + \Gamma\right)\delta u'\right]_{\partial\Omega} + \int_\Omega \underbrace{\left(\gamma u'' + \Gamma\right)'}_{\gamma' u'' \cdot u'' + \gamma u''' + \Gamma'}\,\delta u' +$$

$$+ \int_\Omega \left(\varphi' - \frac{1}{2}\gamma' u''^2 - \frac{S}{(1+u')^2} - \Sigma - \Gamma'\right)\delta u' - \Sigma'\delta u$$

$$= -\left[\left(\gamma u'' + \Gamma\right)\delta u'\right]_{\partial\Omega} + \int_\Omega \left(\underbrace{\varphi' + \frac{1}{2}\gamma' u''^2 + \gamma u''' - \frac{S}{(1+u')^2}}_{A} -\Sigma\right)\delta u' - \Sigma'\delta u$$

$$= -\left[\left(\gamma u'' + \Gamma\right)\delta u'\right]_{\partial\Omega} + \int_\Omega \left(A - \Sigma\right)\delta u' - \Sigma'\delta u$$

$$= -\left[\left(\gamma u'' + \Gamma\right)\delta u'\right]_{\partial\Omega} + \left[\left(A - \Sigma\right)\delta u\right]_{\partial\Omega} - \int_\Omega \left(A - \Sigma\right)'\delta u - \int_\Omega \Sigma'\delta u$$

$$= -\left[\left(\gamma u'' + \Gamma\right)\delta u'\right]_{\partial\Omega} + \left[\left(A - \Sigma\right)\delta u\right]_{\partial\Omega} - \int_\Omega A'\delta u$$

Finally, the Euler-Lagrange equation governing the equilibrium of the membrane is found as a fourth order differential equation in the form:

$$A' = \frac{d}{dx}\left(\varphi' + \frac{1}{2}\gamma' u''^2 + \gamma' u''' - \frac{S(x)}{(1+u')^2}\right)$$

$$= \varphi'' u'' + \frac{1}{2}\left(\gamma'' u'' \cdot u''^2 + 2\gamma' u'' u'''\right) + \gamma' u'' \cdot u''' + \gamma u'''' + \left(\frac{2S\,u''}{(1+u')^3} - \frac{S'}{(1+u')^2}\right)$$

$$= \gamma u'''' + 2\gamma' u'' u''' + \frac{1}{2}\gamma'' u''^3 + \varphi'' u'' + \left(\frac{2S\,u''}{(1+u')^3} - \frac{S'}{(1+u')^2}\right)$$

Appendix E

Matlab codes

This Appendix is devoted to collect all the code written for performing numerical simulations

E.1   Finite Differences

```matlab
function [D0,D1,D2,D3,D4,D5] = funFD1S(n,h)
% SPARSE MATRICES are employed
%
% n = mesh points
% h = discretization step
%
% D0 = function itself (identity)
% D1 = first derivative
% D2 = second derivative
% D3 = third derivative
% D4 = fourth derivative
%

d0 = ones(n,1);
d1 = ones(n-1,1);
d2 = ones(n-2,1);
d3 = ones(n-3,1);
%% == FUNCTION ==
D0 = speye(n);
```

```matlab
21  %% FIRST DERIVATIVE
22  D1 = (diag(d1,1) + diag(-d1,-1));
23  D1 = D1/2/h;
24
25  D1(1,1:3) = [-3/2 2 -1/2]/h;
26  D1(n,n-2:n) = [1/2 -2 3/2]/h;
27  D1 = sparse(D1);
28
29  %% SECOND DERIVATIVE
30  D2 = (diag(-2*d0) + diag(d1,1) + diag(d1,-1));
31  D2(1,1:4) = [2 -5 4 -1];
32  D2(n,n-3:n) = [-1 4 -5 2];
33  D2 = D2/h^2;
34  D2 = sparse(D2);
35
36  %% THIRD DERIVATIVE
37  D3 = diag(-d1,1) + diag(d1,-1) + ...
38      diag(d2/2,2) + diag(-d2/2,-2);
39  D3(1,1:5) = [-5/2 9 -12 7 -3/2];
40  D3(2,1:5) = [-3/2 5 -6 3 -1/2];
41  D3(n-1,n-4:n) = [1/2 -3 6 -5 3/2];
42  D3(n,n-4:n) = [3/2 -7 12 -9 5/2];
43  D3 = D3/h^3;
44  D3 = sparse(D3);
45
46  %% FOURTH DERIVATIVE
47  D4 = diag(6*d0) + ...
48      diag(-4*d1,1) + diag(-4*d1,-1) + ...
49      diag(d2,2) + diag(d2,-2);
50  D4(1,1:6) = [3 -14 26 -24 11 -2];
51  D4(2,1:6) = [2 -9 16 -14 6 -1];
52  D4(n-1,n-5:n) = [-1 6 -14 16 -9 2];
53  D4(n,n-5:n) = [-2 11 -24 26 -14 3];
54  D4 = D4/h^4;
55  D4 = sparse(D4);
56
57
58  %% FIFTH DERIVATIVE
59  D5 = diag(-5*d1/2,-1) + diag(5*d1/2,1) + ...
60      diag(2*d2,-2) + diag(-2*d2,2) + ...
61      diag(-d3/2,-3) + diag(d3/2,3);
62  D5(1,1:7) = [-7/2 20 -(95/2) 60 -(85/2) 16 -(5/2)];
63  D5(2,1:7) = [-(5/2), 14, -(65/2), 40, -(55/2), 10, -(3/2)];
```

276

```
64  D5(3,1:7) = [-(3/2), 8, -(35/2), 20, -(25/2), 4, -(1/2)];
65  D5(n-2,n-6:n) = [1/2, -4, 25/2, -20, 35/2, -8, 3/2];
66  D5(n-1,n-6:n) = [3/2, -10, 55/2, -40, 65/2, -14, 5/2];
67  D5(n,n-6:n) = [5/2, -16, 85/2, -60, 95/2, -20, 7/2];
68  D5 = D5/h^5;
69  D5 = sparse(D5);
```

As an example, see the following script. It is worth noting that some approximations arise at the boundaries (see Figure E.1) if the mesh is not fine enough.

```
1   %% SCRIPT: FINITE DIFFERENCE EXAMPLE
2   clc; clear; close all
3
4   %% exact function and its derivatives
5   syms x
6   u0 = sin(2*pi*x)/3 + exp(x);   %exact solution
7   u1 = diff(u0,1);
8   u2 = diff(u0,2);
9   u3 = diff(u0,3);
10  u4 = diff(u0,4);
11  u5 = diff(u0,5);
12
13  %% conversion to matlab function
14  u0 = matlabFunction(u0);
15  u1 = matlabFunction(u1);
16  u2 = matlabFunction(u2);
17  u3 = matlabFunction(u3);
18  u4 = matlabFunction(u4);
19  u5 = matlabFunction(u5);
20
21  %% mesh
22  xa = 0;
23  xb = 1;
24  nx = 30;
25  xmesh = linspace(xa,xb,nx)';
26  dx = xmesh(2)-xmesh(1);
27
28  %% compute Finite Difference Operators
29  [D0,D1,D2,D3,D4,D5] = funFD1S(nx,dx);
30
31  %% discrete function
32  U0 = u0(xmesh(:));
```

277

```matlab
33  U1 = D1*U0;
34  U2 = D2*U0;
35  U3 = D3*U0;
36  U4 = D4*U0;
37  U5 = D5*U0;
38
39  %% plot result
40  figure('Name','Result','Position',[200 500 800 800])
41  subplot(3,2,1)
42  hold on
43  plot(xmesh,u0(xmesh),'k')
44  plot(xmesh,U0,'ok','MarkerFaceColor','r','MarkerSize',5)
45  grid on
46  title('function')
47
48  subplot(3,2,2)
49  hold on
50  plot(xmesh,u1(xmesh),'k')
51  plot(xmesh,U1,'ok','MarkerFaceColor','r','MarkerSize',5)
52  grid on
53  title('first derivative')
54
55  subplot(3,2,3)
56  hold on
57  plot(xmesh,u2(xmesh),'k')
58  plot(xmesh,U2,'ok','MarkerFaceColor','r','MarkerSize',5)
59  grid on
60  title('second derivative')
61
62  subplot(3,2,4)
63  hold on
64  plot(xmesh,u3(xmesh),'k')
65  plot(xmesh,U3,'ok','MarkerFaceColor','r','MarkerSize',5)
66  grid on
67  title('third derivative')
68
69  subplot(3,2,5)
70  hold on
71  plot(xmesh,u4(xmesh),'k')
72  plot(xmesh,U4,'ok','MarkerFaceColor','r','MarkerSize',5)
73  grid on
74  title('fourth derivative')
75
```

278

```
76  subplot(3,2,6)
77  hold on
78  plot(xmesh,u5(xmesh),'k')
79  plot(xmesh,U5,'ok','MarkerFaceColor','r','MarkerSize',5)
80  grid on
81  title('fifth derivative')
```
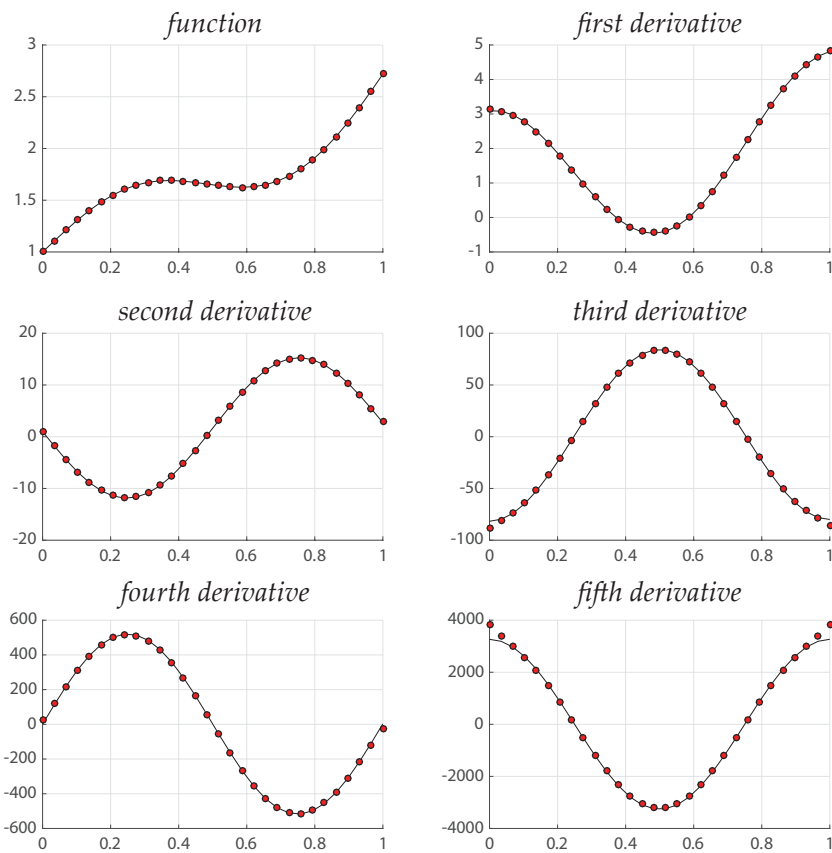

Figure E.1: Example: numerical computation of derivatives by means of Finite Difference Operators.

Bibliography

[1] A. Abdel-Wahab, K. Alam, and V. Silberschmidt. "Analysis of anisotropic viscoelastoplastic properties of cortical bone tissues". *Journal of The Mechanical Behavior of Biomedical Materials* 4 (2011), pp. 807–820 (cit. on pp. 226, 228, 229).

[2] R. Abrol and W. A. Goddard. "Extracellular and intracellular signaling". Ed. by J. A. Adams and K. K. Parker. Royal Society of Chemistry, 2011. Chap. G-protein-coupled receptors: conformational "gatekeepers" of transmembrane signal transduction and diversification (cit. on p. 2).

[3] A. Agrawal and D. Steigmann. "Coexistent Fluid-Phase Equilibria in Biomembranes with Bending Elasticity". *Journal of Elasticity* 93.1 (2008), pp. 63–80 (cit. on pp. 1, 4, 72).

[4] A. Agrawal and D. Steigmann. "Modeling protein-mediated morphology in biomembranes". *Biomechanics and Modeling in Mechanobiology* 8.5 (2009), pp. 371–379 (cit. on pp. 1, 4, 153).

[5] S. Akimov, P. Kuzmin, and Z. J. "An elastic theory for line tension at a boundary separating two lipid monolayer regions of different thickness". *Journal of Electroanalytical Chemistry* 564 (203), pp. 13–18 (cit. on pp. 4, 23).

[6] J. Allard et al. "Mechanical modulation of receptor-ligand interactions at cell-cell interfaces". *Biophysical Journal* 102 (2012), pp. 1–9 (cit. on p. 2).

[7]   G. Amendola, M. Fabrizio, and M. J. Golden. *Thermodynamics of materials with memory: Theory and applications*. ISBN: 978-1-4614-1691-3. Springer, 2002 (cit. on p. 194).

[8]   P. Ammann and R. Rizzoli. "Bone strength and its determinants". *Osteoporosis International* 14 (2003), S13–S18 (cit. on p. 6).

[9]   R. Bagley and P. Torvik. "Fractional Calculus - A different Approach to the Analysis of Viscoelastically Damped Structures". *The American Institute of Aeronautics and Astronautics Journal* 21.5 (1983), pp. 741–748 (cit. on pp. 194, 196).

[10]   R. Bagley and P. Torvik. "On the Fractional Calculus Model of Viscoelastic Behavior". *Journal of Rheology* 30.1 (1986), pp. 135–155 (cit. on pp. 194, 196).

[11]   T. Bartels et al. "Raftlike mixtures of sphingomyelin and cholesterol investigated by solid-state 2H NMR spectroscopy." *Journal of the American Chemical Society* 130 (2008), pp. 14521–32 (cit. on p. 22).

[12]   T. Baumgart, W. Webb, and S. Hess. "Imaging coexisting domains in biomembrane models coupling curvature and line tension". *Nature* 423.821Đ824 (2003) (cit. on pp. 1, 21).

[13]   T. Baumgart et al. "Membrane Elasticity in Giant Vesicles with Fluid Phase Coexistence". *Biophysical Journal* 89 (2005), pp. 1067–1080 (cit. on pp. 1, 4, 72).

[14]   M. Baumgärtel and H. H. Winter. "Interrelation between continuous and discrete relaxation time spectra". *Journal of Non-Newtonian Fluid Mechanics* 44 (1992), pp. 15–36 (cit. on p. 6).

[15]   H. Bermúdez, D. Hammer, and D. Discher. "Effect of Bilayer Thickness on Membrane Bending Rigidity". *Langmuir* 20 (2004), pp. 540–543 (cit. on pp. 1, 4).

[16]   R. Bhowmik et al. "Probing molecular interactions in bone biomaterials: Through molecular dynamics and Fourier transform infrared spectroscopy". *Materials Science and Engineering C* 27 (2007), pp. 352–371 (cit. on p. 6).

[17] C. Biondi et al. "Prostaglandin E2 inhibits proliferation and migration of HTR-8/SVneo cells, a human trophoblast-derived cell line". *Reproductive Biology and Endocrinology* 27.6-7 (2006), pp. 592–601 (cit. on p. 3).

[18] C. Biondi et al. "cAMP efflux from human trophoblast cell lines: a role for multidrug resistance protein (MRP) 1 transporter". *Molecular Human Reproduction* 16.7 (2010), pp. 481–91 (cit. on pp. 3, 63–66, 72, 74, 87).

[19] P. Biscari and F. Bisi. "Membrane-mediated interactions of rod-like inclusions". *The European Physical Journal E* 7 (2002), pp. 381–386 (cit. on pp. 1, 4).

[20] G. Bouligand. "Sur la notion d'ordre de mesure d'un ensemble plan". *Bulletin des Sciences Mathématiques* 53 (1929), pp. 185–192 (cit. on p. 265).

[21] S. Breuer and E. Onat. "On the determination of free energies in linear viscoelastic solids". *Zeitschrift für angewandte Mathematik und Physik* 15.2 (1964), pp. 184–191 (cit. on pp. 168–170).

[22] B. Brown, R. Ekins, and J. Albano. "Saturation assay for cyclic AMP using endogenous binding protein." *Advances in Cyclic Nucleotide Research* 2 (1972), pp. 25–40 (cit. on p. 63).

[23] E. H. Burger. "Bone Mechanics Handbook". Ed. by S. C. Cowin. Second Edition. New York: CRC Pres, 2001. Chap. Experiments on cell mechanosensitivity: bone cells as mechanical engineers (cit. on p. 225).

[24] P. Canham. "The minimum energy of bending as a possible explanation of the biconcave shape of the human red blood cell". *Journal of Theoretical Biology* 26 (1970), 61Ð80 (cit. on pp. 1, 4, 22).

[25] R. S. Cantor. "Lipid composition and the lateral pressure profile in bilayers". *Biophysical journal* 76 (1999), pp. 2625–2639. DOI: `10.1016/S0006-3495(99)77415-1` (cit. on p. 44).

[26] M. Caputo. *Elasticità e Dissipazione*. Bologna: Zanichelli, 1969 (cit. on p. 167).

[27]   L. Chen, M. Johnson, and R. Biltonen. "A Macroscopic Description of Lipid Bilayer Phase Transitions of Mixed-Chain Phosphatidylcholines: Chain-Length and Chain-Asymmetry Dependence". *Biophysical Journal* 80 (2001), pp. 254–270 (cit. on p. 4).

[28]   V. Cherezov et al. "High resolution crystal structure of an engineered human beta2-adrenergic G protein-coupled receptor". *Science* 318.5854 (2007), pp. 1258–65 (cit. on p. 2).

[29]   B. Chini and M. Parenti. "G-protein coupled receptors in lipid rafts and caveolae: how, when and why do they go there?" *Journal of Molecular Endocrinology* 32.2 (2004), pp. 325–38 (cit. on pp. 3, 4).

[30]   R. Choksi, M. Morandotti, and M. Veneroni. "Global minimizers for axisymmetric multiphase membranes". *arXiv preprint* (2012), p. 1204.6673 (cit. on p. 4).

[31]   B. Coleman and D. Newman. "On the rheology of cold drawing. I.Elastic Materials". *Journal of Polymer Science: Part B: Polymer Physics* 26 (1988), pp. 1801–1822 (cit. on pp. 27, 96).

[32]   B. Coleman and D. Newman. "On the rheology of cold drawing II. Viscoelastic materials". *Journal of Polymer Science: Part B: Polymer Physics* 30 (1992), pp. 25–47 (cit. on p. 194).

[33]   S. C. Cowin. "Bone poroelasticity". *Journal of Biomechanics* 32 (1999), pp. 217–238 (cit. on p. 226).

[34]   S. C. Cowin and S. B. Doty. *Tissue Mechanics.* New York: Springer, 2007 (cit. on p. 227).

[35]   S. C. Cowin, L. Moss-Salentijn, and M. L. e Moss. "Candidates for the mechanosensory system in bone". *Journal of Biomechanical Engineering* 113.2 (1992), pp. 191–197 (cit. on p. 225).

[36]   D. Craiem and R. L. Magin. "Fractional order models of viscoelasticity as an alternative in the analysis of red blood cell (RBC) membrane mechanics". *Physical Biology* 7.1 (2010), p. 13001 (cit. on p. 165).

[37]   A. Cuyt et al. *Handbook of Continued Fractions for Special Function.* Heidelberg: Springer, 2008 (cit. on p. 268).

[38] S. Das, A. Tian, and T. Baumgart. "Mechanical Stability of Micropipet-Aspirated Giant Vesicles with Fluid Phase Coexistence". *The Journal of Physical Chemistry B* 112.11625Ð11630 (2008) (cit. on pp. 1, 4, 72).

[39] G. Del Piero and L. Deseri. "On the analytic expression of the free energy in linear viscoelasticity". *Journal of Elasticity* 43 (1996), pp. 247–278 (cit. on pp. 165, 168–170).

[40] G. Del Piero and L. Deseri. "On the concepts of state and free energy in linear viscoelasticity." *Archive for Rational Mechanics and Analysis* 138 (1997), pp. 1–35 (cit. on pp. 165, 168, 169, 194, 195, 198, 201, 230).

[41] G. Del Piero and D. Owen. "Structured Deformations of Continua". *Archive for Rational Mechanics and Analysis* 124 (1993), pp. 99–155 (cit. on p. 37).

[42] G. Del Piero and D. Owen. "Integral-Gradient Formulae for Structured Deformations". *Archive for Rational Mechanics and Analysis* 131 (1995), pp. 121–138 (cit. on p. 37).

[43] L. Deseri, M. Di Paola, and M. Zingales. "Free energy and states of fractional-order hereditariness". *International Journal of Solids and Structures* 51 (2014), pp. 3156–3167 (cit. on pp. 165, 167, 169, 170).

[44] L. Deseri, G. Gentili, and M. Golden. "An Expression for the Minimal Free Energy in Linear Viscoelasticity". *Journal of Elasticity* 54 (1999), pp. 141–185 (cit. on pp. 168, 194).

[45] L. Deseri, M. J. Golden, and M. Fabrizio. "The Concept of a Minimal State in Viscoelasticity: New Free Energies and Applications to PDEs." *Archive for Rational Mechanics and Analysis* 181 (2006), pp. 43–96 (cit. on p. 230).

[46] L. Deseri and M. Golden. "The Minimum Free Energy for Continuous Spectrum Materials." *SIAM Journal on Applied Mathematics* 67.3 (2007), pp. 869–892 (cit. on pp. 165, 168, 194).

[47]   L. Deseri, M. Golden, and M. Fabrizio. "The Concept of a Minimal State in Viscoelasticity: New Free Energies and Applications to PDEs". *Archive for Rational Mechanics and Analysis* 181 (2006), pp. 43–96 (cit. on pp. vi, 165, 168, 194, 195, 198, 201).

[48]   L. Deseri, G. Marcari, and G. Zurlo. "UNESCO". 2009. Chap. Thermodynamics (cit. on p. 44).

[49]   L. Deseri and D. R. Owen. "Toward a field theory for elastic bodies undergoing disarrangements". *Journal of Elasticity* 70.I (2003), pp. 197–236 (cit. on pp. 37, 226).

[50]   L. Deseri and D. R. Owen. "Submacroscopically Stable Equilibria of Elastic Bodies Undergoing Disarrangements and Dissipation". *Mathematics and Mechanics of Solids* 15.6 (2010), pp. 611–638 (cit. on pp. 37, 154, 226).

[51]   L. Deseri and D. R. Owen. "Moving interfaces that separate loose and compact phases of elastic aggregates: a mechanism for drastic reduction or increase in macroscopic deformation". *Continuum Mechanics and Thermodynamics* 25 (2012), pp. 311–341. DOI: 10.1007/s00161-012-0260-y (cit. on pp. 37, 226).

[52]   L. Deseri, M. Piccioni, and G. Zurlo. "Derivation of a new free energy for biological membranes". *Continuum Mechanics and Thermodynamics* 20.5 (2008), pp. 255–273. DOI: 10.1007/s00161-008-0081-1 (cit. on pp. iv, 1, 4, 23, 25, 26, 40, 153, 154, 168, 193).

[53]   L. Deseri and M. Zingales. "Constitutive Model of Hereditary Fluid Mosaic of Lipid Bilayers". *In preparation* (2015) (cit. on p. 154).

[54]   L. Deseri, M. Zingales, and P. Pollaci. "The State of Fractional Hereditary Materials (FHM)". *Discrete and Continuous Dynamical Systems B* 19.7 (2014), pp. 2065–2089 (cit. on pp. v, 5, 197, 202, 204, 208, 211, 217).

[55]   L. Deseri and G. Zurlo. "The stretching elasticity of biomembranes determines their line tension and bending rigidity". *Biomechanics and Modeling in Mechanobiology* 12 (2013), pp. 1233–1242. DOI: doi: 10.1007/s10237-013-0478-z (cit. on pp. iii, iv, 1, 4, 23–26, 30, 40, 72, 153, 154, 168, 193).

286

[56] L. Deseri et al. "Hereditary creep: state and free energy". *In preparation* () (cit. on p. 201).

[57] L. Deseri et al. "Power-law hereditariness of hierarchical fractal bones". *International Journal for Numerical Methods in Biomedical Engineering* 29.12 (2013), pp. 1338–1360 (cit. on pp. v, 5, 6, 227, 228, 230, 233, 234, 238, 239, 241, 243, 245).

[58] L. Deseri et al. "Fractional Hereditariness of Lipid Membranes: Instabilities and Linearized Evolution". *Journal of The Mechanical Behavior of Biomedical Materials* (2015) (cit. on pp. v, 163, 164, 166, 179–181, 183, 185).

[59] M. Deserno. "Fluid lipid membranes: From differential geometry to curvature stresses". *Chemistry and Physics of Lipids* 185 (2014), pp. 11–45 (cit. on pp. iii, 4, 22, 23, 72).

[60] M. Di Paola, F. P. Pinnola, and M. Zingales. "A discrete mechanical model of fractional hereditary materials". *Meccanica* (Jan. 2013). DOI: DOI10.1007/s11012-012-9685-4 (cit. on pp. 194, 234).

[61] M. Di Paola, F. Pinnola, and M. Zingales. "Fractional differential equations and related exact mechanical models". *Computers and Mathematics with Applications* In press (2012) (cit. on pp. 230, 234).

[62] M. Di Paola and M. Zingales. "Exact mechanical models of fractional hereditary materials". *Journal of Rheology* 56.5 (2012), pp. 983–1004 (cit. on pp. 194, 196, 208, 209, 212, 216, 218, 219, 226, 230–232, 241, 243, 246).

[63] M. Di Paola and M. Zingales. "Fractal bodies hereditariness: The power-laws". *Journal of Rheology* (submitted) (cit. on p. 244).

[64] M. T. Drake, S. K. Shenoy, and R. J. Lefkowitz. "Trafficking of G protein-coupled receptors". *Circulation Research* 99.6 (2006), pp. 570–582 (cit. on p. 3).

[65] J.-S. Duan et al. "Eigenvalue problems for fractional ordinary differential equations". *Chaos Solution Fract* 46 (2013), pp. 46–53 (cit. on p. 176).

[66] G. Espinosa et al. "Shear rheology of lipid monolayers and insights on membrane fluidity". *PNAS* 108.15 (2011), pp. 6008–6013. DOI: www.pnas.org/cgi/doi/10.1073/pnas.1018572108 (cit. on pp. v, 154, 165, 167).

[67] M. Fabrizio and M. J. Golden. "Minimum free energies for materials with finite memory". *Journal of Elasticity,* 72 (2003), pp. 121–143 (cit. on p. 194).

[68] M. Fabrizio and A. Morro. "Mathematical problems in linear viscoelasticity". *SIAM Philadelphia* (1992) (cit. on p. 194).

[69] K. Falkoner. *Fractal Geometry: Mathematical Foundetion and Application.* Chicester: John Wiley & Sons, 1990 (cit. on pp. 263, 265).

[70] M. Falkovitz et al. "Theory of periodic structures in lipid bilayer membranes". *PNAS* 79 (1982), pp. 3918–3921 (cit. on pp. 4, 25, 27).

[71] G. W. Feigenson. "Phase boundaries and biological membranes". *Annual Review of Biophysics and Biomolecular Structure* 36 (2007), pp. 63–77 (cit. on p. 22).

[72] D. Filmore. "It's a GPCR world". *Modern Drug Discovery (American Chemical Society)* (Nov. 2004), pp. 24–28 (cit. on p. 2).

[73] A. V. Finkelstein and J. Janin. "The price of lost freedom: entropy of bimolecular complex formation". *Protein Engineering* 3.1 (Oct. 1989), pp. 1–3. ISSN: 0269-2139. URL: http://www.ncbi.nlm.nih.gov/pubmed/2813338 (cit. on pp. 37, 40).

[74] C. Friedrich. "Relaxation and retardation functions of the Maxwell model with fractional derivatives". *Rheologica Acta* 30.2 (1991), pp. 151–158 (cit. on p. 230).

[75] C. Friedrich. "Mechanical stress relaxation in polymers: Fractional integral model versus fractional differential model". *Non-Newtonian Fluid Mechanics* 46 (1993), pp. 307–314 (cit. on p. 230).

[76] C. Friedrich and H. Braun. "Linear viscoelastic behaviour of complex polymeric materials: A fractional mode representation". *Colloid & Polymer Science* 272 (1994), pp. 1536–1546 (cit. on p. 230).

288

[77] A. P. G. Mishuris and E. Radi. "Steady-state propagation of a Mode III crack in couple stress elastic materials". *International Journal of Engineering Science* (2012), pp. 112–128 (cit. on p. 194).

[78] L. Galuppi and G. R. Carfagni. "Laminated beams with viscoelastic interlayer". *International Journal of Solids and Structures* 49 (2012), pp. 2637–2645 (cit. on p. 194).

[79] L. Galuppi and G. R. Carfagni. "The design of laminated glass under time-dependent loading". *International Journal of Mechanical Sciences* 68 (2013), pp. 67–75 (cit. on p. 194).

[80] H. Gao. "Application of fracture mechanics concepts to hierarchical biomechanics of bone and bone-like materials". *International Journal of Fracture* 138 (2006), pp. 101–137 (cit. on p. 6).

[81] H. Gao, W. Shi, and L. Freund. "Mechanics of receptor-mediated endocytosis". *PNAS* 102.27 (2005), pp. 9469–9474 (cit. on pp. 36, 115).

[82] A. Gautieri et al. "Hierarchical Structure and Nanomechanics of Collagen Microfibrils from the Atomistic Scale Up". *American Chemical Society Nano Letters* 11 (2011), pp. 757–766 (cit. on p. 227).

[83] A. Gemant. "A method of analyzing experimental results obtained from elasto-viscous bodies". *Physics* 7 (1936), pp. 311–317 (cit. on p. 194).

[84] G. Gentili. "Maximum recoverable work, minimum free energy and state space in linear viscoelasticity". *Quarterly of Applied Mathematics* 60 (2002), pp. 153–182 (cit. on p. 194).

[85] P. Ghanouni et al. "Functionally different agonists induce distinct conformations in the G protein coupling domain of the beta 2 adrenergic receptor". *The Journal of Biological Chemistry* 276.27 (2001), pp. 24433–6. (Cit. on pp. 3, 37).

[86] A. Gilman. "G proteins: transducers of receptor-generated signals". *Annual Review of Biochemistry* 56.1 (1987), pp. 615–49 (cit. on p. 2).

[87] C. Giorgi and A. Morro. "Viscoelastic solids with unbounded relaxation function". *Continuum Mechanics and Thermodynamics* 4 (1992), pp. 151–165 (cit. on p. 199).

289

[88]   R. Goldstein and S. Leibler. "Structural phase transitions of inter-
        acting membranes". *Physical Review Letters A* 40.2 (1989), pp. 1025–
        1035 (cit. on pp. 2, 4, 25, 27, 28, 72).

[89]   D. Graffi and M. Fabrizio. "Sulla nozione di stato per materiali
        viscoelastici di tipo "rate"". *Atti Accademia dei Lincei, Rendiconti di
        Fisica,* 83 (1989), pp. 201–208 (cit. on p. 194).

[90]   R. Guedes, J. Simoes, and J. Morais. "Viscoelastic behaviour and
        failure of bovine cancellous bone under constant strain rate." *Journal
        of Biomechanics* 39.1 (2006), pp. 49–60 (cit. on p. 6).

[91]   M. Gurtin, E. Fried, and L. Anand. *The Mechanics and Thermo-
        dynamics of Continua*. Cambridge University Press, 2009 (cit. on
        p. 44).

[92]   J. Hanna et al. "Decidual NK cells regulate key developmental
        processes at the human fetal-maternal interface". *Nature Medicine*
        12.1065-1074 (2006) (cit. on p. 3).

[93]   M. A. Hanson et al. "A specific cholesterol binding site is established
        by the 2.8 A structure of the human beta2-adrenergic receptor".
        Structure 16.6 (2008), pp. 897–905 (cit. on p. 2).

[94]   C. W. Harland, M. J. Bradley, and R. Parthasarathy. "Phospholipid
        bilayers are viscoelastic". *PNAS* 107.45 (2010), pp. 19146–19150. DOI:
        `doi:www.pnas.org/cgi/doi/10.1073/pnas.1010700107` (cit. on
        pp. 165, 167).

[95]   F. Hausdorff. "Dimension und äusseres Mass". *Mathematische Annalen*
        19.1-2 (1918), pp. 157–179 (cit. on p. 263).

[96]   W. Helfrich. "Elastic properties of lipid bilayers: theory and possible
        experiments". *Zeitschrift für Naturforschung C* 28.11 (1973), pp. 693–
        703 (cit. on pp. 1, 4, 22, 26).

[97]   C. Hellmich, J. F. Barthélémy, and L. Dormieux. "Mineral-collagen
        interactions in elasticity of bone ultrastructure - a continuum mi-
        cromechanics approach". *European Journal of Mechanics A/Solids*
        23 (2004), pp. 783–810 (cit. on p. 6).

[98] C. Hellmich, D. Celundov, and F. J. Ulm. "Multiporoelasticity of hierarchically structured materials: micromechanical foundations and application to bone." *Journal of Engineering Mechanics* 135.5 (2009), pp. 382–394 (cit. on p. 226).

[99] C. Hellmich and F. Ulm. "Microporodynamics of Bones: Prediction of the "Frenkel-Biot" Slow Compressional Wave". *Journal of Engineering Mechanics* 131.9 (Sept. 2005), pp. 918–927 (cit. on p. 226).

[100] C. Hellmich and F. J. Ulm. "Drained and undrained poroelastic properties of healthy and pathological bone: a poro-micromechanical investigation." *Transport in Porous Media* 58 (2005), pp. 243–268 (cit. on p. 226).

[101] J. Henderson and N. Kosmatov. "Eigenvalue comparison for Fractional Boundary Value Problems with the Caputo Derivative". *Fractional Calculus and Applied Analysis* 17.3 (2014), pp. 872–880 (cit. on p. 176).

[102] U. Hiden et al. "The first trimester human trophoblast cell line ACH-3P: A novel tool to study autocrine/paracrine regulatory loops of human trophoblast subpopulations – TNF-α stimulates MMP15 expression". *BMC Developmental Biology* 7.137 (2007). DOI: `doi:10.1186/1471-213X-7-137` (cit. on p. 42).

[103] A. M. Hofer and K. Lefkimmiatis. "Extracellular calcium and cAMP: second messengers as "third messenger"?" *Physiology (Bethesda)* 22 (2007), pp. 320–7 (cit. on p. 3).

[104] A. Honerkamp-Smith et al. "Line Tensions, Correlation Lengths, and Critical Exponents in Lipid Membranes Near Critical Points". *Biophysical Journal* 95 (2008), pp. 236–246 (cit. on pp. 1, 23).

[105] M. Hu, J. Briguglio, and M. Deserno. "Determining the Gaussian Curvature Modulus of Lipid Membranes in Simulations". *Biophysical Journal* 102.1403Ð1410 (2012) (cit. on p. 1).

[106] M. Hu, P. Diggins IV, and M. Deserno. "Determining the bending modulus of a lipid membrane by simulating buckling". *The Journal of Chemical Physics* 214110 (138). DOI: `doi:10.1063/1.4808077` (cit. on pp. 22, 23).

291

[107] A. Iglic, ed. *Advances in planar lipid bilayers and liposomes*. 1st Edition. Vol. 15. Academic Press, 2012 (cit. on pp. 1, 4).

[108] T. Iyo et al. "Anisotropic viscoelastic properties of cortical bone". *Journal of Biomechanics* 37 (2004), pp. 1433–1437 (cit. on p. 6).

[109] F. Jahnig. "Critical effects from lipid-protein interaction in membranes". *Biophysical Journal* 36 (1981), pp. 329–345 (cit. on pp. 4, 25).

[110] F. Jahnig. "What is the Surface Tension of a Lipid Bilayer Membrane?" *Biophysical Journal* 71 (1996), pp. 1348–1349 (cit. on p. 25).

[111] A. Jaishankar and G. H. McKinley. "Power-law rheology in the bulk and at the interface: quasi-properties and fractional constitutive equations". *Proceedings of the Royal Society A* 469 (2013). DOI: `doi: 10.1098/rspa.2012.0284` (cit. on pp. 5, 193, 194).

[112] J. Jenkins. "Static equilibrium configurations of a model red blood cell". *Journal of Mathematical Biology* 4.2 (1977), pp. 149–169 (cit. on pp. 1, 4).

[113] B. Ji and H. Gao. "Mechanical properties of nanostructure of biological materials". *Journal of Mechanics and Physics of Solids* 52 (2004), pp. 1963–1990 (cit. on p. vii).

[114] D. R. Katti, S. M. Pradhan, and K. S. Katti. "Directional dependence of hydroxyapatite-collagen interactions on mechanics of collagen". *Journal of Biomechanics* 43 (2010), pp. 1723–1730 (cit. on p. 6).

[115] A. A. Kilbas, H. M. Srivastava, and J. J. Trujillo. *Theory and Applications of Fractional Differential Equations*. Amsterdam, Netherlands: Elsevier, 2006 (cit. on p. 167).

[116] C.-I. Kim and D. J. Steigmann. "Distension-induced gradient capillarity in lipid membranes". *Continuum Mechanics and Thermodynamics* 27 (2015), pp. 609–621 (cit. on p. 4).

[117] B. Kobilka and X. Deupi. "Conformational complexity of G-protein-coupled receptors". *Trends in Pharmacological Sciences* 28.8 (2007), pp. 397–406 (cit. on pp. v, 3, 36, 48, 147, 252).

292

[118] A. N. Kolmogorov and S. V. Fomin. *Introductory Real Analysis*. Prentice Hall, 1970 (cit. on pp. 198, 199, 219).

[119] S. Komura and N. Shimokawa. "Tension-Induced Morphological Transition in Mixed Lipid Bilayers". *Langmuir* 22 (2006), pp. 6771–6774 (cit. on p. 27).

[120] S. Komura et al. "Lateral phase separation in mixtures of lipids and cholesterol". *Europhysics Letters* 67.2 (2004), p. 321 (cit. on pp. 4, 27, 72).

[121] G. M. L. Morini A. Piccolroaz and E. Radi. "On fracture criteria for a crack propagating in couple stress elastic materials". *International Journal of Engineering Science* 71 (2013), pp. 45–61 (cit. on p. 194).

[122] R. Lakes. "Materials with structural hierarchy". *Nature* 361 (1993), pp. 511–515 (cit. on pp. vii, 6, 226, 244).

[123] R. Lakes. *Viscoelastic materials*. Cambridge University Press, 2009 (cit. on p. 195).

[124] A. Lasota and M. Mackey. *Chaos, Fractals and Noise. Stochastic aspects of dynamics*. New York: Springer, 1994 (cit. on p. 263).

[125] P. Le Bouteiller and J. Tabiasco. "Killers become builders during pregnancy". *Nature Medicine* 12 (2006), pp. 991–992 (cit. on p. 3).

[126] A. G. Lee. *How lipids affect the activities of integral membrane proteins*. 2004. DOI: 10.1016/j.bbamem.2004.05.012 (cit. on pp. 42, 44).

[127] R. Lefkowitz. "Seven transmembrane receptors: something old, something new". *Acta Physiol* 190 (2007), pp. 9–19 (cit. on pp. v, 3, 36, 48, 147, 252).

[128] J. Li and J. Qi. "Spectral problems for fractional differential equations from nonlocal continuum mechanics". *Adv Differ Equ* 85 (2014), pp. 2–12 (cit. on p. 176).

[129] D. Lingwood and K. Simons. "Lipid rafts as a membrane-organizing principle". *Science* 327.5961 (2010), pp. 46–50 (cit. on p. 4).

[130] R. Lipowsky. "Budding of membranes induced by intramembrane domains". *Journal de Physique II France* 2 (1992), pp. 1825–1840 (cit. on pp. 4, 23, 25).

[131] L. Lunghi et al. "Control of human trophoblast function". *Reproductive biology and endocrinology : RB&E* 5 (2007), p. 6. ISSN: 1477-7827. DOI: 10.1186/1477-7827-5-6 (cit. on pp. 3, 74, 75).

[132] G. G. M. Fabrizio and M. J. Golden. "The minimum free energy for a class of compressible viscoelastic fluids". *Differential and Integral Equations* 7 (2002), pp. 319–342 (cit. on pp. 194, 201).

[133] R. L. Magin. "Fractional calculus models of complex dynamics in biological tissues". *Computers & Mathematics with Applications* 59.5 (2010), pp. 1586–1593 (cit. on pp. 5, 167).

[134] F. Mainardi. "The Fundamental Solutions for the Fractional Diffusion-Wave Equation". *Applied Mathematics Letters* 9.6 (1996), pp. 23–28 (cit. on p. 176).

[135] F. Mainardi. "Fractals and Fractional Calculus in Continuum Mechanics". Wien: Springer Verlag, 1997. Chap. Fractional calculus: Some basic problems in continuum and statistical mechanics, pp. 291–348 (cit. on p. 194).

[136] F. Mainardi. *Fractional Calculus and Waves in Linear Viscoelasticity.* Imperial College Press, 2010 (cit. on pp. 194, 195, 226).

[137] F. Mainardi and G. Spada. "Creep, relaxation and viscosity properties for basic fractional models in rheology". *The European Physical Journal* 193 (2011), pp. 133–160. URL: arXiv:1110.3400 (cit. on p. 194).

[138] M. Maleki, B. Seguin, and E. Fried. "Kinematics, material symmetry, and energy densities for lipid bilayers with spontaneous curvature". *Biomechanics and Modeling in Mechanobiology* 12.5 (2013), pp. 997–1017. DOI: doi:10.1007/s10237-012-0459-7 (cit. on p. 4).

[139] M. Maleki, B. Seguin, and E. Fried. "Kinematics, material symmetry, and energy densities for lipid bilayers with spontaneous curvature". *Biomechanics and Modeling in Mechanobiology* 12.5 (2013), pp. 997–1017 (cit. on p. 153).

[140] B. Mandelbrot. *The Fractal Geometry of Nature.* San Francisco: W. H. Freeman & Co, 1982 (cit. on pp. 263, 265).

[141] B. Mandelbrot. *Fractals and scaling in finance. Discontinuity, concentration, risk.* New York: Springer, 1997 (cit. on p. 263).

[142] D. Marsh. "Lateral pressure profile, spontaneous curvature frustration, and the incorporation and conformation of proteins in membranes". *Biophysical journal* 93 (2007), pp. 3884–3899. DOI: 10.1529/biophysj.107.107938 (cit. on pp. 44, 45, 52).

[143] T. J. Martin and E. Seeman. "Bone remodelling: its local regulation and the emergence of bone fragility". *Best Practice & Research Clinical Endocrinology & Metabolism* 22.5 (2008), pp. 701–722 (cit. on p. 225).

[144] S. Mary et al. "How ligands and signaling proteins affect G-protein-coupled receptors' conformational landscape". *Biochem Soc Trans* 41 (2013), pp. 144–147 (cit. on p. 2).

[145] K. McDonald et al. "Development of a multi-scale finite element model of the osteoporotic lumbar vertebral body for the investigation of apparent level vertebra mechanics and micro-level trabecular mechanics". *Medical Engineering & Physics* 32 (2010), pp. 653–661 (cit. on p. 226).

[146] R. Metzler and J. Klafter. "The random walk's guide to anomalous diffusion: A fractional dynamics approach". *Physics Reports* 399 (2000), pp. 1–77 (cit. on p. 6).

[147] H. Minkowski. "Jahresberichte der Deutschen Mathematike". *Vereinigung* 61 (1908) (cit. on p. 263).

[148] L. Mishnaevsky Jr. "Micromechanics of hierarchical materials: A brief overview". *Review on Advavend Material Science* 30 (2012), pp. 60–72 (cit. on p. vi).

[149] E. F. Morgan, H. H. Bayraktar, and T. M. Keaveny. "Trabecular bone modulus–density relationships depend on anatomic site". *Journal of Biomechanics* 36 (2003), pp. 897–904 (cit. on p. 227).

[150] R. Muller. "Hierarchical microimaging of bone structure and function". *Nature Reviews* 5 (2009), pp. 373–381 (cit. on p. 6).

295

[151]   C. W. Murray and M. L. Verdonk. "The consequences of translational and rotational entropy lost by small molecules on binding to proteins". *Journal of computer-aided molecular design* 16.10 (2002), pp. 741–753. DOI: `10.1023/A:1022446720849` (cit. on p. 37).

[152]   S. Nawaz et al. "Cell viscoelasticity measured with AFM and vertical optical trapping at sub-micrometer deformations". *PLoS ONE* e45297 (2012). DOI: `doi:10.1371/journal.pone.0045297` (cit. on p. 5).

[153]   S. Nikolov and D. Raabe. "Hierarchical Modeling of the Elastic Properties of Bone at Submicron Scales: The Role of Extrafibrillar Mineralization." *Biophysical Journal* 94 (2008), pp. 4220–4232 (cit. on p. 6).

[154]   W. Noll. "A new mathematical theory of simple materials". *Archive for Rational Mechanics and Analysis,* 48 (1972), pp. 1–50 (cit. on pp. 194, 201).

[155]   D. Norouzi, M. Müller, and D. M. "How to determine local elastic properties of lipid bilayer membranes from atomic-force-microscope measurements: A theoretical analysis". *Physical Review Letters E* 74.061914 (2006) (cit. on p. 1).

[156]   P. Nutting. "A new general law of deformation". *Journal of The Franklin Institute* 191 (1921), pp. 679–685 (cit. on pp. 5, 193, 196).

[157]   J. Oates and A. Watts. "Uncovering the intimate relationship between lipids, cholesterol and GPCR activation". *Current Opinion in Structural Biology* 21.6 (2011), pp. 802–7 (cit. on p. 3).

[158]   J. E. Olberding et al. "The non-equilibrium thermodynamics and kinetics of focal adhesion dynamics". *PLoS ONE* 5.8 (2010), e12043 (cit. on pp. 68, 81).

[159]   K. Oldham and J. Spanier. *The Fractional Calculus.* New York: Academic Press, 1974 (cit. on p. 259).

[160]   S. Ollila. *Lateral Pressure in Lipid Membranes and Its Role in Function of Membrane Proteins.* 2010, p. 96. ISBN: 9789521524806. URL: `http://urn.fi/URN:NBN:fi:tty-201011181369` (cit. on pp. 44, 52).

[161] R. S. Ostrom and P. A. Insel. "The evolving role of lipid rafts and cave-olae in G protein-coupled receptor signaling: implications for molec-ular pharmacology". *British of Journal Pharmacology* 143 (2004), pp. 235–45 (cit. on p. 3).

[162] J. Overington, B. Al-Lazikani, and A. Hopkins. "How many drug targets are there?" *Nature Reviews. Drug Discovery* 5.12 (2006), pp. 993–6 (cit. on p. 2).

[163] J. Owicki and H. McConnell. "Theory of protein-lipid and protein-protein interactions in bilayer membranes". *PNAS* 76 (1979), pp. 4750–4754 (cit. on pp. 2, 4, 25, 27).

[164] J. Owicki, M. Springgate, and H. McConnell. "Theoretical study of protein-lipid interactions in bilayer membranes". *PNAS* 75 (1978), pp. 1616–1619 (cit. on pp. 4, 25, 27, 72).

[165] J. Pan, S. Tristram-Nagle, and J. Nagle. "Effect of cholesterol on structural and mechanical properties of membranes depends on lipid chain saturation". *Physical Review E* 80.021931 (2009) (cit. on p. 4).

[166] H. H. Patel, F. Murray, and P. A. Insel. "G-protein-coupled receptor-signaling components in membrane raft and caveolae microdomains". *Handbook of Experimental Pharmacology* 186 (2008), pp. 167–84 (cit. on p. 3).

[167] R. Phillips et al. "Emerging roles for lipids in shaping membrane-protein function". *Nature* 459 (2009), pp. 379–85 (cit. on p. 2).

[168] P. Pivonka et al. "Model structure and control of bone remodeling: A theoretical study". *Bone* 43 (2008), pp. 249–263 (cit. on pp. 225, 226).

[169] I. Podlubny. *Fractional Differential Equation*. Academic, New York, 1998 (cit. on pp. 167, 178, 182, 226, 257, 259–261).

[170] A. A. Poundarik et al. "Dilatational band formation in bone". *PNAS* (2012), pp. 19178–19183. DOI: www.pnas.org/cgi/doi/10.1073/pnas.1201513109 (cit. on p. 227).

[171] G. Puglisi. "Nucleation and phase propagation in a multistable lat-tice with weak nonlocal interactions". *Continuum Mechanics and Thermodynamics* (2007), pp. 299–319 (cit. on p. 155).

[172] J. Qi and S. Chen. "Eigenvalue problems of the model from nonlocal continuum mechanics". *Journal of Mathematical Physics* 52.073516 (2011) (cit. on p. 176).

[173] V. Quaglini, V. La Russa, and S. Corneo. "Nonlinear stress relaxation of trabecular bone". *Mechanics Research Communications* 36 (2009), pp. 275–283 (cit. on pp. 194, 226, 228, 229).

[174] P. Rangamani and D. J. Steigmann. "Variable tilt on lipid membranes". *Proceedings of the Royal Society A* 470 (2015), p. 20140463 (cit. on p. 4).

[175] P. Rangamani et al. "Small scale membrane mechanics". *Biomechanics and Modeling in Mechanobiology* 13 (2014), pp. 697–711 (cit. on p. 4).

[176] W. Rawicz et al. "Effect of Chain Length and Unsaturation on Elasticity of Lipid Bilayers". *Biophysical Journal* 79 (2000), pp. 328–339 (cit. on p. 4).

[177] S. S. Ray, B. P. Poddar, and R. K. Bera. "Analytical solution of a dynamic system containing fractional derivative of order one-half by Adomian decomposition method". *Journal of Applied Mechanics* 72.2 (2005), pp. 290–295. DOI: `doi:10.1115/1.1839184` (cit. on p. 194).

[178] F. Riewe. "Mechanics with fractional derivatives". *Physical Review E* 55 (1997), pp. 3581–3592 (cit. on p. 194).

[179] E. Sackmann. "Handbook of biological physics". Ed. by R. Lipowsky and E. Sackmann. Elsevier, 1995. Chap. 5. Physical Basis of Self-Organization and Function of Membranes: Physics of Vesicles, pp. 213–303 (cit. on pp. 1, 2, 4, 25, 27).

[180] G. Sagvolden et al. "Cell adhesion force microscopy". *PNAS* 96 (1999), pp. 471–476. URL: `http://www.ncbi.nlm.nih.gov/entrez/query.fcgi?cmd=Retrieve%5C&db=PubMed%5C&dopt=Citation%5C&list%5C_uids=9892657` (cit. on p. 75).

[181] S. Sakakibara. "Relaxation properties of fractional derivative viscoelasticity models". *Nonlinear Analysis* 47 (2001), pp. 5449–5454 (cit. on p. 194).

298

[182]   S. G. Samko, A. A. Kilbas, and O. I. Marichev. *Fractional Integrals and Derivatives. Theory and Applications*. Londn - New York: Gordon & Breach Science Publishers, 1987 (cit. on pp. vi, 167).

[183]   S. G. Samko, A. A. Kilbas, and O. I. Marichev. *Fractional Integrals and Derivatives. Theory and Applications*. Londn - New York: Gordon & Breach Science Publishers, 1987 (cit. on pp. 197, 200, 201, 204, 219, 226, 257, 258, 260).

[184]   N. Sarkar and A. Lahiri. "Effect of fractional parameter on plane waves in a rotating elastic medium under fractional order generalized thermoelasticity". *International Journal of Applied Mechanics* 4 (2012). DOI: `doi:10.1142/S1758825112500305` (cit. on p. 5).

[185]   G. Scott Blair. "The role of psychophysics in rheology". *Journal of Colloid Science* 2 (1947), pp. 21–32 (cit. on pp. 5, 193, 230).

[186]   G. Scott-Blair. "Psychoreology: links between the past and the present". *Journal of the Texture Studies* 5 (1974), pp. 3–12 (cit. on p. 167).

[187]   E. Seeman and P. D. Delmas. "Bone Quality — The Material and Structural Basis of Bone Strength and Fragility". *The New England Journal of Medicine* 354 (2006), pp. 2250–2261 (cit. on p. 6).

[188]   V. Sharma et al. "Rheology of globular proteins: apparent yield stress, high shear rate viscosity and interfacial viscoelasticity of bovine serum albumin solutions". *Soft Matter* 7 (2011), pp. 5150–5160. DOI: `doi:10.1039/c0sm01312a` (cit. on p. 5).

[189]   E. J. Shimshack and H. M. McConnell. "Lateral phase separation in phospholipid membranes". *Biochemistry* 12.12 (1973), pp. 2531–2360 (cit. on pp. 1, 22).

[190]   K. Simons and E. Ikonen. "Functional rafts in cell membranes". *Nature* 5.387 (1997), pp. 569–72 (cit. on p. 22).

[191]   D. Steigmann. "A model for lipid membranes with tilt and distension based on three-dimensional liquid crystal theory". *International Journal of Non-Linear Mechanics* 56 (2013), pp. 61–70 (cit. on p. 4).

[192] M. S. Stein et al. "Bone size and mechanics at the femoral diaphysis across age and sex". *Journal of Biomechanics* 31 (1998), pp. 1101–1110 (cit. on p. 226).

[193] M. K. Suchorsky and R. H. Rand. "A pair of van der Pol oscillators coupled by fractional derivatives". *Nonlinear Dynamics* 69 (2012), pp. 313–324. DOI: doi:10.1007/s11071-011-0266-1 (cit. on p. 194).

[194] M. R. Sunny et al. "A modified fractional calculus approach to model hysteresis". *Journal of Applied Mechanics* 77 (2010). DOI: doi:10.1115/1.4000413 (cit. on p. 194).

[195] M. Terzi, K. Dayal, and M. Deserno. "Revisiting the Link between Lipid Membrane Elasticity and Microscopic Continuum Models". *Biophysical Journal* 108.2 (2015), 87a–88a (cit. on p. iii).

[196] J. S. Thomsen et al. "Stochastic simulation of vertebral trabecular bone remodeling". *Bone* 15.6 (1994), pp. 655–666 (cit. on p. 225).

[197] M. Trejo and M. Ben Amar. "Effective line tension and contact angles between membrane domains in biphasic vesicles". *The European Physical Journal E* 34.8 (2011), pp. 2–14 (cit. on p. 23).

[198] N. Triantafyllidis and S. Bardenhagen. "On Higher Order Gradient Continuum Theories in Nonlinear Elasticity Derivation from and Comparison to the Corresponding Discrete Models". *Journal of Elasticity* 33 (1993), pp. 259–293 (cit. on p. 155).

[199] B. Trzaskowski et al. "Action of molecular switches in GPCRs–theoretical and experimental studies". *Science* 318.5854 (2012), pp. 1258–65. DOI: doi:10.1126/science.1150577 (cit. on p. 2).

[200] H. Unal and S. Karnik. "Domain coupling in GPCRs: the engine for induced conformational changes". *Trends in Pharmacological Sciences* 33.2 (2012), pp. 79–88 (cit. on p. 2).

[201] S. Veatch and S. Keller. "Seeing Spots: Complex Phase Behavior in Simple Membranes," *Biochim. Biophys. Acta - Molecular Cell Research* 1746 (2005), pp. 172–185 (cit. on p. 22).

[202] N. Walani, J. Torres, and A. Agrawal. "Endocytic proteins drive vesicle growth via instability in high membrane tension environment". *PNAS* (2015), E1423–E1432. DOI: www.pnas.org/cgi/doi/10.1073/pnas.1418491112 (cit. on pp. 1, 4).

[203] Y. Wang et al. "Experimental study on the viscoelastic properties of cancellous bone of the os calcaneus, os lunatum and os capitalum]". *Journal of Biomedical Engineering* 20.3 (Sept. 2003), pp. 434–438 (cit. on pp. 226, 228, 229).

[204] H. J. Werner et al. "The loss of stiffness as osteoporosis progresses". *Medical Engineering & Physics* 18.7 (1996), pp. 601–606 (cit. on p. 226).

[205] M. Xie et al. "Inactivation of multidrug resistance proteins disrupts both cellular extrusion and intracellular degradation of cAMP". *Molecular Pharmacology* 80 (2011), pp. 281–293 (cit. on pp. 62, 63, 67, 86).

[206] L. Yang and K. Dayal. "Free surface domain nucleation in a ferroelectric under an electrically charged tip". *Journal of Applied Physics* 111 (2012) (cit. on p. 90).

[207] L. Yang and K. Dayal. "Microstructure and stray electric fields at surface cracks in ferroelectrics," *International Journal of Fracture* 174.1 (2012), pp. 17–27 (cit. on p. 90).

[208] P. Yang, Y. C. Lam, and K. Zhu. "Constitutive equation with fractional derivatives for generalized UCM model". *Journal of Non-Newtonian Fluid Mechanics* 165 (2010), pp. 88–97. DOI: doi:http://dx.doi.org/10.1016/j.jnnfm.2009.10.002 (cit. on p. 194).

[209] H. Yao and H. Gao. "Multi-scale cohesive laws in hierarchical materials". *Internatiol Journal of Solids and Structures* 44 (2007), pp. 8177–8193 (cit. on p. vii).

[210] G. Zurlo. "Material and geometric phase transitions in biological membranes". PhD thesis. Doctorate of Philosophy in Structural Engineering, University of Pisa, 2006 (cit. on pp. iii, 1, 4, 23, 25, 27, 40, 72).